

SOUTHWEST RESEARCH INSTITUTE
Post Office Drawer 28510, 6220 Culebra Road
San Antonio, Texas 78284

SI. SKI (IND)
FR. DOWDING
1-80
C

Analysis and Testing of Pipe Response to Buried Explosive Detonations

by
Peter S. Westine
Edward D. Esparza
Alex B. Wenzel

for
The Pipeline Research Committee
American Gas Association

July 1978

Approved:



H. Norman Abramson, Vice President
Engineering Sciences Division

ACKNOWLEDGMENTS

This program was sponsored by the Pipeline Research Committee of the American Gas Association and conducted by Southwest Research Institute. The authors thank the supervisory committee for their guidance and direction, suggestions, and cooperation during the conduct of the program. Members of this committee are:

Mr. Osborne Lucas - Chairman, Columbia Gas Transmission Corp.
Mr. J. M. Holden, American Gas Association
Mr. J. S. Taylor, Consumers Power Company
Mr. J. D. McNorgan, Southern California Gas Company
Mr. R. L. Penning, Panhandle Eastern Pipe Line Company
Mr. C. P. Hendrickson, Northern Illinois Gas Company
Mr. H. E. Russell, Transcontinental Gas Pipe Line Corp.
Mr. J. T. Sickman, Texas Eastern Transmission Corp.
Mr. G. J. Bart, Texas Gas Transmission Corp.

In addition, the authors are very grateful for the support, assistance and cooperation provided by Panhandle Eastern Pipe Line Co., and the Texas Gas Transmission Corp. in conducting the field experiments at the Kansas City and Kentucky remote test sites respectively. Furthermore, funding of part of this program was also provided by Texas Gas Transmission Corp. to conduct the field experiments at the Kentucky site.

At Southwest Research Institute the authors are especially indebted to the following personnel:

Messrs. E. R. Garcia, Jr. and A. C. Garcia - for performing the field experiments
Dr. W. E. Baker - technical consultation and review of analysis
Mr. J. J. Kulesz - assistance in conducting the model experiments
Mr. R. A. Cervantes - assistance in performing model experiments
Mr. J. C. Hokanson - programming of data reduction codes
Meses. T. K. Moseley, P. A. Hugg, and Y. R. Martinez - data reduction
Mr. V. J. Hernandez - final drawing of illustrations

Mmes E. Hernandez, J. Cooke and C. W. Dean - typing of interim and final reports.

Ms. D. J. Stowitts, - for editing and proofing the final report.

The assistance and cooperation of these individuals is greatly appreciated.

EXECUTIVE SUMMARY

This final report describes experimental tests and analytical solutions in a research program to develop procedures for predicting the maximum circumferential and longitudinal stresses in pipelines caused by nearby buried explosive detonations. This study was conducted over a period of 2.5 years by Southwest Research Institute for the Pipeline Research Committee of the American Gas Association.

The approach followed in developing a final solution evolved from a combination of experimental and theoretical studies, specifically:

- Similitude theory
- Model tests on small buried pipes
- Approximate energy procedures based on assumed deformed pipe shapes
- Conservation of mass and momentum principles for shock fronts
- Empirical observation based on past investigations
- Full scale experimental data generated during this study.

To develop this final relationship for predicting pipe stresses, the problem was divided into two parts. The first problem was to estimate the maximum soil particle velocities and displacements at various distances from either buried single detonations (point sources) or multiple detonations (line sources). These ground motions provide the forcing function imparted to the buried pipe. The second problem was to estimate both maximum circumferential and longitudinal stresses in buried pipe caused by these maximum ground motions. After the results of the first solution were substituted into the results of the second solution, pipe stress solutions for circumferential stress σ_{cir} and longitudinal stress σ_{long} were obtained and computed from the equations:

$$\sigma_{cir} = 1.00 \bar{\sigma}$$

$$\sigma_{long} = 0.253 \bar{\sigma}^{1.304} - \bar{\sigma} \quad , \quad \text{for } \bar{\sigma} \leq 2675 \text{ psi} \quad (95a)$$

Or

$$\sigma_{\text{cir}} = 21.70 \bar{\sigma}^{0.740} - 47.55 \bar{\sigma}^{0.584}$$

$$\sigma_{\text{long}} = 47.55 \bar{\sigma}^{0.584}, \text{ for } \bar{\sigma} \geq 2675 \text{ psi} \quad (95b)$$

Where

$$\bar{\sigma} = \frac{46.53 \sqrt{E} (nW)}{\sqrt{h} R^{2.5}} \quad (\text{point source}) \quad (91)$$

Or

$$\bar{\sigma} = \frac{69.76 \sqrt{E} \left(\frac{nW}{\ell}\right)}{\sqrt{h} R^{1.5}} \quad (\text{line source}) \quad (94)$$

and where

- E = modulus of elasticity for the pipe
- nW = equivalent explosive energy weight
- ℓ = length of explosive line
- h = pipe thickness
- R = standoff distance

Forty-three tests measuring ground motions and pipe strains from the detonation of both point and line sources at three different test sites are also presented in this report and are used to demonstrate the validity of this solution. The experiments included tests on 3-, 6- and 16-in. diameter model pipe segments and on 24- and 30-in. diameter pipelines. Although significant scatter occurs, one standard deviation in pipe stress is approximately $\pm 45\%$; no systematic errors are apparent. This scatter appears even in as many as five repeat tests of ideally the same soil, pipe, standoff, and charge conditions.

Before these solutions for pipe stresses generated by blasting can be applied in the field, the stresses in the pipelines from causes, such as manufacturing, pressurization of the pipeline, and thermal changes, must be superimposed on the blast stresses to be sure the pipeline does not yield. Because biaxial rather than uniaxial states of stress are also involved, a failure theory must also be selected. Although failure theories and other causes of pipe stress are discussed later in this report, we do not specifically recommend which approaches should be used. Other considerations such as differing regulations and company policies prevent us from being more specific.

These factors eventually will require each pipeline company to use this research report only as a guide in writing their individual corporate procedures for determining how close to their pipelines blasting can be conducted.

This report is a research report and not a field manual. To help guide corporate development of an appropriate field manual, we present six alternate ways that these equations can be presented, illustrated, and discussed for possible use in field manuals. Tables, nomographs, and figures are used to illustrate different approaches which might be considered in deciding which technique is easier for personnel to apply in computing pipe stresses from blasting.

A sensitivity analysis was also conducted which indicated that pipe stresses from blasting are most sensitive to standoff distance R and least sensitive to the modulus of elasticity of the pipe E and pipe thickness h . Surprisingly, the pipe stresses are independent of the soil density ρ_s , the soil seismic propagation velocity c , and the pipe diameter D . The mathematics of the solution must be studied to understand why these parameters fall out of the analysis. The experimental tests also verified these observations. Dynamic analysis procedures and not static ones must be used to understand these or other conclusions.

As with any analysis procedure, this solution is based upon assumptions which limit its applicability. Three considerations for additional work are suggested in the conclusions and recommendations which could lead to an improved solution. The most important of these is that the explosive is idealized as either a point or a line source. Most problems which will be encountered in the field come from the detonation of an explosive grid. More model tests in this area would be beneficial. Until this work is performed, engineering judgment will be required in order to apply these results to field conditions.

LIST OF ILLUSTRATIONS

Figure		Page
1	Plan View Layout of Model Experiments	21
2	Strain Gage Locations on Model Pipes	23
3	Kansas City Test Site	25
4	Plan View of Test Layout at Kansas City Site	27
5	Strain Gage Locations on 24-Inch Pipe	28
6	Uncovering of Pipeline for Strain Gaging	30
7	Connection and Checkout of Strain Channels	31
8	Backfilling of Hole Around Pipe	32
9	Drilling of Ground Motion Transducer and Charge Holes	33
10	Preparation and Placement of Explosive Charge	35
11	Detonation of Buried 15-lb Explosive Charge	36
12	Craters Made by Buried Detonations	37
13	Kentucky Test Site	38
14	Field Layout of Kentucky Tests	41
15	Strain Gage Locations on 30-Inch Pipe	42
16	Detonation of Buried 5-lb Explosive Charge	43
17	Circuit Diagram for Velocity Transducer	45
18	Circuit Diagram for Accelerometer	46
19	Ground Motion Canister Assembly	48
20	Placement of Velocity Canister Down-Hole	49
21	Strain Gaging of 6-Inch Diameter Pipe	50
22	Field Installation of 3- and 6-Inch Pipes	51
23	Strain Gage Installation and Burial of 16-Inch Diameter Pipe	52
24	Installation of Weldable Strain Gages on 24-Inch Pipe	54-55
25	Installation of Strain Gages on 30-Inch Pipe	57
26	Circuit Diagram for Pipe Strain Gages	58
27	Instrumentation System Block Diagram	59
28	Ground Motions from 0.4-lb Charge at a Radial Distance of 4 Feet	65
29	Ground Motions at 8 ft. from 0.4-lb Charge	66
30	Ground Motions at 3 ft. from 0.21-lb Explosive Line Source	67

TABLE OF CONTENTS (Continued)

	Page
VII. ALTERNATE METHODS OF PREDICTING PIPE STRESSES	131
- Direct Use of Equations	131
- Tabular Format Using $\bar{\sigma}$	133
- Graphical Format Using $\bar{\sigma}$	133
- Solution by Nomograph	136
- Tables for Various Pipe	140
- Graphical Plot of Parameters	146
- General	146
VIII. ANALYSIS OF STRESS SOLUTION	149
- Example Problem	149
- Solution Idealizations	150
- Sensitivity Analysis	150
- Other Stress States	153
- Other Analysis Methods	157
- Factor of Safety	161
IX. CONCLUSIONS AND RECOMMENDATIONS	163
X. REFERENCES	168
XI. LIST OF PARAMETERS AND SYMBOLS	170

LIST OF ILLUSTRATIONS (Continued)

Figure		Page
31	Horizontal Velocities from 0.05-lb. Charge	68
32	Radial Ground Motions at 12 ft. from 15-lb. Charge	71
33	Radial Soil Motions at 12 ft. from a 5-lb Charge	72
34	Radial Soil Motions at 12 ft. from a 5-lb. Charge	75
35	Radial Soil Motions at 12 ft. from a 3-lb Charge	76
36	Circumferential Strain Measurements on 3-Inch Diameter Pipe	78-79
37	Strain Measurements for 6-Inch Pipe	80-81
38	Blast Strain Records for 24-Inch Pipe	85-86
39	Test No. 6 Blast Strains on 24-Inch Pipe	87-88
40	Test No. 6 Blast and Internal Pressure Strains on 24-Inch Pipe	89-90
41	Test No. 4 Strains on 30-Inch Pipe	93-94
42	Ground Displacement in Rock and Soil No Coupling	100
43	Particle Velocity in Rock and Soil No Coupling	102
44	Coupled Displacement in Rock and Soil	105
45	Coupled Particle Velocity in Rock and Soil	106
46	Radial Soil Displacement from Line Charge Detonations	109
47	Maximum Soil Particle Velocity from Line Charge Detonations	110
48	Equation 46 Compared to Displacement Test Data	112
49	Assumed Distribution of Impulse Imparted to a Pipe	115
50	Circumferential Pipe Stress	125
51	Longitudinal Pipe Stress	128
52	Graphical Solution Using $\bar{\sigma}$	135
53	Pipe Stress Nomograph for Point Sources	137
54	Pipe Stress Nomograph for Line Sources	138
55	Graphical Plot of Blasting Pipe Stresses	147
56	Plan View of an Example Field Blasting Problem	151
57	Stress States for Different Yield Theories	155
58	Simplified Yield Theories	156
59	Qualitative Ground Shock Model	157
60	Battelle Circumferential Stress Formula	160

LIST OF TABLES

Table		Page
I	Scale Factors for a Replica Modeling Law	15
II	Summary of Test Conditions for Model Experiments	20
III	Tests Conducted at Kansas City Test Site	26
IV	Kentucky Tests	39
V	Summary of Horizontal Ground Motion Data from Model Tests	63
VI	Radial Soil Motion Data from Kansas City Tests	70
VII	Ground Motion Data	73
VIII	Maximum Strains from Model Experiments	82
IX	Maximum Blast Pipe Stresses for Model Test	83
X	Maximum Strains from Blast Loading on 24-Inch Pipe	91
XI	Combined Blast and Internal Pressure Strains	91
XII	Maximum Blast Stresses on 24-Inch Pipe	91
XIII	Maximum Blast Strains Measured on 30-Inch Pipe	95
XIV	Maximum Blast Stresses in 30-Inch Pipe	95
XV	Measured Durations and Computer Periods	118
XVI	Equivalent Energy Release	129
XVII	Stresses in Pipes from Blasting	134
XVIII	Stress in Buried Pipe from Point Source Blasting	141-144
XIX	Stresses Used in Extrapolation	145
XX	Results of Sensitivity Analysis	152

I. INTRODUCTION

This final report describes a research program to develop functional relationships for predicting the stress in pipelines caused by nearby blasting. This program was conducted during the period of 1975 through 1977 by Southwest Research Institute (SwRI) for the Pipeline Research Committee of the American Gas Association (A.G.A.), under Project No. PR 15-76.

To accomplish the above objective, the program was divided and funded in three phases which had several tasks in each phase. The Phase I effort to formulate an analysis procedure included tasks to:

- Review the literature on ground shock propagation and effects of shock loading on buried pipe-like structures; and
- Qualitatively plan an analytical approach and limited test program for predicting the change in pipe stresses from buried detonations.

The Phase II effort to conduct limited experiments to generate the necessary data for developing a solution included tasks to:

- Quantify procedures for estimating the loads on pipes from both single source and multi-source buried detonations;
- Quantify procedures for predicting the maximum dynamic circumferential and longitudinal stresses in pipe from blast loads; and
- Use model tests on various pipe to experimentally generate and validate the ground shock and pipe stress solutions.

The Phase III effort to validate the solution by conducting actual pipeline tests included tasks to:

- Conduct several field evaluations by measuring additional stresses and ground motions at actual pipeline sites to enhance the solution and demonstrate its validity;
- Present alternate methods for the pipeline industry to use the resulting stress from blasting solution; and
- Complete an engineering report on these efforts.

The resulting solution interrelates type of explosive, amount of explosive, standoff distance, pipe size, pipe properties, and the resultant longitudinal and circumferential pipe stresses caused by blasting. In order to create such a solution, the general problem had to be divided into two separate parts. The first part estimated maximum particle velocity and

maximum soil displacement at various distances from either single detonations (point sources) or multiple detonations (line sources). The second problem was then the estimate of both circumferential and longitudinal maximum dynamic pipe stresses caused by the previously determined maximum ground motions. This division of the general problem into these two separate parts is apparent throughout the report until such time as the solutions are combined to give a final interrelationship.

The solution which finally evolved is in an explicit closed form which can be solved using graphs, tables, or a hand calculator. To accomplish this task, similitude theory had to be combined with theoretical approaches using energy procedures, conservation of mass and momentum principles for shock fronts, and empirical observation before a final solution evolved. The ground shock propagation problem was solved by using similitude theory to create pi terms, empirical observation to combine two of these pi terms, and a vast quantity of test data from both the literature and tests conducted in this study to interrelate scaled energy release and standoff distance to scaled ground motion. The ground motion solution which results from this effort works for small energy releases such as 0.03 lbs. of explosive to large kiloton nuclear blasts. Peak particle displacement predicted from this solution is then combined with the Hugoniot equations for conservation of mass and momentum to estimate the impulse imparted to a buried pipeline. Finally, assumed deformed shapes, a conservation of energy solution, and empirical observation using measured strains on actual buried pipe segments are used to develop the final stress solution.

Forty-three tests measuring ground motions and pipe strains from the detonation of both point and line sources at three different test sites are also described. These experiments include tests on 3-, 6- and 16-in. diameter model pipe segments as well as experiments on actual 24- and 30-in. diameter pipelines. The test results are used to both develop the previously mentioned ground motion and pipe stress solutions and demonstrate the validity of the resulting analyses.

This report is organized into eleven sections, Section II describes the analytical basis using similitude theory for the design of the experiments. The model analysis presented in this section concentrates on developing functional relationships to determine 1) soil particle velocity and displacement

for both a point and line explosive source, and 2) pipe stresses caused by these ground motions. The purpose of this section is to show why model tests could be used in place of full-scale prototype experiments to accumulate the major quantity of test data.

Section III describes the test sites, the experiments performed at each site, and measurement systems used. Model tests using 3-, 6-, and 16-in. diameter pipe were tested at SwRI. Full scale tests on a 24-in. diameter pipe were conducted outside Kansas City, Missouri, and other full scale tests on a 30-in. diameter pipe were conducted in Kentucky. Similar instrumentation and test procedures were used at all sites.

Section IV contains examples of ground motion and pipe strain data traces. In addition, Section IV shows an experiment by experiment compilation of all measured soil particle velocities, soil displacements, circumferential pipe strains, and longitudinal pipe strains.

Section V presents the analyses of ground motions using the test data summarized in Section IV plus additional data from the literature as presented by the Atomic Energy Commission (now part of the Department of Energy) and the Bureau of Mines. These data use explosive energy releases ranging from 0.03 lbs. to 19.2 kilotons (nuclear blast equivalency) to develop empirical relationships for estimating the maximum radial soil particle velocity and displacement from both point and line explosive sources.

The maximum ground motion relationships developed in Section V became the forcing function applied to the pipe in Section VI. Section VI also uses energy procedures to develop an approximate solution for longitudinal and circumferential pipe stresses. Finally, in Section VI the pipe stresses summarized in Section IV are used to empirically perfect a more accurate general pipe solution.

Section VII covers several alternate methods of applying the solution developed in Section VI for predicting pipe stresses in the field. This section is presented to suggest possible field procedures which pipeline companies might consider as better methods for use by their field crews.

Section VIII discusses in greater depth the significance of the pipe stress solution. This section points out that the problem frequently encountered in the field is not simply that of a single source or line source, but rather is that of a matrix of blast holes of some width and depth. Also

in this section is a sensitivity analysis to show how circumferential and longitudinal stresses from blasting vary because another parameter is changed. To place the analysis in perspective, it is emphasized that blasting stresses are not the only ones present. Other stress states caused by internal pipe pressurization, thermal expansion, overburden or surcharge, and from welding or other assembly processes must be superimposed on the blasting stresses to determine the correct state of stress. Also a biaxial rather than a uniaxial state of stress exists in a pipe, so some failure theory must be chosen to decide when yielding begins. It is not specified which failure theory should be selected, but six theories which are in use are shown. Also found in Section VIII is a discussion of present procedures based on other research work and regulatory codes which limit particle velocities. Finally, the section ends with a discussion of safety factors and how they should be chosen.

Conclusions and recommendations for future work are given in Section IX. A list of references is given in Section X, and a list of all the parameters used in this report is given in the foldout sheet, Section XI.

II. ANALYTICAL BASIS FOR THE EXPERIMENTS

General

The objective of this study was to develop an accurate analysis procedure for predicting maximum longitudinal and circumferential stresses in a pipe caused by nearby buried explosive detonations. Although subsequent results arrived at after several years of study infer that soil properties such as density and seismic propagation velocity are relatively unimportant, this observation could not be made initially. At first, it was thought that the soil problem should be approached using either 1) a finite difference or finite element computer code, or 2) an empirical approach. The analytical computer program was rapidly ruled out for two reasons. First, no generally accepted equation-of-state exists for various soils exposed to severe ground shock from nearby detonations. Any equation used would be subject to criticism and in general might compromise the study. Secondly, a computer program which had to be exercised every time a new problem was encountered would not be used by field crews and engineers concerned with day to day pipeline operations. This line of reasoning rapidly indicated that an empirical approach was attractive.

An empirical method was used; however, it was supplemented with approximate analysis procedures. Experimental testing to obtain data on actual pipelines would have been very expensive. Hence, the approach became a compromise in which model experiments were conducted on 3-, 6-, and 16-in. diameter pipe using small charges buried at shallow depths as a stimulation of large full scale pipeline conditions. A large amount of data was accumulated using models. A limited number of full scale or prototype experiments were conducted on a 24-in. diameter pipeline near Kansas City, Missouri and on a 30-in. diameter pipeline in Kentucky to demonstrate that actual pipeline conditions.

The solution was divided into two parts. One part was to determine the peak radial particle velocity U and radial maximum displacement X in the soil when a detonation occurs in the vicinity. This ground motion solution was subdivided into two problems--(1) ground motion from a single source (point source solution) and (2) a multi-source detonation (line source solution). The other solution was a pipe stress solution for determining both

circumferential and longitudinal stresses in a pipe because of ground motions. In Section VI these two solutions are combined to give an overall solution.

In the beginning of this study, model tests and the associated similitude theory were an important part in both the ground shock and pipe stress solutions. Therefore, this section provides at least a minimal modeling background so that the test program is properly understood.

Pi Theorem and Its Significance

Many parameters must be combined through testing or analysis if a solution is to be developed in any study. Dimensional analysis or similitude theory provides a technique for combining any complete list of parameters into a smaller list of dimensionless combinations of these parameters. If these dimensionless ratios, often called pi terms, should remain invariant between model and full-scale (prototype) tests, the two systems are equivalent. Note that each parameter does not have to be the same for the systems to be equivalent, only the pi terms (π terms) need to be equal in equivalent systems. The implications of this rule are that if all pertinent physical parameters are indeed identified in defining a physical problem and further, if all π terms are kept invariant between model and prototype, then tests on small size models will truly predict results for full-scale items. The set of π terms for any given problem defines the model law in the mathematical form:

$$f_1 (\pi_1, \pi_2, \dots \pi_n) = 0 \quad (1)$$

where f_1 is an unknown functional form. Alternatively, Equation (1) can be written:

$$\pi_i = f_2 (\pi_1, \pi_2, \pi_i, \pi_{i+1} \dots \pi_n) \quad (2)$$

where again f_2 is some unknown functional form different from f_1 . Equation (2) can be stated as follows:

"Any dimensionless group (π term) can be expressed as some function of all of the other dimensionless groups defining the problem."

In addition to establishing that the functional relationships such as those of Equations (1) and (2) do indeed exist, the model law also establishes certain interrelations between scale factors for all of the physical parameters involved. It does not, however, irrevocably fix individual scale factors unless other assumptions are made. In a model law involving a number of π terms, a set of interrelations equal to the number of π terms is defined.

Other attributes of the sets of dimensionless groups resulting from dimensional analysis are:

- (1) The number of such groups usually equals the number of original dimensional parameters minus the number of fundamental physical dimensions (usually three).
- (2) No given set of π terms is unique for the problem. New terms may be generated by such manipulations as inverting, taking to powers or roots, multiplying or dividing one or more terms together, etc. The total number of π terms is not altered by such manipulations.
- (3) Although different sets of dimensionless groups can be easily generated for the same problem, the final implications of the resulting model law are the same regardless of which set is chosen.

In order to understand similitude methods, one must know the limitations, or apparent limitations, of dynamic modeling. The first of these is readily apparent: one must be able to identify and list the physical dimensions of the parameters governing the problem. No model analysis is possible unless this first step can be taken. A corollary to the first limitation is that no information can be obtained on scaling of a physical parameter if that parameter is not originally included in the analysis. (Strictly speaking, these "limitations" are not truly limitations on similitude theory, but instead only indicate poor or incomplete definition of the problem.) The most important true limitation is that model law cannot, by itself, determine the actual functional form of dependence of one dimensionless parameter on others. That is, forms f_1 and f_2 in Equations (1) and (2) must be determined in some other way. The methods for such determination are

two fold: (1) mathematical analysis (including numerical solution by computer codes), and (2) experimentation. Only by using one or both of these methods can the actual functional forms be determined. The strength of the dimensional analysis, on the other hand, lies in the generalization of the results obtained by experimental or mathematical solution.

The major advantages for using model analysis are:

- (1) The number of quantities being interrelated can be greatly reduced. This means that fewer experiments are needed, or, in the case where enough experimental data exist, one can develop a more extensive solution, provided the dimensional data are appropriately interpreted.
- (2) If experiments are conducted, it becomes less expensive because physically smaller items can be tested. These financial advantages of scale are achieved because the π terms can be identical in both large and small systems, making these systems equivalent even though they differ in physical size.

In this program, we took full advantage of the above features, resulting in a general solution to a very complicated problem, with a limited number of experiments.

This introduction about modeling and its advantages is short by necessity. For additional reading, we recommend references 1 through 4.

Modeling of Ground Shock Propagation

For a single concentrated explosive source, assume that a buried energy release W is instantaneously detonated at some standoff distance R from a location in the soil where we wish to know the peak radial velocity U and the maximum radial soil displacement X . The soil is assumed to be a semi-infinite, homogeneous, isotropic medium of mass density ρ_s and seismic P-wave propagation velocity c . These two parameters account for both inertial and compressibility effects in the soil. Finally, later observation infers that perhaps atmospheric pressure p_0 or some other pressure quantity also influences ground motions. This definition of the problem leads to six-parameter spaces of dimensional variables which, in functional format, can be written as:

$$U = f_U (R, W, \rho_s, c, p_o) \quad (3)$$

$$X = f_X (R, W, \rho_s, c, p_o) \quad (4)$$

Our task for attempting to experimentally interrelate all six parameters in the above solution is simplified by conducting a similitude analysis.

Begin this analysis by writing an equation of dimensional homogeneity with an engineer's system for fundamental units of measure of force F, length L, and time T. The exponents $\alpha_1, \alpha_2, \alpha_3, \alpha_4, \alpha_5$ and α_6 in this equation of dimensional homogeneity are as yet undetermined integers.

$$U^{\alpha_1} R^{\alpha_2} W^{\alpha_3} \rho_s^{\alpha_4} d^{\alpha_5} p_o^{\alpha_6} \stackrel{d}{=} F^{\circ} L^{\circ} T^{\circ} \quad (5)$$

The symbol $\stackrel{d}{=}$ means "dimensionally equal to." This equation of dimensional homogeneity states that, if all parameters are listed so that the problem is completely defined, various products of these parameters exist that will be nondimensional. The next step is to substitute the fundamental units of measure for each parameter in Equation (5).

$$\left(\frac{L}{T}\right)^{\alpha_1} (L)^{\alpha_2} (FL)^{\alpha_3} \left(\frac{FT^2}{L^4}\right)^{\alpha_4} \left(\frac{L}{T}\right)^{\alpha_5} \left(\frac{F}{L^2}\right)^{\alpha_6} \stackrel{d}{=} F^{\circ} L^{\circ} T^{\circ} \quad (6)$$

Then collect exponents for each of the fundamental units of measure to obtain:

$$(L)^{\alpha_1 + \alpha_2 + \alpha_3 - 4\alpha_4 + \alpha_5 - 2\alpha_6} (F)^{\alpha_3 + \alpha_4 + \alpha_6} (T)^{-\alpha_1 + 2\alpha_4 - \alpha_5} \stackrel{d}{=} F^{\circ} L^{\circ} T^{\circ} \quad (7)$$

Equating exponents on the left- and right-hand sides of Equation (7) then yields three equations interrelating the five α coefficients:

$$L: \alpha_1 + \alpha_2 + \alpha_3 - 4\alpha_4 + \alpha_5 - 2\alpha_6 = 0 \quad (8-a)$$

$$F: \alpha_3 + \alpha_4 + \alpha_6 = 0 \quad (8-b)$$

$$T: -\alpha_1 + 2\alpha_4 - \alpha_5 = 0 \quad (8-c)$$

Solving for α_2 and α_4 and α_5 in terms of the other two coefficients yields:

$$\alpha_2 = -3\alpha_3 \quad (9-a)$$

$$\alpha_4 = -\alpha_3 - \alpha_6 \quad (9-b)$$

$$\alpha_5 = -\alpha_1 - 2\alpha_3 - 2\alpha_6 \quad (9-c)$$

Substituting Equations (9) into the original equation of dimensional homogeneity, Equation (5) then gives:

$$U^{\alpha_1} R^{-3\alpha_3} W^{\alpha_3} \rho_s^{-(\alpha_3+\alpha_6)} c^{-(\alpha_1+2\alpha_3+2\alpha_6)} P_o^{\alpha_6} \stackrel{d}{=} F^\circ L^\circ T^\circ \quad (10)$$

Finally, collecting parameters with similar exponents yields:

$$\left(\frac{U}{c}\right)^{\alpha_1} \left(\frac{W}{\rho_s c^2 R^3}\right)^{\alpha_3} \left(\frac{P_o}{\rho_s c^2}\right)^{\alpha_6} \stackrel{d}{=} F^\circ L^\circ T^\circ \quad (11)$$

Because the products and quotients inside each parenthesis in Equation (11) are nondimensional, the α_1 , α_3 , and α_6 exponents are undetermined and can conceptually take on any value. These three nondimensional ratios in Equation (11) are called pi terms. Equation (11) restates the more complex Equation (3) as:

$$\frac{U}{c} = f_{U/c} \left[\frac{W}{\rho_s c^2 R^3}, \frac{P_o}{\rho_s c^2} \right] \quad [\text{point source}] \quad (12)$$

The functional format for Equation (12) cannot be explicitly written until either experimental test data or theoretical analyses furnish additional information. The major advantage in conducting this model analysis was that the six-parameter space given by Equation (3) has been reduced to a three-parameter space of nondimensional numbers.

The same procedure can next be applied to Equation (4) for maximum radial soil displacement. Algebraic procedures are not repeated as these

are almost the same as those followed in Equations (5) through (11) with the exception that X is in the analysis rather than U. The nondimensional equation which results from this application of similitude theory to Equation (21) is:

$$\frac{X}{R} = f_{X/R} \left[\frac{W}{\rho_s c^2 R^3}, \frac{P_o}{\rho_s c^2} \right] \quad [\text{point source}] \quad (13)$$

To complete the shock propagation efforts, relationships for particle velocity and soil displacement when line sources generate the shock were needed. Precisely the same procedure was used as described, except now the source is characterized by the energy release per unit length W/ℓ rather than by the total energy release W . The line charge counterparts to the point source dimensional Equations (3) and (4) are:

$$U = f_U (R, W/\ell, \rho_s, d, p_o) \quad (14)$$

$$X = f_X (R, W/\ell, \rho_s, c, p_o) \quad (15)$$

A similitude analysis applied to Equations (14) and (15) yields the following two nondimensional equations for shock wave propagation from a line source.

$$\frac{U}{c} = f_{U/c} \left[\frac{W/\ell}{\rho_s c^2 R^2}, \frac{P_o}{\rho_s c^2} \right] \quad [\text{line source}] \quad (16)$$

$$\frac{X}{R} = f_{X/R} \left[\frac{W/\ell}{\rho_s c^2 R^2}, \frac{P_o}{\rho_s c^2} \right] \quad [\text{line source}] \quad (17)$$

The derivations of equations (12), (13), (16) and (17) do not give a final functional format. This was done in Section V by applying experimental test data on explosive sources ranging from 0.03 lbs. to 19.2 kilotons (nuclear blast equivalency). The experimental data for explosive sources ranging from 0.03 lb to 15 lb were obtained by SwRI through experiments conducted under

this program. Data for charge weights up to 19.2 kilotons were obtained from published literature by the Atomic Energy Commission (AEC) and the Bureau of Mines. The data applied for the derivation of the final functional format of the above equation covered nine orders of magnitude in scaled charge weight $W/\rho_s c^2 R^3$. A more detailed description of the SwRI experiments as well as the derivation of the final functional equation for soil particle velocity and displacement is given in Sections II, IV and V of this report. This final functional equation empirically derived became the forcing function for the pipe structural response solution described below.

Modeling Stresses in Pipes

Similitude theory was also applied to determine the state of stresses in the buried pipes resulting from underground detonations. Tests were conducted on small models rather than large pipes because more information could be accumulated for a given outlay of money. Small-scale testing means test sites do not have to be as remote, smaller quantities of explosive can be used, excavation problems are greatly reduced, and test crews can be smaller because equipment is not large and bulky. On the other hand, these financial advantages would only be meaningful provided the experiments on smaller test systems were indeed representative of structural response conditions in large prototype gas mains. To demonstrate that small structural response models could represent large-scale prototype conditions and provide data, this model analysis was conducted.

Assume that an infinitely long circular pipe of radius r , wall thickness h , mass density ρ_p , and modulus of elasticity E is exposed to ground shock motions of particle velocity U and displacement X from either line or point explosive sources. The explosive source is located at a standoff distance R in a soil with a mass density ρ_s and a seismic P-wave propagation velocity c . The response of interest to us, is the maximum elastic change in circumferential and longitudinal stresses σ_{\max} caused by the passage of this shock over the buried pipe. No need exists for simulating the state of stress in the pipe from internal pipe gas pressures, as these elastic stresses can be superimposed on those caused by a shock loading. This definition of the problem accounts for the load imparted to the pipe, inertial plus compressibility effects in both pipe as well as soil, the geometry of all major aspects of this problem, and for any effective mass of earth that might vibrate with a deforming pipe segment. All the parameters later included in this theoretical pipe response calculations are included in this

definition of the problem. In functional format, the stress in the pipe would be given by:

$$\sigma_{\max} = f_{\sigma} (R, h, r, E, \rho_p, \rho_s, c, U, X) \quad (18)$$

Writing a statement of dimensional homogeneity gives the equation:

$$\sigma_{\max}^{\alpha_1} R^{\alpha_2} h^{\alpha_3} r^{\alpha_4} E^{\alpha_5} \rho_p^{\alpha_6} \rho_s^{\alpha_7} c^{\alpha_8} U^{\alpha_9} X^{\alpha_{10}} \doteq F^{\circ} L^{\circ} T^{\circ} \quad (19)$$

Substituting the fundamental units of measure gives:

$$\left(\frac{F}{L^2}\right)^{\alpha_1} (L)^{\alpha_2} (L)^{\alpha_3} (L)^{\alpha_4} \left(\frac{F}{L^2}\right)^{\alpha_5} \left(\frac{FT^2}{L^4}\right)^{\alpha_6} \left(\frac{FT^2}{L^4}\right)^{\alpha_7} \left(\frac{L}{T}\right)^{\alpha_8} \left(\frac{L}{T}\right)^{\alpha_9} (L)^{\alpha_{10}} \doteq F^{\circ} L^{\circ} T^{\circ} \quad (20)$$

Collecting exponents for each of the fundamental units of measure gives the result:

$$\begin{aligned} (L) \quad & -2\alpha_1 + \alpha_2 + \alpha_3 + \alpha_4 - 2\alpha_5 - 4\alpha_6 - 4\alpha_7 + \alpha_8 + \alpha_9 + \alpha_{10} \quad (F) \quad \alpha_1 + \alpha_5 + \alpha_6 + \alpha_7 \\ & \times (T) \quad 2\alpha_6 + 2\alpha_7 - \alpha_8 - \alpha_9 \quad \doteq \quad F^{\circ} L^{\circ} T^{\circ} \end{aligned} \quad (21)$$

Equating exponents on the left and right sides of Equation (21) yields:

$$L: -2\alpha_1 + \alpha_2 + \alpha_3 + \alpha_4 - 2\alpha_5 - 4\alpha_6 - 4\alpha_7 + \alpha_8 + \alpha_9 + \alpha_{10} = 0 \quad (22-a)$$

$$F: \alpha_1 + \alpha_5 + \alpha_6 + \alpha_7 \quad (22-b)$$

$$T: 2\alpha_6 + 2\alpha_7 - \alpha_8 - \alpha_9 \quad (22-c)$$

Solving for α_2 , α_7 , and α_8 in terms of the other seven coefficients in Equations (22) gives:

$$\alpha_2 = -\alpha_3 - \alpha_4 + \alpha_{10} \quad (23-a)$$

$$\alpha_7 = -\alpha_1 - \alpha_5 - \alpha_6 \quad (23-b)$$

$$\alpha_8 = -2\alpha_1 - 2\alpha_5 - \alpha_9 \quad (23-c)$$

Substituting Equations (23) into Equation (19) then gives:

$$\sigma_{\max}^{\alpha_1} R^{-\alpha_3-\alpha_4+\alpha_{10}} h^{\alpha_3} r^{\alpha_4} E^{\alpha_5} \rho_p^{\alpha_6} \rho_s^{-\alpha_1-\alpha_5-\alpha_6} c^{-2\alpha_1-2\alpha_5-\alpha_9} U^{\alpha_9} X^{\alpha_{10}} \stackrel{d}{=} F^{\circ}L^{\circ}T^{\circ} \quad (24)$$

Finally, gathering terms with like coefficients gives the seven pi terms:

$$\left(\frac{\sigma_{\max}}{\rho_s c^2}\right)^{\alpha_1} \left(\frac{h}{R}\right)^{\alpha_3} \left(\frac{r}{R}\right)^{\alpha_4} \left(\frac{E}{\rho_s c^2}\right)^{\alpha_5} \left(\frac{\rho_p}{\rho_s}\right)^{\alpha_6} \left(\frac{U}{c}\right)^{\alpha_9} \left(\frac{X}{R}\right)^{\alpha_{10}} \stackrel{d}{=} F^{\circ}L^{\circ}T^{\circ} \quad (25)$$

In nondimensional format, Equation (25) permits us to rewrite Equation (18) as:

$$\left(\frac{\sigma_{\max}}{\rho_s c^2}\right) = f_{\sigma_{\max}/\rho_s c^2} \left(\frac{h}{R}, \frac{r}{R}, \frac{E}{\rho_s c^2}, \frac{\rho_p}{\rho_s}, \frac{U}{c}, \frac{X}{R}\right) \quad (26)$$

As was the case in the previous section the functional format of Equation (26) could not be explicitly written until experimental test data were generated to measure the maximum circumferential stress and the maximum longitudinal stress in the pipe from the ground motions associated with a buried detonation.

Design of Experiments

For experimental design, Equation (12) for U/c and Equation (13) for X/R were substituted into Equation (26). This substitution means that:

$$\left(\frac{\sigma_{\max}}{\rho_s c^2}\right) = f_{\sigma_{\max}} / \rho_s c^2 \left[\frac{h}{R}, \frac{r}{R}, \frac{E}{\rho_s c^2}, \frac{\rho_p}{\rho_s}, \frac{P_o}{\rho_s c^2}, \frac{W}{\rho_s c^2 R^3} \right] \quad (27)$$

Tests were conducted on several different sizes of pipe including diameters of 3-, 6-, and 16-in. and eventually 24- and 30-in. Equation (27) can be the same in a 3-in. diameter pipe as in a 30-in. diameter pipe, if the other parameters are scaled correctly. A replica model in particular makes model and prototype systems equivalent by scaling all geometries h , R , and r by a geometric scale factor λ and all soil and pipe properties remain the same or have a scale factor of 1.0. The pi term $W/\rho_s c^2 R^3$ indicates that the energy release or size of the charge W must be scaled as λ^3 if this pi term is to be invariant, and the term $\sigma_{\max}/\rho_s c^2$ indicates that the measured stresses will be the same in both model and prototype systems. Table I summarizes the scale factors which can satisfy Equation (27) for stress or, in a similar manner, Equations (12) and (13) for ground motion.

TABLE I.
SCALE FACTORS FOR A REPLICA MODELING LAW

<u>Symbols</u>	<u>Parameters</u>	<u>Scale Factor</u>
h, R, r, X	geometric lengths or distances	λ
ρ_s, ρ_p	mass density	1.0
E	modulus of elasticity	1.0
P_o	atmospheric pressure	1.0
c, U	velocity	1.0
W	explosive energy release	λ^3

Equation (27) is shown to be invariant by substituting the scale factors from Table I for a model system. A bar over each symbol indicates that Equation (27) is being written for a second system. This substitution gives:

$$\left[\frac{1 \bar{\sigma}_{\max}}{1 \bar{\rho}_s (1\bar{c})^2} \right] = f_{\sigma_{\max}} \frac{1 \bar{\sigma}_{\max}}{\rho_s c^2} \left[\frac{\lambda \bar{h}}{\lambda \bar{R}}, \frac{\lambda \bar{r}}{\lambda \bar{R}}, \frac{1 \bar{E}}{1 \bar{\rho}_s (1\bar{c})^2}, \frac{1 \bar{\rho}_p}{1 \bar{\rho}_s}, \frac{1 \bar{P}_o}{1 \bar{\rho}_s (1\bar{c})^2}, \frac{\lambda^3 \bar{W}}{1 \bar{\rho}_s (1\bar{c})^2 (\lambda \bar{R})^3} \right] \quad (28)$$

Or after factoring out the λ 's which are constants and canceling:

$$\left(\frac{\bar{\sigma}_{\max}}{\bar{\rho}_s \bar{c}^2} \right) = f_{\sigma_{\max}} \left[\frac{\bar{h}}{\bar{R}}, \frac{\bar{r}}{\bar{R}}, \frac{\bar{E}}{\bar{\rho}_s \bar{c}^2}, \frac{\bar{\rho}_p}{\bar{\rho}_s}, \frac{\bar{p}_o}{\bar{\rho}_s \bar{c}^2}, \frac{\bar{W}}{\bar{\rho}_s \bar{c}^2 \bar{R}^3} \right] \quad (29)$$

Note that Equation (29) is exactly the same as Equation (27). This observation means that the systems are equivalent; they have the same equation, provided properties are scaled as in Table I.

To illustrate how a 3-in. diameter steel pipe with a wall thickness of 0.060 in. buried 6 in. and loaded with single explosive charge weighing 0.05 lb located 1.5 ft away could be used to correspond to some prototype 30-in. diameter pipe, the 30-in. prototype would also be made of steel, have a 0.60-in. wall thickness, be buried 60 in. (5 ft) deep, would be loaded with a 50-lb charge, and would be located 15 ft away. The maximum longitudinal and circumferential stresses in both of these pipes would be the same.

In addition to the strain measurements made on pipes to record stress, ground motion transducers were installed to measure maximum particle velocity and soil displacement. These motions also scale according to the parameters in Table I. At the pipe or any other scaled location, the velocity would be the same and the displacements scale as the geometric scale factor λ . Both ground motions and pipe strains were recorded in experiments so information would be obtained for studying and generating both the ground motion and the pipe stress solutions.

Actually, any one model test simulates a variety of different prototype conditions. A test on a 3-in. diameter pipe models a certain set of conditions on a 24-in., 60-in., or any other size pipe at the same time that it is simulating a 30-in. pipe. This type of generalized thinking emphasizes that a whole spectrum of conditions is being studied provided the results of a test are interpreted properly. The final variations for charge weights, standoff distances, etc., were selected to give several orders of magnitude variation in any given prototype condition. Different sizes of pipe were tested to emphasize that indeed the solution is a general one. In particular, as results are studied in Section V for ground motion and Section VI for

pipe stress, the reader will become aware that the scaled standoff distances are closer to the charge than in other earlier ground motion and pipe stress studies. The reader will realize that a buried pipe is a strong structure capable of withstanding much more severe buried blasting conditions than have generally been accepted in the past. Furthermore, the results given in Section IV and analyzed in Sections V and VI clearly demonstrate that the approach selected and the solutions obtained are valid for a wide range of explosive weights, materials, energies and geometries, as well as standoff distances and soil properties.

III. THE EXPERIMENTS

General

Tests were conducted to record ground motion and pipe strain data from different scale model as well as full scale experiments, to generate and validate the ground shock and pipe stress solutions which are presented in Sections II, V and VI of this report. The experiments were divided into three groups and were performed at three different test sites. The first group of tests were fired at SwRI and consisted of 31 experiments using three different sized scaled model pipes (nominal 3-, 6-, and 16-in. diameter). Pipe strains, as well as soil particle velocities and displacements, were obtained for different charge weights, distances from charge to pipe, and for single and multiple explosive charges.

The second group of tests (eight experiments) were conducted at a site near Kansas City, Missouri using an out-of-service length of 24-in. diameter pipe made available by Panhandle Eastern Pipe Line Company (PEPLC). On three of these tests using the full-scale pipe, there was zero gage pressure within the pipe, the same as in the first group of scaled experiments performed at SwRI. On the other five full-scale experiments, the pipe length was pressurized with air to 300 psig. Similar ground motion and pipe strain data were gathered as in the smaller scale experiments with the exception that only single (point) explosive charges were used on all full scale tests.

The third and final group of four tests were fired at a site near Madisonville, Kentucky in a joint effort between Texas Gas Transmission Company (TGTC), the A.G.A. and SwRI. These experiments used one of TGTC's operational 30-in. pipelines with a reduced gas pressure of 400 psig. Ground motion and pipe strain measurements on a full-scale pipeline were again made on these tests to record the loading from a point explosive source.

Tests on Model Pipes

Three different pipes were used in performing the 31 model tests in this program to obtain data using three different geometric scales. These pipes were nominally 3-in. diameter by 24-ft long, 6-in. diameter by 40-ft long, and 16-in. diameter by 7-ft long. The 3-in. and 6-in. diameter pipes were to have been 1/8- and 1/4-scale models of a 24-in. diameter, 3/8-in. thick

gas pipe buried 4 ft (2 pipe diameters) to its center line. However, after grinding the exterior surface of the two scaled pipes, the inaccuracies in this process caused the 3-in. diameter pipe to be slightly thicker. The 16-in. pipe had a thickness-to-diameter ratio that was twice that ratio in the other pipes in order to obtain data on pipe which was not geometrically similar or a model of the other pipes. Both single and multiple explosive charges, (to simulate a line source) buried to the same depth as the center line of the pipe, were used to generate the ground shock loading on these pipes and the ground motion transducers used. The center of the pipe was arbitrarily located at a depth of two diameters below the surface of the ground. The length of the two smaller pipes was selected to simulate a semi-infinite length as would be encountered in the field. Because of the line explosive sources used to load these pipes, a sufficient length of pipe was required so that the ends of the pipe would remain sufficiently anchored during the loading as would be the case in a real line.

The experiments were conducted in a relatively homogeneous, semi-infinite field of sandy loam on the grounds of SwRI during the summer and early fall of 1976. At five locations, cores were taken down to 6 ft in depth to ensure that the soil was in fact homogeneous over the test area and to relatively large depths. Table II summarizes the pipe and explosive charge parameters used in each of the model experiments. In this table, each test is identified, and the pipe description is given by the outside diameter, thickness, and burial depth measured from the ground surface to the center of the pipe. This same depth applied to the charge, whether point or line source. The standoff distance was measured horizontally from the center of the charge to the center of the pipe. To be able to make the small spherical charges in single or multiple configuration, a plastic explosive, C-4, was used.

In most of the 31 model tests, four velocity transducers and one accelerometer (mounted at the same location as the closer-in velocity sensor) were used to obtain horizontal ground motion data. In some cases a second accelerometer was also used. Figure 1-a shows a sketch of the plan view of a typical field setup using a concentrated point explosive source. Figure 1-b shows a similar sketch for a line explosive source. Note that three different transducer lines were used to minimize interference as the shock waves propagated through the ground. Although the spacing varied between canisters for different

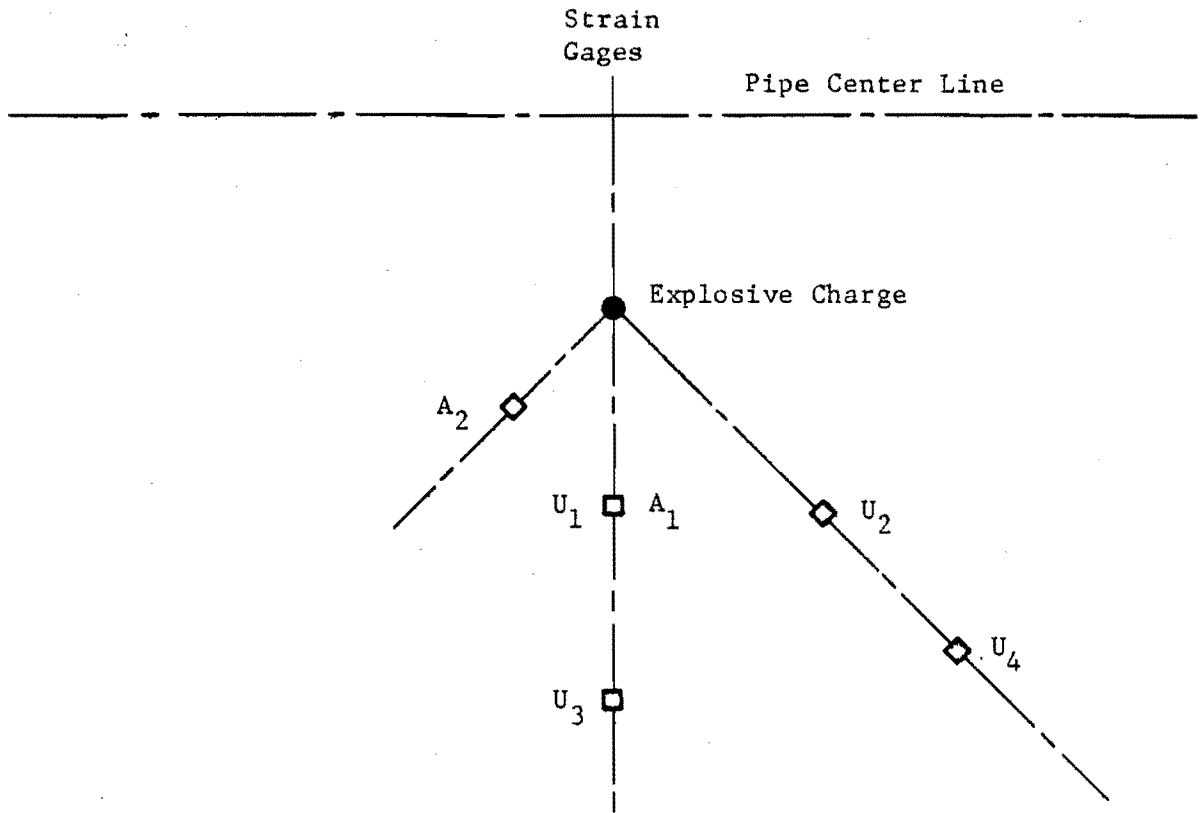
TABLE II. SUMMARY OF TEST CONDITIONS FOR
MODEL EXPERIMENTS

Test No.	Pipe Diameter (in.)	Pipe Thickness (in.)	Depth of Burial (in.)	Charge Weight (lb)	Type of Source	Line Length (ft)	Standoff Distance (ft)
1	2.95	0.059	6	0.05	point	--	1.5
2	2.95	0.059	6	0.05	point	--	1.5
3	2.95	0.059	6	0.05	point	--	1.5
4	2.95	0.059	6	1.00	point	--	11.0
5	5.95	0.093	12	0.40	point	--	3.0
6	5.95	0.093	12	0.40	point	--	3.0
7	5.95	0.093	12	1.00	point	--	11.0
8	5.95	0.093	12	0.03	point	--	2.0
9	5.95	0.093	12	0.03	point	--	1.0
10	2.95	0.059	6	0.03	point	--	0.75
11	5.95	0.093	12	0.35	line	10.5	5.0
12	5.95	0.093	12	2.80	line	14.4	8.0
13	5.95	0.093	12	2.80	line	9.0	5.0
14	5.95	0.093	12	2.80	line	9.0	5.0
15	2.95	0.059	6	0.35	line	4.5	2.5
16	2.95	0.059	6	0.35	line	4.5	2.5
17	2.95	0.059	6	0.21	line	9.0	5.0
18	2.95	0.059	6	2.80	line	5.4	3.0
19	5.95	0.093	12	0.21	line	2.7	1.5
20	16.0	0.515	32	0.03	point	--	3.0
21	16.0	0.515	32	0.03	point	--	1.5
22	16.0	0.515	32	0.03	point	--	1.0
23	16.0	0.515	32	0.03	point	--	1.0
24	16.0	0.515	32	0.06	point	--	1.5
25	16.0	0.515	32	0.06	point	--	1.25
26	2.95	0.059	6	0.35	line	19.8	8.0
27	2.95	0.059	6	0.35	line	19.8	8.0
28	2.95	0.059	6	0.05	point	--	1.5
29	2.95	0.059	6	0.05	point	--	1.5
30	5.95	0.093	12	0.40	point	--	3.0
31	5.95	0.093	12	0.40	point	--	3.0

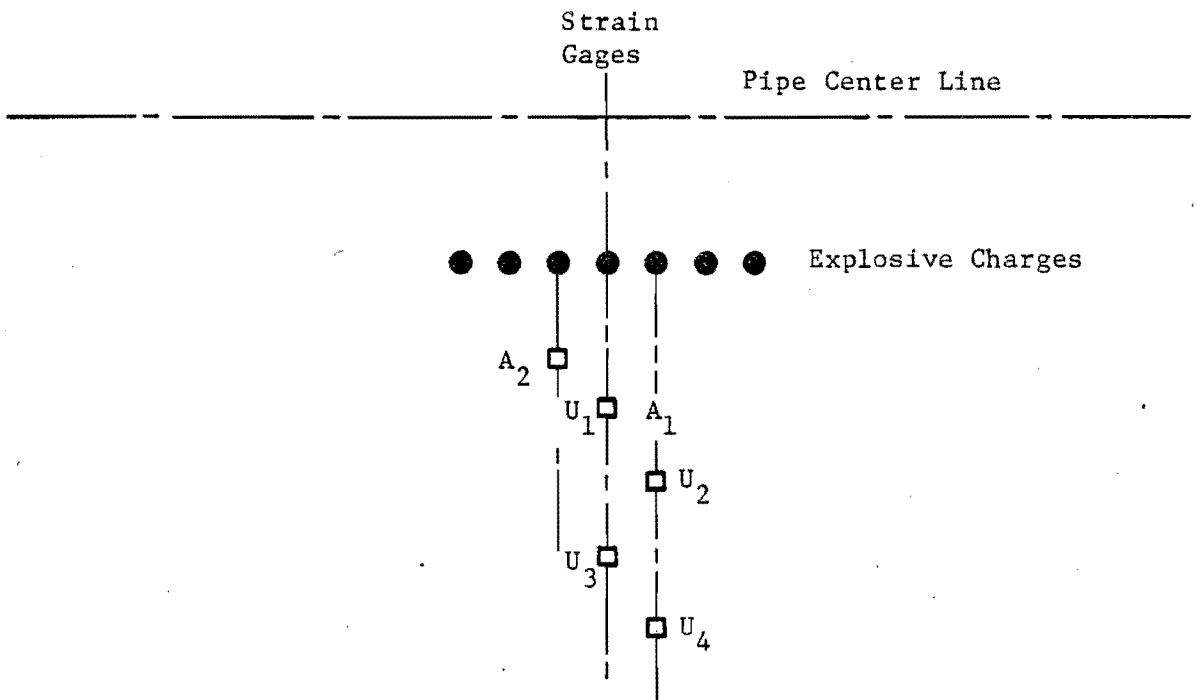
6-IN

6-IN

6-IN



(A) FOR POINT SOURCE



(B) FOR LINE SOURCE

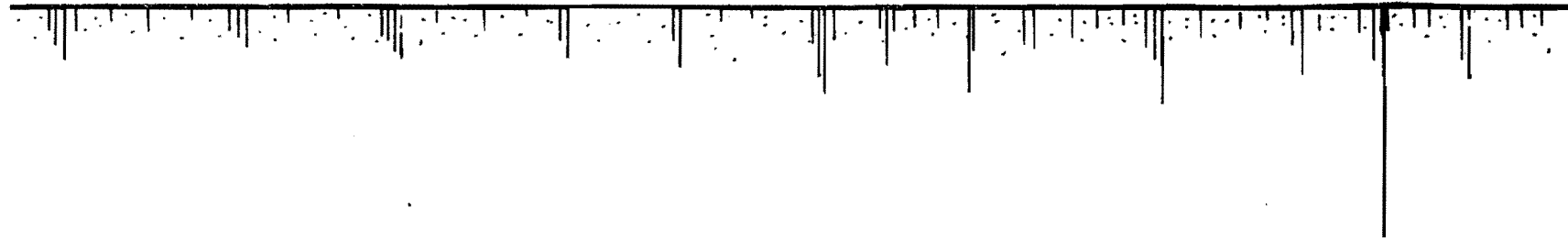
FIGURE 1. PLAN VIEW LAYOUT OF MODEL EXPERIMENTS

test conditions, the first canister was usually buried at the same distance from the charge (or charge line) as the pipe being tested.

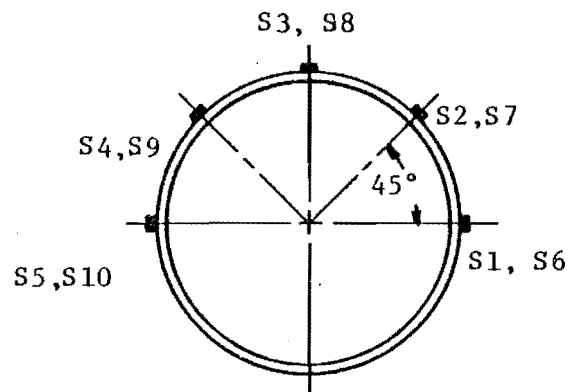
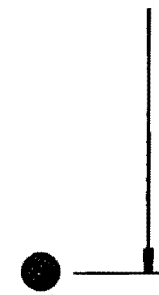
To measure the response of these pipes, strain gages were epoxy-bonded at five different stations along the upper half-circumference of each pipe. Two-element strain gage rosettes were used so that both circumferential and longitudinal measurements were possible at each station. Each pipe was gaged with a set of five rosettes at the longitudinal center of the pipe. In addition, an extra set of gages was mounted 1 ft from the center so that in case a gage malfunctioned, or was damaged from the blast load or the environment, another one could be substituted without having to unbury the pipe to remount a strain gage. Figure 2 shows the strain gage locations and their sensing axes (circumferential and longitudinal) on the pipe.

A typical model experiment was conducted after the pipe had been strain gaged and buried in the ground. For a given charge type and weight, and its standoff distance from the pipe, the motion transducer locations were selected. Estimates of the expected peak ground motions and pipe strains were then made using the ground motion data from the literature and some engineering judgment for the strains. From these estimates, the amplifier gains and record levels of the instrumentation used to record the data were computed and set. Once each motion measurement channel was completely wired end-to-end and checked for proper operation, the transducer was buried by hand to its proper depth. The holes were backfilled and the soil tamped to approximately the same compactness. Water content in the soil and density were checked prior to testing. An electrical calibration was then recorded to facilitate playback and data reduction and then a countdown sequence was recorded on the voice channel of the tape recorder. The explosive charge was then buried, the hole backfilled and soil tamped in a similar fashion as the motion transducer locations. The tape recorder was started and the charge was fired at the end of the countdown sequence. The data were played back into an oscillograph recorder for quick-look analysis of the records before setting the whole system for the following test. The area around the hole made by the charge in the soil was dug, back filled and tamped before making a new hole for the test that followed.

Ground Surface



Twice Pipe O. D.



Gages S1-S5 Sense Circumferentially

Gages S6-S10 Sense Longitudinally

FIGURE 2. STRAIN GAGE LOCATIONS ON MODEL PIPES

Tests on Full-Scale Pipe - Kansas City

Twelve experiments were conducted using full-scale pipelines in the operating field environment. Eight of these experiments were done on a 98-ft length of 24-in. diameter pipe located near Kansas City, Mo., during the summer of 1977. This section of pipe, with a thickness of 0.312 in. and buried 5 ft to its center, had recently been taken out of service by PEPLC due to re-routing of a transmission line near new highway construction. Prior to complete removal of this section of line, it was made available for conducting the first group of full-scale verification experiments. The location of the test pipe was surveyed and soil samples taken by PEPLC. The section tested was adjacent and parallel to a small creek. Figure 3 shows pictures of the test area. The soil samples taken from two test holes indicated a 2-ft upper layer of black loam, followed by 6 ft of sandy clay, and clay mixed with small sandstone for the bottom 3 ft of the test holes. Subsequent digging around the pipe, and augering of holes for soil instrumentation and charges confirmed the uniformity of the layering in the test area soil.

Two types of experiments were fired using single charges buried to the same depth as the pipe: one set without any line pressure and the other with an air pressure of 300 psig. The section of test pipe was capped at both ends and connections welded for air pressurization. High pressure air cylinders were used to raise the pressure in the pipe. Two sizes of charges were used in these tests; 5 and 15 lb of ammonium nitrate fuel oil (AN-FO) explosive. Table III shows the tests performed at the Kansas City test site. The original test plan called for conducting only five tests. However, conditions in the field indicated that some revisions to the test plan would provide additional data which would increase the confidence level of the field measurements. Therefore two tests, Nos. 2 and 4, were repeated as Tests 3 and 6, respectively. In addition, Test 7 was conducted on a second set of strain gages which were installed 6 ft from a coupling in the line. This test was included to determine if a difference in strain levels could be detected on measurements made near a coupled joint in the pipe. As had originally been planned, the final test was designed to yield the pipe from the higher loading of a closer-in charge.



(a) View looking west from across bend of creek.



(b) View looking south from record van location.

FIGURE 3. KANSAS CITY TEST SITE

TABLE III. TESTS CONDUCTED AT KANSAS CITY
TEST SITE

Test No.	Charge Weight (lb)	Standoff Distance (ft)	Pipe Pressure (psig)
1	15	9.4	0
2	5	6.0	0
3	5	6.0	0
4	15	13.0	300
5	5	9.0	300
6	15	13.0	300
7	15	13.0	300
8	15	6.0	300

In all eight tests, three velocity transducers were used to obtain the horizontal ground motion. These electromechanical devices were the same ones used in the model experiments at SwRI and were housed in the same protective canister used previously. The big difference, of course, in their field installation was that they were buried 60 in. instead of the 6 to 32-in. depths used in the model tests in accordance with the model law. This entailed a much more time consuming effort to bury the transducer and to move them as required from test to test. Furthermore, the procedure required the use of an auger and a back-hoe. This mechanical support was provided by PEPLC as it was needed. Figure 4 is a sketch showing the locations of the soil particle velocity transducers and charges fired in the Kansas City tests.

The pipe response to the shock wave loading from the single explosive charges was measured using strain gages at three locations on the pipe: on the front (side nearer charge), on the top, and on the back. Circumferential and longitudinal strain gage orientations were used at each location. Two sets of strain gages were installed at each of two stations on the pipe approximately 25 ft apart. These additional installations provided substitute gages in case of malfunctioning at any location during the testing program in an effort to insure 100% operational strain measurement channels for each test without having to excavate down to the pipe and remounting additional gages, a more time-consuming operation. The drawing in Figure 5

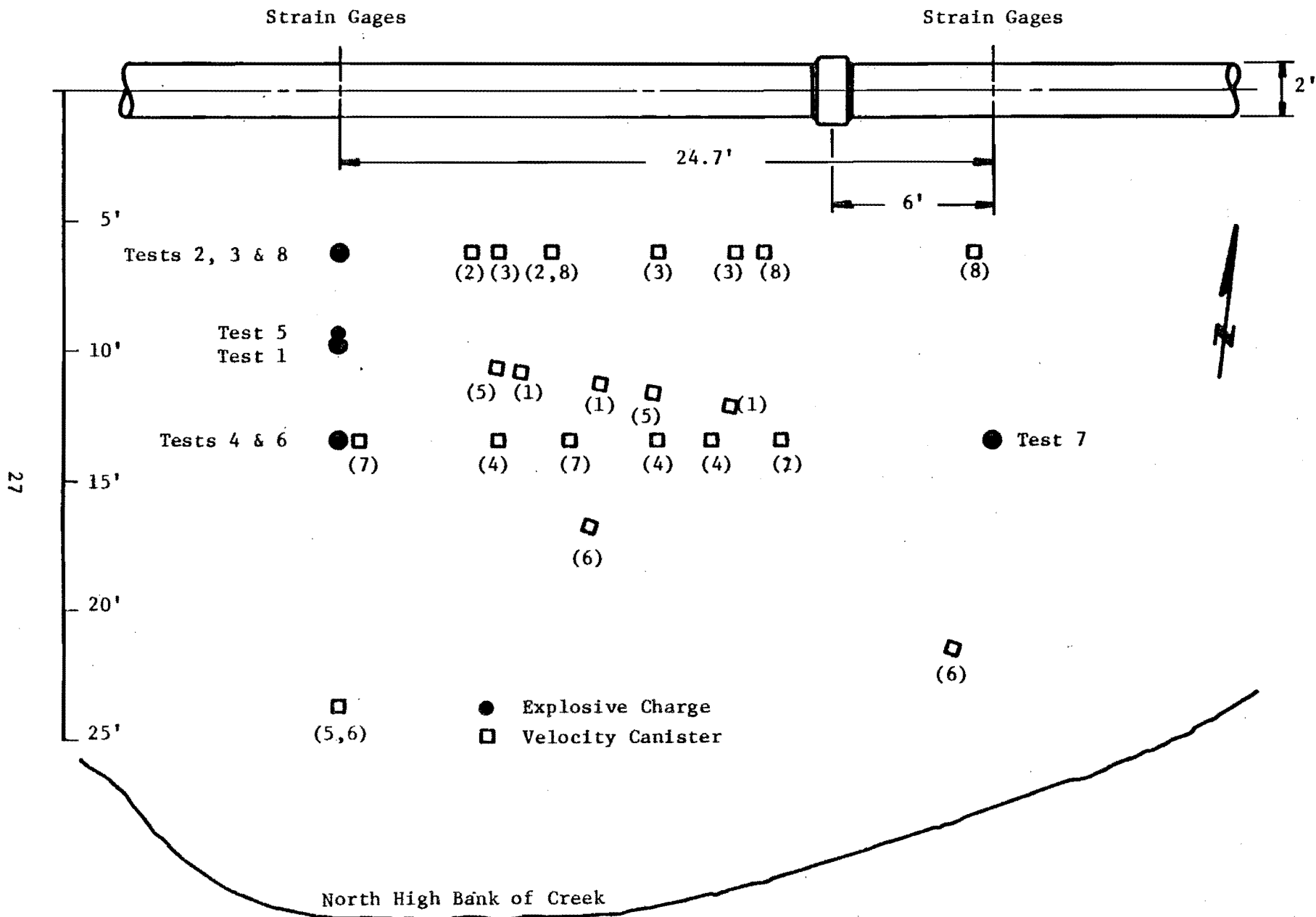
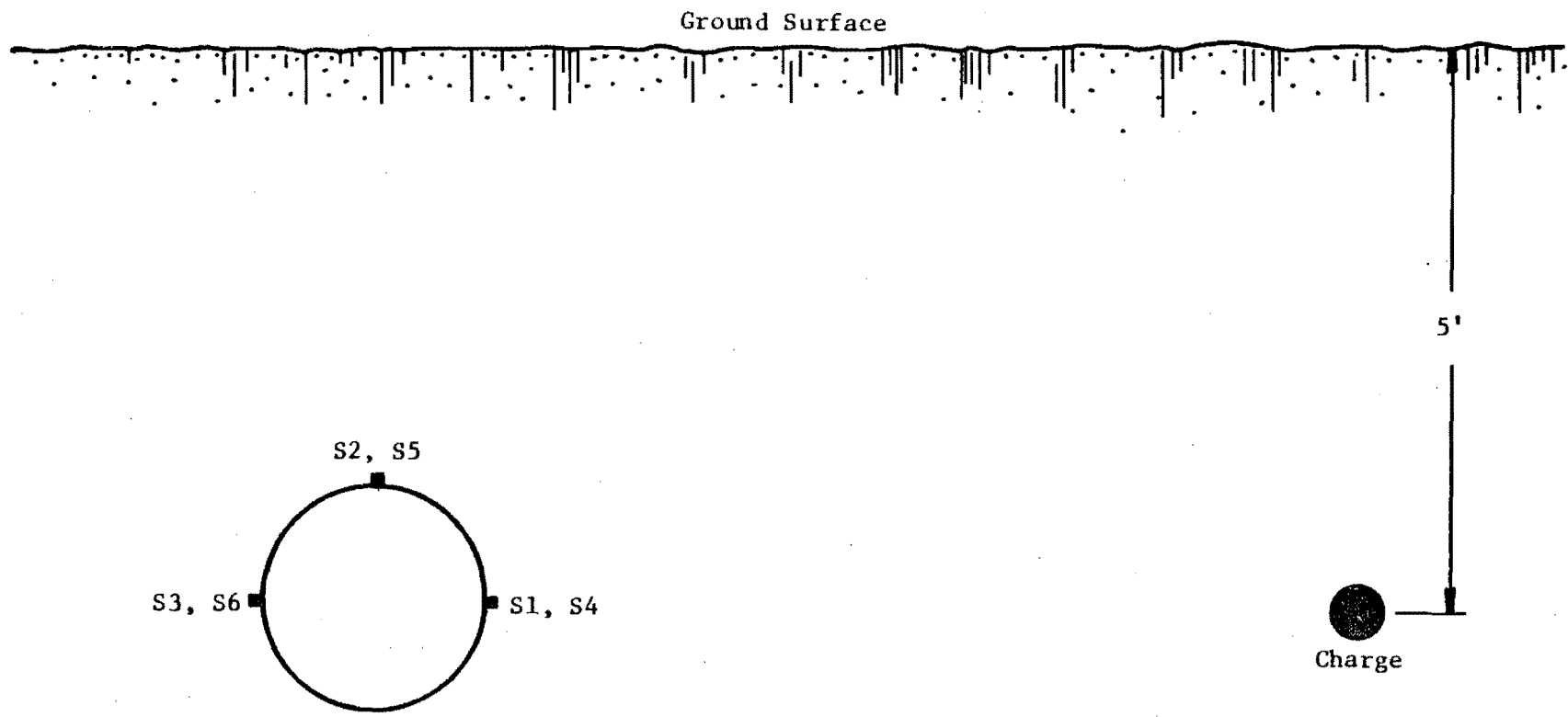


FIGURE 4. PLAN VIEW OF TEST LAYOUT AT KANSAS CITY SITE



Gages S1-3 Sense Circumferentially
Gages S4-6 Sense Longitudinally

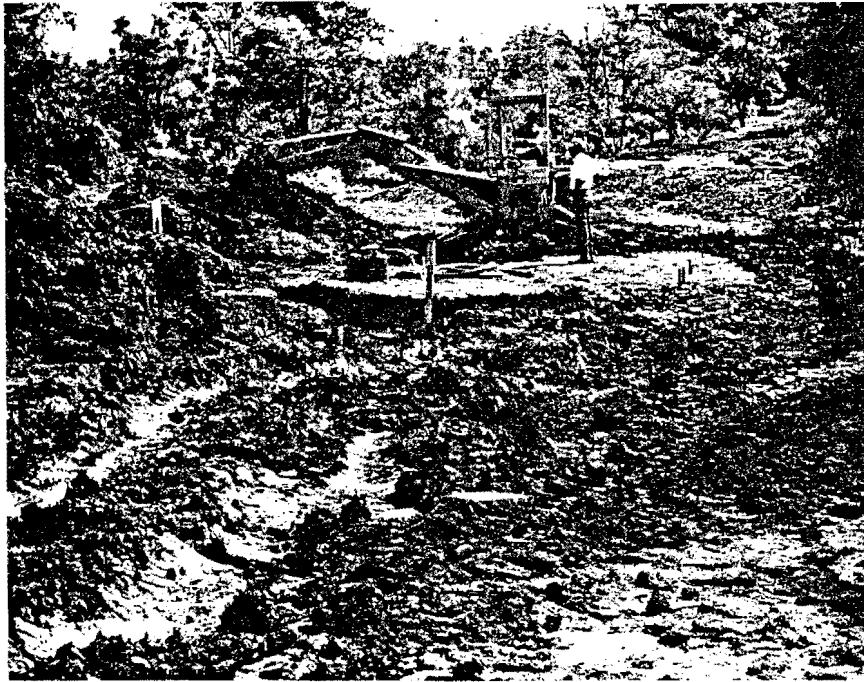
FIGURE 5. STRAIN GAGE LOCATIONS ON 24-INCH PIPE

details the locations of one set of strain gages. All other sets of gages were installed at similar points around the pipe.

To perform the eight full-scale experiments at the Kansas City site, the test section of pipe was first uncovered at two separate places 25 ft apart as shown in Figure 6-a. The holes were excavated large enough to allow working room for sanding and cleaning the pipe surface and installing the strain gages. Each hole turned out to be deep and large enough to keep the seeping water level from rising too rapidly. As a result, during the strain gaging of the pipe the water in the hole only had to be pumped out every three or four hours. Figure 6-b shows the exposed test pipe with a standing water level as was typically found prior to pumping.

Once the pipe was exposed, the outer coating was removed and the pipe surface was then finished with emery cloth of decreasing coarseness until the surface was free of rust, scale, oxides and surface irregularities. The area was then thoroughly degreased and washed with solvent just prior to spot welding of the strain gages. The gages were then mounted, lead wires connected and the entire installation heavily coated for environmental and physical protection. The lead wires for each set of gages were routed up through rubber hosing to an adjacent junction-box (J-box) for connecting to the long cable lines going back to the electronic instrumentation housed in a mobile office trailer. Figure 7-a shows the connecting of the strain gage lead wires to the long lines. Each strain channel was then tested end-to-end for proper connections and operation. After every channel checked out, the exposed pipe was very carefully backfilled. Figure 7-b shows the beginning of this operation. All the backfill near the pipe was placed and tamped by hand to preclude any damage to the strain gages and their cable. Once the pipe was well covered, the rest of the hole was filled and tamped in layers by machine until the ground was level. Part of this procedure is shown in Figure 8.

Once the pipe strain gage operation was completed, the holes for the velocity transducers and the explosive charge to be used on the first test were made using an auger as shown in Figure 9. The completed array of holes is also pictured in this figure. The velocity transducers were then connected to the J-box, tested end-to-end, and placed down-hole in their respective locations. The holes were backfilled and tamped by hand in layers in an effort to restore the disturbed soil to its original condition. Knowing the



(a) Excavation around test pipe.

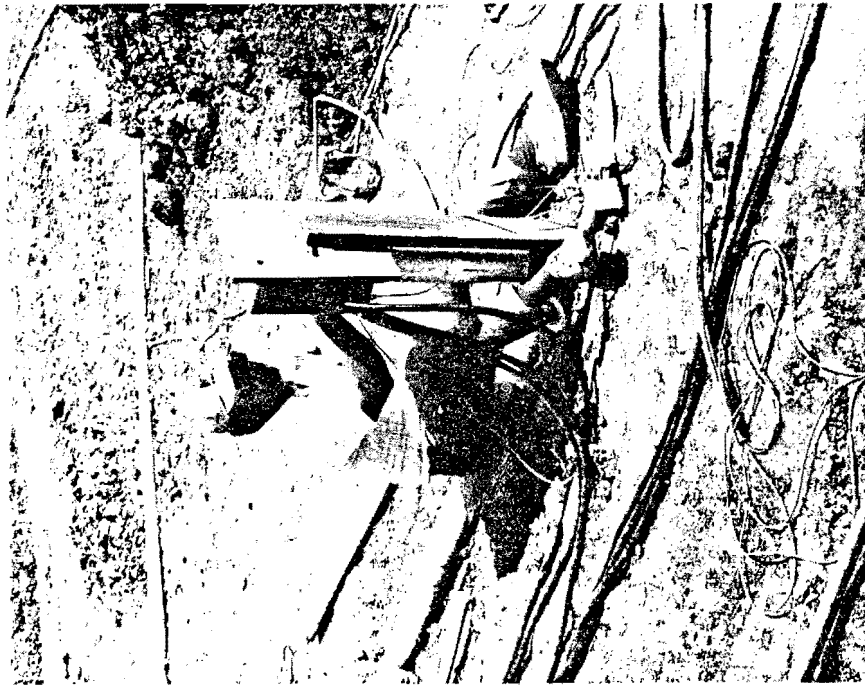


(b) Exposed 24-in. pipeline.

FIGURE 6. UNCOVERING OF PIPELINE FOR STRAIN GAGING



(b)



(a)

FIGURE 7. CONNECTION AND CHECK-OUT OF STRAIN CHANNELS

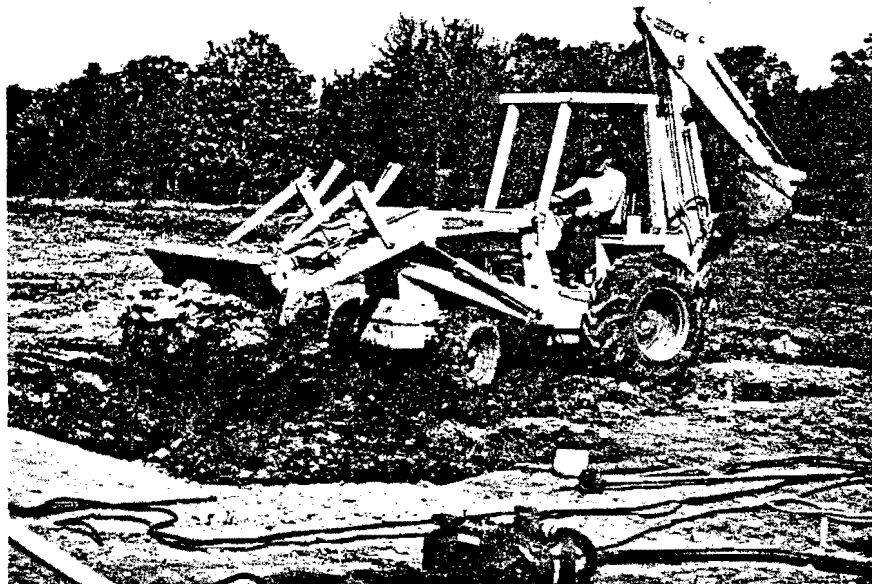


FIGURE 8. BACKFILLING OF HOLE AROUND PIPE

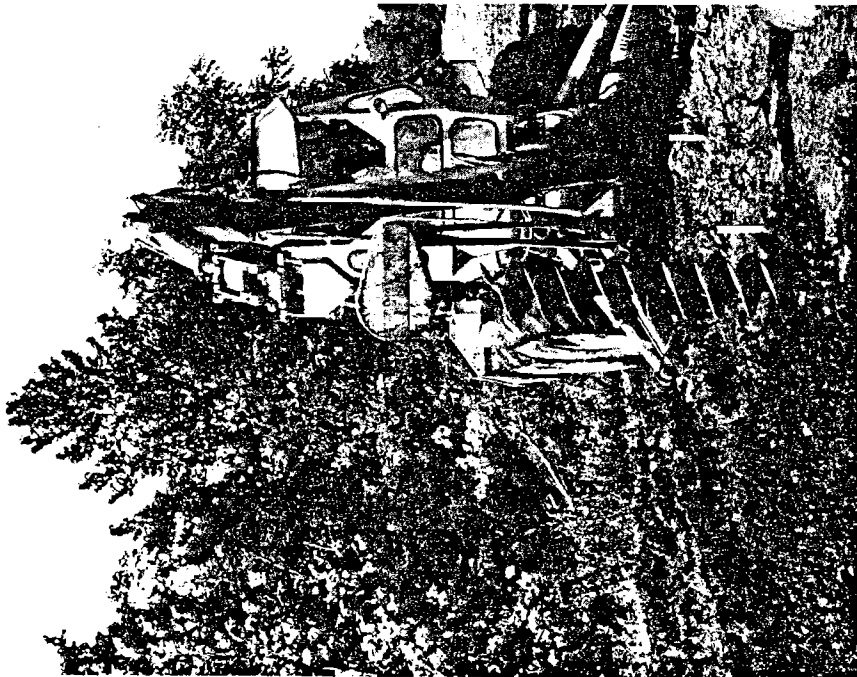


FIGURE 9. DRILLING OF GROUND MOTION TRANSDUCER AND CHARGE HOLES

charge weight and its standoff from the pipe, the ground motions and pipe strains expected were estimated using the results of the model experiments. The gains and recording levels were then set for each measurement channel. A countdown sequence and electrical calibration voltages were then recorded for each measurement channel on the magnetic tape recorder. Once the complete measurement system was ready for testing, the AN-FO explosive charge was prepared by placing the cap, booster and the required amount of explosive in a thin plastic container to protect it from any water or moisture. The plastic bag was then sealed and placed down-hole as shown in Figure 10. At the same time the site area was cleared of all personnel except for the ordnance technician, and danger signs and audible flashers were placed at the entrance road to the site to warn any unexpected visitors. Once the charge hole was backfilled with tamped soil, the firing circuit was checked one last time for continuity, and the power supply turned on for charging the firing capacitor. The tape recorder was then started and the countdown sequence played back. At time-zero, the charge was detonated. Figure 11 is a photograph of one of the tests being fired using a 15-lb explosive charge. The following two photographs, Figure 12, show the craters made by a 15-lb charge and a 5-lb charge. After each test, the area around the crater was excavated out about 2-ft past visible cracks in the soil and down 2 ft below the location of the charge. The hole was then refilled in layers and tamped in an effort to restore the ground back to its undisturbed condition. Velocity transducers which required moving to a new location were dug up and the hole refilled and tamped. The velocity transducer and explosive hole layout for the next experiment was then laid out and the holes redrilled. The same procedures were followed for each subsequent test until all eight experiments were completed.

Tests on Full-Scale Pipe-Kentucky

The last four experiments using a full-scale pipeline were conducted during late fall of 1977, on an operational 30-in. diameter line near Madisonville, Kentucky. The site was located on the TGTC right-of-way on the edge of a cornfield and adjacent to a soybean field. Figure 13 shows two photographs of the test site. The last mile to the site was accessible most of the time only by foot or tracked vehicles because of the snow and rain making the soft



FIGURE 10. PREPARATION AND PLACEMENT OF EXPLOSIVE CHARGE

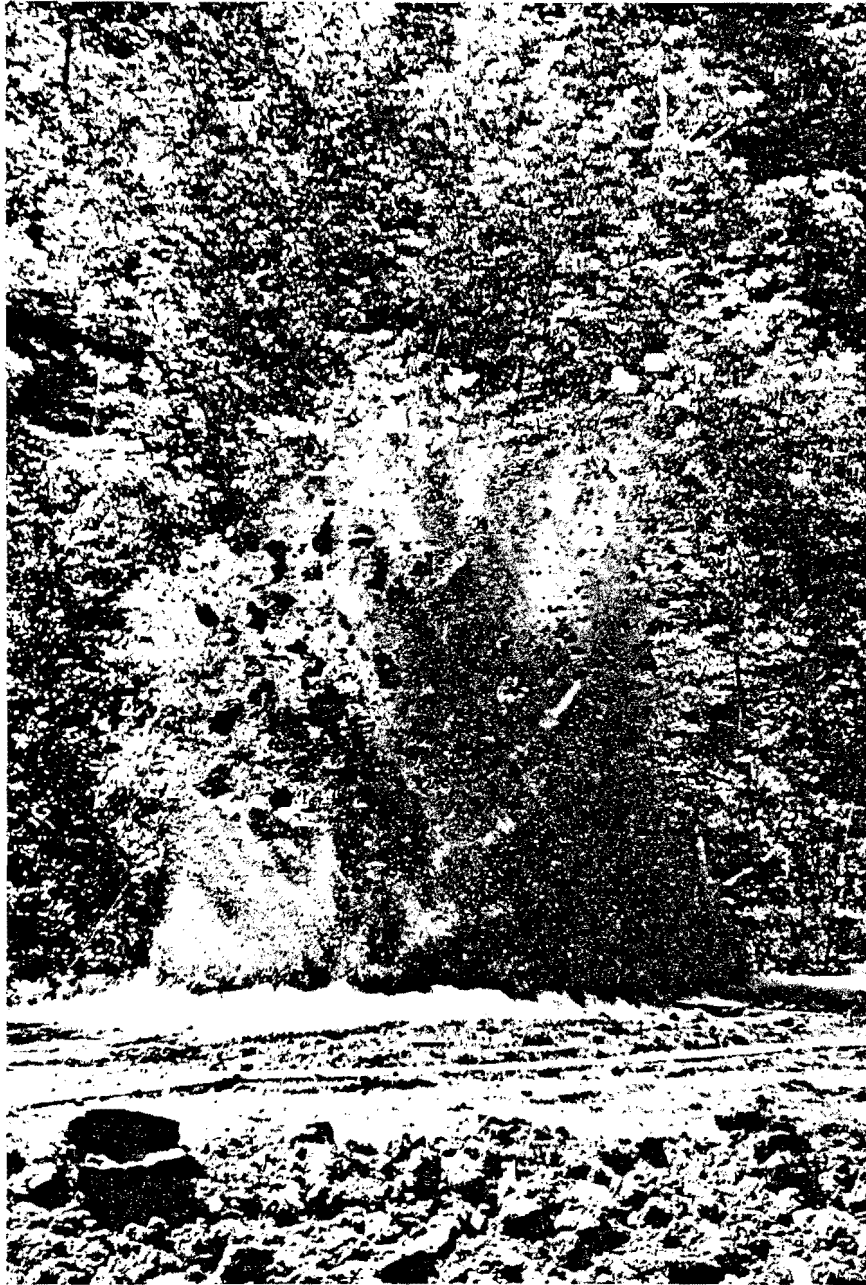


FIGURE 11. DETONATION OF BURIED 15-LB.
EXPLOSIVE CHARGE



(A) 15 LB. CHARGE



(B) 5 LB. CHARGE

FIGURE 12. CRATERS MADE BY BURIED DETONATIONS



(a) View looking northwest from corn field.



(b) View looking east toward entrance to site.

FIGURE 13. KENTUCKY TEST SITE

ground extremely muddy. The pipe at the test site is buried approximately 5.5 ft to its centerline and its thickness is 0.344 in. The excavation around the test pipe indicated a very uniform layer of soft, reddish clay down to at least 7.5 ft in depth. Although four tests were fired, five were actually setup. Test No. 5 resulted in a misfire in the booster used which precluded detonation of the AN-FO explosive. A subsequent rain made conditions in the field impossible for setting up the test again the following day. An ensuing snowstorm and extremely cold weather forecast for the week, plus the necessity of placing the 30-in. line back in service prompted TGTC to cancel a try for a fifth test and declare the program complete. The test plan for the Kentucky site as originally outlined called for five point source experiments with the charge (5 lb) buried to the same depth as the pipe on three of them, and with the charge buried much deeper on the other two. However, the plan was slightly modified in the field. The charge weights used were decreased on some tests so that a test at the closer standoff distance could be conducted without loading the pipe past a maximum combined blast and pressure stress set by TGTC. Also because of the extremely muddy conditions and very soft soil in the test area, the holes for the explosive charges had to be dug using a post hole digger. Consequently, a maximum charge depth of only 7.5 ft could be obtained. Therefore, only one deeper charge test was attempted. Unfortunately, it was to have been Test No. 5, which had the misfire. Table IV lists the tests performed at the Kentucky test site.

TABLE IV. KENTUCKY TESTS

Test No.	Charge Weight (lb)	Standoff Distance (ft)	Line Pressure (psig)
1	5	15	400
2	4	15	400
3	3	9	400
4	3	15	400

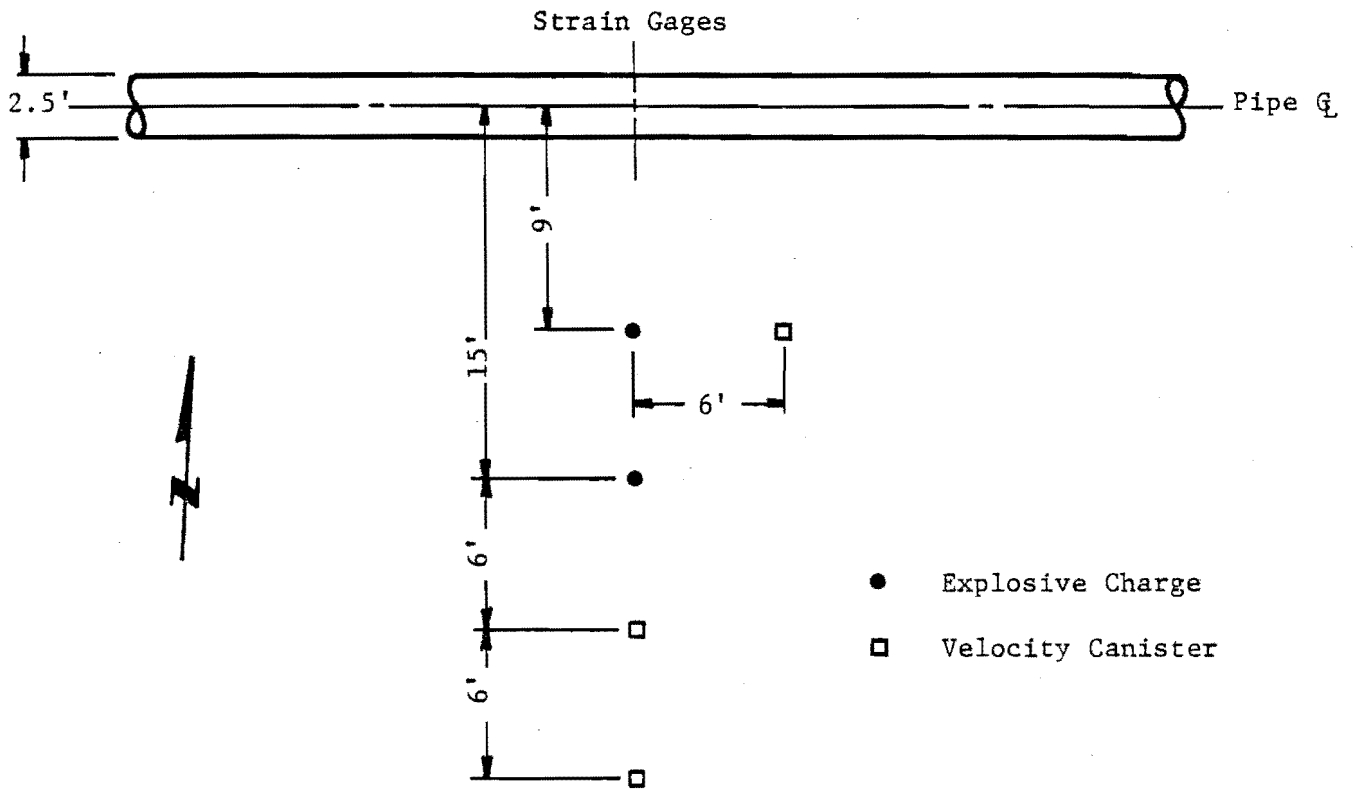
At least two ground motion transducers and six strain gages were recorded on each test in a similar way as was done in the Kansas City experiments. Field support for uncovering the pipe, burying the transducers, and preparing

the ground after each test was provided by TGTC. The location of the velocity transducers and the explosive charges used in these tests are shown in Figure 14. Circumferential and longitudinal strain gages were installed at the locations shown in Figure 15. One set of gages, plus a back-up set, were installed as in the Kansas City tests: on the front, top and back of the pipe. A second set of gages were mounted and rotated 45° from the first to be used on the deeper charge tests.

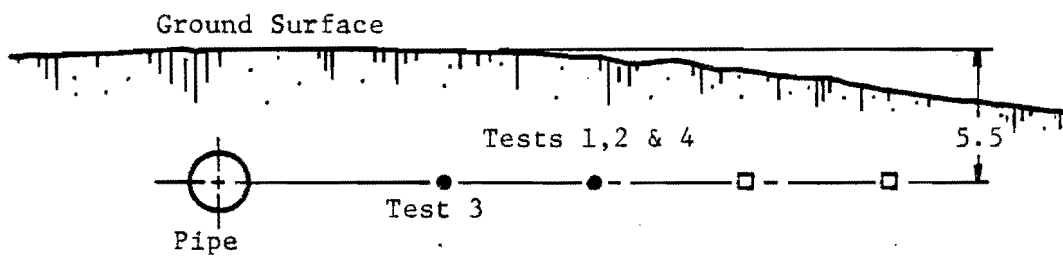
To instrument this 30-in. pipe, a similar procedure was followed as in the Kansas City tests. The pipe was first uncovered and an area of pipe cleaned down to the bare metal for mounting the strain gages. Water in the hole was again a problem and it was pumped out several times during the day while installation of gages took place. The gages were then coated and the clean section of pipe recovered prior to back-filling. After all the strain gage channels were connected and checked out with their electronics, the hole was filled and tamped. The holes were then dug for installing the velocity transducers and the first charge. These channels were also checked end-to-end before back-filling. The record instrumentation was then set-up, calibrated and a countdown sequence recorded. The AN-FO charge, properly water-proofed, was then buried and at time-zero it was detonated. Figure 16 shows the 5-lb charge being fired. As in all the other full-scale tests, after each test the area around the crater was excavated with a back-hoe, and the hole back-filled and tamped before the charge hole for the following test was dug. This same procedure was followed until the testing program was completed.

Ground Motion Transducers

The preliminary analysis for predicting pipe response to buried explosive detonations indicated that maximum horizontal soil particle velocity and displacement were required to determine the forcing function. To measure these two parameters, motion transducers were required to be placed at the locations of interests in both the model and full-scale experiments. Because this program was primarily designed for conducting tests using available technology for making the required measurements, no efforts were undertaken to develop new measurement methods or hardware. Existing transducers and techniques were modified for application in this program. Most commercially available motion

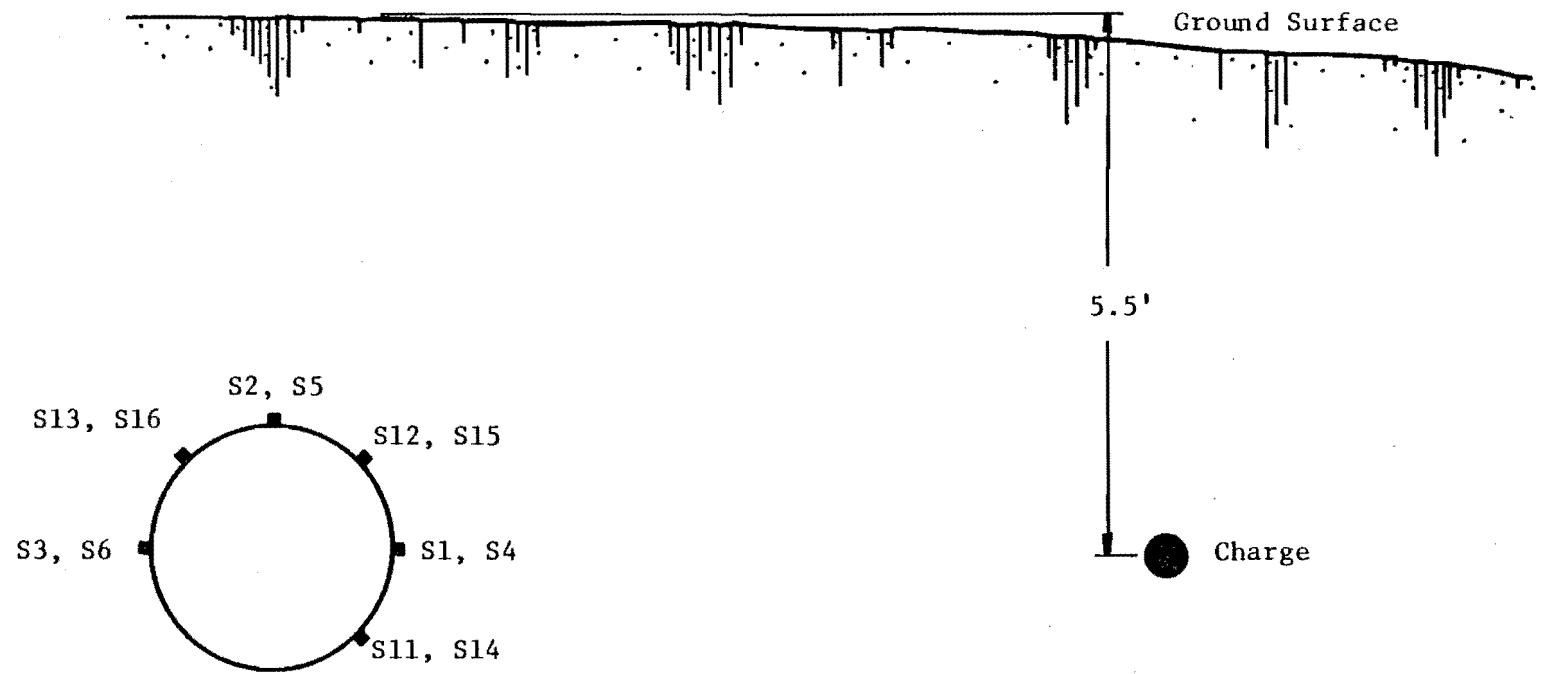


PLAN VIEW



ELEVATION VIEW

FIGURE 14. FIELD LAYOUT OF KENTUCKY TESTS



Gages S1-3 and S11-13 are circumferential.
 Gages S4-6 and S14-16 are longitudinal.

FIGURE 15. STRAIN GAGE LOCATIONS ON 30-INCH PIPE

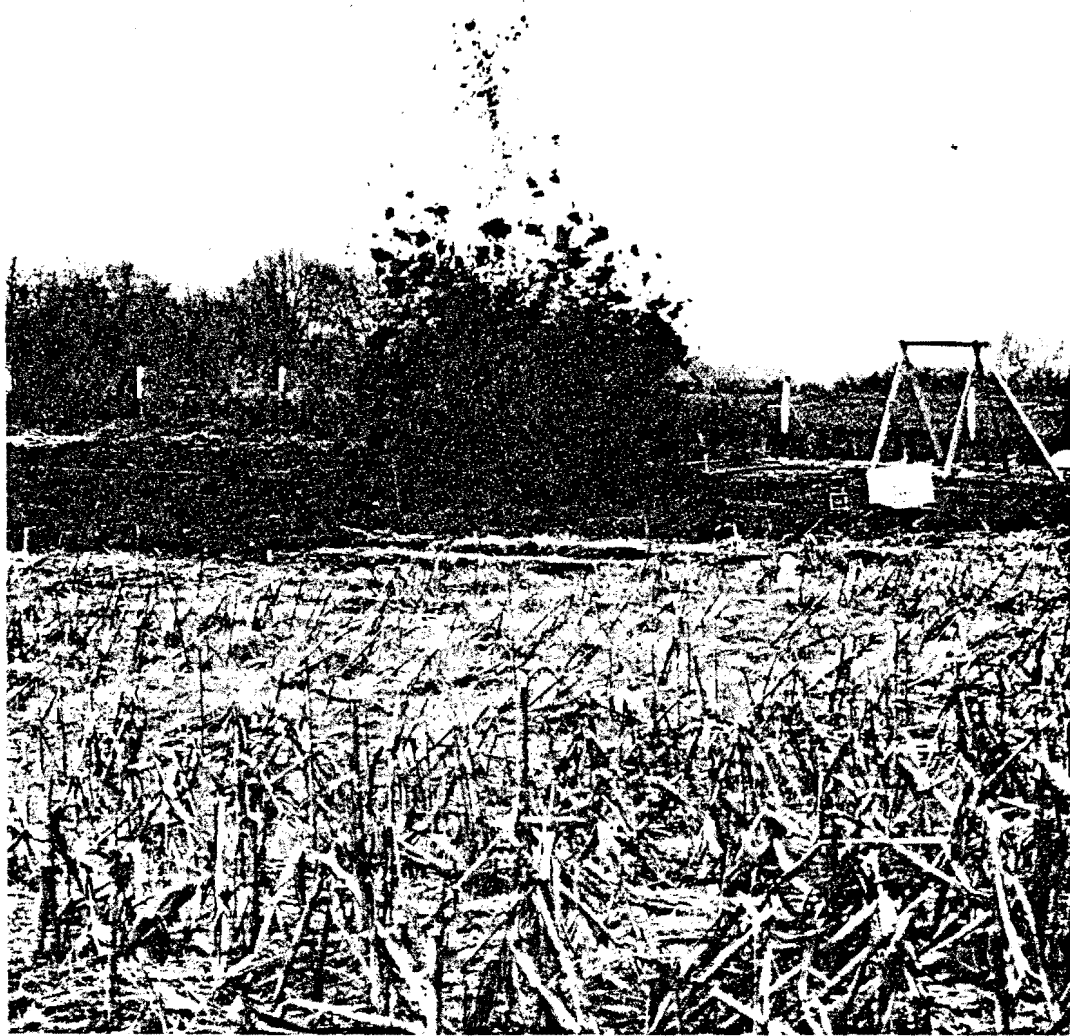


FIGURE 16. DETONATION OF BURIED 5-LB.
EXPLOSIVE CHARGE

transducers are not designed for an environment of high-pressure or external stress exerted on the transducer housing, as in the case of a high-explosive generated stress wave in soil. Therefore, the transducers were installed in a protective canister which also simplified placement procedure in the field and provided weatherproofing. From data in the literature, a range of magnitudes and rise times of particle velocity and displacement that could be expected in these tests were obtained. Bell and Howell Type 4-155 piezoelectric velocity transducers were chosen as the primary sensor for making the soil velocity measurements. Peak displacement measurements were obtained by integrating the velocity trace using a manual digitizer and plotter with a Hewlett-Packard Model 9830 microcomputer. The Type 4-155 transducer is a small, rugged vibration transducer with a high natural frequency which allows a linear response over a wide frequency range. The high sensitivity makes it desirable for low level velocity measurements which can be externally integrated to provide displacement signals. Each unit combines within its housing a piezoelectric accelerometer, an electrical impedance which allows the use of long interconnecting cables between the sensor and the recording instrumentation. The usable velocity range of this type of sensor is 0.2 to 100 ips, with a dynamic frequency response of 1 to 2000 Hz. The velocity transducer can withstand a shock acceleration of 100 g's peak without damage and is sealed water tight. Figure 17 shows how this velocity sensor was connected in all the tests performed to a power supply and a magnetic tape recorder used to record the data. By recording the data at 15 or 30 ips and playing it back at 1-7/8 ips, a time amplification factor of 16 allowed good time resolution for recording the playback data on oscillograph recorder.

Since some of the scale model experiments required detonations very close to the pipes and measurement of ground motions were wanted at comparable distances, a second type of sensor was also used in these experiments. These transducers were piezoelectric accelerometers, PCB Model 302M46, with a full-scale range of 2500 g's and a frequency response of 0.05 to 10,000 Hz. Since the velocity transducers previously described can withstand only 100 g's of shock acceleration, the accelerometers were used to determine how close to the explosives ground motion measurements could be made without damaging the velocity gage. The accelerometers were connected to the tape recorder as shown in Figure 18. The canisters used to house the velocity gages were

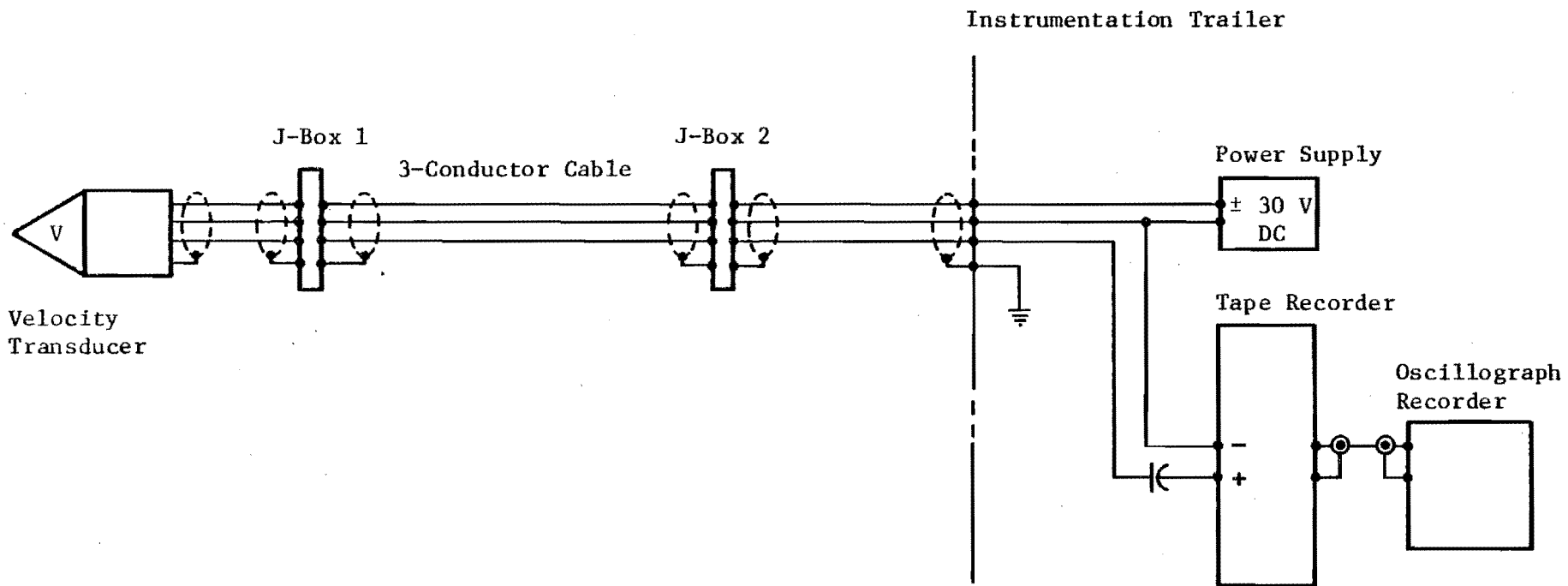
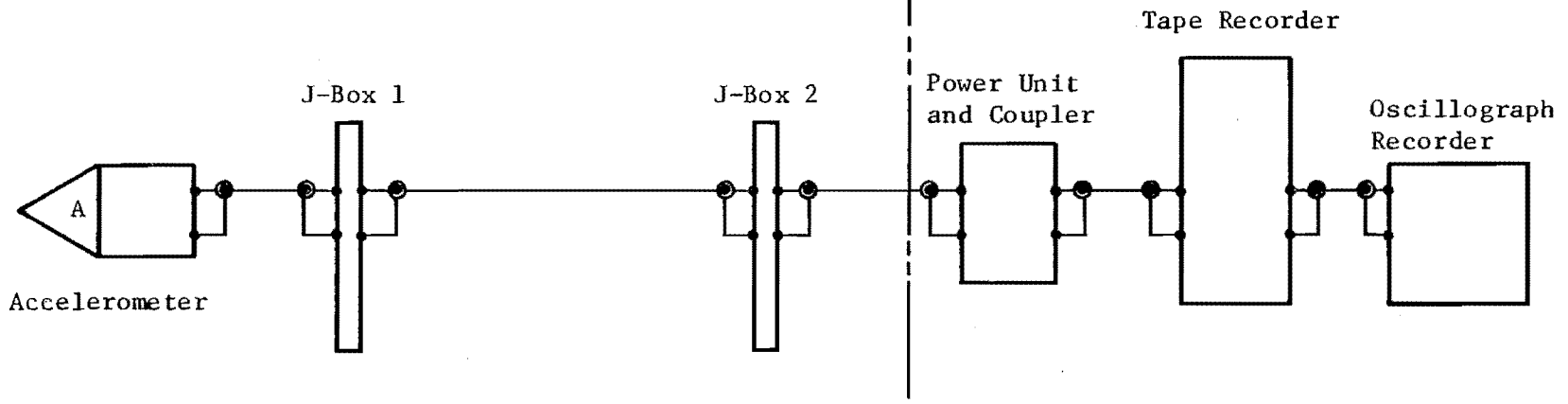


FIGURE 17. CIRCUIT DIAGRAM FOR VELOCITY TRANSDUCER

Instrumentation Trailer



46

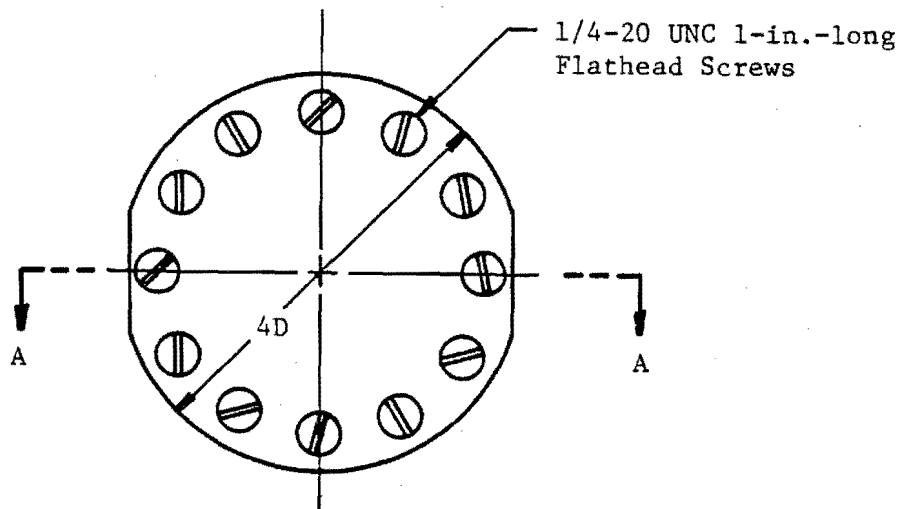
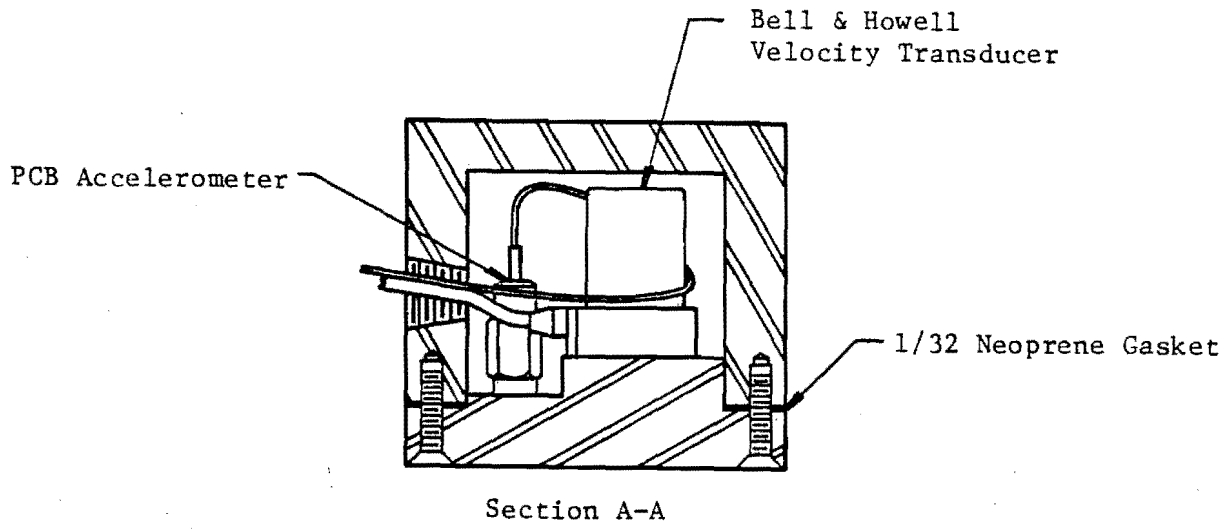
FIGURE 18. CIRCUIT DIAGRAM FOR ACCELEROMETER

designed so that an accelerometer could also be mounted at the same time. The canisters were similar to some previously designed, tested, and used by the U. S. Army Waterways Experiment Station to make ground motion measurements. A sketch showing how a velocity gage and an accelerometer were mounted in a canister is shown in Figure 19. A hose and fitting were used to route the interconnecting cable from the canister to a junction-box above ground. The hose provided physical and environmental protection to the cable. The accelerometer data were also played back onto oscillograph paper, then digitized and integrated to obtain velocity data to compare to that of the velocity transducer. In some tests, an accelerometer was used by itself close-in to the explosive charge. In these cases a similar, though smaller, canister was used since no velocity transducer was included. Because most of the acceleration measurements and their integrated velocities were made to determine whether the velocity gage could be used at a given close-in standoff distance, the data were not used in checking the analysis. Instead, the direct velocity measurements, which are more accurate, and their integrated displacements were used. In the case of the displacements, which turned out to be the controlling parameter in the analysis for most detonations near gas lines, a double integration would have been required on the acceleration data, thus increasing errors and inaccuracies. Consequently, no double integrations were attempted.

The placement of the motion transducers in the field experiments required the digging of holes of the proper depth and slightly larger than the canister used. Each velocity transducer and accelerometer was first inspected when received from the manufacturer by checking the factory calibration over a frequency range of 20 to 400 Hz using a shake table at SwRI. Then it was placed in a canister and the whole assembly mounted on the shake table again to insure that the sensitivity remained constant. Then it was taken to the field for placement. On the full-scale experiments the holes made were up to 6 ft in depth. Figure 20 shows a typical canister placement down-hole for the full-scale experiments.

Strain Gages

To measure the response of the pipes tested, strain gages were used at various locations on the surface of each pipe. Two primary techniques for



Scale: 1/2" = 1'

FIGURE 19. GROUND MOTION CANISTER ASSEMBLY

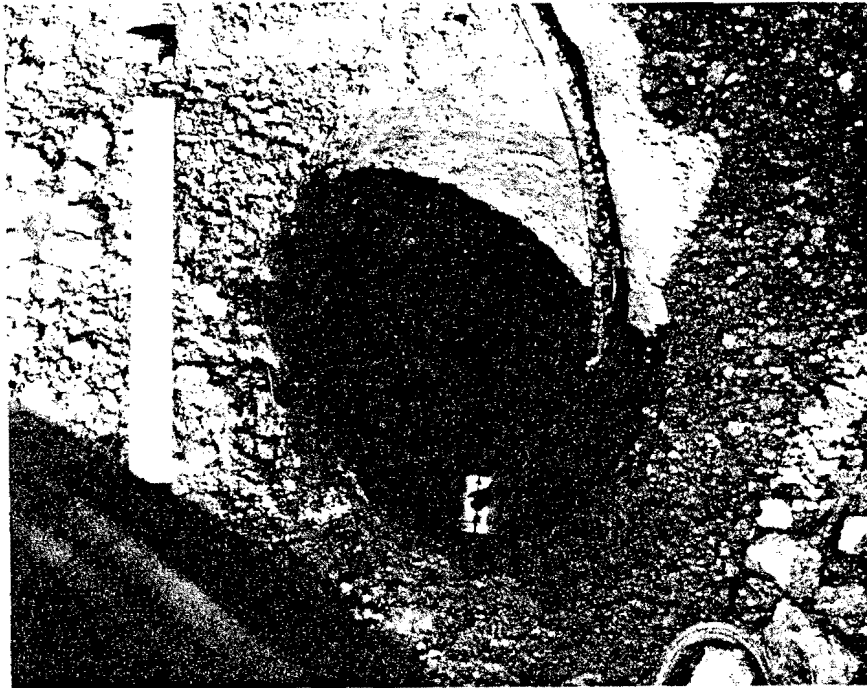
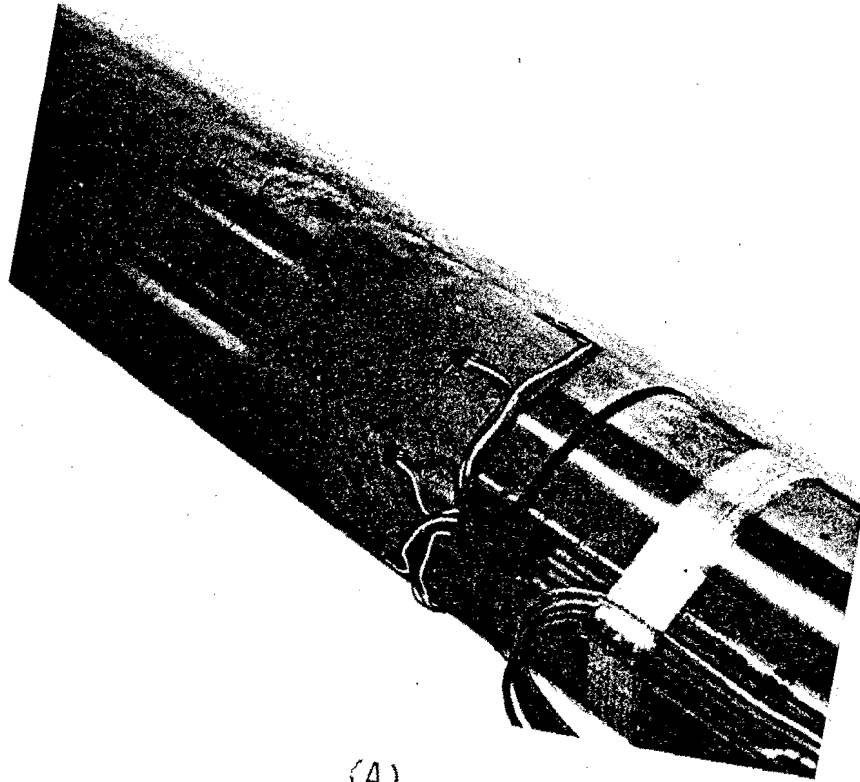
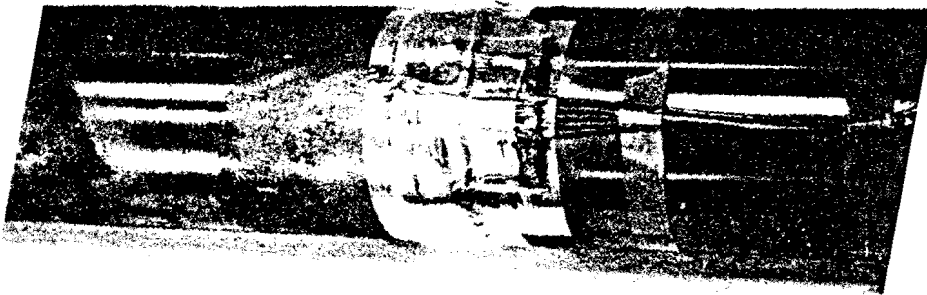


FIGURE 20. PLACEMENT OF VELOCITY CANISTER DOWN-HOLE

mounting strain gages on specimens are available to the user: adhesive bonding and spot welding. For most applications adhesive bonding of strain gages is the common technique used, particularly if the size of the structure is such that it can be taken inside during the installation. On the three pipes used in the model scale experiments the Micro-Measurements Type CEA-06-125ÜT-350, two element, 90° strain gage rosettes were bonded with M-BOND AE-10 epoxy adhesive. Because all the gages were mounted along a longitudinal or circumferential sensing direction, an orthogonal rosette was chosen to decrease installation time. Each rosette was connected to a four-conductor shielded cable, with one pair of conductors attached to each gage element. After the rosette installation was complete it was protected against the environment using M-COAT F coating. Figure 21 shows the 6-in. pipe with one set of strain gages installed and wired, and with the protective coating in place. After all the gages were tested for proper operation, the instrumented pipes were placed in the ground as shown in Figure 22 for the 3- and 6-in. pipes. In a similar fashion, the last of the model pipes was instrumented. Figure 23 shows the

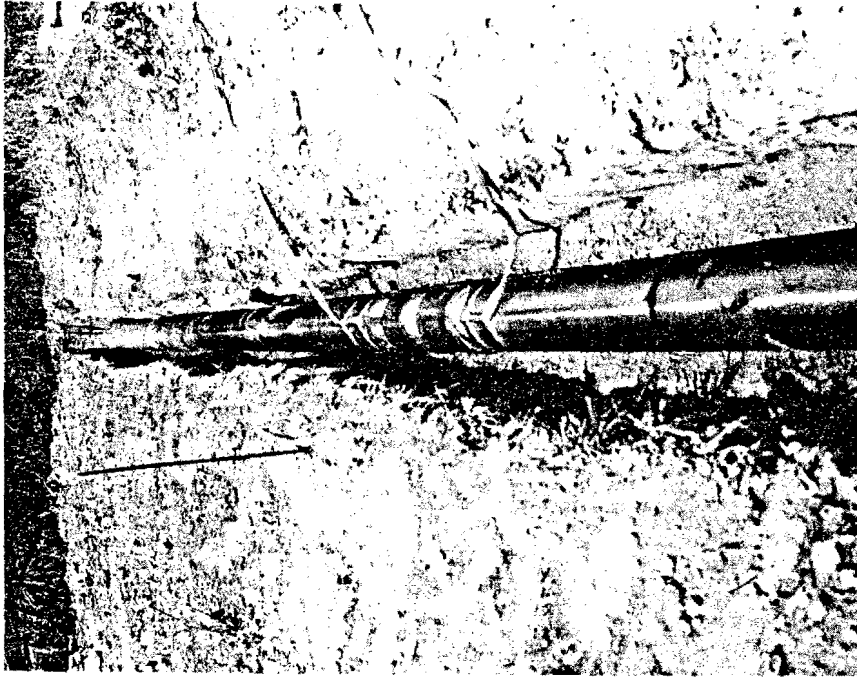


(A)

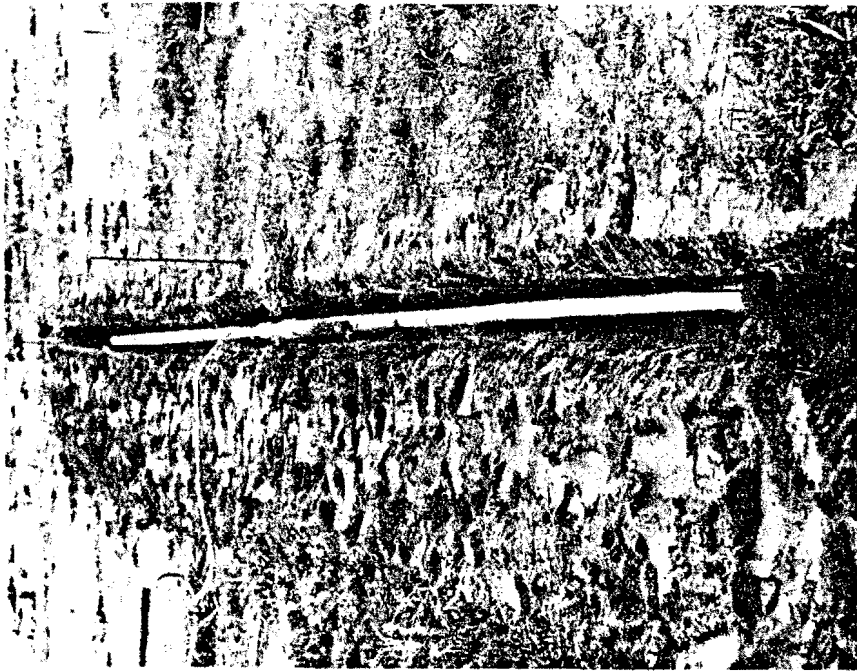


(B)

FIGURE 21. STRAIN GAGING OF 6-IN. DIAMETER PIPE



(B) 6-IN. DIAMETER PIPE



(A) 3-IN. DIAMETER PIPE

FIGURE 22. FIELD INSTALLATION OF 3- AND 6-IN. PIPES

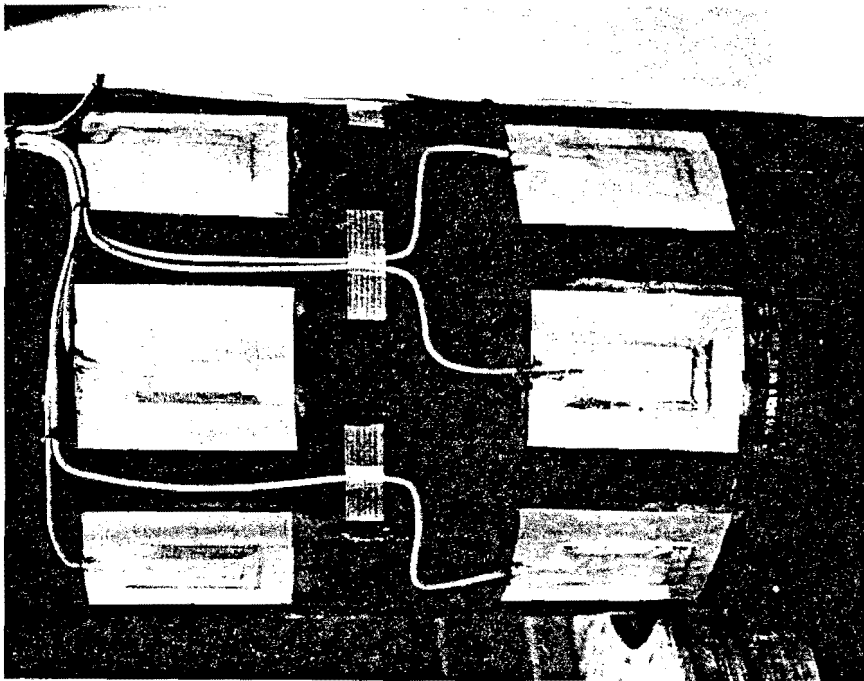
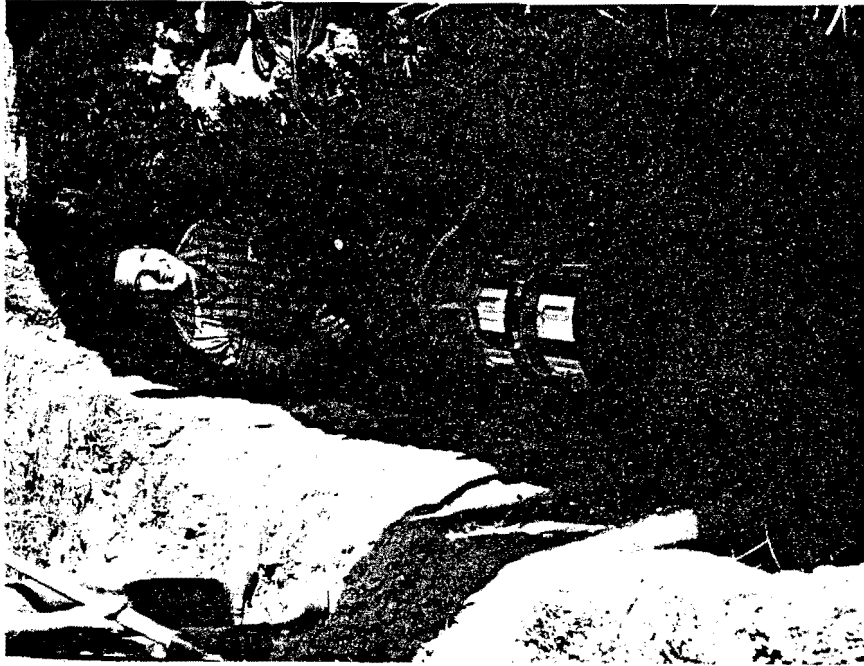


FIGURE 23. STRAIN GAUGE INSTALLATION AND BURIAL OF
16-IN. DIAMETER PIPE

strain gage installation completed and the pipe being buried carefully so as not to damage the strain gages and their connecting cables. The cables were routed above ground to a nearby weatherproof, portable J-box which was placed near the pipes as each was being tested.

For the two full scale pipes tested in Kansas City and Kentucky, weldable strain gages were chosen because conditions in the field would have made adhesive bonding of gages a very difficult and time consuming operation. The weldable gages used, made also by Micro-Measurements, are precision foil strain gages carefully bonded by the manufacturer to a metal carrier, Series 17 stainless steel, for spot welding to structures by the user. Spot welding is easily accomplished with a portable, hand-probe spot welder which is equipped to operate from either AC or internal DC power. Surface preparation is not as critical for the weldable gage which further simplifies their installation. The same type of environmental protection was applied to the weldable gages as was done to the adhesive bonded gages on the model pipes. The 24-in. pipe tested in Kansas City used Type CEA-06-W250C-120 weldable strain gage rosettes. These two-element, 90° rosettes simplified installation of orthogonal gages at each location. For the 30-inch pipe tested in Kentucky, however, weldable rosettes were not available from the manufacturer, and Type CEA-06-W250A-120 single gages were purchased and installed in orthogonal pairs at each sensing location to measure the longitudinal and circumferential strains.

Installation of the weldable strain gage rosettes used on the 24-in. pipe was begun by removing the coating on the pipe and grinding the metal to remove any rust, scale and surface irregularities. This procedure was completed by handgrinding with silicon-carbide paper until the surface was smooth, and thoroughly degreasing and washing with solvent to remove all residue. After the surface is properly prepared a sample metal carrier supplied with each package of gages is used to determine the proper weld-energy setting and electrode force required to obtain a good spot weld. A setting of approximately 10 watt-seconds with an electrode force of 4 lb will usually produce satisfactory welds. Once these settings are determined, the gage or rosette was aligned on the pipe and held in place with a piece of drafting tape. The metal carrier was then tacked in place by single spot welds on each side and the tape removed. The gage is then spot welded all around by two rows of alternating spot welds. Figure 24a shows a rosette being spot welded in place



(A)



(B)

FIGURE 24. INSTALLATION OF WELDABLE STRAIN GAGES ON 24-IN. PIPE

and the portable welder. Figure 24-b is a closer view of the welding operation. After the rosette was installed, cable leads were soldered to each strain gage element and the element electrically checked before the complete installation was covered with protective coating starting with a layer of butyl-rubber, one of the components of the M-COAT F. This operation is shown in Figure 24-c. For mechanical protection a patch of neoprene rubber is placed over the butyl-rubber before aluminum tape is used as the final cover. A liquid sealant is then used around all the edges of the aluminum tape. Figure 24-d shows two complete installations of a pair of rosettes. This figure also shows the lead wires completely sealed and placed into a rubber hose for additional protection. This hose routed the cables to a near-by J-box.

For the individual weldable gages used on the 30-in. pipe in Kentucky, the installation of the gages was about the same as the rosettes in Kansas City. However, because individual gages were used alignment at each location prior to spot welding took more time. And, the one installation required down 45° from horizontal was more difficult to do than the rest. Figure 25-a shows the spot welding of the gages at this location. The attachment of cables and environmental protection, as shown on Figure 25b was essentially the same.

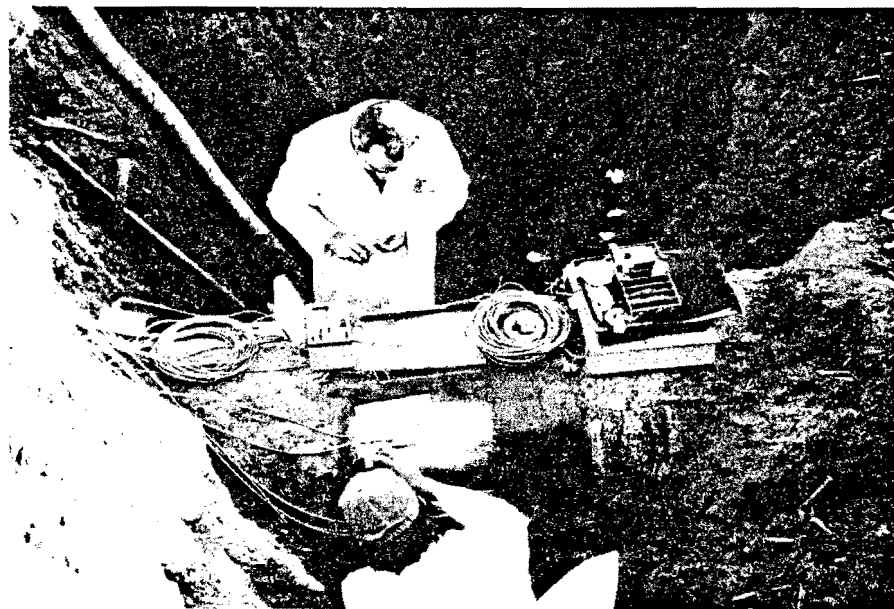
Regardless of whether bondable or weldable gages were being used, each element of the strain rosettes or individual gage was connected as a single active arm of a Wheatstone bridge, using a three-wire hook-up and remote electrical calibration connections. B&F Model 1-700 SG signal conditioner units provided bridge completion and balance, excitation voltage to the bridge, and a two-point electrical calibration. The output of each bridge was amplified with a B&F Model 702A-10D differential, wide-band amplifier and recorded on the same tape recorder used for the ground motion measurements. Figure 26 shows the circuit diagram for the strain gages.

Record and Playback System

For the majority of the experiments, six recording tracks of a tape recorder were allocated for strain measurements as shown on Figure 27. Two to four tracks were used for velocity channels and in some of the scale model experiments two accelerometer channels were recorded also. Two of the 14

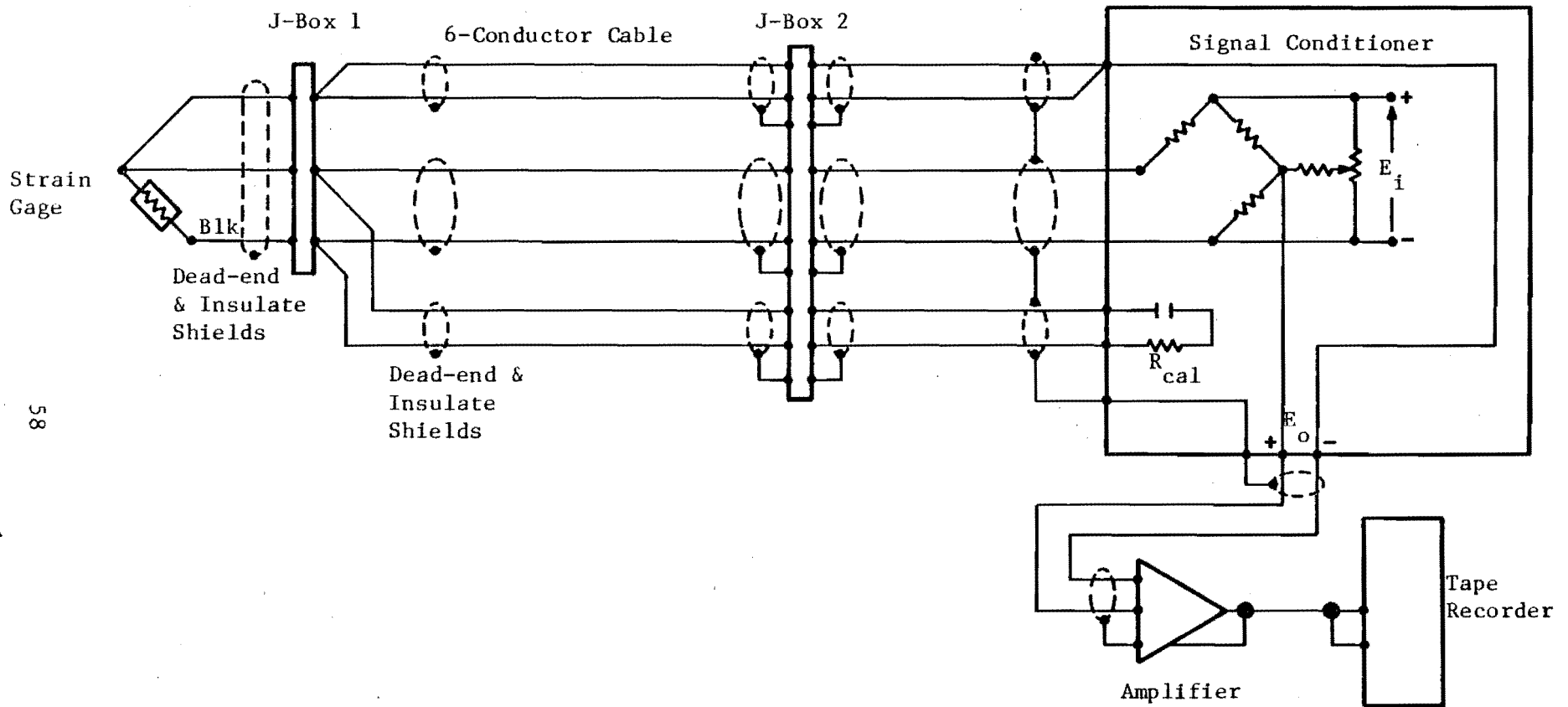


(A)



(B)

FIGURE 25. INSTALLATION OF STRAIN GAGES
ON 30-IN. PIPE



58

FIGURE 26. CIRCUIT DIAGRAM FOR PIPE STRAIN GAGES

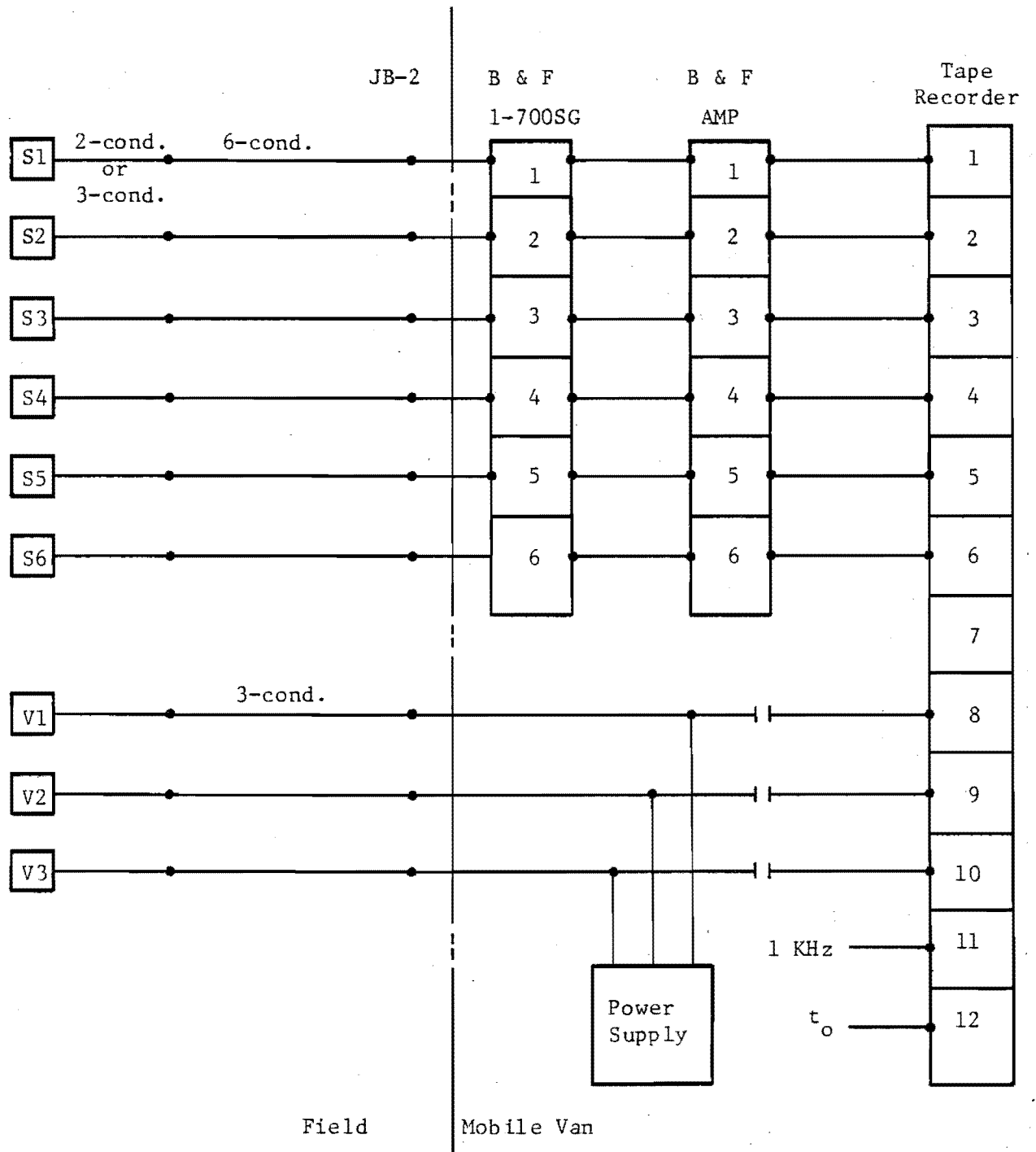


FIGURE 27. INSTRUMENTATION SYSTEM BLOCK DIAGRAM

tracks available were reserved in all cases for recording time-zero and a real-time reference signal. The data for the scale model experiments were recorded on an Ampex FR-1900 tape recorder. The field data taken in the Kansas City and Kentucky tests were recorded on a Honeywell Model 5600C system. The recorded data were played back into a Bell & Howell Model 5-164 oscillograph system for quick-look data analysis and subsequent data reduction. The data were time extended on playback by factors of 16 or 32, and using galvanometers having at least an 1,000 Hz upper frequency response the data were not attenuated below a frequency of 16 kHz.

The oscillograph records were digitized at SwRI, manipulated, scaled and plotted using a Hewlett-Packard Model 9830 microcomputer system. From these plots, peak particle velocity, computed particle displacement and pipe strain data were obtained for use in the analysis.

IV. EXPERIMENTAL RESULTS

General

The experimental data obtained from this program are presented in this section. For each set of experiments conducted, the horizontal ground motion data and pipe strain data are presented separately. For most of the 31 model-scale experiments, four velocity transducers, one accelerometer and six strain gage elements were recorded. Twenty of these experiments used a single explosive charge as the source for loading the pipes. On the remaining eleven model experiments, multiple charges representing a line source were used. For the eight full-scale experiments done at the Kansas City test site, single explosive charges were used in all cases to shock load the pipe tested with and without internal pressure. The other four full-scale tests, which were conducted at the Kentucky test site, used an operational pipeline with internal pressure, and single explosive charges were detonated. Two to three velocity transducers and six strain gages were recorded on the full-scale tests. In addition to the ground motion and pipe strain measurements, other data such as average seismic velocity in the soil, spot checks of soil water content, and small soil sample densities were also measured throughout the testing programs. These data will also be presented.

Ground Motions

To determine the forcing function which causes buried transmission lines to be stressed due to nearby buried explosive detonations, maximum horizontal soil particle velocity and displacement were measured in all field experiments conducted in this program. In most of the 31 model tests conducted, four velocity transducers and one accelerometer (mounted on the same canister as the closer-in velocity sensor) were used to obtain the ground motion data. In some cases a second accelerometer was also used in a separate canister. Figure 1 (section III) shows the location of these transducers in both the single and multicharge tests. Note that three different transducer lines were used to minimize interference as the shock waves propagated through the ground. Although the spacing varied between canisters for different test conditions, the first canister was usually

buried at the same distance from the charge (or charge line) as the pipe being tested.

The type and size of explosive used, and ground motion data obtained in the 31 model experiments are summarized in Table V. This table lists each test by number, the total charge weight used, whether the charge was a point or a line source, and if a line source, the length of the line. The line sources were composed of seven equal weight charges spaced equidistant, the center charge aligned with the center of the pipe, and the charge line parallel to the pipe. Each charge was buried below the surface the same distance as the center of the pipe in a given test. This distance from the surface of the ground to the center of each charge is also listed in the table. All the ground motion data are radial horizontal measurements for the point sources and horizontal measurements along lines perpendicular to the line sources. The headings in the table used to identify each measurement correspond to those shown in Figure 1. For example, R_1 is the distance between the charge and the first ground motion canister containing a velocity transducer, U_1 , and sometimes also an accelerometer, A_1 . The displacement X_{U1} was obtained by integrating the velocity-time trace of U_1 . The velocity U_{A1} was obtained by integrating the acceleration-time trace of A_1 . As previously mentioned, the data from A_1 were primarily to insure that the first velocity gage had not been exposed to a shock environment that would have damaged and invalidated its data, and as a check for the peak velocity measured. The second, third, and fourth (when used) velocity sensors are listed in the table with their corresponding distances from the charge and displacements obtained by integration. A second accelerometer, A_2 , was used in some tests primarily to monitor close-in accelerations for determining whether the first velocity transducer could be placed closer to the explosive source. Integrated velocities were also obtained for these very close-in measurements and are reported here for completeness, even though it was felt that they were not accurate enough to be used in the analysis. In many cases these measurements were so close to some of the line charges that the shock waves had not traveled a sufficient distance to have formed a line source. Therefore, the data could not have been used in the analysis anyway.

The last column lists the average seismic velocity obtained in each test. This propagation velocity was obtained by determining the arrival time

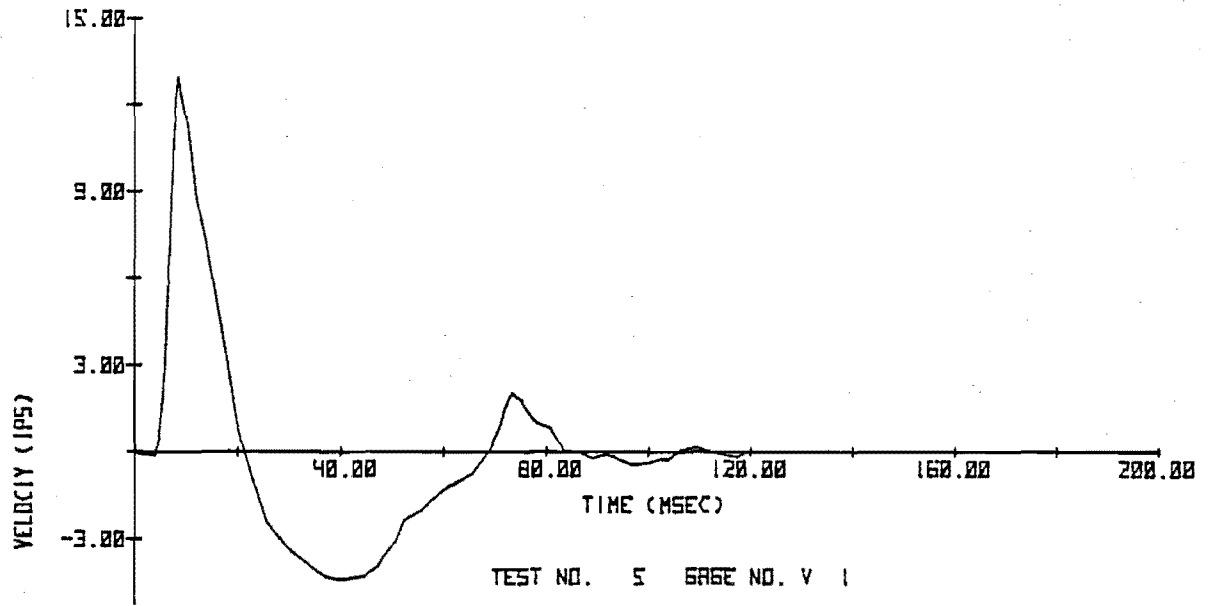
TABLE V. SUMMARY OF HORIZONTAL GROUND MOTION DATA FROM MODEL TESTS

Test No.	Charge Weight (lb)	Type of Source	Line Length (ft)	Depth of Burial (in.)	Motion Parameters																Average Seismic Velocity (fps)	
					R ₁ (ft)	U ₁ (ips)	X _{U1} (in.)	A ₁ (ips ²)	U _{A1} (ips)	R ₂ (ft)	U ₂ (ips)	X _{U2} (in.)	R ₃ (ft)	U ₃ (ips)	X _{U3} (in.)	R ₄ (ft)	U ₄ (ips)	X _{U4} (in.)	R _{A2} (ft)	A ₂ (ips ²)		U _{A2} (ips)
1	0.05	point	--	6	3.0	--	--	4,437	9.5	--	--	--	--	--	--	--	--	--	--	--	--	--
2	0.05	point	--	6	3.0	12.4	0.042	6,491	9.2	4.5	3.0	0.012	6.0	2.26	0.013	--	--	--	--	--	--	958
3	0.05	point	--	6	3.0	--	--	--	--	--	--	--	--	--	--	--	--	--	--	--	--	--
4	1.00	point	--	6	7.0	23.0	0.234	8,000	18.3	11.0	5.8	0.056	15.0	2.47	0.030	--	--	--	--	--	--	922
5	0.40	point	--	12	4.0	13.0	0.105	5,900	10.0	8.0	5.8	0.050	12.0	2.1	0.016	--	--	--	--	--	--	929
6	0.40	point	--	12	4.0	24.2	0.150	14,200	27.0	8.0	8.9	0.066	12.0	3.0	0.022	--	--	--	--	--	--	895
7	1.00	point	--	12	7.0	15.4	0.160	--	--	11.0	10.3	0.118	15.0	2.7	0.038	--	--	--	3.0	31,230	54	1038
8	0.03	point	--	12	2.0	10.9	0.053	--	--	4.0	2.3	0.018	6.0	0.8	0.005	--	--	--	1.0	34,000	48	958
9	0.03	point	--	12	2.0	7.4	0.031	--	--	4.0	1.7	0.011	6.0	0.92	0.006	--	--	--	1.0	46,000	45	751
10	0.03	point	--	6	1.0	33.4	0.050	46,000	41.0	3.0	4.3	0.019	5.0	1.6	0.007	--	--	--	0.5	290,000	90	1014
11	0.35	line	10.5	12	2.0	19.2	0.195	15,500	22.0	2.0	18.9	0.130	4.0	13.0	0.170	6.0	6.4	0.073	1.0	63,500	48	1110
12	2.80	line	14.4	12	5.0	25.9	0.41	--	--	8.0	12.3	0.195	11.0	11.5	0.16	14.0	5.8	0.094	--	--	--	738
13	2.80	line	9.0	12	5.0	36.3	1.35	--	--	10.0	9.1	0.166	15.0	3.2	0.065	20.0	1.6	0.025	--	--	--	679
14	2.80	line	9.0	12	5.0	39.6	1.46	--	--	10.0	9.1	0.136	15.0	2.2	0.044	20.0	1.6	0.023	3.0	24,400	72	780
15	0.35	line	4.5	6	2.5	50.1	0.48	14,850	57.0	5.0	14.1	0.200	7.5	5.8	0.082	10.0	1.5	0.023	1.5	57,100	90	945
16	0.35	line	4.5	6	2.5	72.8	0.55	--	--	5.0	17.2	0.240	7.5	7.9	0.108	10.0	2.0	0.031	1.5	110,000	128	771
17	0.21	line	9.0	6	3.0	21.7	0.19	7,003	18.0	5.0	8.1	0.114	7.0	5.0	0.051	10.0	--	0.017	--	--	--	829
18	2.80	line	5.4	6	5.0	51.5	1.49	--	--	10.0	6.8	0.13	15.0	4.6	0.075	20.0	3.0	0.043	3.0	54,800	130	734
19	0.21	line	2.7	12	1.5	66.5	0.52	--	--	3.0	19.8	0.27	6.0	6.1	0.12	9.0	1.8	0.035	1.0	140,000	150	564
20	0.03	point	--	32	1.5	14.0	0.029	10,300	13.0	3.0	4.7	0.011	4.0	2.13	0.005	5.0	1.3	0.003	1.0	32,100	27.5	1138
21	0.03	point	--	32	1.5	10.4	0.039	--	--	3.0	3.0	0.011	4.5	1.49	0.005	6.0	0.82	0.003	1.0	15,050	33	964
22	0.03	point	--	32	1.0	57.4	0.185	47,050	60.0	2.5	2.2	0.010	4.0	1.50	0.004	5.5	0.57	0.001	0.5	270,000	140	1100
23	0.03	point	--	32	1.0	44.2	0.113	40,620	46.0	2.5	3.3	0.015	4.0	1.4	0.0057	5.5	0.69	0.003	0.5	200,000	124	975
24	0.06	point	--	32	1.5	57.7	0.39	18,200	69.0	3.0	5.5	0.030	4.5	3.1	0.0018	6.0	1.33	0.006	1.0	95,500	97	866
25	0.06	point	--	32	1.75	40.5	0.187	24,050	50.0	3.2	5.1	0.029	4.75	3.0	0.0187	6.2	1.1	0.007	1.0	140,000	123	675
26	0.35	line	19.8	6	5.0	4.5	0.0415	--	--	8.0	2.53	0.021	11.0	2.0	0.014	14.0	1.8	0.011	--	--	--	701
27	0.35	line	19.8	6	5.0	4.71	0.041	--	--	8.0	3.0	0.0225	11.0	2.5	0.018	14.0	2.0	0.013	--	--	--	645
28	0.05	point	--	6	1.5	44.2	0.270	--	--	3.0	9.0	0.085	4.5	3.9	0.040	6.0	2.0	0.021	1.0	120,000	110	568
29	0.05	point	--	6	1.5	46.0	0.230	65,700	56.0	3.0	12.2	0.110	4.5	5.3	0.056	6.0	2.9	0.028	1.0	102,000	91	612
30	0.40	point	--	12	3.0	60.0	0.670	19,100	49.0	6.0	8.6	0.179	12.0	1.0	0.017	18.0	0.7	0.009	--	--	--	592
31	0.40	point	--	12	3.0	52.0	0.480	--	--	6.0	8.2	0.180	12.0	0.8	--	18.0	0.75	--	2.0	150,000	128	447

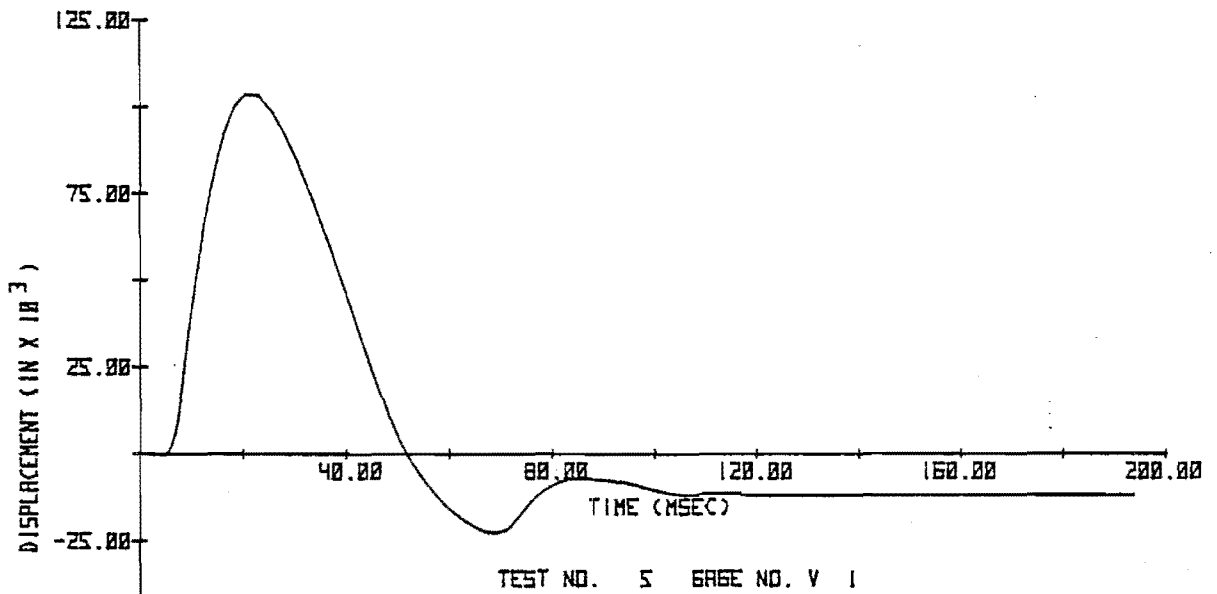
* See explanation in text.

of the seismic wave at each velocity transducer and dividing into their respective distances from the charge. The three or four values thus obtained in most tests were then averaged, and this average value is the one listed. The seismic velocity is one of the characteristic parameters of the soil and accounts for different soil conditions from test to test, as can be caused by changes in water content. The water content of the soil at the surface and at the depth of burial of the charge was spot checked whenever it was felt that the soil was drier or wetter than "normal." In most cases, water content was an average of 8-10%, although a few tests were conducted with water content as low as 3% and as high as 14% at the surface during a dry spell and after some heavy rains, respectively. The second parameter used in the analysis to characterize the soil is its density. The value used in the analysis on all the data was 102 lb/ft³, which was the average density measured from the survey cores taken before the test program. Small sample density measurements were made in some tests, and, in general, the results did not vary much from the average value obtained from the cores.

Examples of velocity and displacement measurements are shown in Figures 28 and 29 taken from Test No. 5 which used a point explosive source. Figure 28-a is the velocity-time plot obtained from velocity sensor U₁ by digitizing the record from the oscillograph and plotting it with engineering units, using the microcomputer and its plotter. Figure 28b is the displacement-time plot obtained by integrating the digitized velocity trace. Smaller amplitude measurements of velocity and displacement are shown in Figure 29. These traces are from sensor U₂ used in the same test, but at a more distant location. In addition to the smaller amplitudes, also note the later arrival time of the blast at this location. Similar examples of velocity and displacement records from a line explosive source used in Test No. 17 are presented as Figure 30. An additional set of horizontal velocity traces recorded in the model experiments using single charges is shown in Figure 31 for Test No. 29. Again, the time histories are very similar to the others, and smaller amplitudes with later arrival times were recorded as the distance of the transducer increased away from the charges. All these traces show in general the look of the signatures of the velocity data recorded in the model experiments.



(A) VELOCITY



(B) DISPLACEMENT

FIGURE 28. GROUND MOTIONS FROM 0.4-LB CHARGE AT A RADIAL DISTANCE OF 4 FT

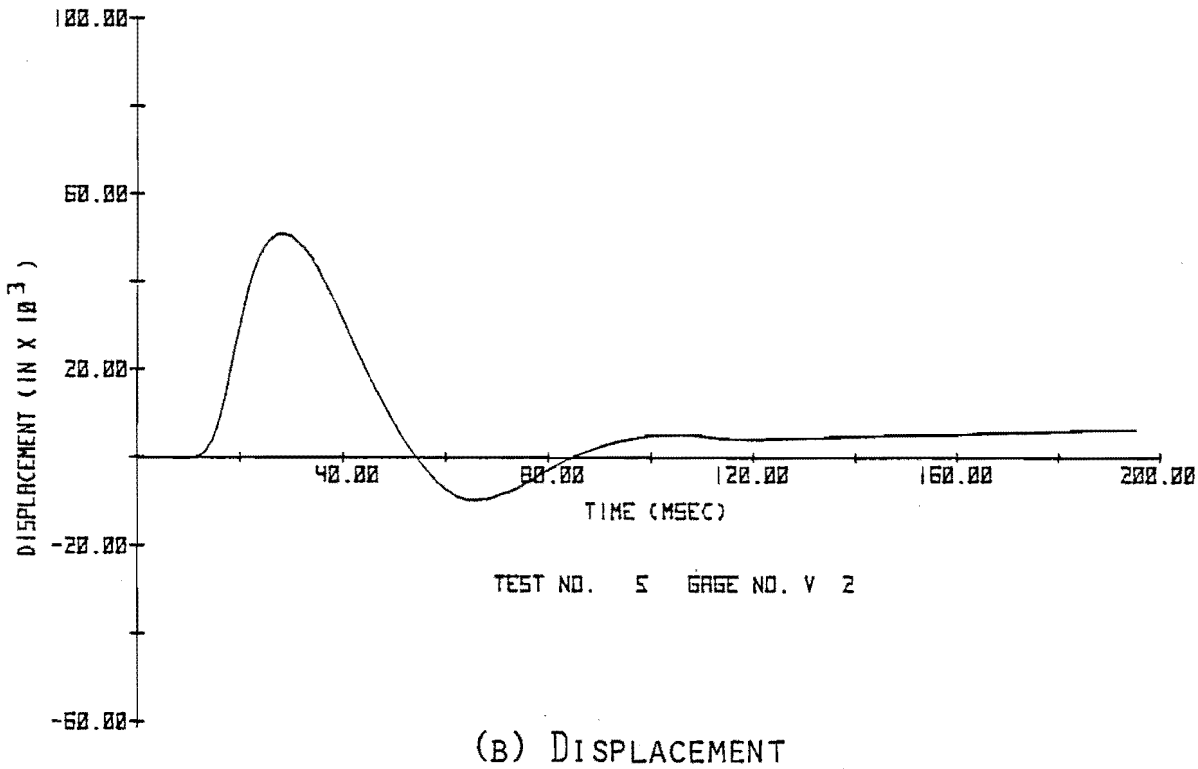
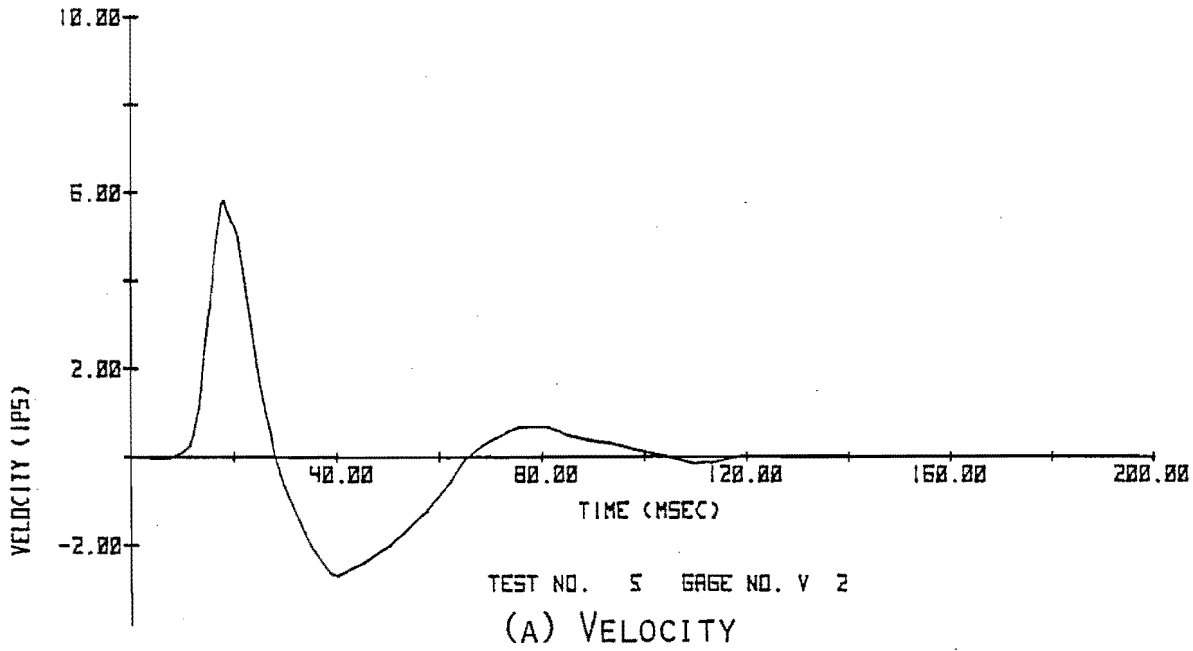
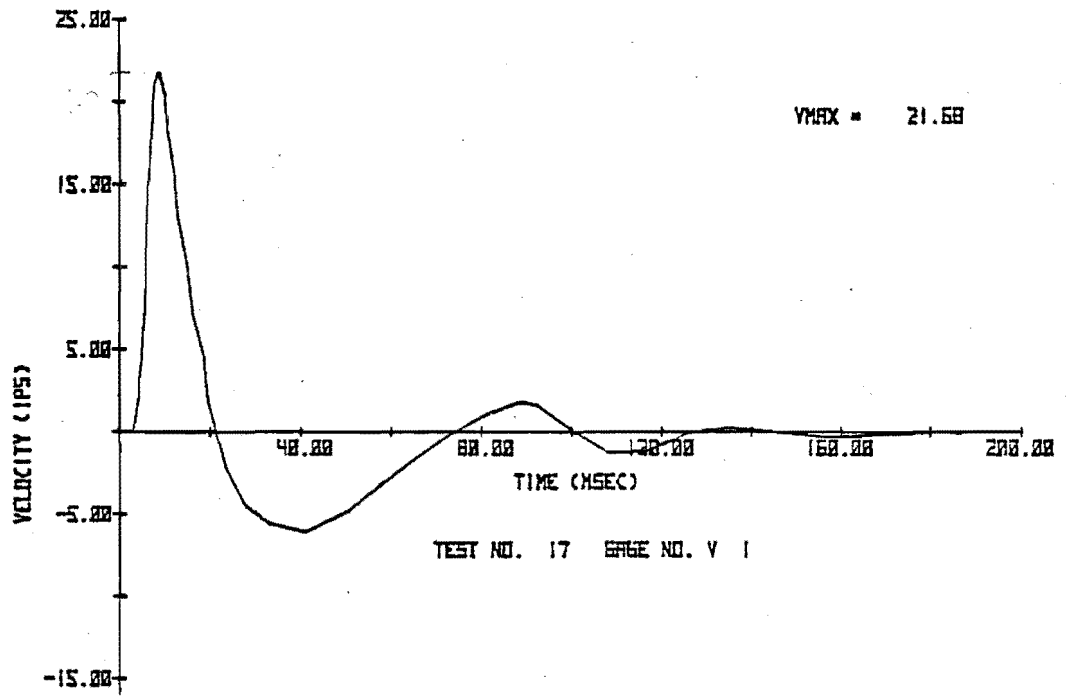
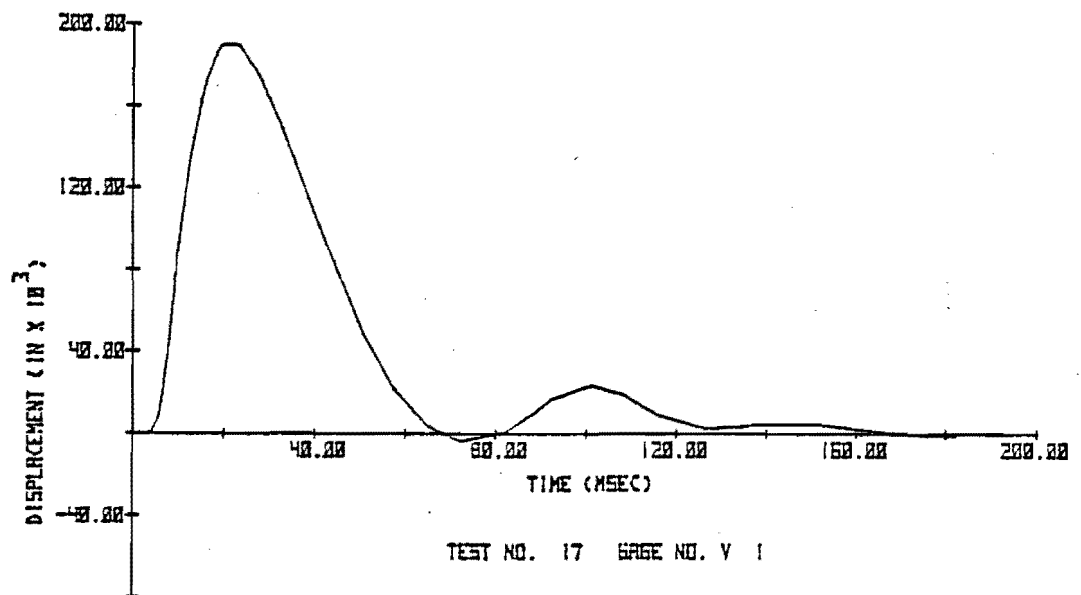


FIGURE 29. GROUND MOTIONS AT 8 FT FROM 0.4-LB CHARGE



(A) VELOCITY



(B) DISPLACEMENT

FIGURE 30. GROUND MOTIONS AT 3 FT FROM 0.21-LB EXPLOSIVE LINE SOURCE

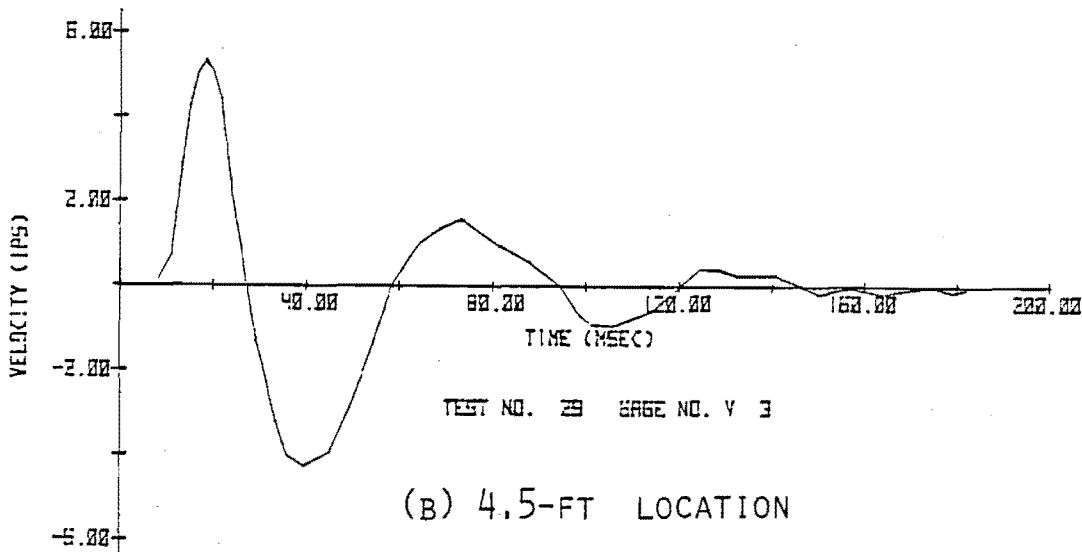
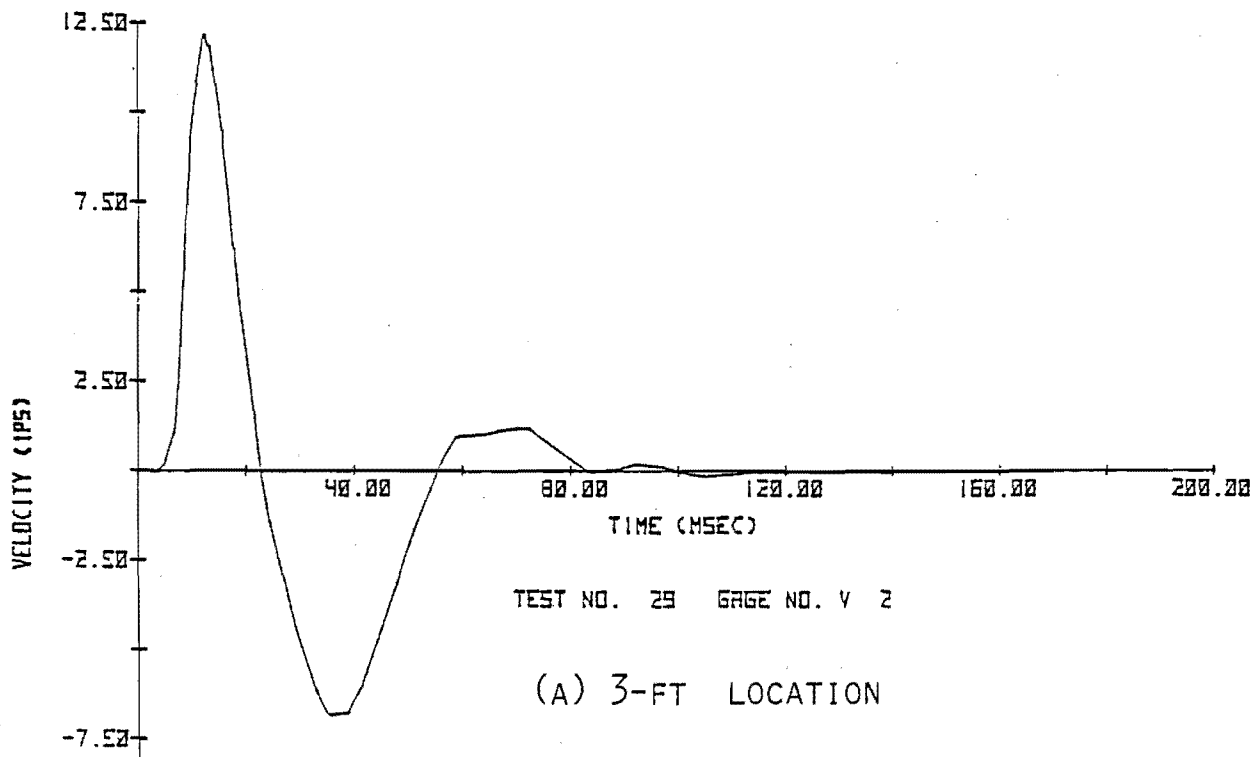


FIGURE 31. HORIZONTAL VELOCITIES FROM 0.05-LB CHARGE

In the eight experiments conducted at the Kansas City test site, three velocity transducers were used to obtain the horizontal ground motion data. These transducers were placed in the ground at the same depth as the center of the pipe, as was the case in all the model experiments. They were located as shown in Figure 4 such that the first two transducers would bracket the horizontal distance between the center of pipe and the explosive. The third transducer used was then located further out to obtain data over a reasonable range of distance. The peak soil velocities and displacements obtained from the Kansas City experiments are shown in Table VI by test number and distance of the velocity transducers from the single charge sources used. For example in Test No. 4, which used a 15-lb charge, the second canister containing velocity transducer U_2 was located a distance R_2 of 12 ft away from the charge. The velocity-time trace recorded by this channel is shown in Figure 32 along with its integration to obtain the displacement. An example of the ground motions recorded from a 5-lb charge is given in Figure 33.

Note that these data examples show particle velocities of the same order of magnitude as those measured in the model experiments, an expected result since the larger distances used for placing the transducers in the full-scale tests were selected so that similar velocity amplitudes would result. However, the velocity pulse durations would necessarily become longer on the larger scale experiments. This was confirmed by the data. Likewise, displacement amplitudes and durations were of larger magnitude in the full-scale experiments.

The seismic wave propagation was also determined in the Kansas City tests from the time of arrival of the wave at each canister location. The average value for each test is also given in Table VI. Small soil samples near the surface from the holes made for placing the charge and velocity transducers on each test were checked for water content and density. The water content was measured to be between 10-12% on all the Kansas City tests and the density averaged close to $100 \text{ lb}_m / \text{ft}^3$.

The soil particle velocity and displacement data recorded in the four full-scale tests conducted at the Kentucky test site were of similar nature as those obtained in Kansas City. Table VII shows the peak values recorded. The transducers were placed so as to obtain data at approximately the same distance as that between the charge and the center of the pipe. At least

TABLE VI. RADIAL SOIL MOTION DATA FROM KANSAS CITY TESTS

Test No.	Charge Weight (lb)	R ₁ (ft)	U ₁ (ips)	X _{U1} (in)	R ₂ (ft)	U ₂ (ips)	X _{U2} (in)	R ₃ (ft)	U ₃ (ips)	X _{U3} (in)	Seismic Velocity (fps)
1	15	7.0	55.4	0.92	10.0	14.3	0.28	15.0	3.6	0.057	900
2	5	5.0	159.7	2.62	8.0	80.0	2.18	--	--	--	573
3	5	6.0	88.0	2.17	12.0	8.7	0.33	15.0	3.0	0.70	519
4	15	6.0	118.8	1.96	12.0	47.7	1.86	14.0	36.0	1.21	1232
5	5	6.0	82.4	2.04	12.0	10.4	0.35	14.0	3.4	0.11	582
6	15	10.0	76.3	2.35	14.0	13.0	0.51	23.5	2.5	0.032	735
7	15	8.0	98.6	5.5	16.0	8.2	0.25	24.0	3.6	0.11	792
8	15	8.0	138.0	4.78	16.0	6.2	0.34	24.0	1.24	0.049	622

Motion away from the charge is positive.

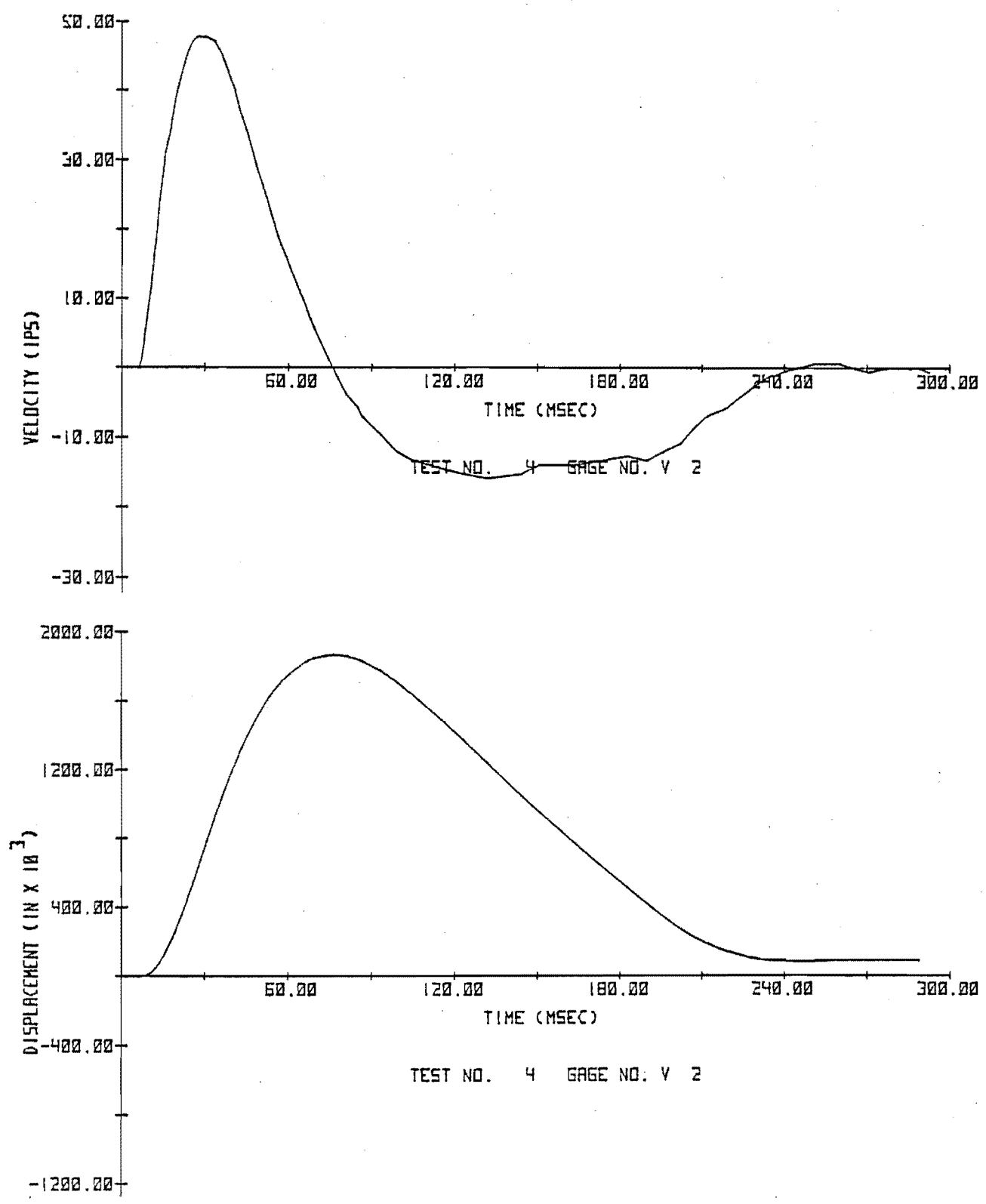


FIGURE 32. RADIAL GROUND MOTIONS AT 12 FT FROM 15-LB CHARGE

TABLE VII. GROUND MOTION DATA

Test No.	Charge Weight (lb)	R ₁ (ft)	U ₁ (ips)	X _{U1} (in)	R ₂ (ft)	U ₂ (ips)	X _{U2} (in)	R ₃ (ft)	U ₃ (ips)	X _{U3} (in)	Seismic Velocity (fps)
1	5	6	--	--	12	22.0	0.29				1,230
2	4	6	80.7	1.51	12	--	--				--
3	3	6	72.5	0.79	12	14.1	0.33	18	2.1	0.036	974
4	3	6	93.0	1.57	12	18.8	0.25				1,480

Motion away from charge is positive.

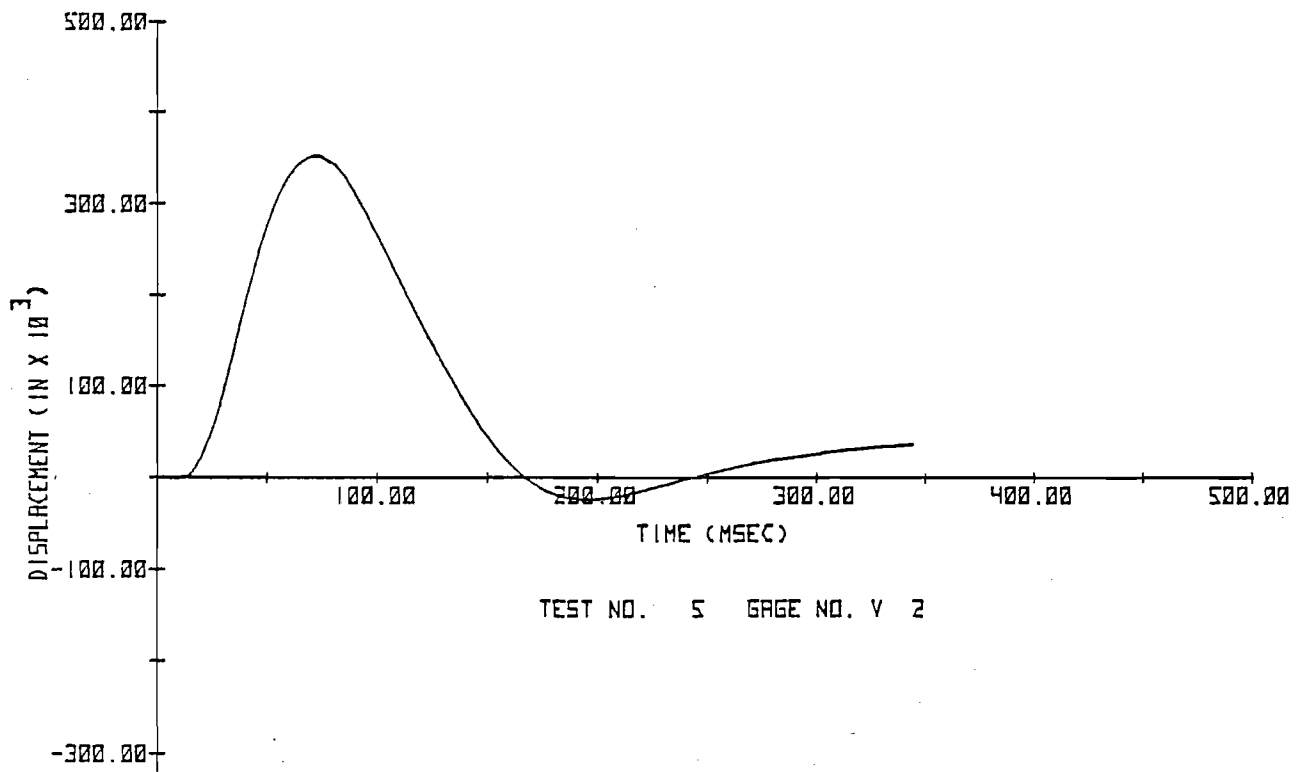
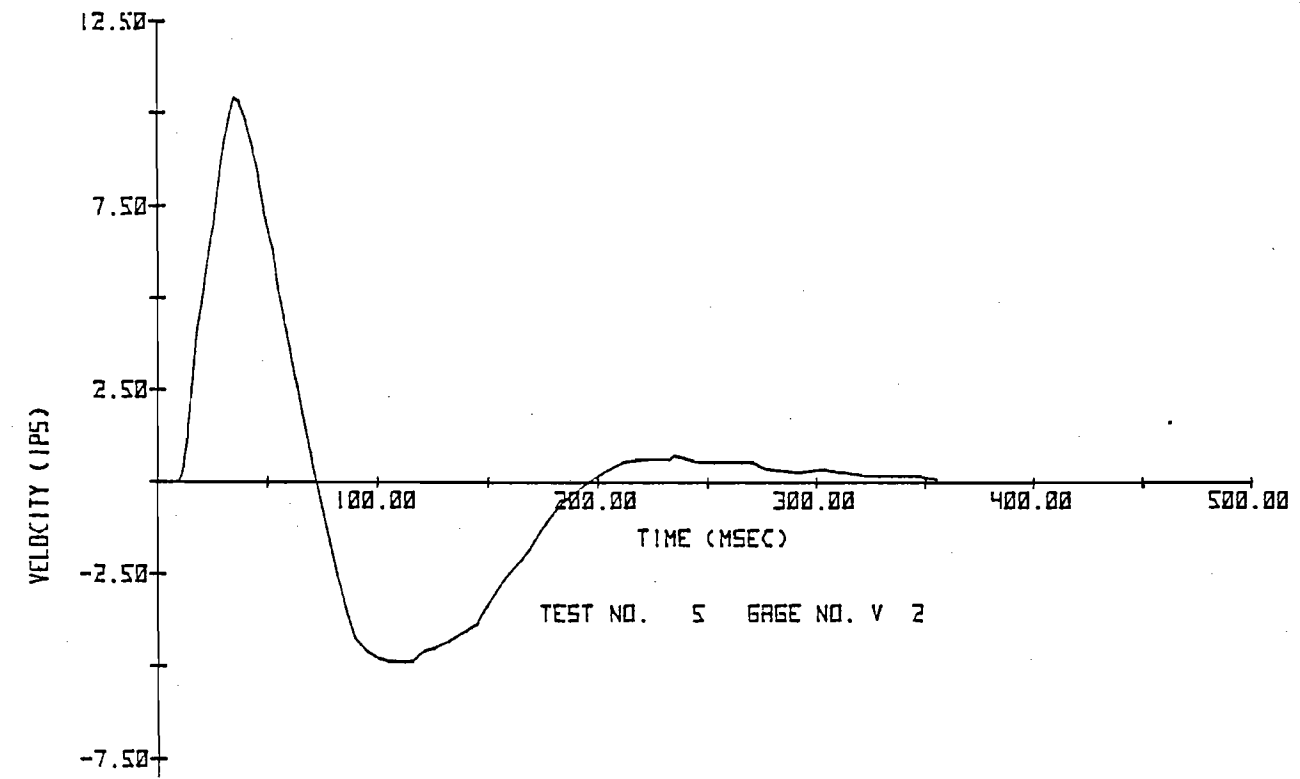


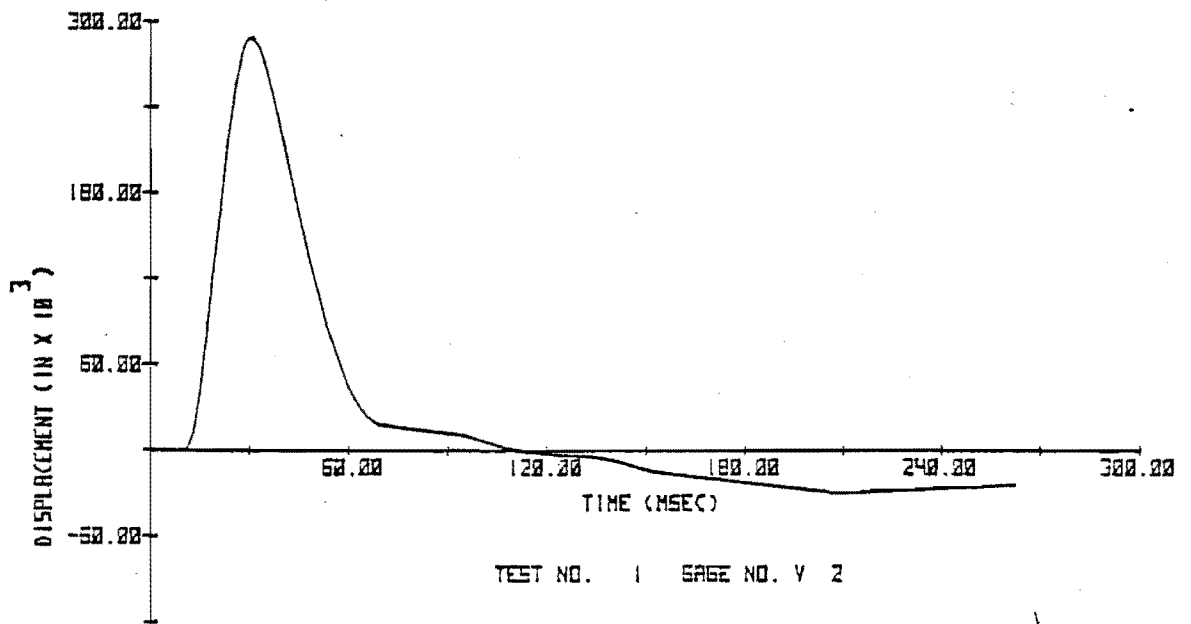
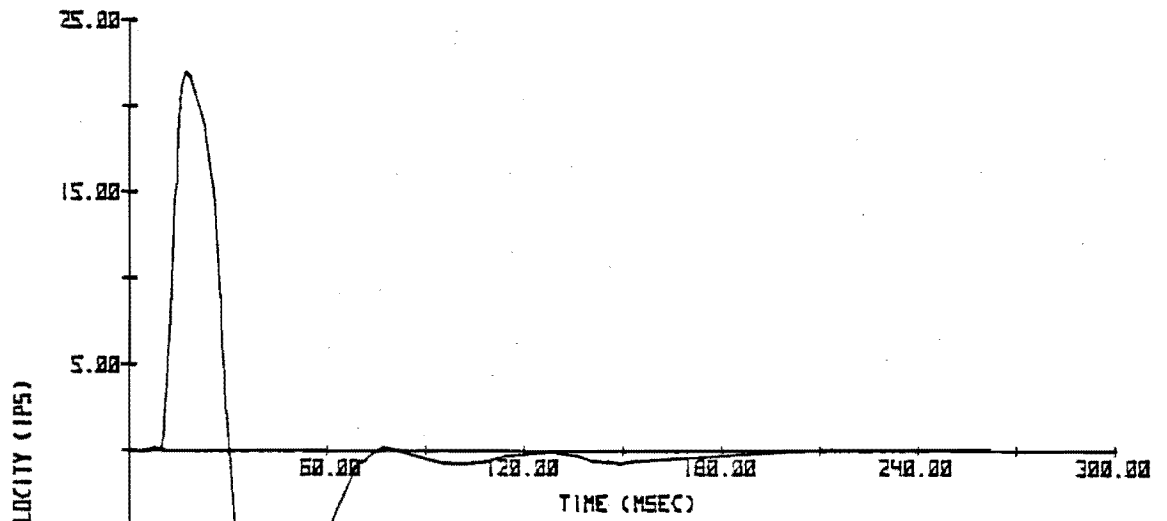
FIGURE 33. RADIAL SOIL MOTIONS AT 12 FT FROM A 5-LB CHARGE

two measurements were attempted on each test as shown in Figure 14. However, two data points were lost due to over-ranging the transducer in one case, and severing of a cable splice in the second before data had been recorded. Seismic velocity when obtainable is also shown in this table. Water content in the soil measured near the surface ranged from 14-16% and soil density averaged right at $101 \text{ lb}_m/\text{ft}^3$. Two examples of the soil motion data are shown as Figures 34 and 35. Both of these measurements were at the same distance of a similar size charge as the ones in Figure 33 from the Kansas City tests. However, the Kentucky data seems to have a higher peak velocity with a much smaller duration. Because of the difference in seismic velocities in these two sets of tests and because the data are plotted in dimensionless form, the differences in amplitudes become small. This will be shown in a later section of this report. Furthermore, the parameter that controls the pipe response in the realm of interest is the soil displacement which, in its dimensionless form, also plots well regardless of the test site.

Pipe Strains and Stresses

Strain measurements were made on both the model and full scale experiments conducted in this program to quantitatively determine the response of pipelines to nearby underground detonations. For use as the 3- and 6-inch pipes, MT-1020 carbon steel tubing with a manufacturer specified minimum ultimate tensile strength of 65,000 psi was used. The specified minimum yield strength (SMYS) was 55,000 psi. However, tensile tests performed on coupons from these pipes at SwRI showed the ultimate tensile strength to be about 80,000 psi which would give an estimated yield strength of about 68,000 psi. The 16-in. pipe used was ASTM A53, Grade B with a SMYS of 35,000 psi. Because the principal modes of pipe response were not known, the 31 model experiments used five different strain gage locations around the upper half-circumference of each model pipe as shown in Figure 2. Two-element rosettes were used so that both circumferential and longitudinal strain measurements would be possible at each location.

The testing program was begun by recording the five circumferential strains since it was felt that these would be the larger strains. Also, the mode of the pipe response in this direction needed to be determined so that those gages recording redundant or lower peak strains could be dropped



50-5.4

FIGURE 34. RADIAL SOIL MOTIONS AT 12 FT FROM A 5-LB CHARGE

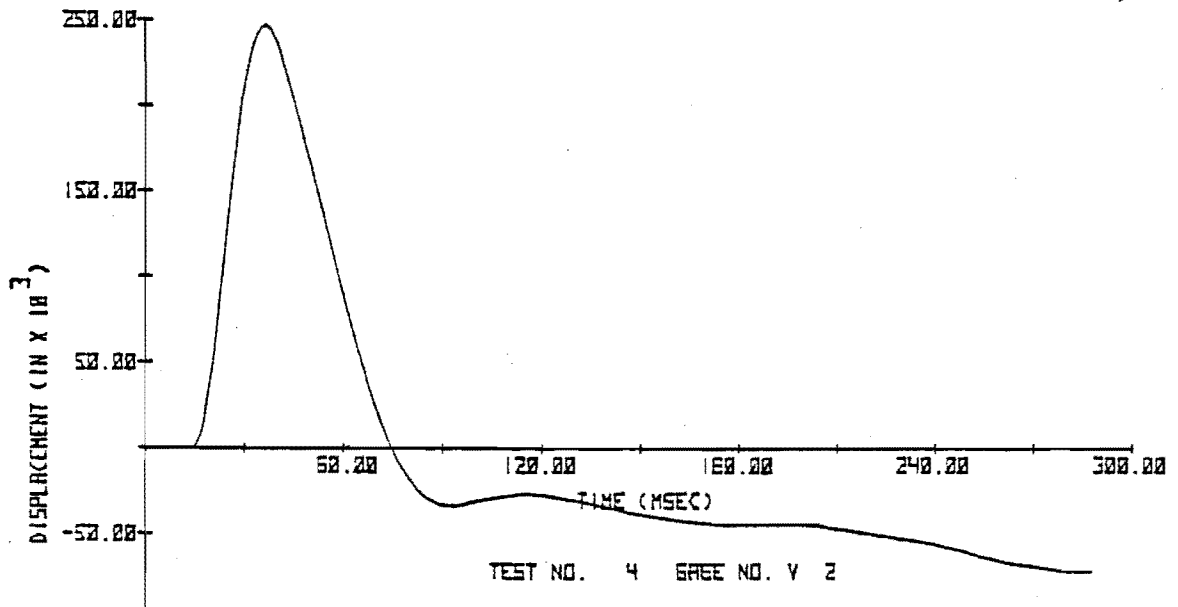
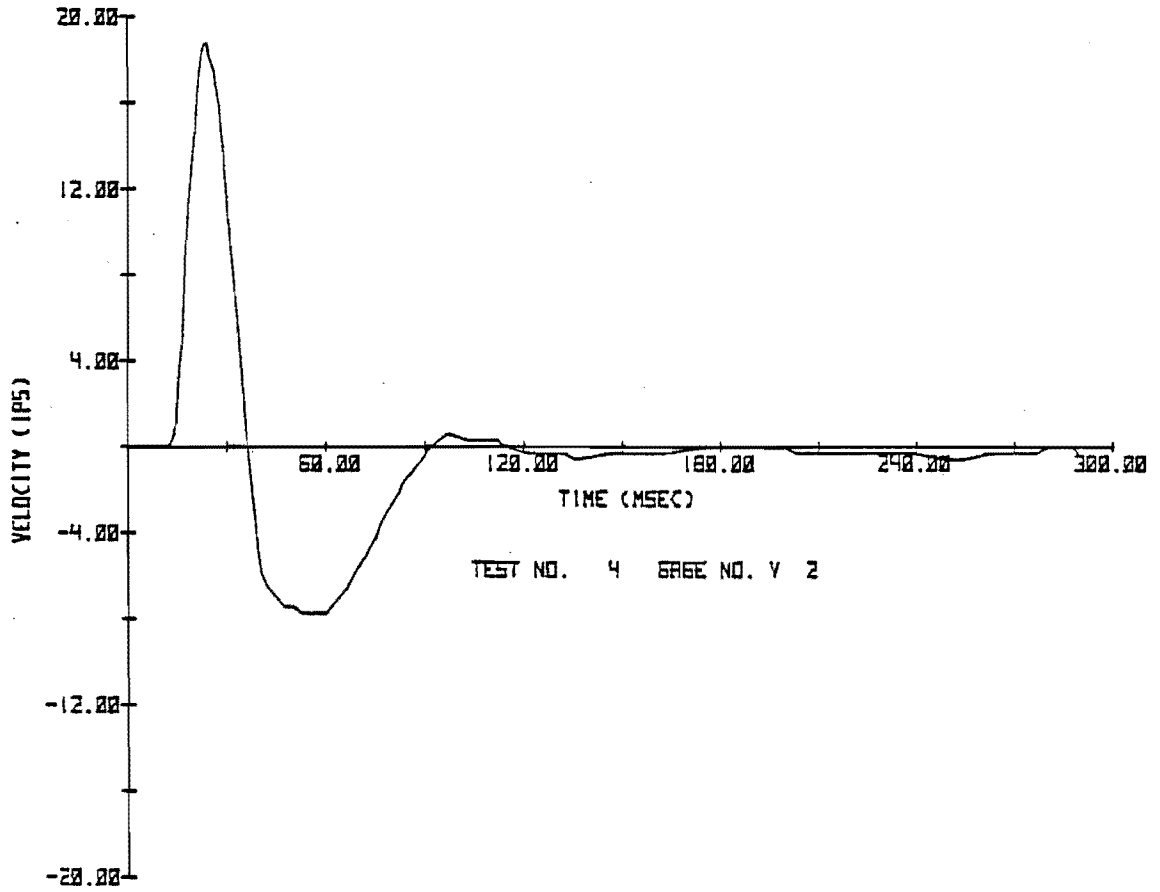


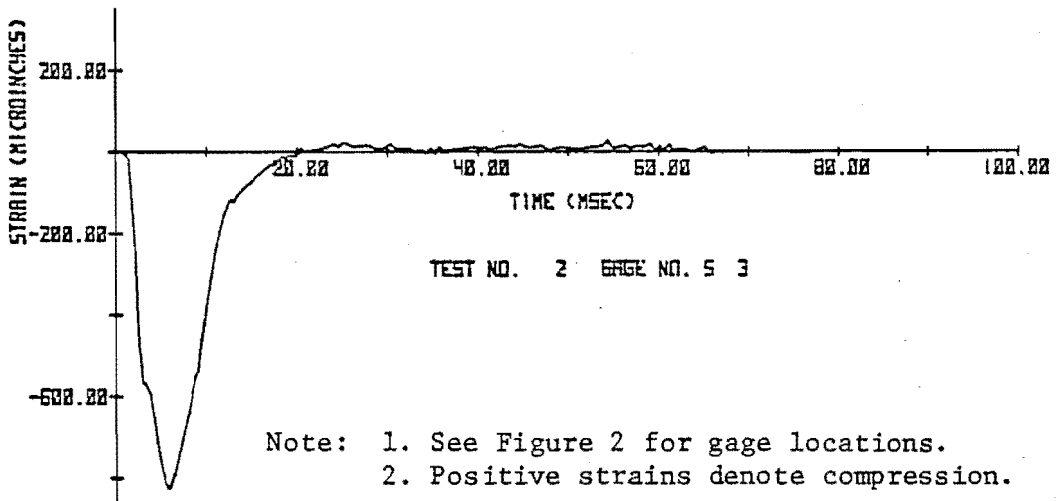
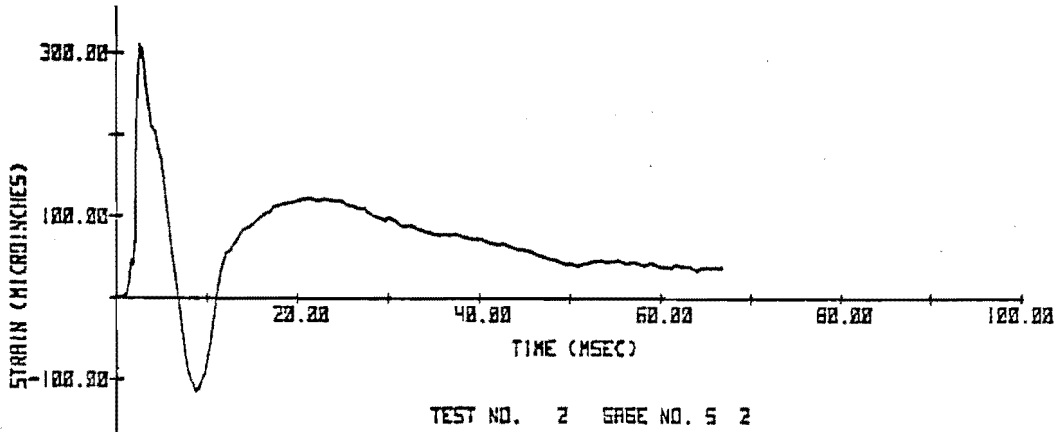
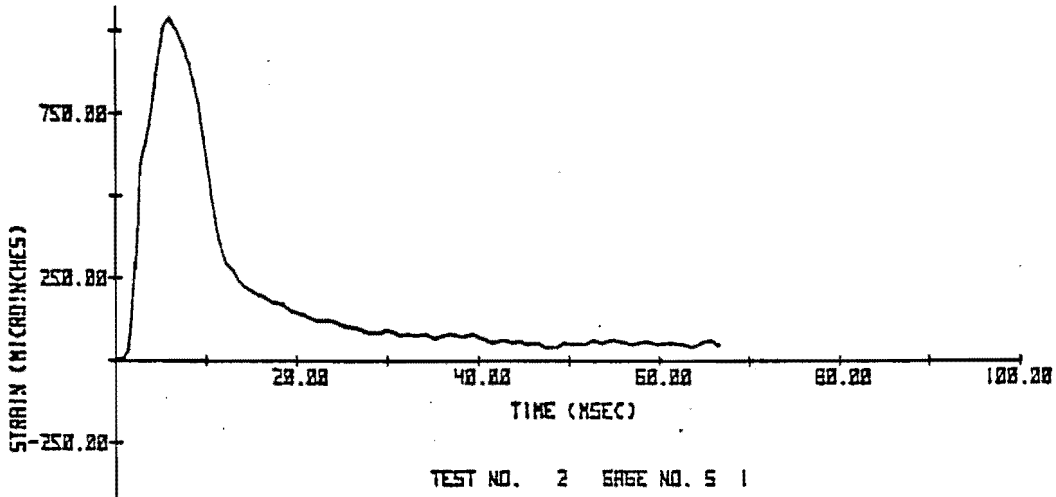
FIGURE 35. RADIAL SOIL MOTIONS AT 12 FT FROM A 3-LB CHARGE

and longitudinal gages substituted. From the first five model tests, it was determined that the pipe was ovaling and that the significant circumferential strains were at the front, top, and back locations on the pipe. Figure 36 shows the five circumferential strains measured in Model Test No. 2 using the 3-in. pipe. Therefore, longitudinal strain gages were recorded instead of the two circumferential gages located at 45° between the top and side locations. The first few longitudinal measurements indicated that the pipe was bending significantly away and upward from the charge. Therefore, for the majority of the remaining model experiments, as well as all of the full-scale tests, longitudinal strains were measured and recorded at the same locations as the circumferential ones: on the front, top and back side of each pipe. Figure 37 is an example of the strains measured in both directions on the 6-in. pipe in Model Test No. 30.

The strain data recorded in the 31 model experiments are presented in Table VIII. Each test is identified by test number, the size of the pipe used, the distance between the charge and the center of the pipe, the size of the explosive charge, and whether the charge was either a point or line source. The circumferential and longitudinal strains are identified by subscripts which correspond to the strain measurement locations shown in Figure 2. Because maximum stresses caused by the blast loading are the quantities used in the analysis and plotting of the data in later sections of this report, Table IX lists the absolute peak stress values computed from the measured strains using the uniaxial strain to stress formula. A biaxial stress formula, including Poisson's effect, was not used because of the order of magnitude increase in complexity which would have been required in the data reduction. Generally the maximum error caused by this distortion should be no more than 10%; an increase in accuracy which did not seem realistic when the magnitude of the scatter was considered. The treatment of these blast stresses in the overall solution of the problem and the contribution they make in determining the overall load on a transmission line is covered later in the report.

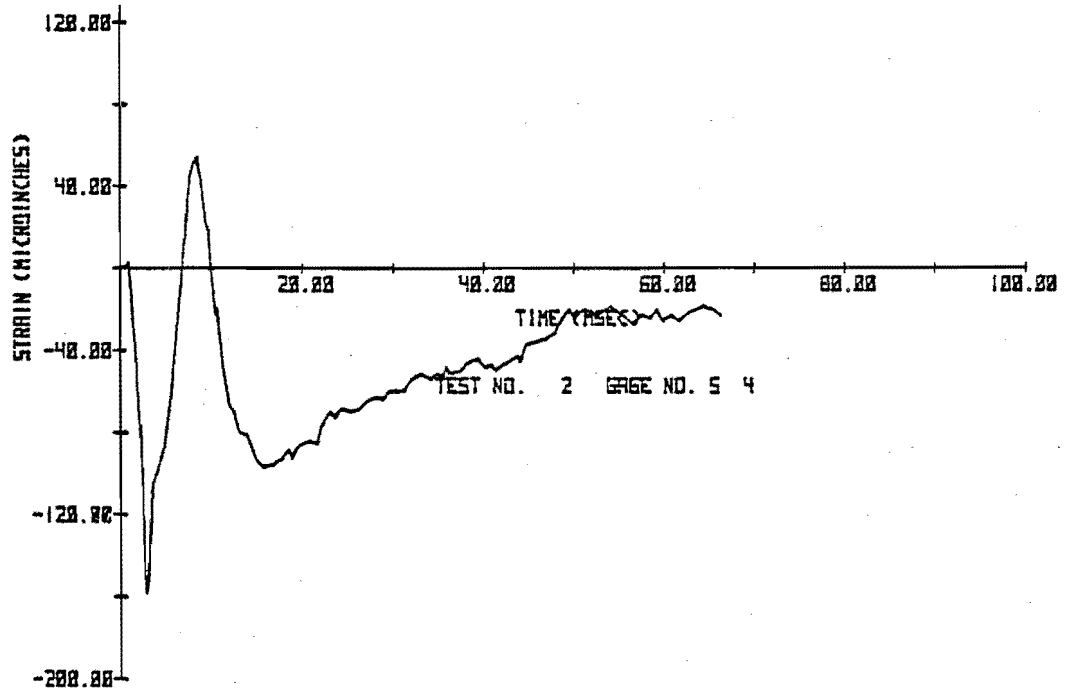
30%
POSSIB.
?

The Panhandle Eastern 24-in. pipe tested in Kansas City was also strain-gaged on the top, on the front (side nearer charge), and on the back. Circumferential and longitudinal orientations were used at each location as shown in Figure 5. All tests used a single explosive charge buried to the same



Note: 1. See Figure 2 for gage locations.
 2. Positive strains denote compression.

FIGURE 36. CIRCUMFERENTIAL STRAIN MEASUREMENTS ON 3-IN. DIAMETER PIPE



Note: 1. See Figure 2 for gage locations.
 2. Positive strains denote compression.

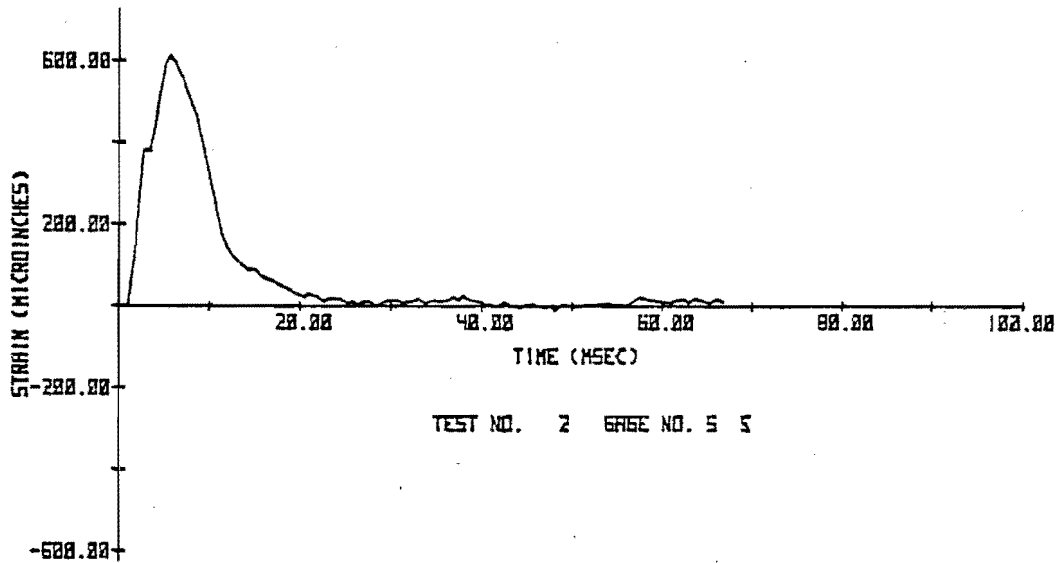
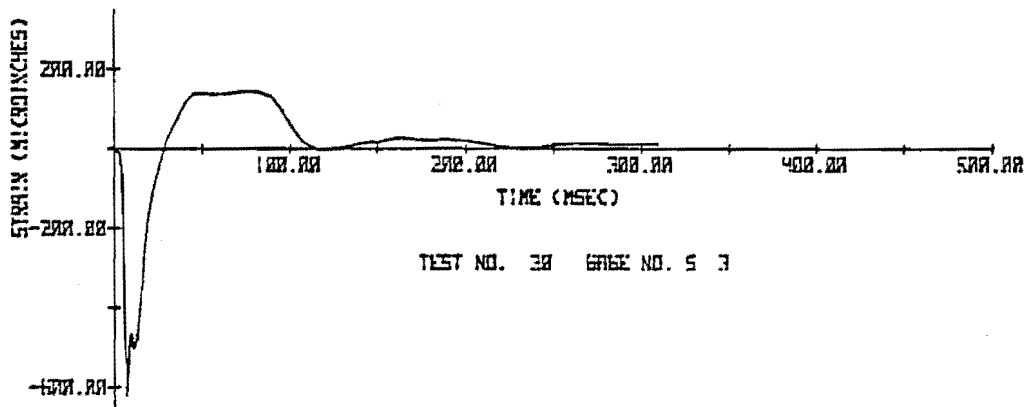
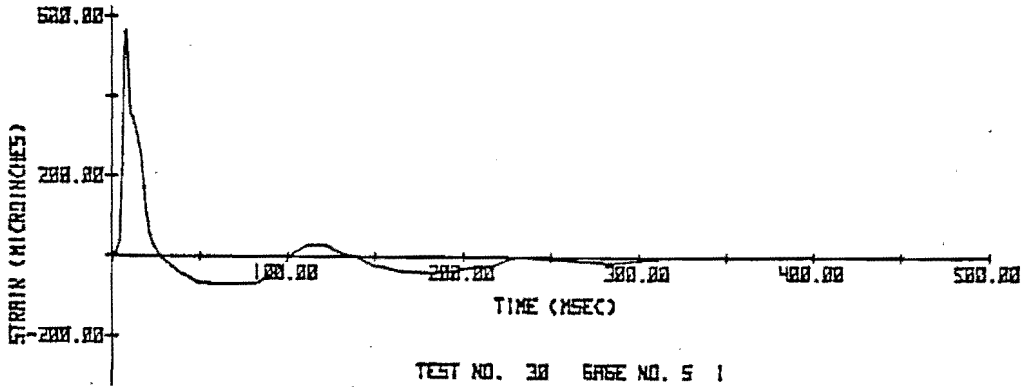
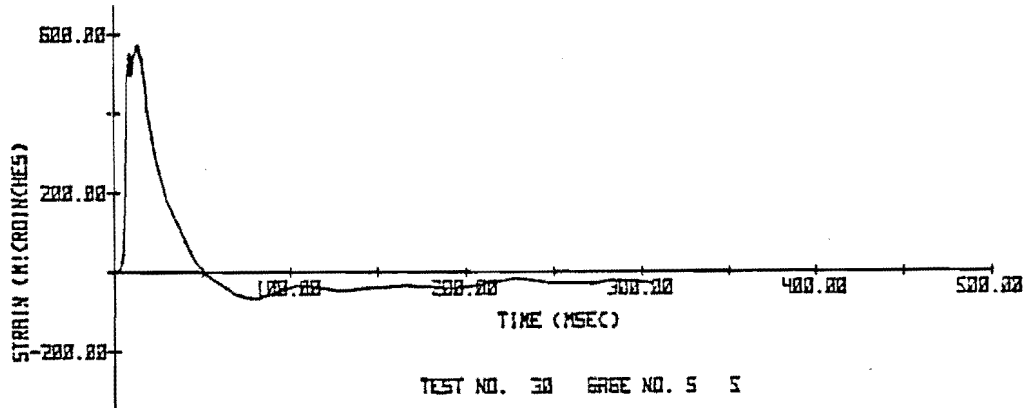


FIGURE 36. CIRCUMFERENTIAL STRAIN MEASUREMENTS ON
 3-IN. DIAMETER PIPE (CONT'D.)

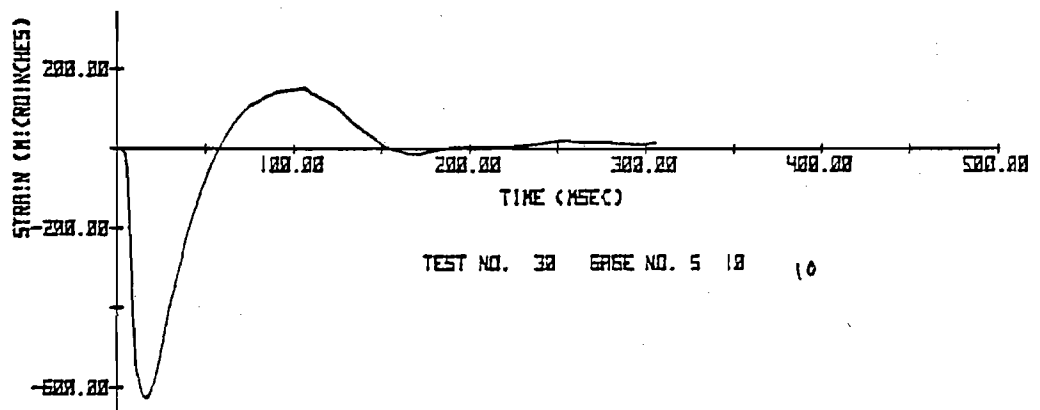
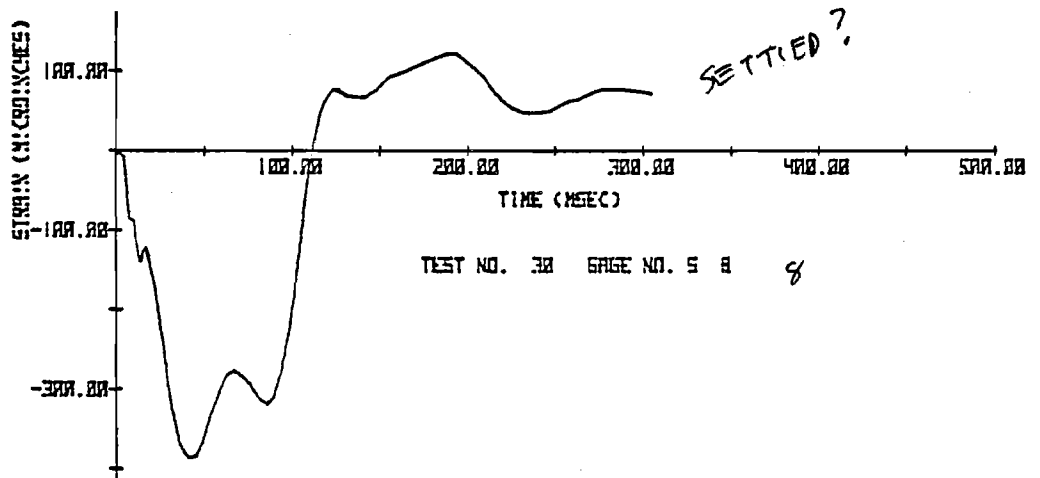
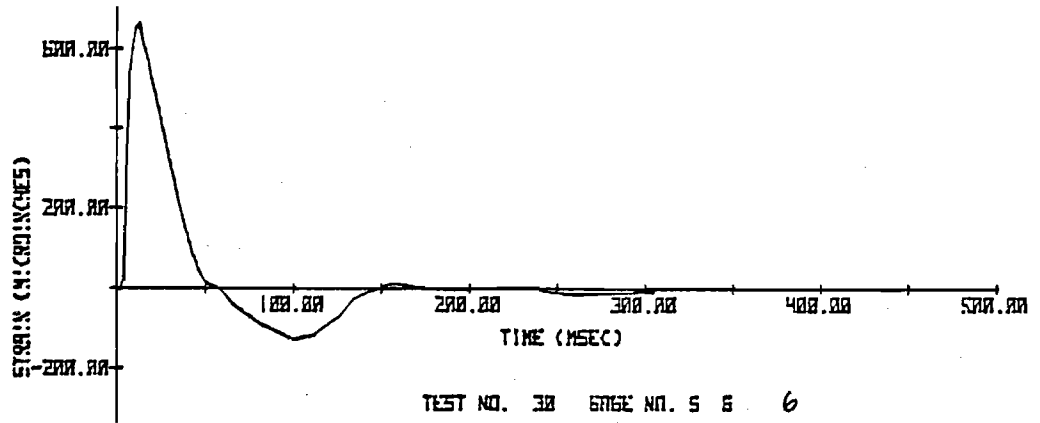


Note: 1. See Figure 2 for gage locations.
 2. Positive strains denote compression.



(A) CIRCUMFERENTIAL STRAINS

FIGURE 37. STRAIN MEASUREMENTS FOR 6-IN. PIPE



(B) LONGITUDINAL STRAINS

FIGURE 37. STRAIN MEASUREMENTS FOR 6-IN. PIPE
(CONT'D.)

TABLE VIII. MAXIMUM STRAINS FROM MODEL EXPERIMENTS

Test No.	O.D. Pipe (in)	Standoff Distance (ft)	Charge Weight (lb)	Type of Source	Circumferential Strains					Longitudinal Strains		
					S1 ($\mu\epsilon$)	S2 ($\mu\epsilon$)	S3 ($\mu\epsilon$)	S4 ($\mu\epsilon$)	S5 ($\mu\epsilon$)	S6 ($\mu\epsilon$)	S8 ($\mu\epsilon$)	S10 ($\mu\epsilon$)
1	2.95	1.5	0.05	pt.	474	--	-360	-175	253			
2	2.95	1.5	0.05	pt.	1,039	311	-830	-158	612			
3	2.95	1.5	0.05	pt.	844	443	-590	--	875			
4	2.95	11.0	1.00	pt.	80.7	74.9	-80	-37	112			
5	5.95	3.0	0.40	pt.	466	171	-590	241	608			
6	5.95	3.0	0.40	pt.	707	-90	-930		849	592		-520
7	5.95	11.0	1.00	pt.	90.6		-120		102	127	-44	-137
8	5.95	2.0	0.03	pt.	156		-135		106	169	-73	-117
9	5.95	1.0	0.03	pt.	996		-600		629	548	-238	--
10	2.95	0.75	0.03	pt.	1,075		-980		1,217	580	-215	868
11	5.95	5.0	0.35	line	140		-230		--	239	-76	--
12	5.95	8.0	2.8	line	302		-360		339	276	-190	-285
13	5.95	5.0	2.8	line	673		-850		942	724	-338	-825
14	5.95	5.0	2.8	line	424		-520		713	734	-435	-850
15	2.95	2.5	0.35	line	1,355		-1,025		1,084	600	-480	-535
16	2.95	2.5	0.35	line	1,395		-1,080		998	620	-570	-583
17	2.95	5.0	0.21	line	109		-67		115	140	-51	--
18	2.95	3.0	2.8	line	3,898		-2,640		2,308	1,550	-1,780	-1,396
19	5.95	1.5	0.21	line	1,147		-1,750		1,371	1,304	-255	-1,125
20	16.0	3.0	0.03	pt.	27.4		-15.0		19.4	16.7	-5.0	--
21	16.0	1.5	0.03	pt.	477		-240		238	205	-105	70
22	16.0	1.0	0.03	pt.	312		-168		155	158	-85	--
23	16.0	1.0	0.03	pt.	--		-865		572	--	-270	246
24	16.0	1.5	0.06	pt.	214		-152			119	-85	
25	16.0	1.25	0.06	pt.	564		-330			298	-153	
26	2.95	8.0	0.35	line	42		-27		37	48	46	-42.4
27	2.95	8.0	0.35	line	43		-29		42	54	-51	-61
28	2.95	1.5	0.05	pt.	337		-200		192	490	-263	-410
29	2.95	1.5	0.05	pt.	463		-380		342	620	-260	-565
30	5.95	3.0	0.40	pt.	564		-620		574	666	-390	-620
31	5.95	3.0	0.40	pt.	473		-560		518	627	-410	-560

Positive strains denote compression.

TABLE IX. MAXIMUM BLAST PIPE STRESSES FOR MODEL TESTS

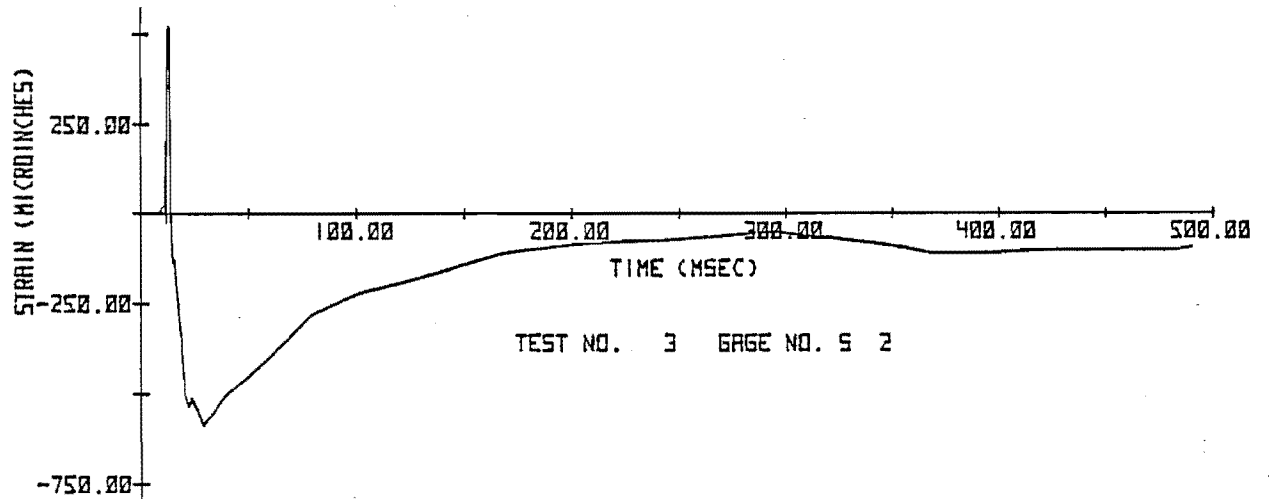
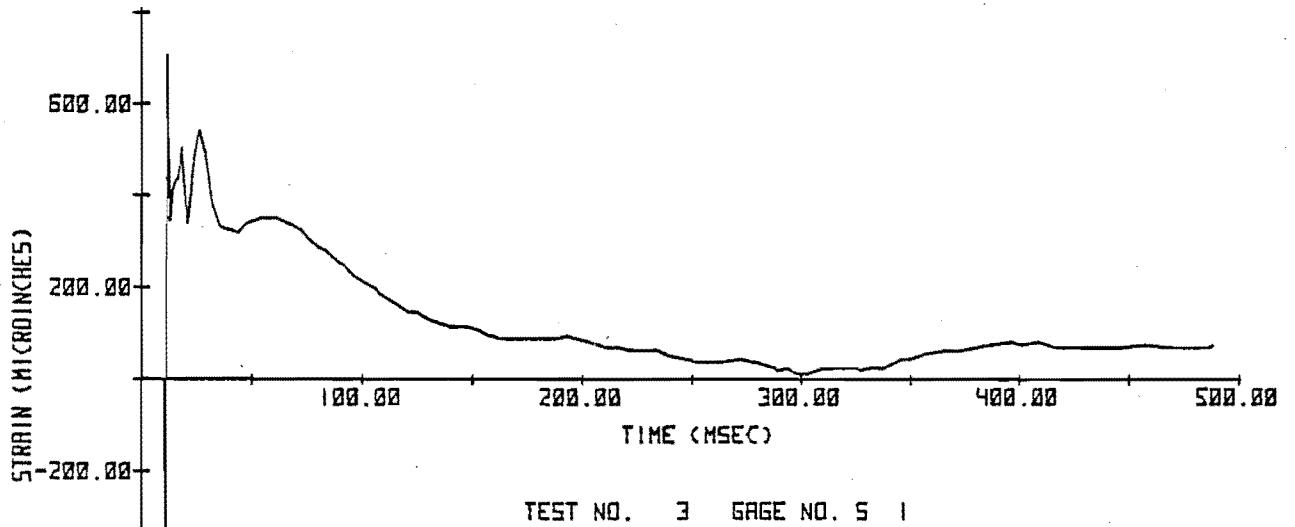
Test No.	Pipe (in)	Standoff Distance (ft)	Charge Weight (lb)	Type of Source	Circumferential Stress (psi)	Longitudinal Stress (psi)
1	2.95	1.5	0.05	pt.	14,200	
2	2.95	1.5	0.05	pt.	31,200	
3	2.95	1.5	0.05	pt.	26,300	
4	2.95	11.0	1.00	pt.	3,400	
5	5.95	3.0	0.40	pt.	18,200	
6	5.95	3.0	0.40	pt.	27,900	17,800
7	5.95	11.0	1.00	pt.	3,600	4,100
8	5.95	2.0	0.03	pt.	4,700	5,100
9	5.95	1.0	0.03	pt.	29,900	16,400
10	2.95	0.75	0.03	pt.	36,500	26,000
11	5.95	5.0	0.35	line	6,900	7,200
12	5.95	8.0	2.8	line	10,800	8,600
13	5.95	5.0	2.8	line	28,300	24,800
14	5.95	5.0	2.8	line	21,400	25,500
15	2.95	2.5	0.35	line	40,700	18,000
16	2.95	2.5	0.35	line	41,900	18,600
17	2.95	5.0	0.21	line	3,500	4,200
18	2.95	3.0	2.8	line	plastic yield	53,400
19	5.95	1.5	0.21	line	52,500	39,100
20	16.0	3.0	0.03	pt.	820	500
21	16.0	1.5	0.03	pt.	14,300	6,200
22	16.0	1.0	0.03	pt.	9,400	4,700
23	16.0	1.0	0.03	pt.	26,000	8,100
24	16.0	1.5	0.06	pt.	6,400	3,600
25	16.0	1.25	0.06	pt.	16,900	8,900
26	2.95	8.0	0.35	line	1,300	1,400
27	2.95	8.0	0.35	line	1,300	1,800
28	2.95	1.5	0.05	pt.	10,100	14,700
29	2.95	1.5	0.05	pt.	13,900	18,600
30	5.95	3.0	0.40	pt.	18,600	20,000
31	5.95	3.0	0.40	pt.	16,800	18,800

depth as the center of the pipe. This out-of-service length of pipe was tested with no internal pressure on the first three tests, and with a pressure of 300 psig for the last five tests. Typical strain data recorded in the unpressurized full-scale experiments are shown in Figure 38 for Test No. 3 in which three circumferential and three longitudinal measurements were made. Note that the character of these time histories are very similar to those from the model experiments shown earlier except that time durations are longer.

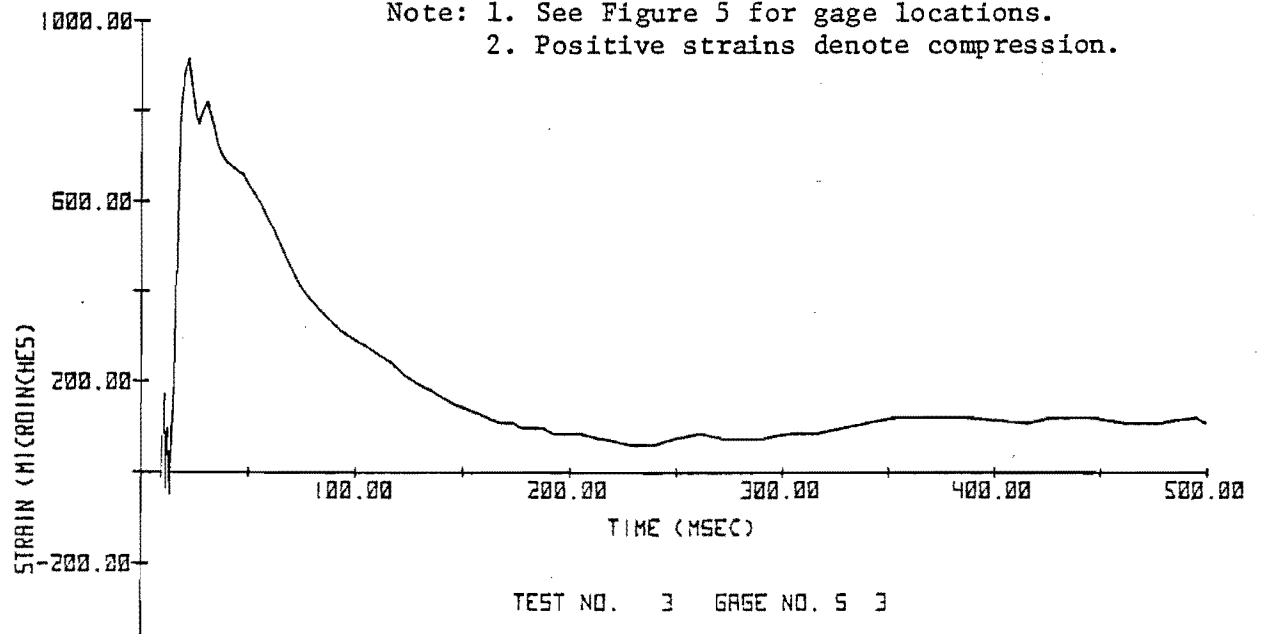
For the pressurized tests, the recorded strains for each test were also blast-induced because each strain channel was reset before each test. However, the strain gages had been recorded during the pressurization process to determine the strain levels seen by each strain gage due to the internal pressure only right after pressurization. The three circumferential channels recorded an average tensile strain of about $310\mu\epsilon$ and the three longitudinal channels an average tensile strain of about $75\mu\epsilon$. Allowing for some restraint to the pipe by the soil around it, these strains agree well with the levels that would be expected from the 300 psig internal pressure. Therefore, these strains can be superimposed on those resulting from the blast loading to obtain a composite strain-time history. For example, Figure 39 shows the strains recorded on Test No. 6 from the blast only while Figure 40 shows the composite strains due to the blast and internal pressure load.

The blast strain measurements made in the Kansas City full-scale experiments are listed in Table X by test number. The size of the single charge used and its distance to the pipe are also given. The circumferential and longitudinal strains are identified by subscripts which are defined in Figure 5. In a similar way, the combined peak strains from the blast loading and the 300 psig internal pipe pressure are presented in Table XI for Test Nos. 4-8. The absolute value of the maximum stresses due to the blast loading only computed from the measured peak strains are listed in Table XII. These data points are also used in developing the solution for predicting pipe response to buried detonations in later sections of this report.

Finally, the last set of strain measurements were made on a Texas Gas Transmission Corporation 30-in. operational line with a specified minimum yield strength of 52,000 psi located in Kentucky. This pipe was strain gaged in a similar fashion as the Kansas City line. Circumferential and

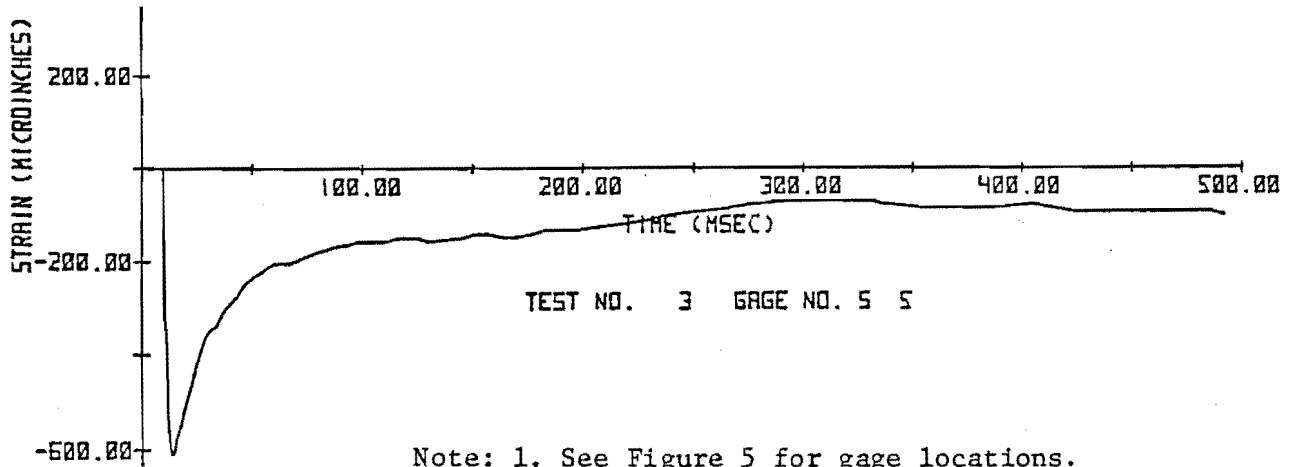
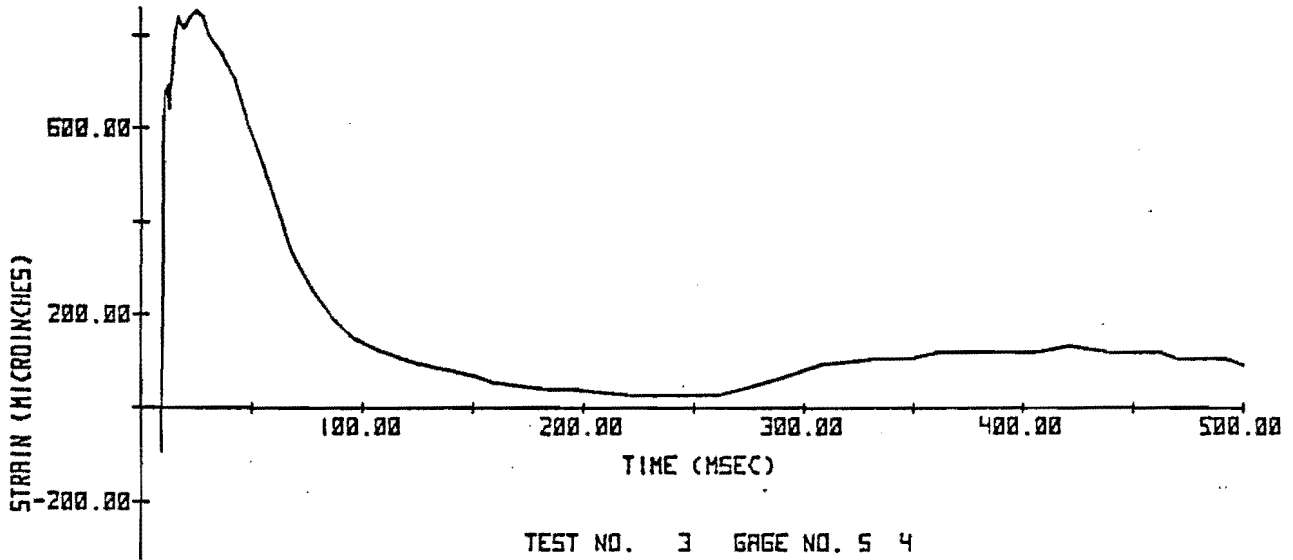


Note: 1. See Figure 5 for gage locations.
 2. Positive strains denote compression.

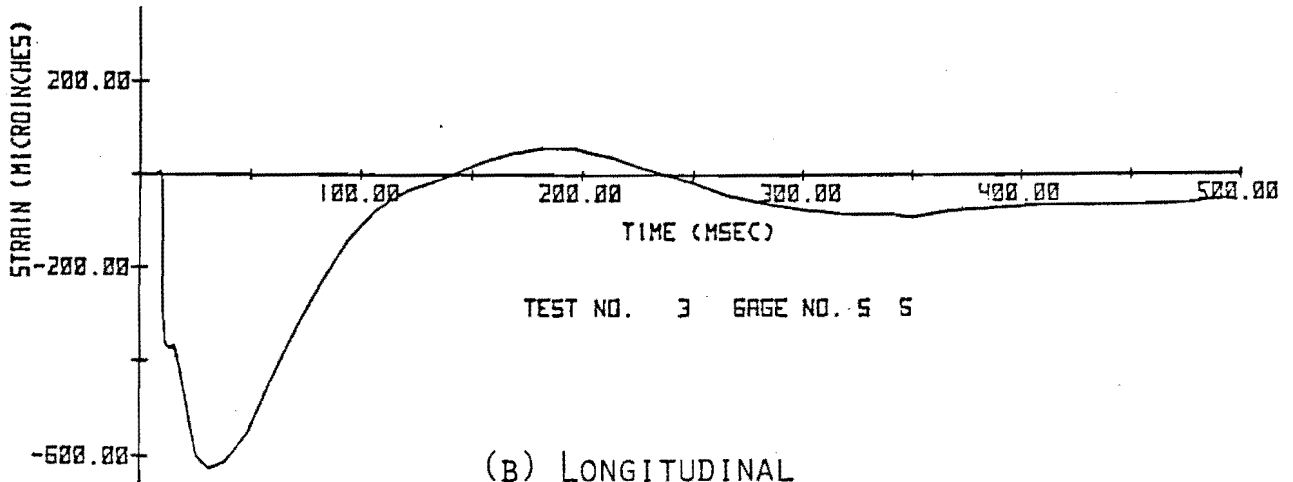


(A) CIRCUMFERENTIAL

FIGURE 38. BLAST STRAIN RECORDS FOR 24-INCH PIPE

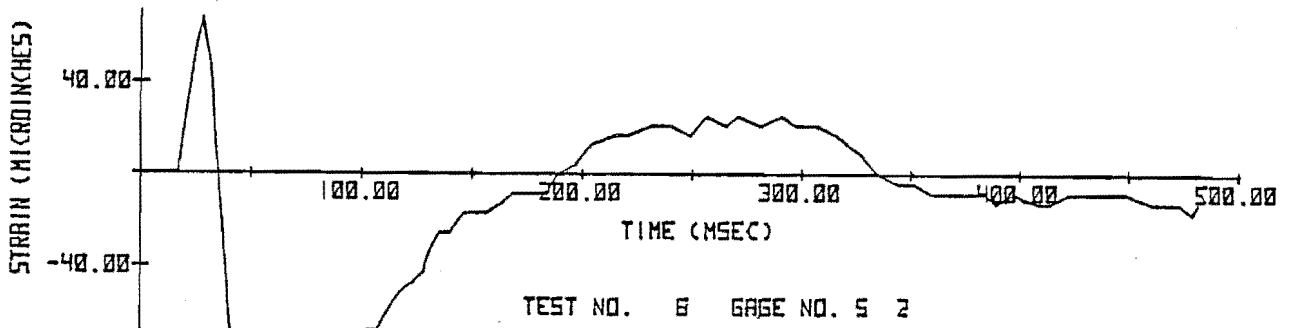
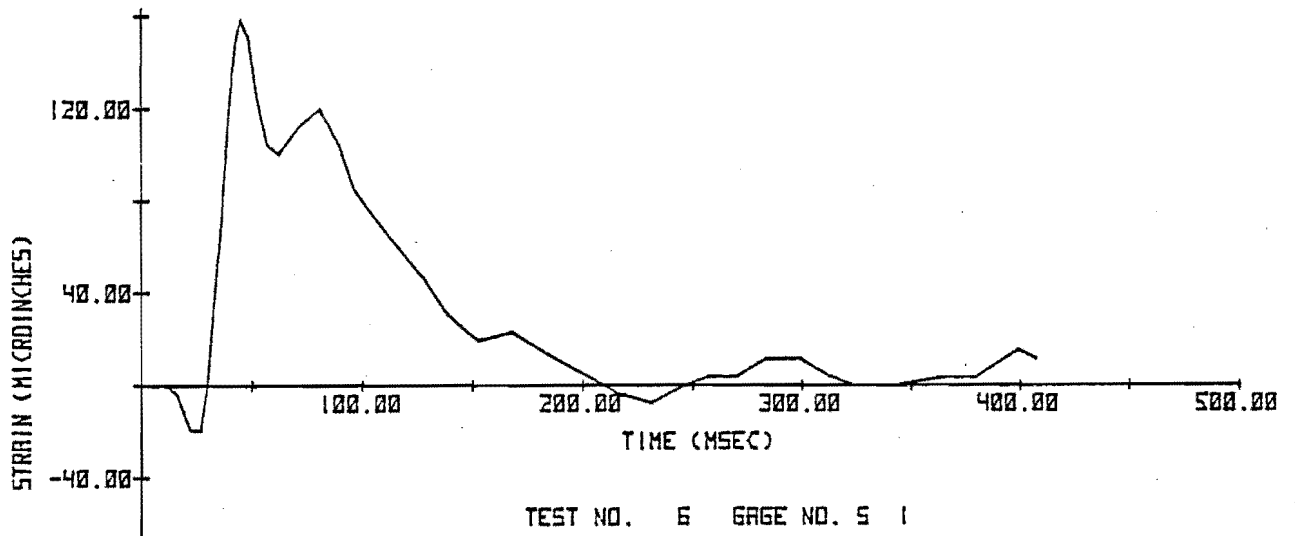


Note: 1. See Figure 5 for gage locations.
 2. Positive strains denote compression.

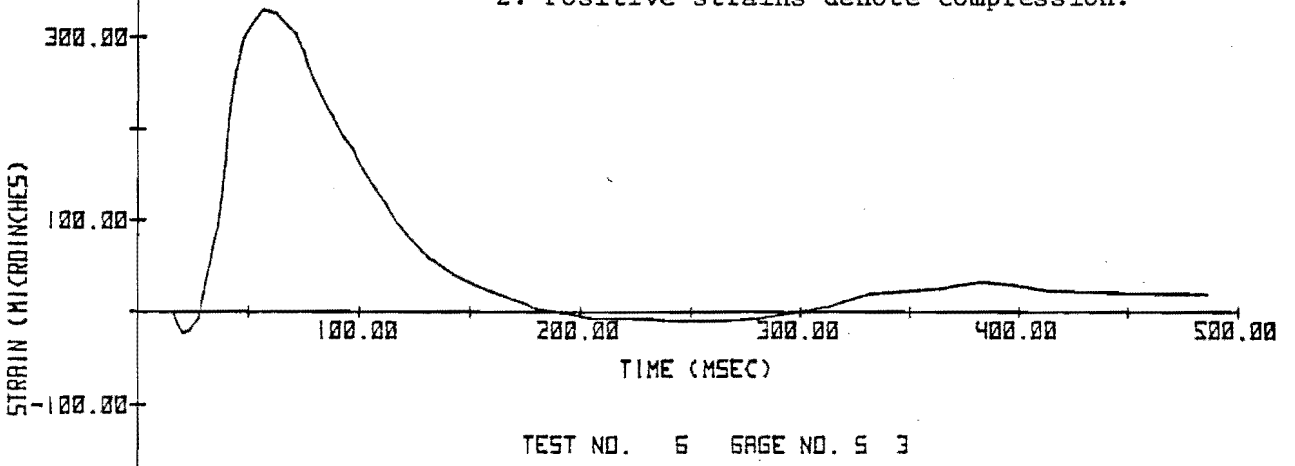


(B) LONGITUDINAL

FIGURE 38. (CONTINUED)

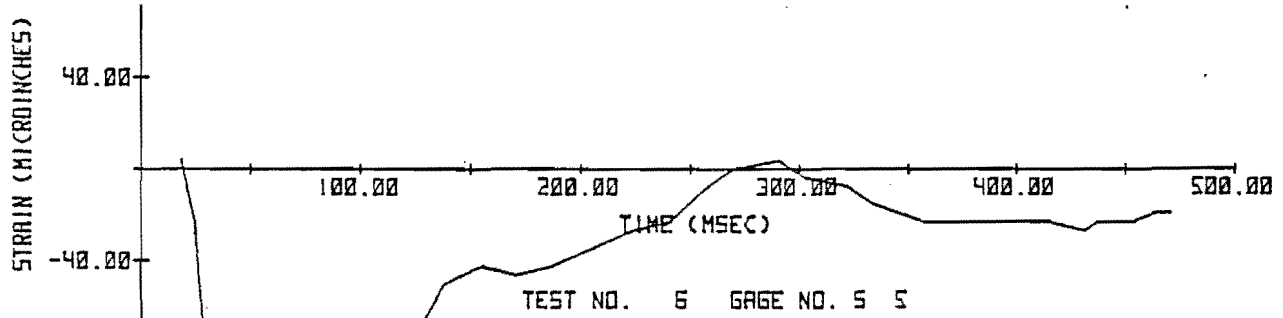
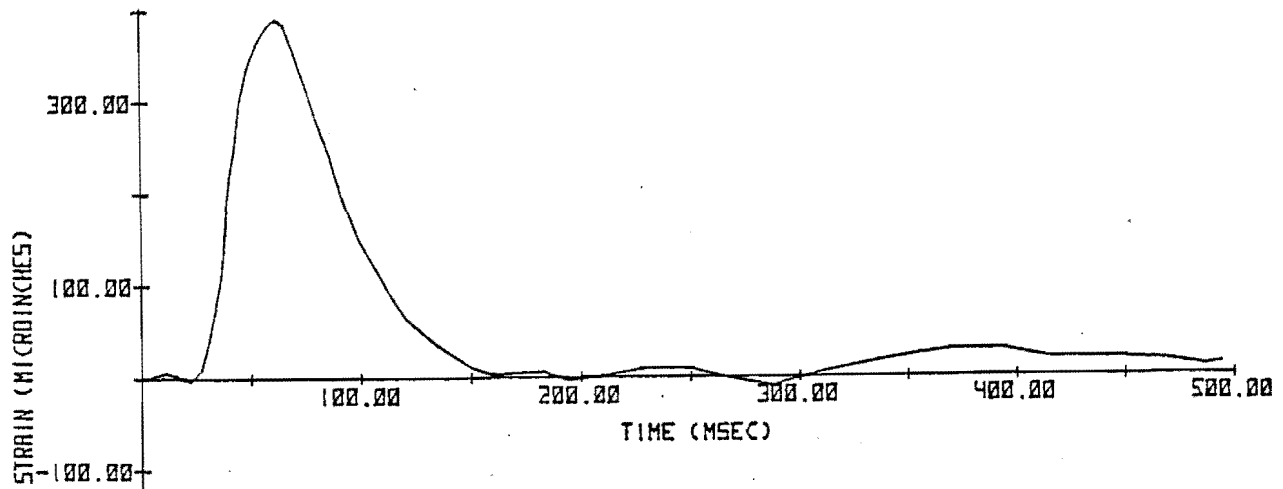


Note: 1. See Figure 5 for gage locations.
 2. Positive strains denote compression.

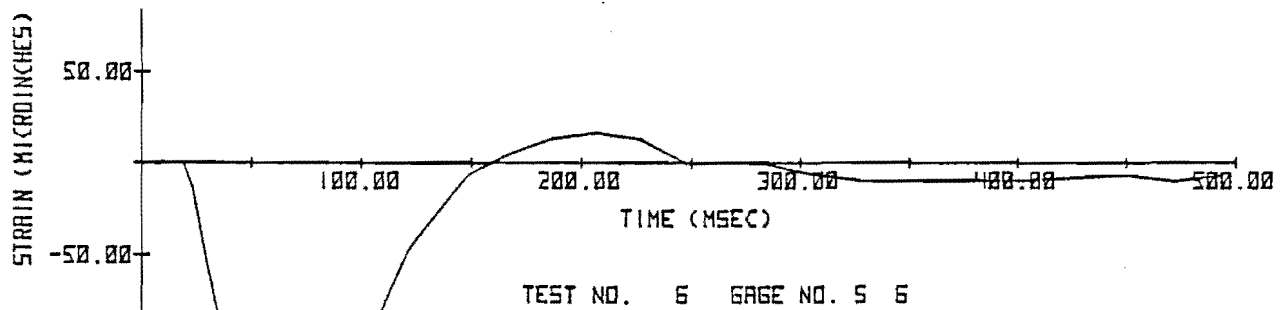


(A) CIRCUMFERENTIAL

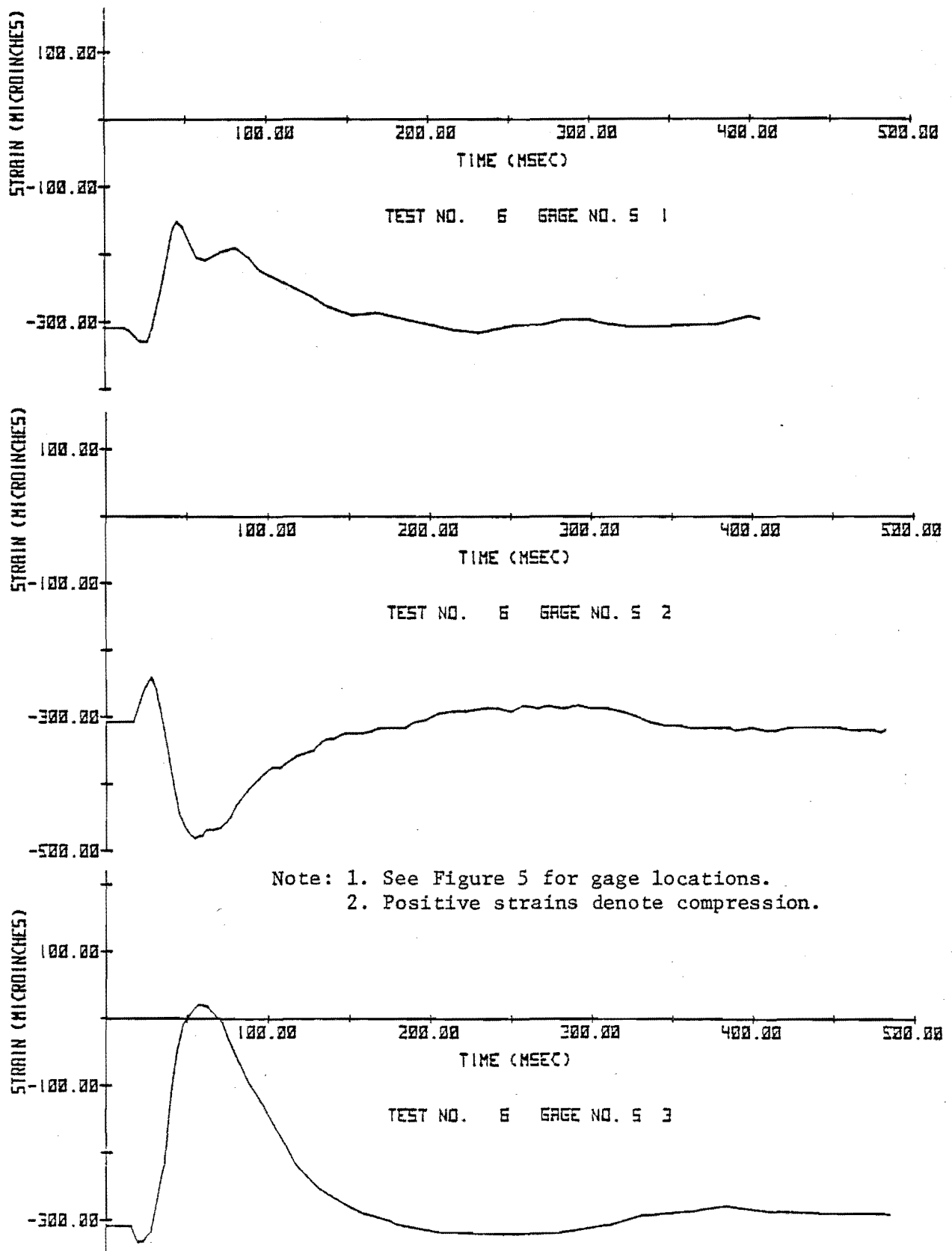
FIGURE 39. TEST No. 6 BLAST STRAINS ON 24-IN. PIPE



Note: 1. See Figure 5 for gage locations.
 2. Positive strains denote compression.

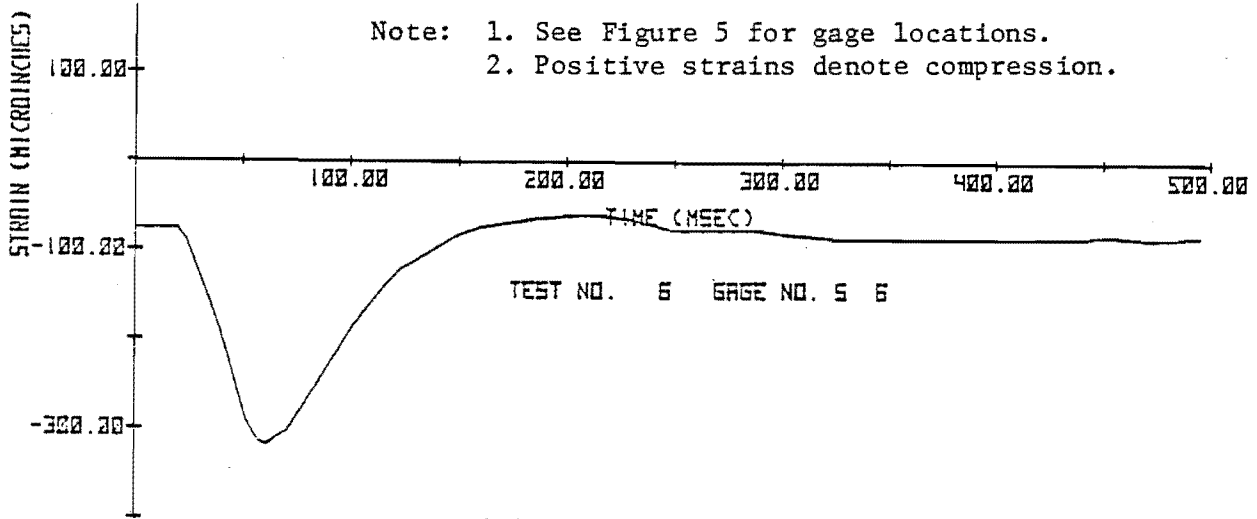
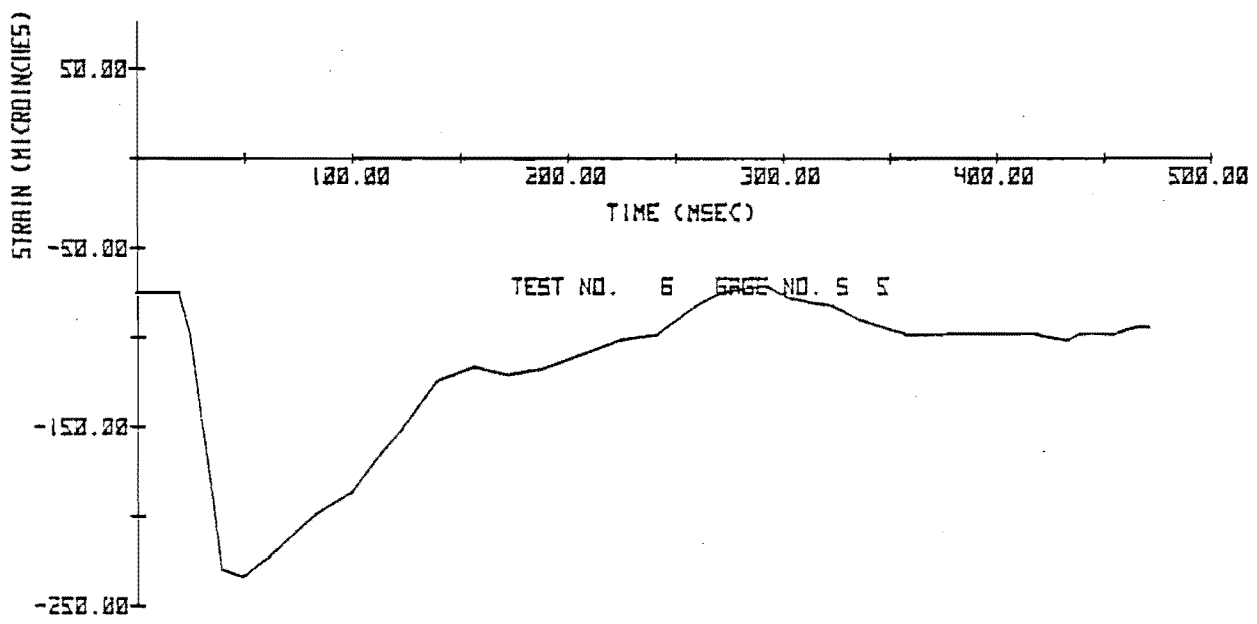
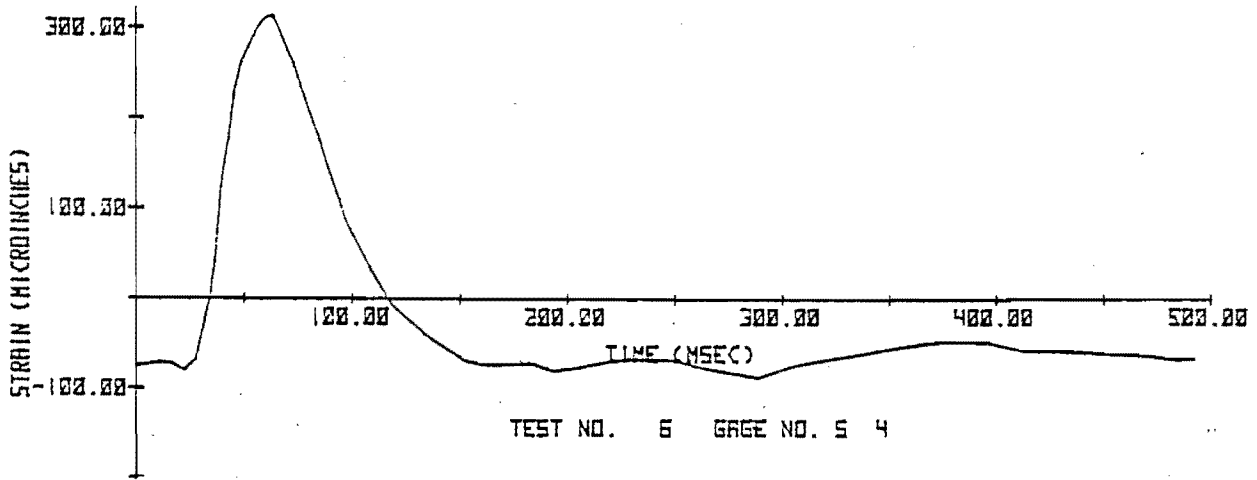


(B) LONGITUDINAL
 FIGURE 39 (CONTINUED)



(A) CIRCUMFERENTIAL

FIGURE 40. TEST NO. 6 BLAST AND INTERNAL PRESSURE STRAINS ON 24-INCH PIPE



Note: 1. See Figure 5 for gage locations.
 2. Positive strains denote compression.

(B) LONGITUDINAL
 FIGURE 40, (CONTINUED)

$h = .312$

TABLE X. MAXIMUM STRAINS FROM BLAST LOADING ON 24-IN. PIPE

Test No.	Charge Weight (lb)	Standoff Distance (ft)	Circumferential			Longitudinal		
			S1 (μE)	S2 (μE)	S3 (μE)	S4 (μE)	S5 (μE)	S6 (μE)
1	15	9.4	219	-268	352	360	-229	-309
2	5	6.0	856	-974	--	--	-933	--
3	5	6.0	708	-586	917	854	-615	-628
4	15	13.0	264	-214	537	588	-303	-786
5	5	9.0	248	-219	404	454	-280	-492
6	15	13.0	159	-175	330	390	-159	-243
7	15	13.0	150	-149	274	336	-183	-317
8	15	6.0	-2800	1352	3815	5865	-1283	-6783

Positive strains denote compression

TABLE XI. COMBINED BLAST AND INTERNAL PRESSURE STRAINS

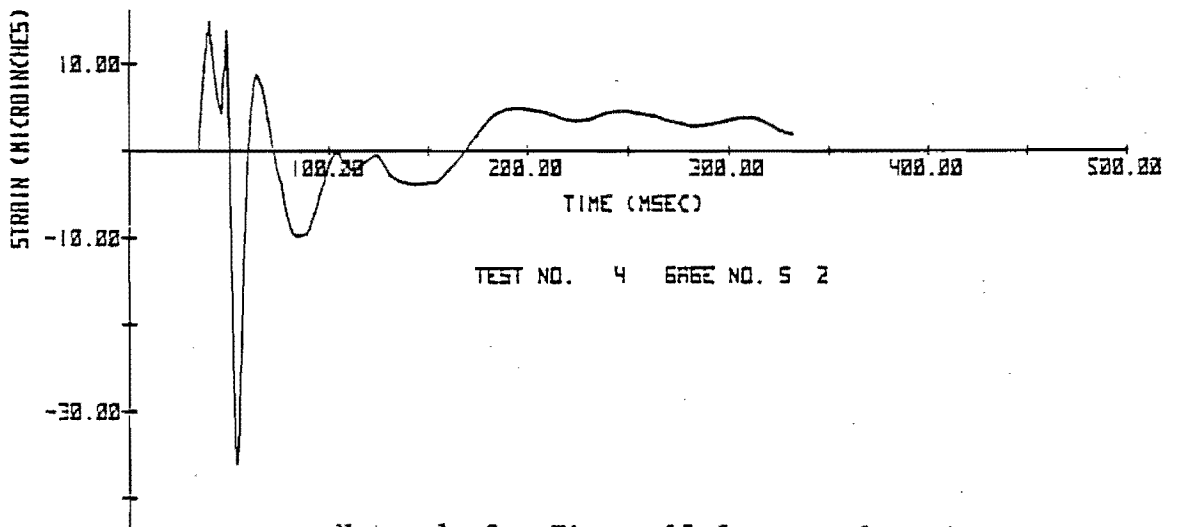
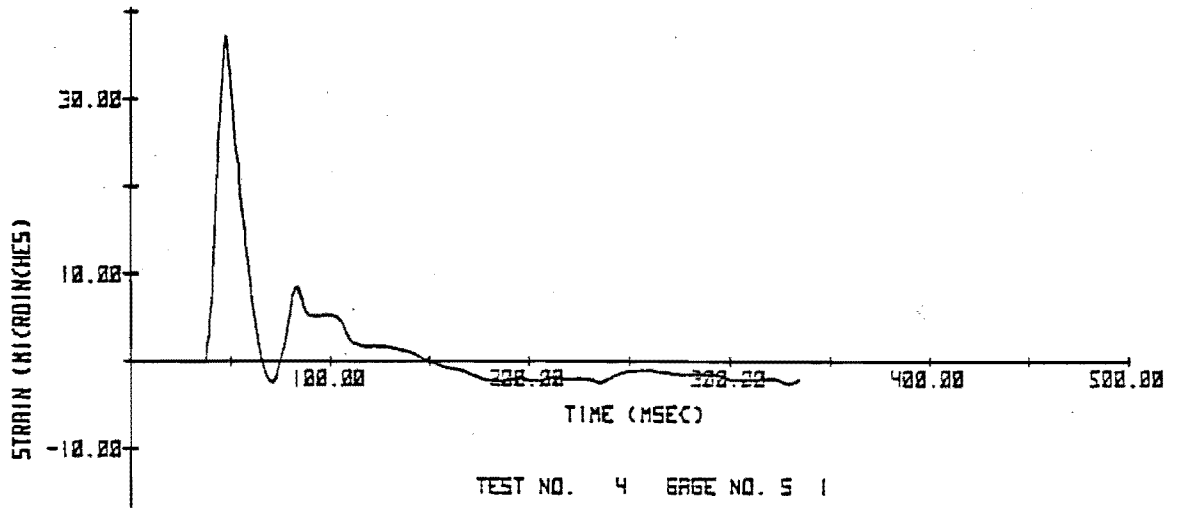
Test No.	Circumferential			Longitudinal		
	S1 (μE)	S2 (μE)	S3 (μE)	S4 (μE)	S5 (μE)	S6 (μE)
4	-405	-531	-342	513	-378	-861
5	-429	-534	-332	379	-355	-567
6	-335	-476	-348	315	-234	-318
7	-383	-470	-342	261	-258	-392
8	-2,875	-1,052	3,478	5,790	-1,358	-6,858

TABLE XII. MAXIMUM BLAST STRESSES ON 24-IN. PIPE

Test No.	Charge Weight (lb)	Standoff Distance (ft)	Circumferential	Longitudinal
			Stress (psi)	Stress (psi)
1	15	9.4	10,600	10,800
2	5	6.0	29,200	28,000
3	5	6.0	27,500	25,600
4	15	13.0	16,100	23,600
5	5	9.0	12,100	14,800
6	15	13.0	9,900	11,700
7	15	13.0	8,200	10,000
8	15	6.0	Beyond elastic limit	

measurements were again made as defined in Figure 15. This pipeline was loaded with single explosive charges buried to the same depth as the pipe and tested at a reduced pressure of 400 psig. Normal operation pressure is about 800 psig. The data records obtained were very good in spite of the bad weather encountered during this part of the program and of the generally lower strain amplitudes recorded due to the smaller blast loading used to insure the line would be in no danger of getting close to yield from the combined stresses. The signature of the time histories behaved pretty much as expected and were similar to those recorded at SwRI and Kansas City. For example, Figure 41 shows the strains recorded in Test No. 4. As in the previous test data, gages S1 and S2 produced similar traces of opposite polarity. Likewise S4 and S6 recorded mirror image traces.

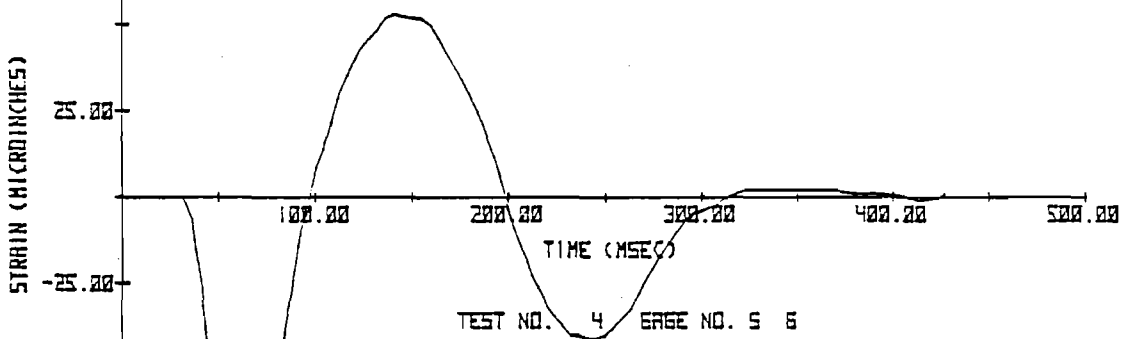
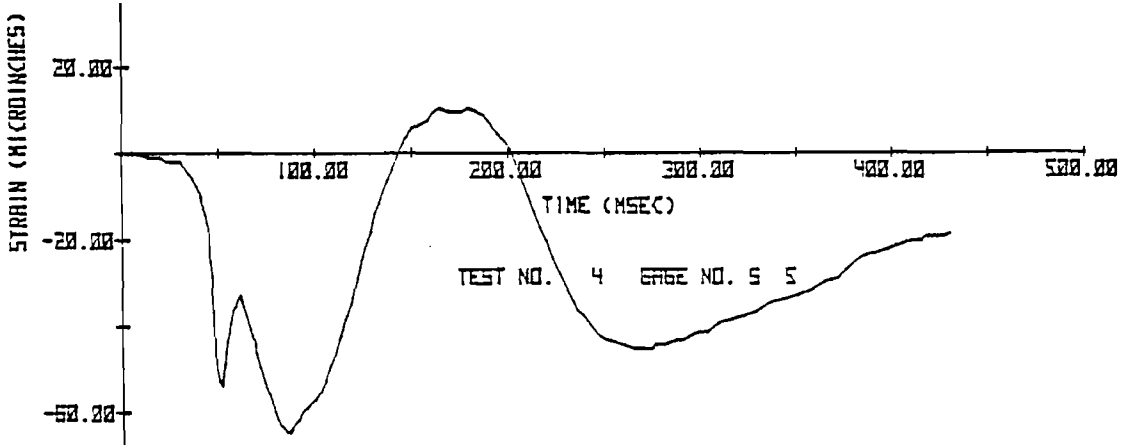
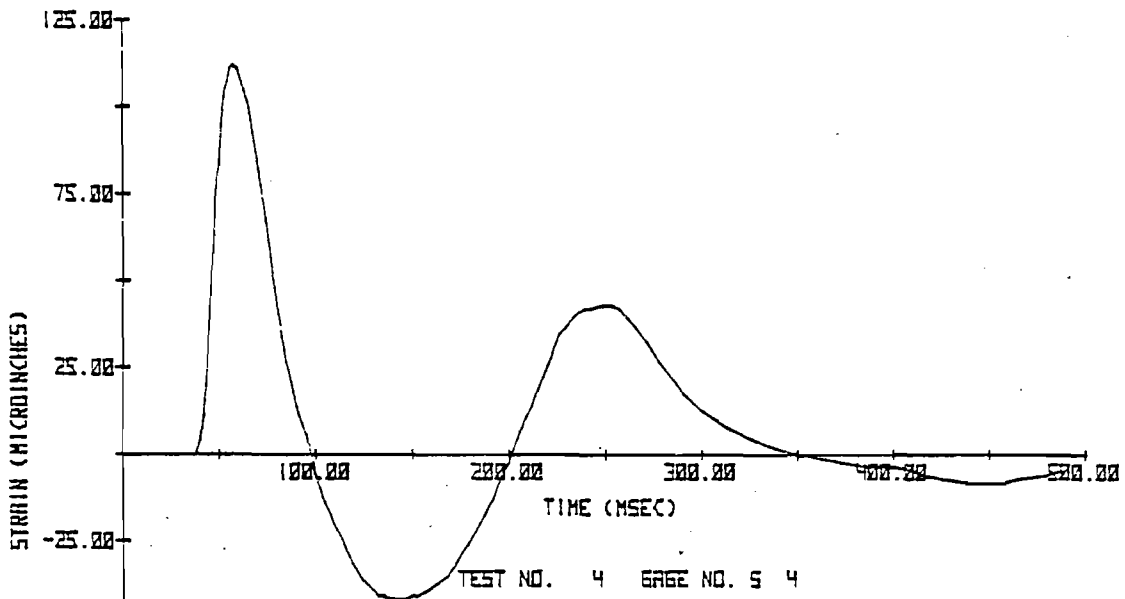
The peak strains recorded from the loading of the 30-in pipe by single explosive detonations are listed by the test number on Table XIII. Each strain channel corresponds to the locations shown in Figure 15. The absolute value of the stresses computed from the peak strains measured are listed in Table XIV. The data presented in this table were also manipulated and used to develop the theoretical and empirical stress solution presented later in this report.



Note: 1. See Figure 15 for gage locations.
 2. Positive strains denote compression.

(A) CIRCUMFERENTIAL

FIGURE 41. TEST NO. 4 STRAINS ON 30-INCH PIPE



Note: 1. See Figure 15 for gage locations.
 2. Positive strains denote compression.

(B) LONGITUDINAL
 FIGURE 41 (CONTINUED)

h = 344

TABLE XIII. MAXIMUM BLAST STRAINS MEASURED ON 30-INCH PIPE

Test No.	Charge Weight (lb)	Standoff Distance (ft)	Circumferential			Longitudinal			
			S1 (μϵ)	S2 (μϵ)	S13 (μϵ)	S4 (μϵ)	S5 (μϵ)	S6 (μϵ)	
1	23.7	5	15	101	-34	--	126	-88	-166
2	25.6	4	15	40	-31	--	73	-40	-80
3	16.9	3	9	251	-195	186	389	-141	-235
4	28.2	3	15	37	-36	39	112	-64	-123

TABLE XIV. MAXIMUM BLAST STRESSES ON 30-INCH PIPE

Test No.	Charge Weight (lb)	Standoff Distance (ft)	Circumferential Stress (psi)	Longitudinal Stress (psi)
1	5	15	3,000	5,000
2	4	15	1,200	2,400
3	3	9	7,500	11,700
4	3	15	1,200	3,700

V. GROUND MOTION RELATIONSHIPS

Introduction

New empirical relationships were developed for predicting maximum radial soil velocity and displacement when buried explosive charges are detonated in soil or rock. These relationships are needed because the ground motion defines the forcing function applied to a buried pipe from blasting. In addition, some state laws have a safe blasting criteria for any structure (buildings, pipes, houses, etc.) which is based on limiting the maximum soil particle velocity to less than 2.0 in/sec. This statement does not say we agree with the basis for such laws; however, these laws are used. The relationships which will be discussed for explosive point sources are given by Equation 30, radial displacement, and Equation 31, radial particle velocity.

$$\frac{X}{R} \left(\frac{p_o}{\rho c^2} \right)^{1/2} = \frac{0.04143 \left(\frac{W}{\rho c^2 R^3} \right)^{1.105}}{\tanh^{1.5} \left[18.24 \left(\frac{W}{\rho c^2 R^3} \right)^{0.2367} \right]} \quad (30)$$

$$\frac{U}{c} \left(\frac{p_o}{\rho c^2} \right)^{1/2} = \frac{6.169 \times 10^{-3} \left(\frac{W}{\rho c^2 R^3} \right)^{0.8521}}{\tanh \left[26.03 \left(\frac{W}{\rho c^2 R^3} \right)^{0.30} \right]} \quad (31)$$

where

- X = maximum radial soil displacement
- U = peak radial soil particle velocity
- R = standoff distance
- W = explosive energy release (use radio-chemical energy release for nuclear sources)
- ρ = mass density of the soil or rock
- c = seismic P-wave velocity in the soil or rock
- p_o = atmospheric pressure

Any self consistent set of units may be used in applying these relationships for all terms; $X/R (p_o/\rho c^2)^{1/2}$, $U/c (p_o/\rho c^2)^{1/2}$, and $W/\rho c^2 R^3$ are nondimensional. Experimental test data on explosive sources ranging from 0.03 lbs to 19.2 Kt (nuclear blast equivalency) will be used in subsequent discussion to demonstrate the validity of these relationships. The data used in substantiating the validity of these results cover nine orders of magnitude in scaled explosive energy release, the quantity $W/\rho c^2 R^3$ from approximately 4.4×10^{-11} to 4.4×10^{-2} .

Major differences separate these empirical equations from others that predict ground motions. This new procedure is not log linear; test results cover more orders of magnitude, and a coupling term $(\rho c^2/p_o)^{1/2}$ is divided into the scaled displacement and velocity. The presence of atmospheric pressure in the prediction relationships does not mean atmospheric pressure is a physical phenomena influencing the results. The quantity ρc^2 is a measure of the compressibility of the shock propagation media. Hence, the quantity p_o is a standard (compressibility of air) and introduces empirically relative compressibilities for different media such as soil and rock. This point will be elaborated later.

Historical Background

Two different groups of ground shock propagation procedures have been used in the past for empirical relationships interrelating charge weight, standoff distance and ground motion. The approach generally used by statisticians was to propose a propagation law of the form

$$A = K W^{n_W} R^{n_R} \quad (32)$$

where

- A = is the peak amplitude for either velocity or displacement
- n's = are constant exponents
- K = is a constant

This format is popular because the logarithm can be taken of both sides to obtain:

$$[\ln A] = [\ln K] + n_W [\ln W] + n_R [\ln R] \quad (33)$$

Because this equation is linear, a least squares curve fit can be made to obtain the three coefficients $\ln K$, n_W , and n_R . The weakness of this statistical approach is that this format is assumed regardless of what happens physically. The resulting equations are dimensionally illogical. A serious problem is the statistician's use of an incomplete expression. Other parameters enter the ground shock propagation problem, especially soil properties, which are ignored. Because these properties are ignored, the definition of the problem is incomplete, and the results do not represent a general solution.

Using the statistical approach, various investigators obtain different results depending upon the amount and range of their data. Typical values found in the literature^[5-15] have a range for n_W from 0.4 to 1.0 and for n_R from -1 to -2 with A as particle displacement or velocity. This situation arises because investigators use data from different segments of the curve as given by Equations 30 and 31).

The second group of individuals, usually these associated with the Atomic Energy Commission, present their results in the format:

$$U \propto \left(\frac{W^{1/3}}{R} \right)^{n_W} \quad (34)$$

$$\frac{X}{W^{1/3}} \propto \left(\frac{W^{1/3}}{R} \right)^{n_X} \quad (35)$$

This approach is an extension of the Hopkinson-Cranz scaling law for air blast waves, and is a dimensional version of a model analysis. If soil properties such as ρ and c are treated as constants; and dropped from the resulting pi terms in a model analysis, the dimensional versions as presented in Equations (34) and (35) are obtained. An example of curve fits for displacement and velocity to Equations (34) and (35) is given in Murphey.^[15]

$$\frac{U R^{1.65}}{W^{0.55}} = \text{constant} \quad (36)$$

$$\frac{X R^{1.5}}{W^{0.833}} = \text{constant} \quad (37)$$

Murphey's data were all obtained for chemical explosive detonations in Halite (salt domes) and cover scaled charge weight over three orders of magnitude. The authors certainly agree with Murphey and other AEC investigators on using modeling principles. These curve fits will be expanded by including data obtained over nine orders of magnitude and by including an additional parameter.

Problems With The Conventional Modeling Approach

If the soil properties ρ and c are listed in a model analysis together with the explosive energy release W , standoff distance R , and either of the response parameters U or X , then two dimensionless pi terms are obtained for either displacement or velocity as in the following functional relationships:

$$\frac{X}{R} = f_X \left(\frac{W}{\rho c^2 R^3} \right) \quad (38)$$

$$\frac{U}{c} = f_U \left(\frac{W}{\rho c^2 R^3} \right) \quad (39)$$

Experienced modelers can readily see that with ρ and c considered as invariant, these equations amount to Equations (36) and (37). No reason exists to presume that the general but unspecified functional format given by Equations (38) and (39) should be log linear. The functional format can be obtained by nondimensionalizing experimental test data and plotting the results provided the analysis is completely defined.

Figures 41 and 42 are plots of scaled deformation and scaled velocity using limited amounts of test data for chemical explosive detonations. The displacement data seen in Figure 42 come from only two sources, References 15 and the test results obtained in this program at the SwRI test site. Murphey (Reference 15) describes two types of Halite experiments. In one group of tests, the soil is in contact with the explosive charge. In another group of tests, 6- to 15-ft cavities placed an air gap between the soil and the explosive charge. These tests described by Murphey called "Cowboy" used 200, 500, and 1000 pound charges. The tests denoted by circles in Figure 42 were conducted in this program at the SwRI test site.

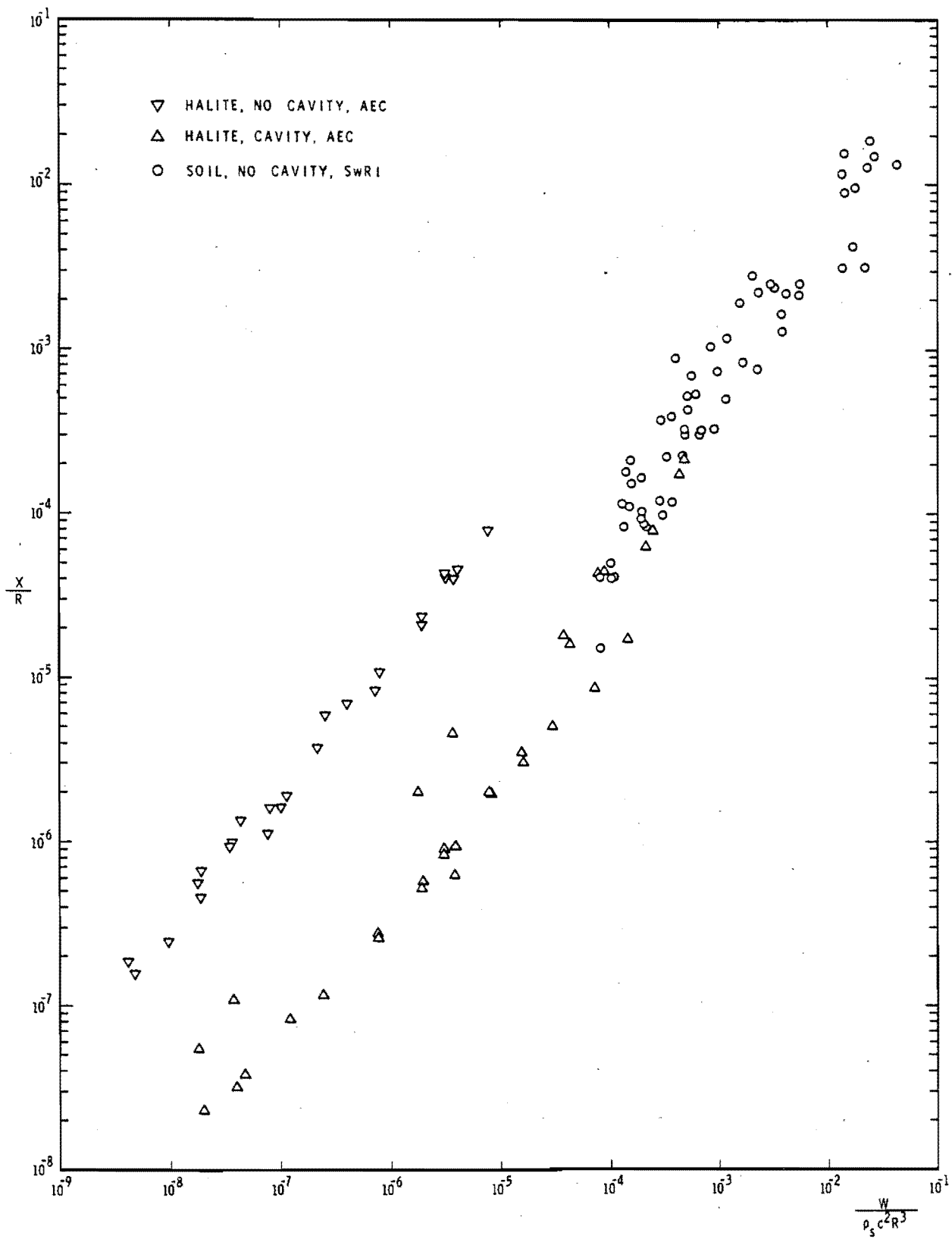


FIGURE 42. GROUND DISPLACEMENT IN ROCK AND SOIL NO COUPLING

All of these tests were in silty clay soils with various moisture contents. The charges ranged from 0.03 to 1.00 lb of explosive. Although more data could be plotted in Figure 42, correlation will not occur. Obviously some phenomena are present in Figure 42 which are not reflected in a solution as given by Equation (38).

The same lack of correlation which became apparent in Figure 42 for displacement is also apparent in Figure 43 for peak particle velocity. An additional compilation of data not contained in Figure 42, has been included in the Figure 43 velocity plot. Harry Nicholls, et al [16] summarize velocities obtained from blasting in stone quarries. If only single explosive source detonations are used in this compilation, approximately 50 data points can be obtained for a variety of charge weights, site locations and standoff distances. In addition to this new data, the peak particle velocity data corresponding to halite, both with and without cavity, and soil tests are included in Figure 43.

Although the data in both Figures 42 and 43 fail to correlate, they do show some systematic tendencies. Increasing values of $W/\rho c^2 R^3$ result in increasing values of scaled ground motion, and the slopes associated with the various data points are almost identical. The figures infer that some phenomena not included in the analysis should be added. In particular, both figures indicate that a different coupling must exist between different soils or rock and the explosive source. Obviously the poorest coupling exists when an air gap or cavity separates the transmitting media from the explosive source as in some of Murphey's halite experiments. Figures 42 and 43 show that the resulting ground motions are less for experiments with a cavity in halite. However, a weak rock, such as halite, should have a better coupling than soil when both are in contact with explosives. Figures 42 and 43 indicate that ground motions are greater for detonations in rock than for similar detonations in soil. From these detonations, a coupling term could be added to Equations (38) and (39) to achieve better correlation.

Addition Of An Impedance Term

The term which was added to either the scaled displacement X/R or the scaled velocity U/c terms was the square root of the soil compressibility relative to a standard compressibility, the compressibility of air. This

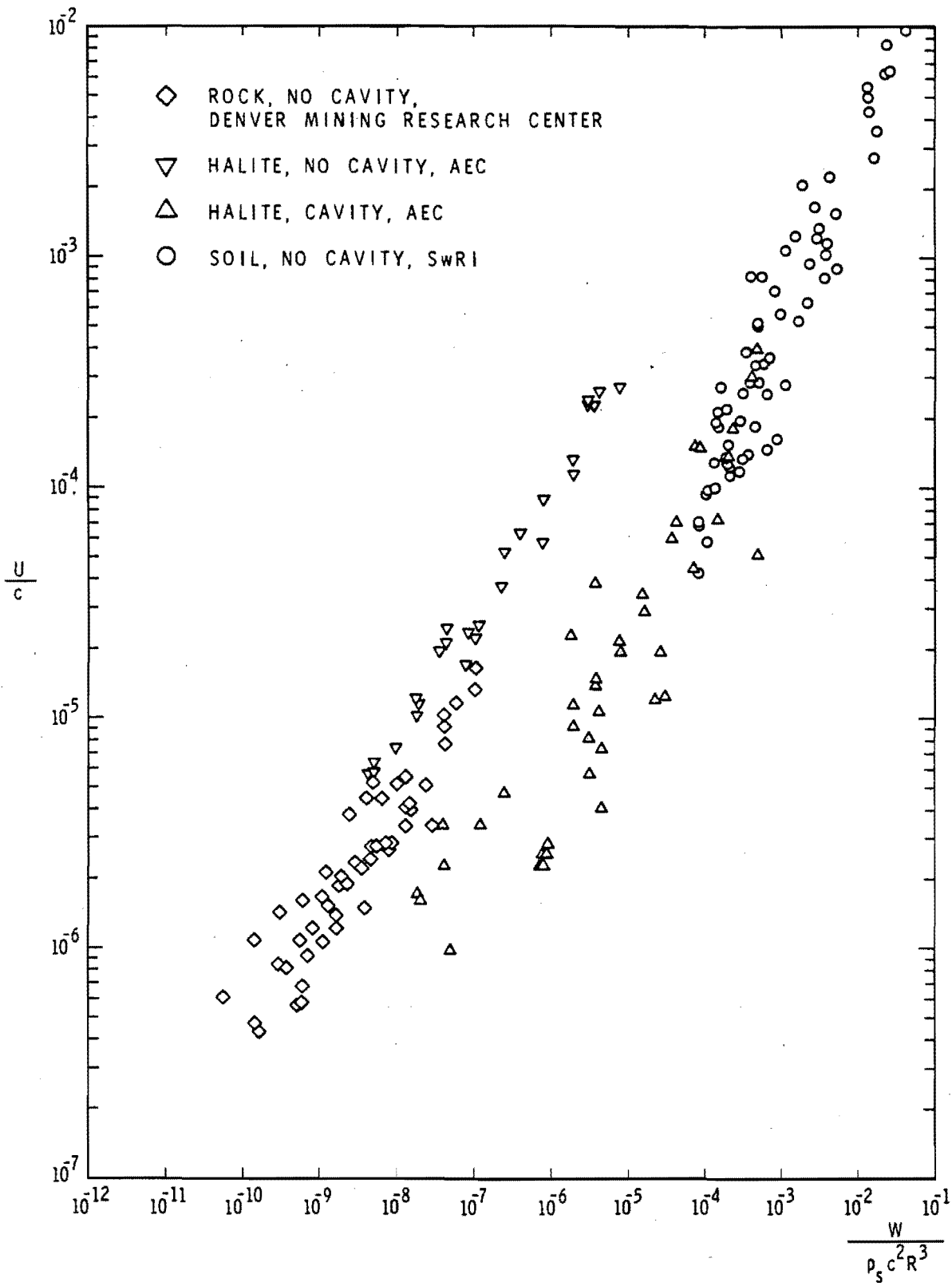


FIGURE 43. PARTICLE VELOCITY IN ROCK AND SOIL NO COUPLING

quantity $\sqrt{\rho c^2/p_o}$ was divided into the nondimensionalized ground motions to obtain the functional equations, (40) and (41).

$$\frac{X}{R} \left(\frac{p_o}{\rho c^2}\right)^{1/2} = f_{X/R} \left(\frac{W}{\rho c^2 R^3}\right) \quad (40)$$

$$\frac{U}{c} \left(\frac{p_o}{\rho c^2}\right)^{1/2} = f_{U/c} \left(\frac{W}{\rho c^2 R^3}\right) \quad (41)$$

Creation of the terms $(X/R) (p_o/\rho c^2)^{1/2}$ and $(U/c) (p_o/\rho c^2)^{1/2}$ was based entirely on empirical observation. A functional format could also be created by plotting the dependent and independent variables in Equations (40) and (41). In addition to using the no cavity data presented in Figures 42 and 43, the ground motion data obtained in this program at the Kansas City and Kentucky test sites, and additional AEC data were plotted using results from some buried nuclear detonations. The cavity test results in halite were not replotted because this empirical approach does not account for ground shock propagation when charges are placed in cavities.

The AEC data, which were also plotted, come from References 17 and 18. Both soil displacement and maximum particle velocity were reported in Reference [17] on Project Salmon, a nuclear blast yield of 5.3 kilotons; hence, this data will appear in both scaled velocity and displacement plots. Reference [18] is a summary of displacement and acceleration, but not velocity, for numerous large AEC buried detonations. Maximum scaled displacement data are included for such projects as a 19.2 kiloton detonation named Blanca, a 77 ton detonation named Tamalpais, a 13.5 ton detonation named Mars, a 30 ton detonation named Evans, and a 5.0 kiloton detonation named Logan. The writers in References 17 and 18 are not clear; we believe they are quoting equivalent blast yields for nuclear detonations. Test results indicate that for buried nuclear detonations the radio chemical yield is more appropriate than the equivalent air blast yield. The radio chemical yield is twice as great as the equivalent air blast yield, so all of the blast yields listed in this paragraph were doubled before plotting any data points. In addition, the energy W had to be converted to foot pounds of energy by

multiplying explosive weight by $1.7 \times 10^{+6}$ ft-lbs/lb, or the appropriate conversion factor, so the quantity $W/\rho c^2 R^3$ would be nondimensional. The density is a bulk mass (not weight) density, a total density of the media, and c is the seismic P-wave propagation velocity. Other soil data might exist, but only results in which c was measured and reported could be used in this evaluation. Obviously, the gas industry has little interest in nuclear explosions, however, the inclusion of this data emphasizes the broad applicability of these results.

Figures 44 and 45, respectively, are plots of nondimensionalized displacement and nondimensionalized velocity as given by Equations (40) and (41). Because the data appear to collapse into a unique function, these results give a graphical solution. Scatter does exist; however, no experiments or test site appears to yield systematic errors. The range in any test condition is larger than ranges in any previous ground shock propagation reports. The scaled charge weight $W/\rho c^2 R^3$ ranges over nine orders of magnitude from approximately 4.4×10^{-11} to 4.4×10^{-2} . The charge weight itself ranges from 0.03 lb of chemical explosive to the radio chemical yield of 38.4 kilotons in Blanca, a factor of over one billion. The range in soil or rock densities is small because nature offers only a small variation, but the wave velocity c ranges from approximately 500 fps to 15,000 fps, a factor of 30. The soil data measured in this program are at much closer standoff distances to the charge than other results, but the transition does seem to be a continuous one.

The continuous lines placed through the data in Figures 44 and 45 were presented as Equations (30) and (31). Both are the result of "eye-balling" curve fits to the test data. One standard deviation for the test results about either line is approximately $\pm 50\%$. Although straight lines can be curve fit to segments of the results in Figures 44 and 45, the rate of change for either X or U with respect to either W or R varies dependent upon the scaled charge weight $W/\rho c^2 R^3$. These variations are reasonably close to those given by others and discussed in the historical background presented earlier in this section. Closest to the charge where these slopes are greatest, are slightly larger exponents than those which were previously reported; however, the earlier observations did not include data obtained in this study.

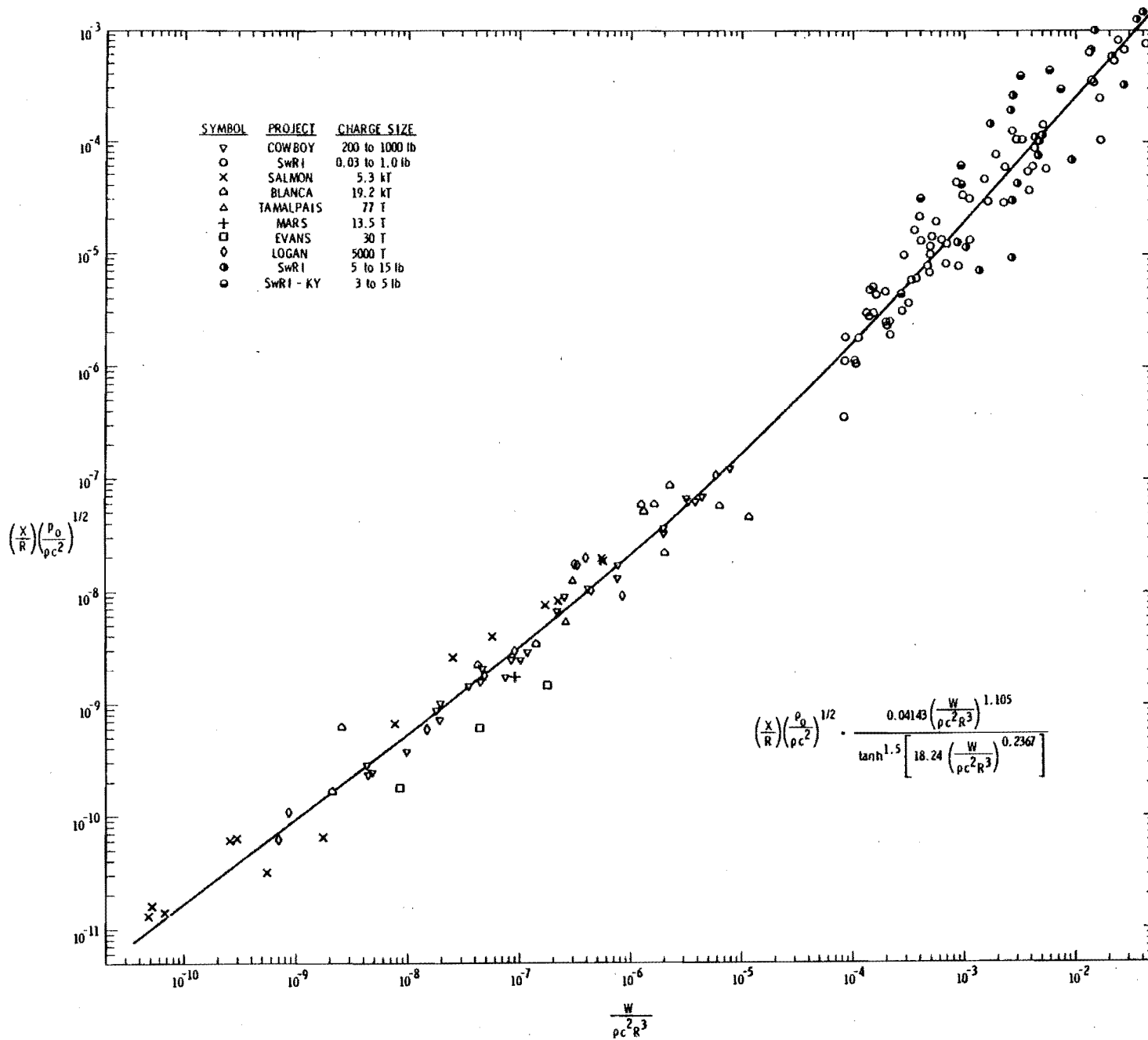


FIGURE 44. COUPLED DISPLACEMENT IN ROCK AND SOIL

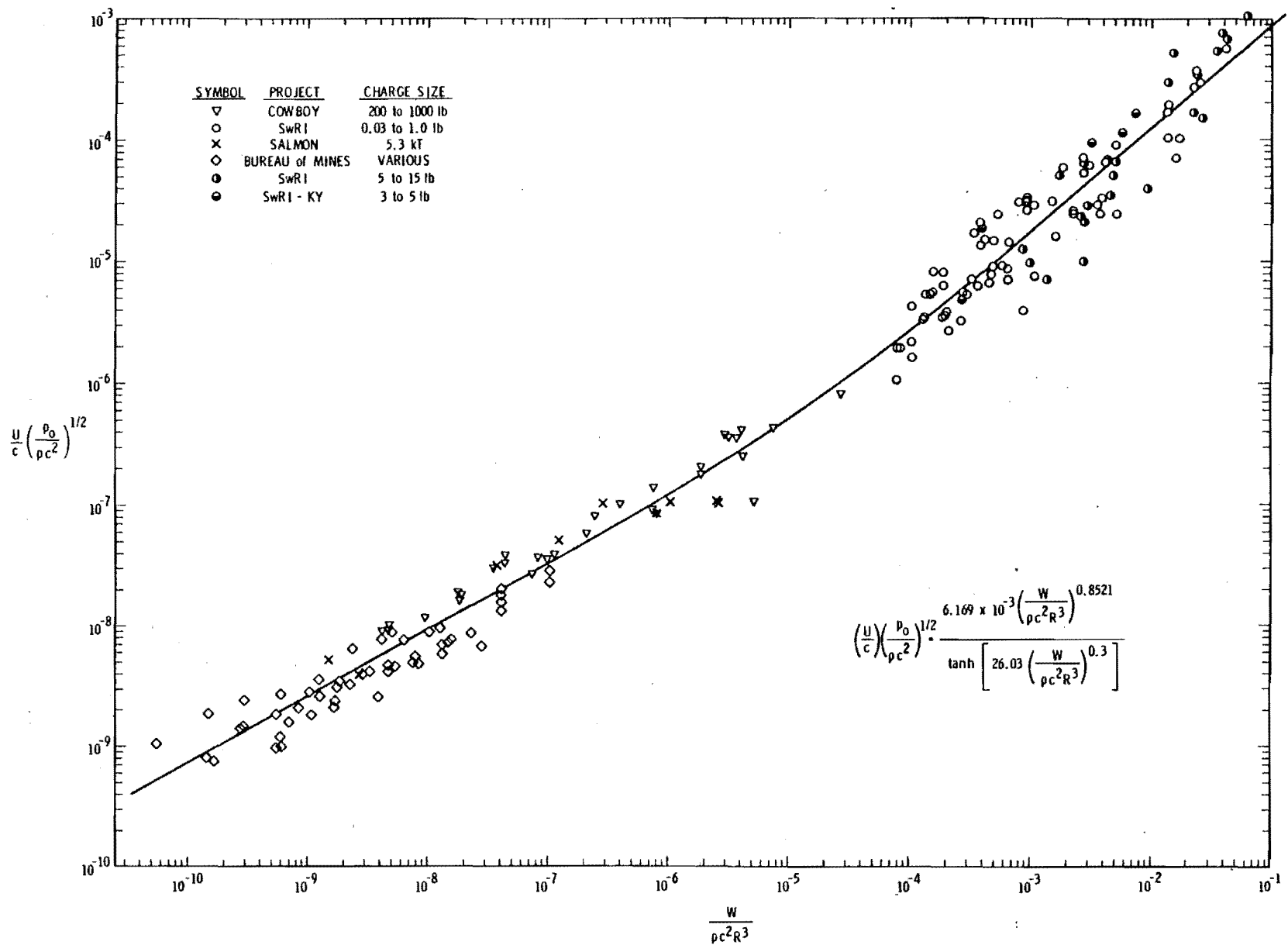


FIGURE 45. COUPLED PARTICLE VELOCITY IN ROCK AND SOIL

Discussion Of Coupling Term

The term $(\rho c^2/p_0)^{1/2}$ which is divided into the scaled velocity term U/c and scaled displacement term X/R is an empirical factor which seems to work. The fact that the compressibility of the soil (ρc^2) is proportional to a modulus of elasticity (E) is related to the compressibility of air, does not mean that atmospheric pressure is actually a parameter physically entering this problem. If these ground shocks were to be propagated on the moon where essentially no atmosphere exists, the amplitudes of the response would be finite rather than infinite as inferred by this solution. The atmospheric pressure p_0 was just a convenient constant which non-dimensionalized ρc^2 .

Perhaps p_0 enters pore pressure considerations and actually does belong in these calculations; however, this is doubtful. Other parameters which have the dimensions of pressure could be considered, but those parameters would essentially have to be constants in all soils. Examples of possible substitutes for p_0 could include: (1) η (the density times the heat of fusion) if one believes significant amounts of energy are dissipated in phase changes, (2) $\rho c_p \theta$ (the heat capacity times an increase in temperature) if thermal heating is important, (3) the energy per unit volume (area under a stress-strain curve) in a hysteresis loop if material damping is important, and (4) others or combinations of all of these effects. No satisfactory explanation has been drawn. The point which makes all hypotheses difficult to accept is that p_0 or its counterpart must be essentially constant in all soil and rock tests. A numerical value other than 14.7 psi does not invalidate this solution; a different constant only translates all curves.

Ground Shock Around Line Sources

Sometimes more than one buried charge is detonated simultaneously. If many equally spaced charges are strung along a line as in explosive ditch digging, the ground motion must be predicted for a line rather than point source. The major difference in these line solutions is that the term $W/\rho c^2 R^3$ becomes $W/\ell/\rho c^2 R^2$ where W/ℓ is the energy release per unit length of line. The ground motion equations in functional format then become:

$$\frac{X}{R} \left(\frac{p_o}{\rho c^2} \right)^{1/2} = f_X \left(\frac{W/l}{\rho c^2 R^2} \right) \quad (42)$$

$$\frac{U}{c} \left(\frac{p_o}{\rho c^2} \right)^{1/2} = f_U \left(\frac{W/l}{\rho c^2 R^2} \right) \quad (43)$$

Experimental test data were needed to complete the functional format for these line source equations. Not every experiment is applicable because these solutions are for infinitely long lines. The standoff distance cannot be much greater than the length of the line, and must be large relative to the spacing between successive charges if an infinitely long line source is to be approximated. In this program a large amount of line source displacement and velocity data were obtained for experiments in soil. Reference 16 supplements the velocity data (no displacement data) at an entirely different range of scaled standoff distances with measurements at the Littleville Dam construction site. Although other multiple detonation data is reported in Reference 16, it cannot be used as line sources because either successive charges were delayed or the standoff distances were much larger than the length of the explosive train.

Figure 46 for radial soil displacement from line sources and Figure 47 for maximum particle velocity from line sources present this data in the formats suggested by Equations (42) and (43). Straight lines have been curve fitted to this data. The functional formats are given by Equations (44) and (45).

$$\frac{X}{R} \left(\frac{p_o}{\rho c^2} \right)^{1/2} = 0.0792 \left(\frac{W/l}{\rho c^2 R^2} \right)^{1.125} \quad (44)$$

$$\frac{U}{c} \left(\frac{p_o}{\rho c^2} \right)^{1/2} = 0.7905 \left(\frac{W/l}{\rho c^2 R^2} \right)^{1.010} \quad (45)$$

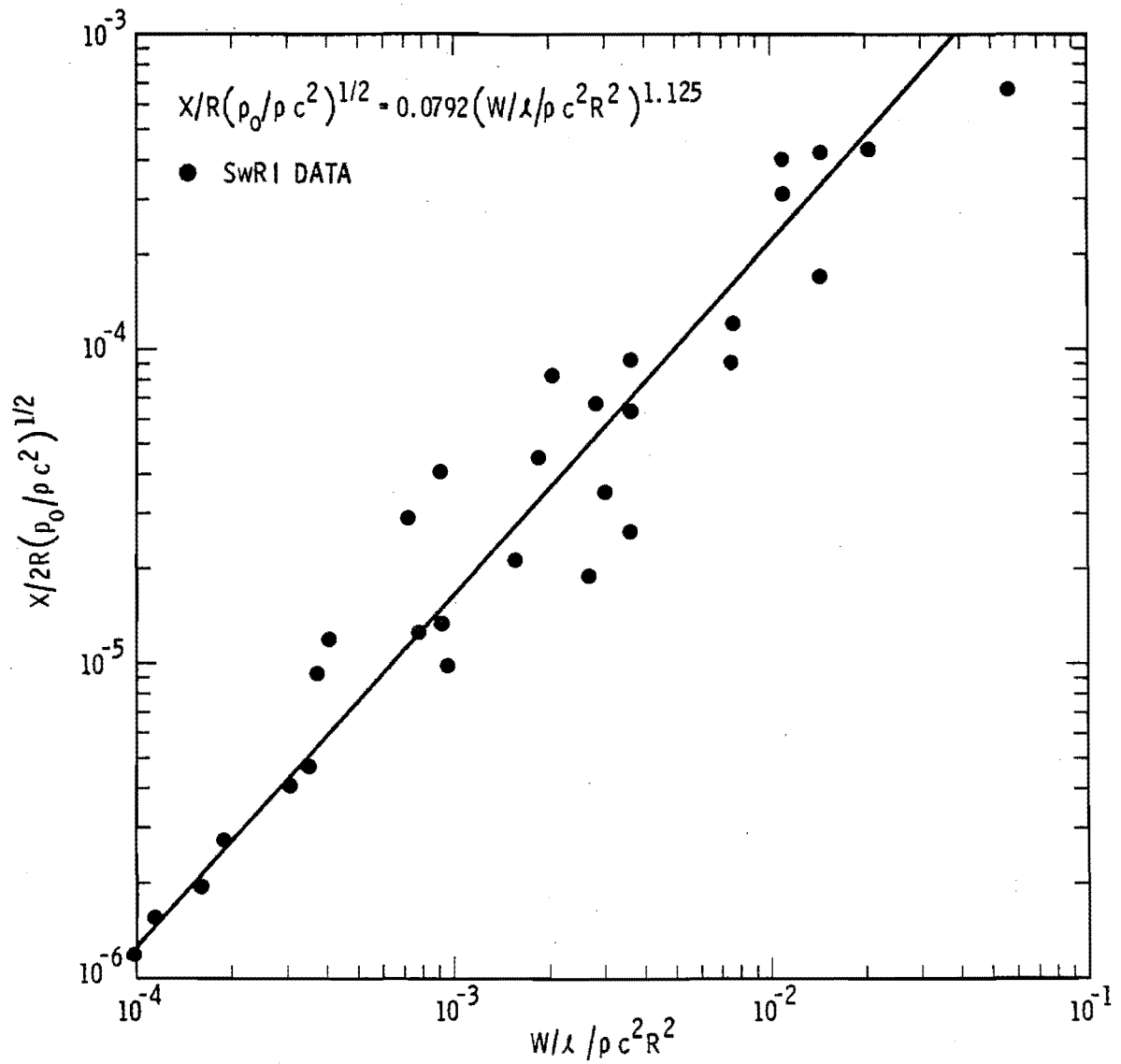


FIGURE 46. RADIAL SOIL DISPLACEMENT FROM LINE CHARGE DETONATIONS

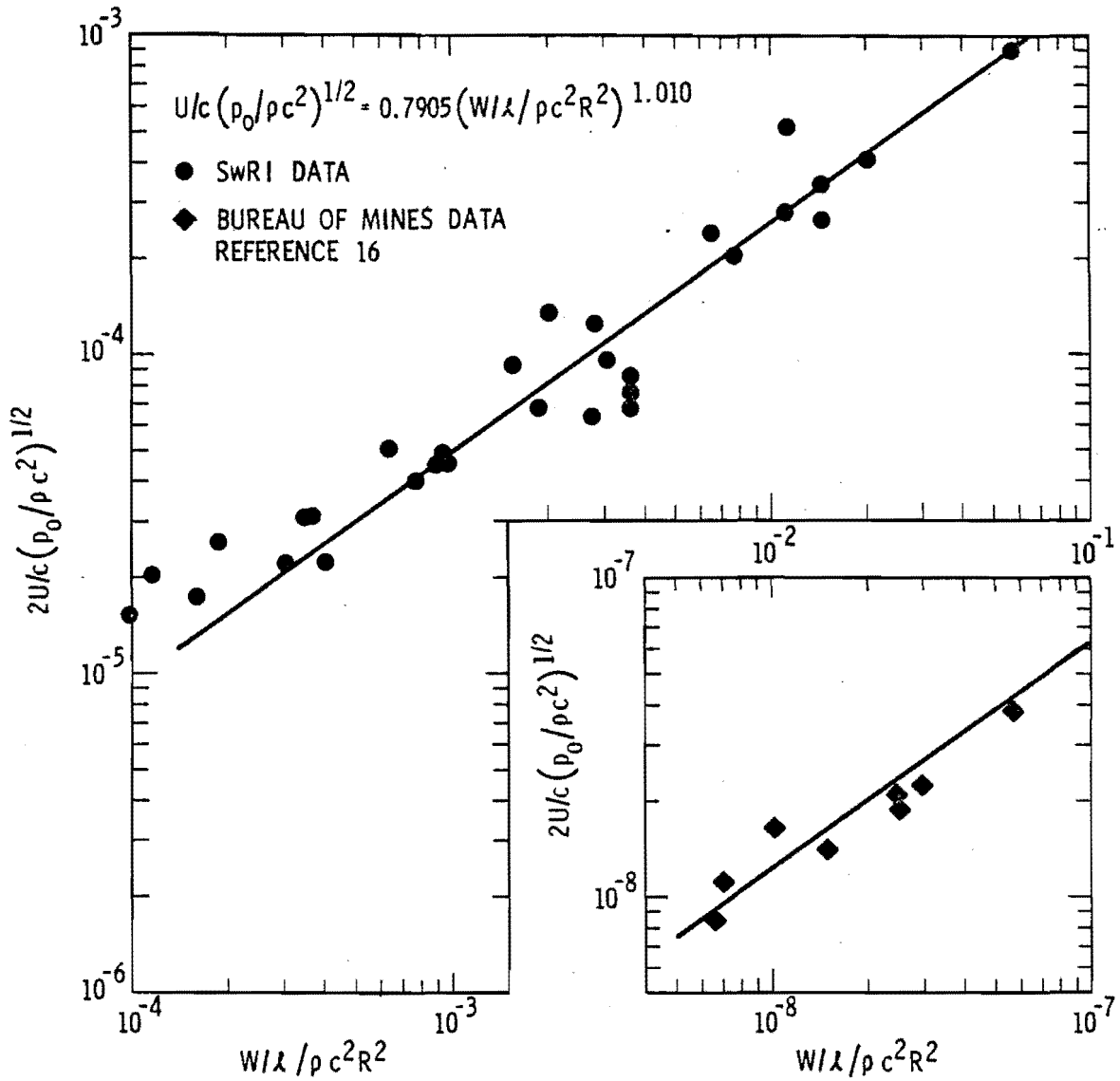


FIGURE 47. MAXIMUM SOIL PARTICLE VELOCITY FROM LINE CHARGE DETONATIONS

Ideally, more data would be available over a wider range in scaled charge weights and at several sites so more confidence would exist in Equations (44) and (45) as prediction equations. The range of validity is not as great, and c was estimated rather than measured at the Littleville Dam site. Equations (44) and (45) although helpful, should be given only tentative acceptance.

Further Approximation For Displacement

The results presented in this discussion are those which will be used to determine the load imparted to a buried pipe. Equations (30) and (31) for buried point sources and Equations (44) and (45) for buried line sources are more accurate than other curve fits which were discussed earlier in this section. One further simplification can be made as an approximation to Equation (30). Over a limited range in $\frac{W}{\rho c^2 R^3}$ of from 1×10^{-7} to 4×10^{-2} , Equation (46) is the most accurate log-linear relationship.

$$\frac{X}{R} \left(\frac{p_o}{\rho c^2} \right)^{1/2} = 0.025 \left(\frac{W}{\rho c^2 R^3} \right) \quad (46)$$

Equation (46) is a fairly accurate prediction equation. When in error, it generally overestimates the displacement X ; thus, is conservative. At values of $\frac{W}{\rho c^2 R^3}$ less than 1×10^{-7} , Equation (46) begins to underestimate the displacement, and becomes dangerous. For conventional pipeline applications, the use of Equation (46) for values of $\frac{W}{\rho c^2 R^3}$ less than 1×10^{-7} presents no problems as the associated scaled displacements are too small to threaten a pipeline. Only if blasting charges exceed 100 tons, as in large nuclear simulations, would the use of Equation (46) present problems. Equation (46) is a much simpler equation to use than Equation (30) with its hyperbolic form. All of the blasting performed in this program was for values of $\frac{W}{\rho c^2 R^3}$ greater than 1×10^{-4} . This observation means that the simpler form given by Equation (46) can be used. Figure 48 shows Equation (46) plotted versus the test results from Figure 44, and indicates that these conclusions are correct. In analytical derivations, Equation (46) rather than Equation (30) is used. Many simplifications will result in the final solution because of this approximation.

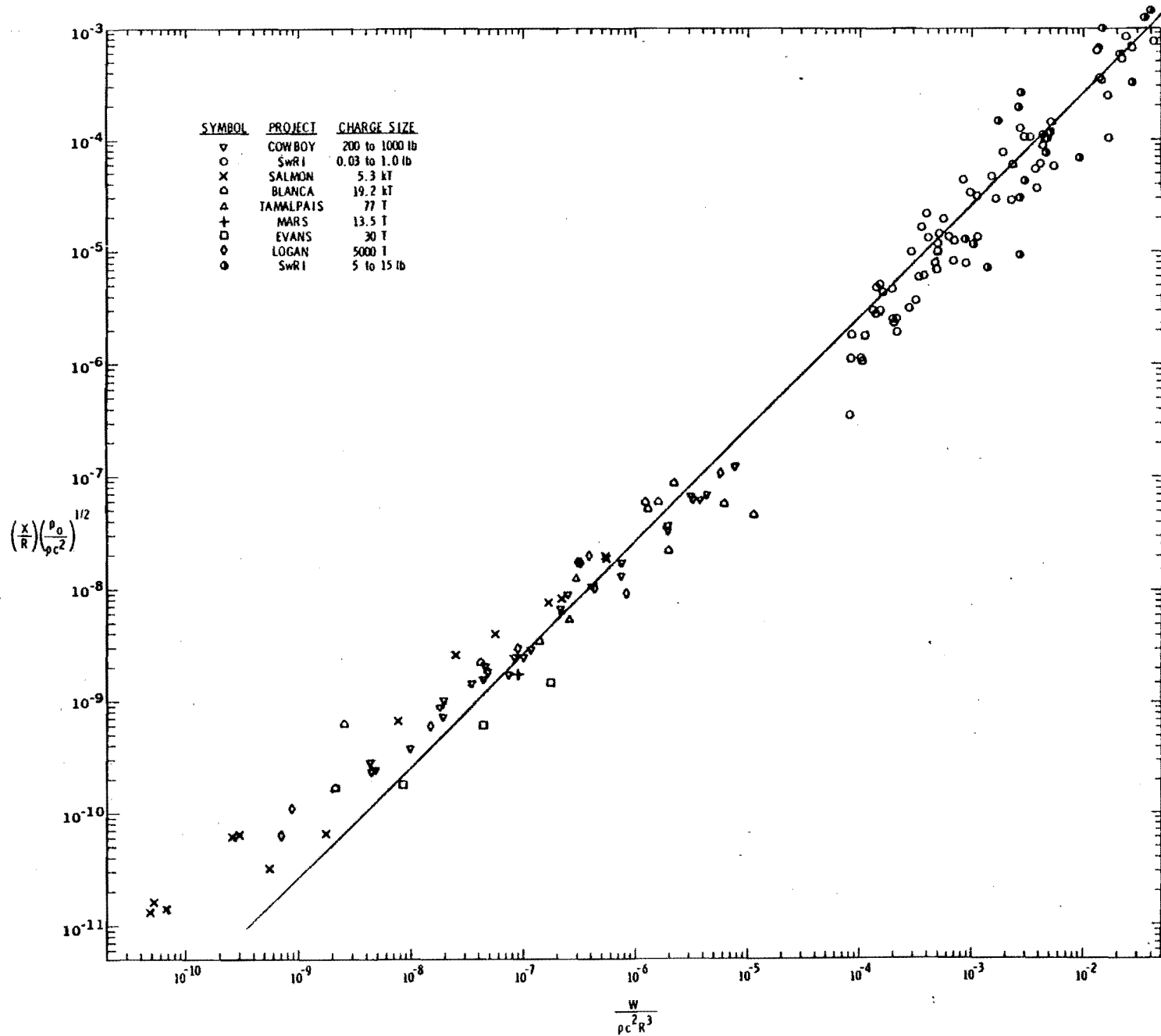


FIGURE 48. EQUATION 46 COMPARED TO DISPLACEMENT TEST DATA

VI. ANALYTICAL DERIVATION OF PIPE STRESS FORMULA

Introduction

The ground motions predicted in the previous chapter impart a shock loading to a buried pipe. Basically, this load takes the form of an impulse imparting kinetic energy to a buried pipe. This kinetic energy is dissipated by changing to strain energy. Significant strains were recorded and are reported in Section IV in both circumferential and longitudinal directions. The purpose of this analysis is to derive an approximate formula to interrelate maximum pipe stress in both directions to the various pipe, soil, and explosive parameters of importance.

The solution which follows uses both approximate analysis procedures to interrelate variables and empirical test results to develop the final functional format. Only elastic analysis procedures will be used because it is considered unacceptable to permit any stress to exceed yield in a pipeline. All pipe stress data used in this derivation comes from the data reported in Section IV. These data are used to both derive and evaluate the accuracy of the resulting expressions.

Predicting Impulse Imparted to Pipes

Before structural calculations can be made, the impulse distribution imparted to a pipe from a ground shock must be estimated. This load becomes the forcing function needed in structural calculations.

The side-on pressure and subsequent impulse must be determined without a pipe present before the impulse imparted to a pipe can be determined. Fortunately, soil particle velocity and displacement, predicted in Section V, relate directly to free-field or side-on pressures and impulses. To calculate pressure from particle velocity, we use the Rankine-Hugoniot relationships for conservation of mass and momentum. For a stationary coordinate system with a shock front moving at velocity V , these equations are:

$$-\rho_s V = \rho_a (U - V) \quad (47)$$

$$\rho_s V^2 = p_s + \rho_a (U - V)^2 \quad (48)$$

where ρ_a is the density behind the shock front and p_s is the side-on overpressure. Multiplying both sides of Equation (47) by $(U - V)$ and then subtracting the new Equation (47) from Equation (48) gives:

$$p_s = \rho_s V U \quad (49)$$

Equation (49) states that peak side-on overpressure is the product of soil density, shock front velocity, and peak particle velocity. In a fairly incompressible medium such as soil with its massive particles, the shock front propagation velocity V very rapidly decays to c . Substitution of c for V is a common practice in hydraulic shock studies and would appear to be equally valid in soil. This final substitution yields the equation which will be used to relate side-on overpressure and particle velocity.

$$p_s = \rho_s c U \quad (50)$$

Either Equation (46) for point sources or Equation (44) for line sources can be substituted into Equation (50) to determine p_s . To determine the side-on specific impulse i_s , we will treat ρ_s and c as constants and integrate Equation (50). Because the time integral of pressure is impulse and the time integral of velocity is displacement, integrating Equation (50) gives:

$$i_s = \rho_s c X \quad (51)$$

Equation (51) also can be used for values of X from either point or line charges. Next, the distribution of impulse imparted to a buried pipe by side-on impulses must be estimated. Figure 49 shows a pipe loaded by an assumed distribution of applied impulse. It is known that at the top and bottom of the pipe, the applied impulse will be i_s . Also, that at a lower limit at the front of the pipe the impulse will equal at least $2 i_s$. Between the top and front edge of the pipe, some distribution will exist which is not known. Therefore assuming some distribution, a convenient mathematical expression, Equation (52), which reaches the correct limits, was selected.

$$i = i_s \left(1 + \frac{2\theta}{\pi} \right) \text{ for } 0 < \theta < \frac{\pi}{2}$$

$$i = i_s \left(1 - \frac{2m\theta}{\pi} \right) \text{ for } 0 > \theta > -\frac{\pi}{2}$$

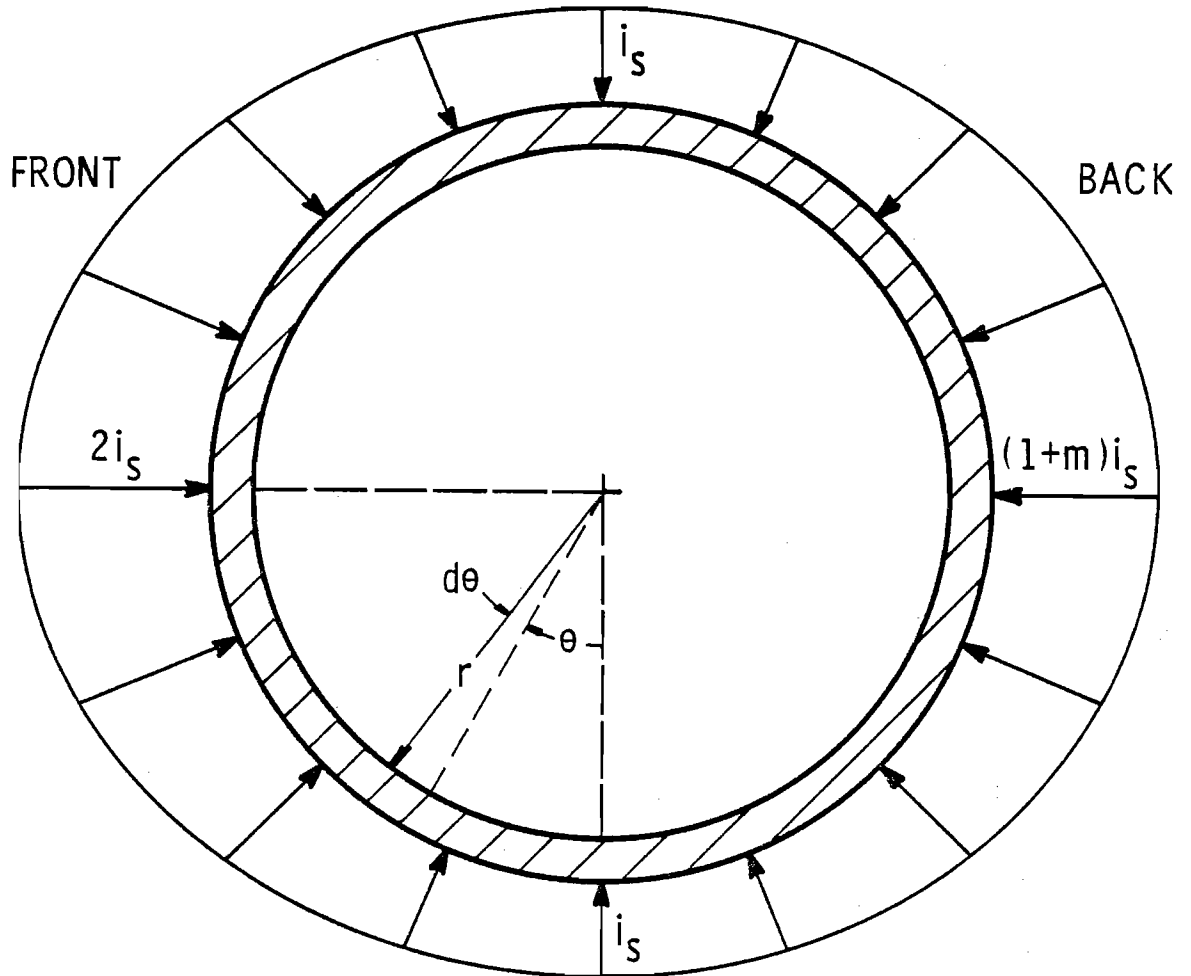


FIGURE 49. ASSUMED DISTRIBUTION OF IMPULSE IMPARTED TO A PIPE

$$i = i_s \left(1 + \frac{2\theta}{\pi} \right) \quad \text{for } 0 < \theta < \pi/2 \quad (52)$$

The back side of the pipe will also be loaded by the shock wave diffracting around the pipe. At $\theta = -\pi/2$, on the very rear surface of the pipe, the impulse could very easily exceed i_s ; however, no one knows the exact magnitude. This was solved by assuming that the applied specific impulse equals $(1 + m)i_s$ at the back of the pipe where m is some number between 0 and 1. Experimentally measured stresses will be used later to assign a constant numerical value to m . The distribution of impulse over the back surface of the pipe is similar to that used over the front surface and is

$$i = i_s \left(1 - \frac{2m\theta}{\pi} \right) \quad \text{for } 0 > \theta > -\pi/2 \quad (53)$$

A minus sign appears in Equation (53) because the angle θ is measured in a negative direction.

The total impulse I imparted to a pipe by the specific impulse distributions given in Equations (52) and (53) can now be computed. For a dx differential length of pipe, this impulse is given by:

$$\frac{I}{(dx)} = 2 \int_0^{\pi/2} \left(i_s + \frac{2i_s}{\pi} \theta \right) (\sin \theta) r \, d\theta - 2 \int_0^{\pi/2} \left(i_s + \frac{2m i_s}{\pi} \theta \right) (\sin \theta) r \, d\theta \quad (54)$$

Or, after simplifying algebraically:

$$\frac{I}{(dx)} = \frac{4(1-m)}{\pi} i_s r \int_0^{\pi/2} \theta \sin \theta \, d\theta \quad (55)$$

Performing the required integration gives:

$$I = \frac{4}{\pi} (1-m) i_s r (dx) \quad (56)$$

Equation (56) is the total impulse imparted to a ring segment. This equation can also be written as:

$$I = C_D i_s A \quad (57)$$

where

$A = 2 r (dx)$, the projected area

$C_D = \frac{2}{\pi} (1 - m)$, a diffraction coefficient

Equation (57) states that the total impulse is the specific impulse times the project areas times a constant diffraction coefficient. The constant diffraction coefficient will be determined empirically from test results. Determining C_D amounts to determining m , as they are both related through the definition of C_D . It should be emphasized that C_D as created in this analysis is not a drag coefficient and is specifically called a diffraction coefficient because it is associated with a diffraction process.

Derivation of Pipe Stress Formulae

To determine pipe stresses, calculate kinetic energy and strain energy. The first of these, kinetic energy (KE), is given by:

$$KE = \sum_{\text{pipe}} \frac{1}{2} m V_o^2 = \sum_{\text{pipe}} \frac{I^2}{2m} = 2 \int_0^{\ell/2} \frac{I^2}{2m} \quad (58)$$

Substituting Equation (57) for I and assuming that an effective mass of earth from the center of the charge to the center of the pipe moves with the pipes gives the result:

$$KE = \int_0^{\ell/2} \frac{C_D^2 i_s^2 (2r)^2 (dx)^2}{\rho_s (2r) R (dx)} \quad (59)$$

This assumption of a large effective mass of earth moving with the pipe causes the mass of the pipe itself to be insignificant. It is based on

empirical observations made during pipe tests reported in Section IV. For bending in a ring, the fundamental natural frequency ω is given by:

$$\omega = 2.6833 \sqrt{\frac{EJ}{\mu r^4}} \quad (60)$$

where

$$J = \frac{1}{12} (dx) h^3, \text{ the second moment of area}$$

$$\mu = \text{the mass per unit length}$$

When it was assumed that the mass of earth was $\rho_s (dx) R$, rather than the mass of the pipe; substituting this mass in Equation (60) and computing the period τ from the frequency ω gave:

$$\tau = 8.11 \sqrt{\frac{\rho_s R r^4}{E h^3}} \quad (61)$$

Calculated periods using Equation (61) agreed well with observed durations in the pipe strain records on early model tests, as shown in Table XV. These strain records also showed pipe ovaling; hence, inferring that pipe bending is a correct mode of response.

TABLE XV. MEASURED DURATIONS AND COMPUTED PERIODS

Test No.	Observed Durations (m.s.)	Calculated Periods (m.s.)
1	16	11.7
2	11	11.7
3	13	11.7
4	25	31.6
5	35	34.8
6	36	34.8
7	71	66.8

If we now return to Equation (59) and perform the required integration, we obtain:

$$KE = \frac{C_D^2 i_s^2 r \ell}{\rho_s R} \quad (62)$$

Substituting Equation (51) for i_s in Equation (62) finally yields:

$$KE = \frac{C_D^2 \rho_s c^2 r \ell X^2}{R} \quad (63)$$

Next, the strain energy SE must be calculated because of the pipe responding in either a longitudinal bending mode or a circumferential mode. For longitudinal bending, this computation is done by assuming a deformed shape given by:

$$Y = W_o \cos \left(\frac{\pi X}{\ell} \right) \quad (64)$$

where

$$\begin{aligned} W_o &= \text{mid-span deformation} \\ \ell &= \text{total length of the deforming pipe} \end{aligned}$$

Differentiating Equation (64) twice and substituting into the elastic moment-curvature relationship gives:

$$M = -EJ \frac{d^2 Y}{dx^2} = \frac{\pi^2 EJ W_o}{\ell^2} \cos \left(\frac{\pi X}{\ell} \right) \quad (65)$$

But the strain energy is given by:

$$SE = 2 \int_0^{\ell/2} \frac{M^2 dx}{2 EJ} \quad (66)$$

Substituting Equation (65) into Equation (66) gives:

$$SE = \frac{\pi^4 EJ W_o^2}{\ell^4} \int_0^{\ell/2} \cos^2 \left(\frac{\pi X}{\ell} \right) dx \quad (67)$$

Which after integrating gives:

$$SE = \frac{\pi^4 EJ w_o^2}{4 \ell^3} \quad (68)$$

Next we wish to substitute for J and w_o . The second moment of area J for a pipe is given by:

$$J = \frac{\pi}{4} (r_o^4 - r_i^4) \quad (69)$$

Substituting (r_i+h) for r_o , this becomes:

$$J = \frac{\pi r_i^4}{4} \left[\left(1 + \frac{h}{r_i} \right)^4 - 1 \right] \quad (70)$$

Using the binomial expansion and retaining only the first two terms because h/r_i is small gives:

$$J = \frac{\pi r_i^4}{4} \left[1 + 4 \left(\frac{h}{r_i} \right) + \dots - 1 \right] \quad (71)$$

Equation (71) reduces to:

$$J \approx \pi r^3 h \quad (72)$$

The deformation w_o is related to the maximum stress by substituting into:

$$\sigma_{\max} = \frac{M_{\max} c}{J} \quad (73)$$

But M_{\max} occurs when the $\cos \frac{\pi x}{\ell}$ equals 1.0 in Equation (65), hence:

$$\sigma_{\max} = \frac{\pi^2 EJ w_o}{\ell^2} \frac{r}{j} \quad (74)$$

Which gives, when solved for w_o :

$$w_o = \frac{\sigma_{\max} \ell^2}{\pi^2 E r} \quad (75)$$

Substituting Equations (72) and (75) into Equation (68) finally gives the longitudinal strain energy:

$$SE_{\text{long.}} = \frac{\pi \sigma_{\max}^2 r h \ell}{4 E} \quad (76)$$

If it is assumed that the pipe goes into an ovaling bending mode as was indicated by the recorded strains and by the calculated and observed durations associated with vibrating pipes, the strain energy in the circumferential direction is computed from an assumed deformed shape given by:

$$Y = w_o \cos 2\theta \quad (77)$$

The elastic bending moment, as computed from two derivatives of Equation (77), is:

$$M = -EJ \frac{d^2 Y}{r^2 d\theta^2} = \frac{4 EJ w_o}{r^2} \cos 2\theta \quad (78)$$

The strain energy SE is given by:

$$SE = 8 \int_0^{\pi/4} \frac{M^2 r d\theta}{2 EJ} \quad (79)$$

Which, after substitution of Equation (78) into Equation (79), yields:

$$SE = \frac{64 EJ w_o^2}{r^3} \int_0^{\pi/4} \cos^2 (2\theta) d\theta \quad (80)$$

Integration of Equation (80) gives the result:

$$SE = \frac{8 \pi EJ w_o^2}{r^3} \quad (81)$$

Substitution of the maximum moment from Equation (78) when $\cos 2\theta$ equals 1.0 into Equation (73) gives:

$$\sigma_{\max} = \frac{4 EJ w_o}{r^2} \frac{h/2}{J} \quad (82)$$

Or, after solving for w_o :

$$w_o = \frac{\sigma_{\max} r^2}{2 E h} \quad (83)$$

The second moment of area J in the circumferential direction is given by:

$$J = \frac{1}{12} \ell h^3 \quad (84)$$

Finally, substituting Equations (83) and (84) into Equation (81) gives for the circumferential strain energy:

$$SE_{\text{cir}} = \frac{\pi}{6} \frac{\sigma_{\max}^2 r h \ell}{E} \quad (85)$$

Approximate solutions which interrelate the variables are obtained by equating the kinetic energy, Equation (63), to the strain energy, Equation (76) for longitudinal stress or Equation (85) for circumferential stress. This computation gives the result:

$$\frac{\pi}{4} \frac{\sigma_{\text{long}}^2 h(r \ell)}{E} = \frac{C_D^2 \rho_s c^2 X^2 (r \ell)}{R} \quad (86)$$

Or:

$$\sigma_{\text{long}} = \left(\frac{4 C_D^2}{\pi} \right)^{1/2} \frac{E^{1/2} \rho_s^{1/2} c X}{h^{1/2} R^{1/2}} \quad (87)$$

Similarly, this procedure for circumferential stress yields the result:

$$\sigma_{\text{cir}} = \left(\frac{6 C_D^2}{\pi} \right)^{1/2} \frac{E^{1/2} \rho_s^{1/2} c X}{h^{1/2} R^{1/2}} \quad (88)$$

Notice that in Equation (86) the quantity $(r \ell)$ on the strain energy or left hand side of the equation cancels with $(r \ell)$ on the kinetic energy or right hand side of this equation. This observation means that the stresses will be independent of both the pipe length ℓ and the pipe radius r . Static analysis procedures do not yield this conclusion, and cannot be used to draw valid conclusions in this dynamic problem. Dynamically, this solution infers that doubling the radius r or size of the pipe doubles the kinetic energy imparted to the pipe; however, this process doubles the amount of material available for absorbing the input energy through strain energy. The net result is that the pipe radius r cancels out of the analysis and the stresses are independent of pipe radius. The experimental data obtained in this program on 3-in, 6-in, 16-in, 24-in, and 30-in diameter pipes will be used later in comparisons which uphold this analytical observation.

The other major observation which should be made concerning Equations (87) and (88) is that in both orthogonal directions the maximum stress

appears to equal the same quantity $\left(\frac{E^{1/2} \rho_s^{1/2} c X}{h^{1/2} R^{1/2}} \right)$ times a constant which

differs for maximum circumferential stress σ_{cir} and longitudinal stress σ_{long} . This observation suggests that the final solution can be obtained

by two plots, one for circumferential stress of σ_{cir} versus $\left(\frac{E^{1/2} \rho_s^{1/2} c X}{h^{1/2} R^{1/2}} \right)$

and the other for longitudinal stress of σ_{long} versus $\left(\frac{E^{1/2} \rho_s^{1/2} c X}{h^{1/2} R^{1/2}} \right)$.

This procedure is precisely the one which was followed to develop the final quantitative functional formats for predicting pipe stresses from buried detonations.

Use of Data to Complete the Solution

In Section IV, pipe stresses from buried detonations are reported for tests at SwRI, Kansas City, and in Kentucky. Experiments were conducted using both line and point sources for explosive charge sizes varied by greater than 2 orders of magnitude. All of these stress results are tabulated in Tables IX, XII, and XIV from Section IV. These results are used to empirically complete this derivation because formulæ are needed in terms of charge size rather than in terms of soil displacement. Equation (46) from Section V was substituted into Equation (88) to obtain:

$$\sigma_{\text{cir}} = [0.03455 C_D] \frac{\sqrt{E} W}{\sqrt{p_o} \sqrt{h} R^{2.5}} \quad (89)$$

Equation (89) is nondimensional; however, it was written in a dimensional format because R is inches and W is in-lbs of energy release and is not very convenient for users in the field. Using the quantity (n W) as equivalent lbs of AN-FO in place of an energy release, substituting 14.7 psi for p_o , and making the appropriate substitutions so R would be in feet, E in psi, and h in inches gives:

$$\sigma_{\text{cir}} \text{ (psi)} = [333.8 C_D] \frac{\sqrt{E \text{ (psi)}} [n W \text{ (lbs AN-FO)}]}{\sqrt{h \text{ (in)}} [R \text{ (ft)}]^{2.5}} \quad (90)$$

Now plot the left hand of Equation (90) against the right hand side of this equation. Figure 50 is this plot with the open symbols, the points for a single explosive source. The shaded symbols are the test results for line sources which will be discussed later. The line through the data in Figure 50 has a slight curve but if the straight segment was associated with the smaller values of σ_{cir} , it would have C_D in Equation (90) equal to 0.1394 so Equation (90) could be written as:

$$\bar{\sigma} \text{ (psi)} = [46.53] \frac{\sqrt{E \text{ (psi)}} [n W \text{ (lbs AN-FO)}]}{\sqrt{h \text{ (in)}} [R \text{ (ft)}]^{2.5}} \quad (91)$$

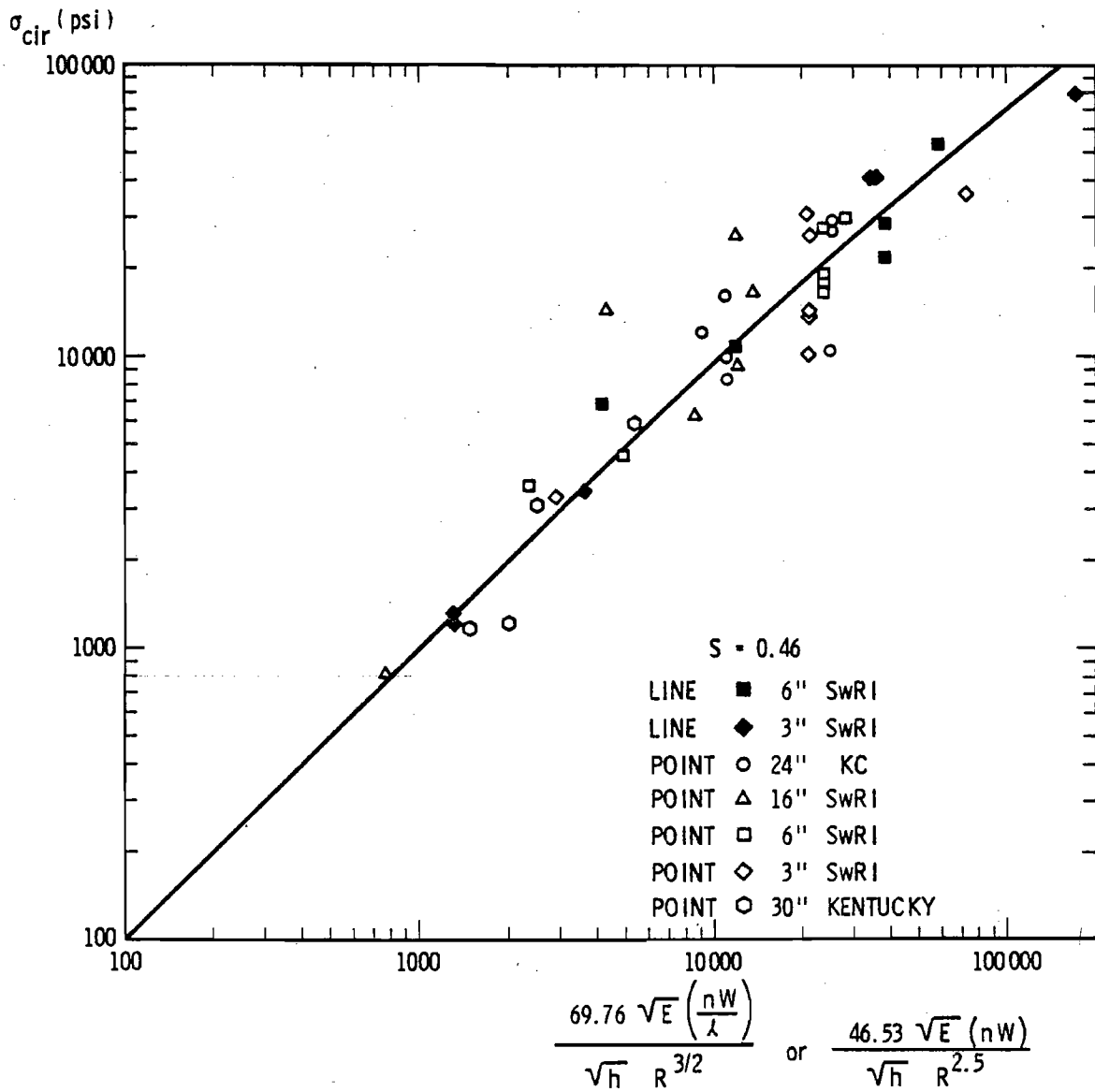


FIGURE 50. CIRCUMFERENTIAL PIPE STRESS

The symbol $\bar{\sigma}$ has been substituted for the maximum circumferential stress σ_{cir} in Equation 91 because $\bar{\sigma}$ only equals σ_{cir} for values of $\bar{\sigma}$ less than 2675 psi. For larger values of $\bar{\sigma}$, σ_{cir} almost equals $\bar{\sigma}$ but not quite. The line actually drawn through the data points in Figure 50 is given by:

$$\sigma_{\text{cir}} = 1.0 \bar{\sigma} \quad \text{for } \bar{\sigma} \leq 2675 \text{ psi} \quad (92a)$$

$$\sigma_{\text{cir}} = 21.7 \bar{\sigma}^{0.740} - 47.55 \bar{\sigma}^{0.584} \quad \text{for } \bar{\sigma} \geq 2675 \text{ psi} \quad (92b)$$

The fact that the line curves in Figure 50 is not distressing. The analytical solution was created by assuming a deformed shape. In addition, it is assumed that other modes of response do not occur and that the deformed shaped does not change with the intensity of the loading. Any or both of these effects would cause transitions which have been handled in this solution by using empirical observation.

Experimental tests on the 3- and 6-in diameter pipe also used explosive line sources. These data points are the shaded symbols in Figure 50. Equation (88) applies to line or point explosive sources, however, a different ground motion relationship must be used in substituting for ground motion X. For the point source solution we used Equation (46) as an approximation for the more complex Equation (30), and substituted Equation (46) into Equation (88) to eventually obtain Equation (91). Similarly for a line source solution, we wrote Equation (93) as an approximation to the more complex Equation (15).

$$\frac{x}{R} \left(\frac{\rho_o}{\rho_s c^2} \right)^{1/2} = 0.0375 \left(\frac{W/\ell}{\rho_s c^2 R^2} \right) \quad (93)$$

Given that a series of equal weight charges are spaced in a straight line with an equal gap between each charge and are detonated, then a line source solution is applicable if ℓ (the length of the explosive line) is greater than $2/3R$ and ℓ is also less than NR . Equation (93) for a line source was then substituted into Equation (88) and the proper dimensional substitutions were made to obtain the following dimensional equation.

$$\bar{\sigma} \text{ (psi)} = [69.76] \frac{\sqrt{E \text{ (psi)}} \left[\left(\frac{n W}{\ell} \frac{\text{lbs AN-FO}}{\text{ft}} \right) \right]}{\sqrt{h \text{ (in)}} [R \text{ (ft)}]^{1.5}} \quad (94)$$

Equation (94) is the line source counterpart to Equation (91) for point sources. All of the observations made about Equation (91) pertain to Equation (94). For values of $\bar{\sigma}$ less than 2675 psi, the quantity $\bar{\sigma}$ in Equation (94) for a line source equals σ_{cir} . For large values of $\bar{\sigma}$ the solution for the line source also diverges slightly from Equation (94) as it did for point sources. Hence, Equations (92) pertain to either point or line sources provided the correct equation for $\bar{\sigma}$ is applied.

In addition, to predicting circumferential stress, we also need to predict maximum longitudinal stress from blasting σ_{long} . Because Equation (87) for longitudinal stress is similar to Equation (88) for circumferential stress except for a constant, longitudinal stress σ_{long} should plot as only a slightly different function of $\bar{\sigma}$. Figure 51 is this longitudinal stress plot using the longitudinal stress test data also summarized in Section IV. Both point source and line source data may also be seen in Figure 51. The same symbol shapes are used in Figure 51 as in Figure 50. The abscissa in both Figures 50 and 51 use the same equations and format for determining $\bar{\sigma}$. The major difference seen in Figures 50 and 51 is that a more pronounced break in the curve appears at a $\bar{\sigma}$ of 2675 psi in the longitudinal stress curve, Figure 51.

The equations which have been curve fitting to the data in Figure 51 are given by:

$$\sigma_{\text{long}} = 0.253 \bar{\sigma}^{1.304} - \sigma \quad \text{for } \bar{\sigma} \leq 2675 \text{ psi} \quad (95a)$$

$$\sigma_{\text{long}} = 47.55 \bar{\sigma}^{0.584} \quad \text{for } \bar{\sigma} \geq 2675 \text{ psi} \quad (95b)$$

Equations (95) for longitudinal stress are the counterparts to Equations (92) for circumferential stress. The more pronounced break in longitudinal stress infers that a change in mode of pipe response occurs around a $\bar{\sigma}$ of 2675 psi which has a very pronounced effect on longitudinal response and only a small effect on circumferential response. Probably this change in

σ_{long} (psi)

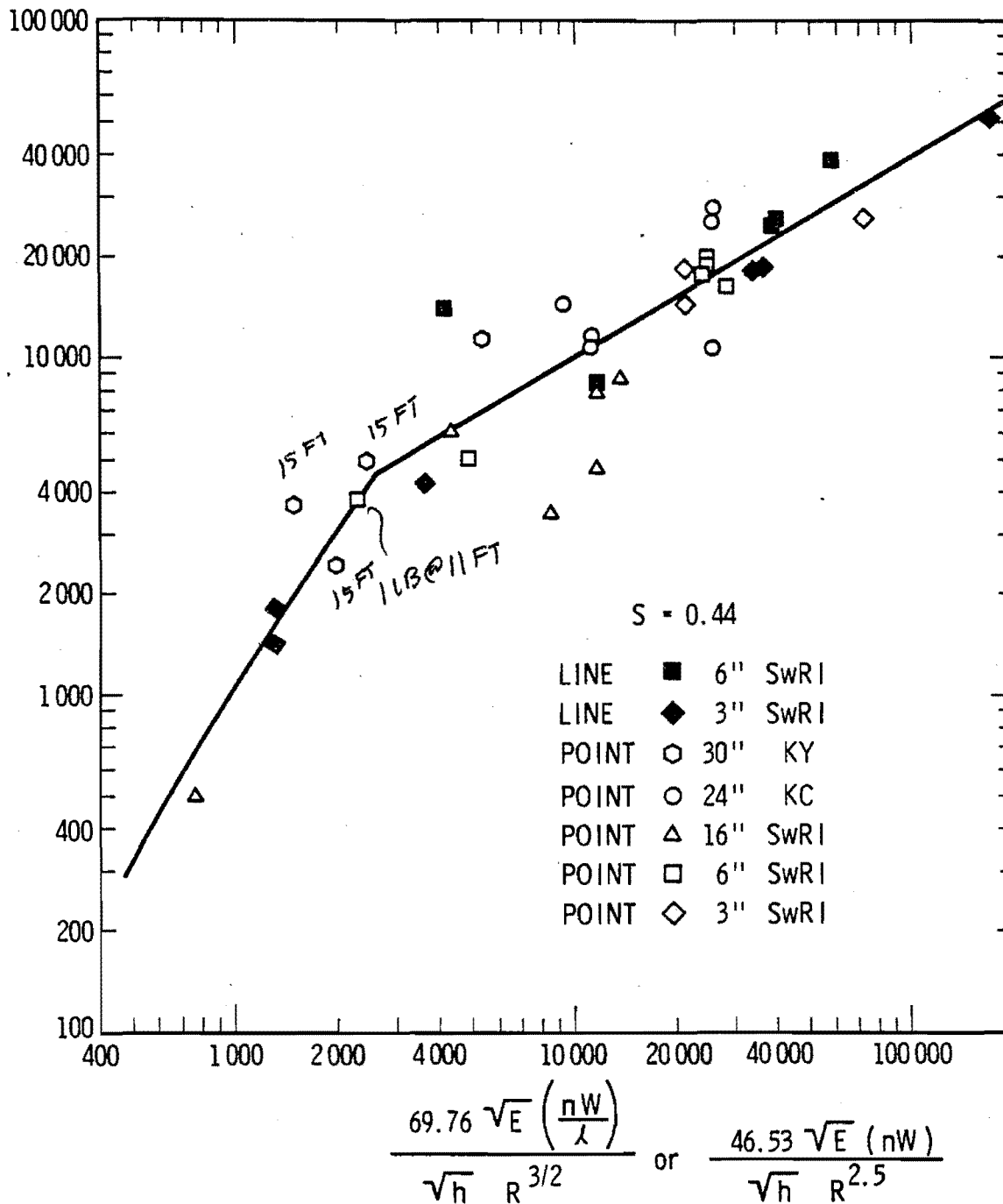


FIGURE 51. LONGITUDINAL PIPE STRESS

mode is the difference between shock fronts with little or no curvature enveloping a long cylindrical pipe, and shock fronts with very pronounced curvature for close in changes diffracting around the same long cylindrical pipe. Our analysis procedure assumed that shock fronts with little or no analysis also comes the closest to predicting stresses for $\bar{\sigma}$ less than 2675 psi, the plane wave condition. Empirical procedures were used to estimate the effects of the more difficult procedures associated with extremely close in changes.

Equations (92) and (95) or their graphical representations in Figures (50) and (51) are the pipe stress solutions which are used in all further discussion in Sections VII and VIII. This section ends with two supplemental discussions concerning two details in this solution.

Supplemental Analysis Observations

Most explosives which are chemical energy releases have almost the same explosive energy per unit weight. This observation permits us to write a quantity such as (n W) in place of W. The quantity n relates other chemical explosives to the energy release in AN-FO (94/6). AN-FO has an n of 1.00; whereas, those explosives which are more energetic have n greater than 1.00, and those which are less energetic have n less than 1.00. Table XVI lists values of n for some common as well as commercial explosives. Notice that n varies little more than a factor of $\pm 20\%$ from the smallest n of 0.83 to the larges of 1.16. This observation means that if n is not known, a pipe stress can still be calculated whose answer will be essentially correct. Only small increases in accuracy occur by knowing what explosive is to be used.

TABLE XVI. EQUIVALENT ENERGY RELEASES

<u>Explosive</u>	<u>n</u>
Pentolite (50/50)	1.11
TNT	0.98
RDX	1.16
Comp B (60/40)	1.12
HBX-1	0.83
NG Dynamite (40%)	1.05
NG Dynamite (60%)	1.12
AN Low Density Dynamite	0.99
AN-FO (94/6)	1.00

Because Figures (50) and (51) have lines through the data, standard deviations were calculated for the scatter in data about these lines. The standard deviations were calculated by dividing an observed stress by its calculated value to create a fraction and increase the sample size. By assuming that this new distribution is a normal one, one standard deviation S can then be calculated by:

$$S = \frac{\sum_1^n \left[\left(\frac{\sigma_{\text{obs}}}{\sigma_{\text{cal}}} - 1 \right)^2 \right]}{(n - 1)} \quad (96)$$

Both the circumferential stress and longitudinal stress are estimated using Equations (92) and (95) to essentially be the same degree of accuracy. One standard deviation for the circumferential stress equalled 46%, whereas, it equalled 44% for the longitudinal stress. Irrespective of the size of the pipe or of the test site location, data points for any one condition fall below as well as above the lines in Figures 50 and 51. This observation infers that the scatter is random rather than systematic. Additional discussion about standard deviation, its meaning, and its inferences with respect to selections of a safety factor are presented in Section VIII. The closest charges to the pipe were at standoff distances of only 0.75 pipe diameters from the center of a pipe. These two shots exhibited large scatter, so we are inclined to limit this solution to standoff distances of 1.5 or greater pipe diameters from the center of a pipe.

This report will now proceed by showing different methods of presenting this solution in company field manuals.

VII. ALTERNATE METHODS OF PREDICTING PIPE STRESSES

Eventually the solution which has been developed must be applied in the field. This report is not a field manual; however, it seems appropriate that some alternate ways of predicting the pipe stress solutions should be presented, illustrated and discussed so each corporation can elect for itself a procedure which is best for its personnel. All of the procedures which will be illustrated use the same relationships to compute stress. Each approach is nothing more than a different sequence for arriving at the same answers. Six different procedures are presented.

Direct Use of Equations

This approach is the most obvious one. It states that one of two different equations must be used to compute $\bar{\sigma}$. Once $\bar{\sigma}$ is obtained, the circumferential stress and longitudinal stress from blast are obtained by substituting into one of two different groups of equations dependent upon whether $\bar{\sigma}$ is less than or greater than 2675 psi. The equations being used are those that have already been used in discussions.

$$\bar{\sigma} = \frac{46.53 \sqrt{E} (nW)}{\sqrt{h} R^{2.5}} \quad \text{(Point Source)} \quad (91)$$

$$\bar{\sigma} = \frac{69.76 \sqrt{E} \frac{nW}{l}}{\sqrt{h} R^{1.5}} \quad \text{(Line Source)} \quad (94)$$

And

$$\begin{aligned} \sigma_{\text{cir}} &= 1.0 \bar{\sigma} \\ \sigma_{\text{long}} &= 0.253 \bar{\sigma}^{1.304} - \bar{\sigma} \quad \text{for } \bar{\sigma} \leq 2675 \text{ psi} \end{aligned} \quad (95a)$$

Or

$$\begin{aligned} \sigma_{\text{cir}} &= 21.70 \bar{\sigma}^{0.740} - 47.55 \bar{\sigma}^{0.584} \\ \sigma_{\text{long}} &= 47.55 \bar{\sigma}^{0.584} \quad \text{for } \bar{\sigma} \geq 2675 \text{ psi} \end{aligned} \quad (95b)$$

To illustrate the use of these equations assume that a single AN-FO explosive charge weighing 40 lb is placed 32 ft from a steel pipe 24-in. in diameter and 0.5-in. thick. Find the maximum circumferential stress σ_{cir} and longitudinal stress σ_{long} caused by the blast wave propagated through the soil. The modulus of elasticity for steel is $29.5 \times 10^{+6}$ psi.

First look up the equivalent energy release for AN-FO in a table of explosive energy releases. Because all computations in this report have been based on AN-FO (94/6), the energy equivalency n equals 1.0, and we have a single 40-lb energy release for the product (nW). All parameters needed to compute $\bar{\sigma}$ have been listed in the previous paragraph. Using Equation (91) for a point source gives:

$$\bar{\sigma} = \frac{46.53 \sqrt{29.5 \times 10^{+6}} (40)}{\sqrt{0.5} (32)^{2.5}} = 2468 \text{ psi} \quad (97)$$

Because $\bar{\sigma}$ is less than 2675 psi, we use Equation (95a) to obtain σ_{cir} and σ_{long} . These quantities equal:

$$\begin{aligned} \sigma_{cir} &= 1.0 (2468) = 2468 \text{ psi} \\ \sigma_{long} &= 0.253 (2468)^{1.304} - (2468) = 4242 \text{ psi} \end{aligned} \quad (98)$$

These stresses are the elastic contributions due to blast loading. To determine the total state of stress in the pipe, the stresses due to pressurization, temperature changes, pipe settlement, and other causes must be superimposed and some biaxial failure theory used to determine if the pipe yields.

The advantage to this approach is that fairly simple relationships exist which are easily accessible and can be substituted into the equation to calculate blasting stress contributions. In the field, crews might have difficulty using these equations because they will not know how to compute stresses using exponents such as 1.304, 0.740, and 0.584. In addition, if field crews were forced to transform these equations so that a charge weight or standoff distance had to be determined, most would find this task to be an impossible one.

Tabular Format Using $\bar{\sigma}$

Table XVII is the solution to Equations (95a) and (95b) presented in tabular format. The solution is applied by using Equation (91) to compute $\bar{\sigma}$, and Table XVII to read off σ_{cir} and σ_{long} for some specific value of $\bar{\sigma}$. Naturally, extrapolation must be used whenever $\bar{\sigma}$ falls between tabulated values.

In this example a 40-lb charge of AN-FO was placed 32 ft. from a steel pipe 0.5-in thick. Using Equation (91) for a point source to compute $\bar{\sigma}$ gives:

$$\bar{\sigma} = \frac{46.53 \sqrt{29.5 \times 10^{+6}} (40)}{\sqrt{0.5} (32)^{2.5}} = 2468 \text{ psi} \quad (99)$$

Table XVII gives a circumferential stress σ_{cir} of 2000 psi for $\bar{\sigma}$ equal to 2000 and 3000 psi for $\bar{\sigma}$ equal to 3000 psi. Extrapolation means that the circumferential stress σ_{cir} equals 2468 psi as given by Equation (100).

$$\sigma_{\text{cir}} = 2000 + \frac{(2468 - 2000)}{(3000 - 2000)} (3000 - 2000) = 2468 \text{ psi} \quad (100)$$

Similarly extrapolation gives 4036 psi for the longitudinal stress as indicated by Equation (101).

$$\sigma_{\text{long}} = 3097 + \frac{(2468 - 2000)}{(3000 - 2000)} (5103 - 3097) = 4036 \text{ psi} \quad (101)$$

These answers are close to those given by the previous procedure, though the longitudinal stresses from blasting differ slightly. The procedure is easier for those capable of taking relatively easy roots such as 0.5, 1.5, and 2.5. In addition, the energy release or standoff distances can be solved for directly without using an iteration procedure. Problems may arise in attempts to extrapolate, and perhaps field personnel will have difficulty taking the 1.5 or 2.5 roots of standoff distance.

Graphical Format Using $\bar{\sigma}$

Figure 52 is a graphical rather than tabular solution to Equations (95a) and (95b). Every data point tabulated in Table XVII would appear to fall

TABLE XVII
STRESSES IN PIPES FROM BLASTING

Point Charge	$\frac{46.53 \sqrt{E} \text{ (nW)}}{\sqrt{h} R^{2.5}}$		
Line Charge	$\frac{69.76 \sqrt{E} \frac{\text{nW}}{l}}{\sqrt{h} R^{1.5}}$	σ_{cir} (psi)	σ_{long} (psi)
	100	100	2.5
	150	150	23.9
	200	200	53.1
	300	300	129
	400	400	225
	600	600	460
	800	800	743
	1,000	1,000	1,064
	1,500	1,500	2,003
	2,000	2,000	3,097
	3,000	3,000	5,103
	4,000	3,993	6,036
	6,000	5,888	7,648
	8,000	7,700	9,048
	10,000	9,447	10,307
	15,000	13,603	13,061
	20,000	17,537	15,450
	30,000	24,949	19,579
	40,000	31,928	23,161
	60,000	45,010	29,349
	80,000	57,277	34,718
	100,000	68,957	39,550

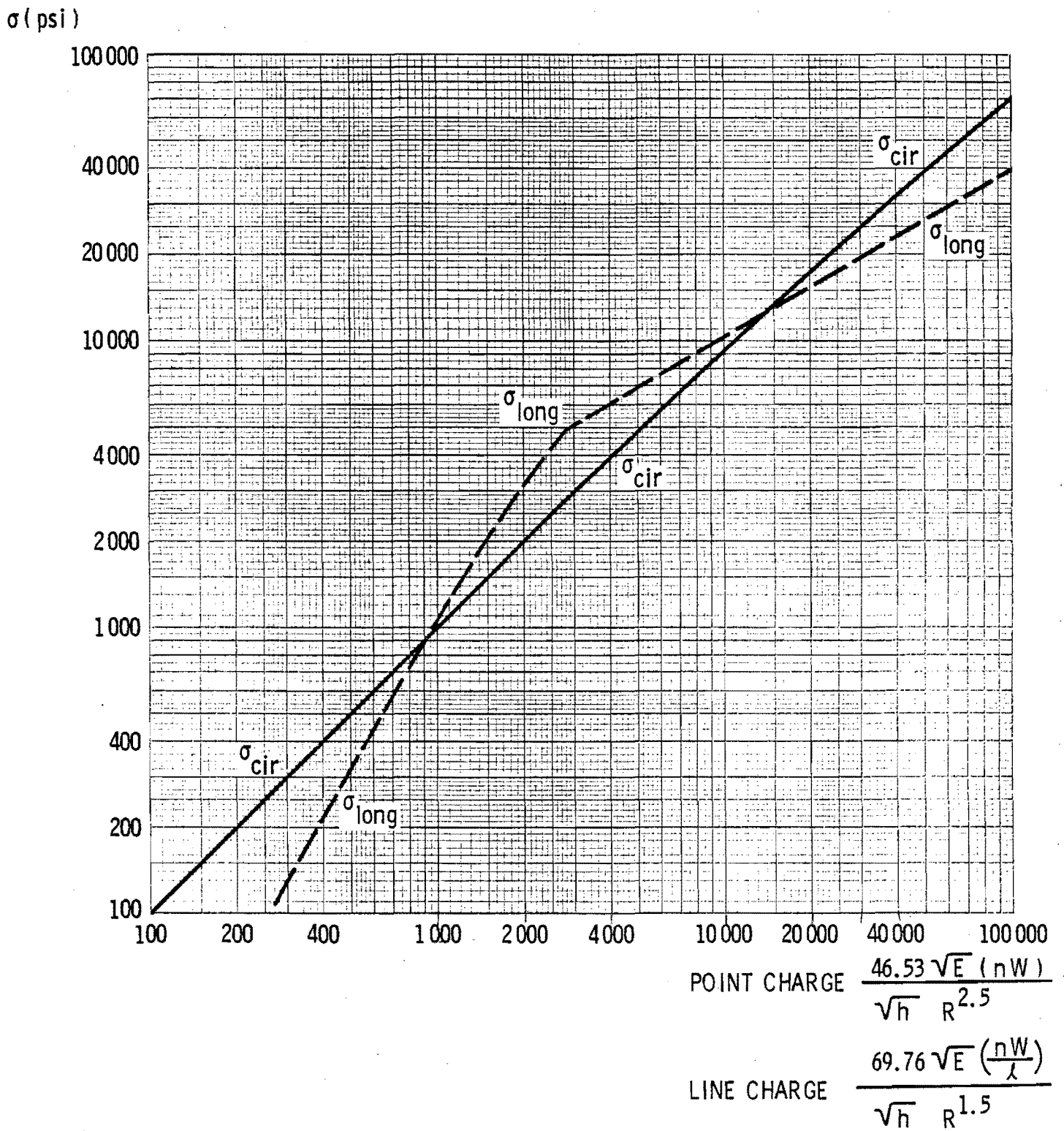


FIGURE 52. GRAPHICAL SOLUTION USING $\bar{\sigma}$

exactly on either the longitudinal stress σ_{long} or circumferential stress lines in Figure 52.

As in the example used throughout previous discussions, a 40-lb charge of AN-FO is placed 32 ft from a steel pipe 0.5-in. thick. Using Equation (91) for a point source to compute $\bar{\sigma}$ gives:

$$\bar{\sigma} = \frac{46.53 \sqrt{29.5 \times 10^{+6}} (40)}{\sqrt{0.5} (32)^{2.5}} = 2468 \text{ psi} \quad (102)$$

Now we enter Figure 52 for a $\bar{\sigma}$ of 2468 and read off of the ordinate that the circumferential stress σ_{cir} equals 2450 psi, and the longitudinal stress σ_{long} equals 4200 psi. These answers differ slightly from the actual ones because of the accuracy which may be obtained from such a graph.

Most of the advantages and disadvantages remain the same as in the previous presentation. Probably the one added advantage is that no extrapolation procedure needs to be learned to use Figure 52. Both axes in Figure 52 are, of necessity, log axes. Some engineers in the field might have difficulty in using this type of graph paper.

Solution by Nomograph

The previous solutions all required that some computation be done before obtaining the blasting stresses from a graph, table, or computation. It is possible to present a nomograph with all the parameters shown separately. Figures 53 and 54 are these nomographs for point and line explosive sources respectively. One begins in these nomographs by finding the modulus of elasticity for pipe material on the vertical line. A horizontal line is then run from this modulus over to the appropriate pipe thickness in the contours in the lower left of the figures. From the pipe thickness, a vertical line is run up to the appropriate equivalent energy release (lbs. of AN-FO) in the contours in the upper left of these figures. From the energy release, a horizontal line is run over to the appropriate standoff distance in the contours in the upper right of the figures. Finally the circumferential stress from blasting and the longitudinal stress are read by dropping a vertical line from the standoff distance to intersect the circumferential stress and longitudinal stress axes.

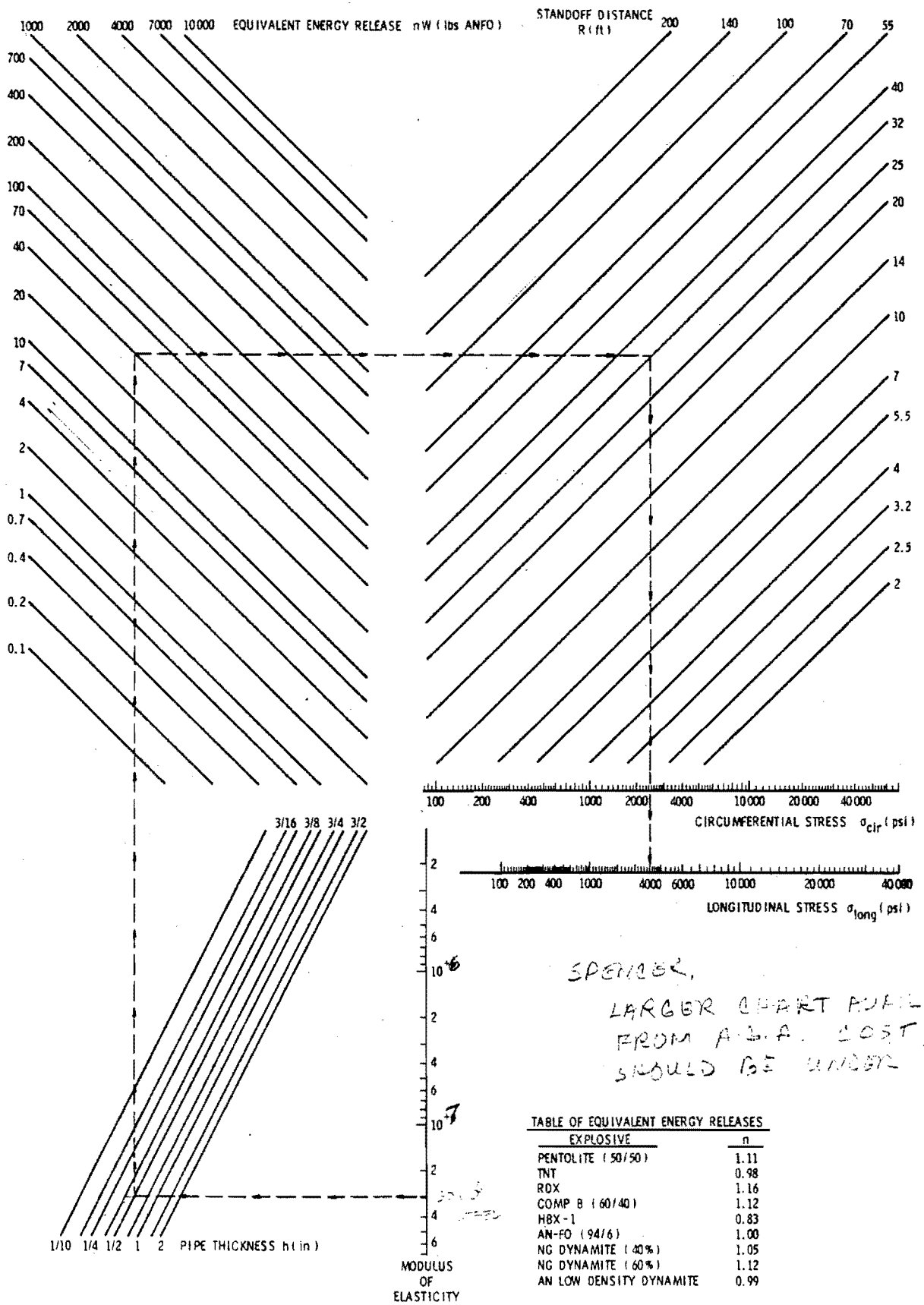


FIGURE 53. PIPE STRESS NOMOGRAPH FOR POINT SOURCES

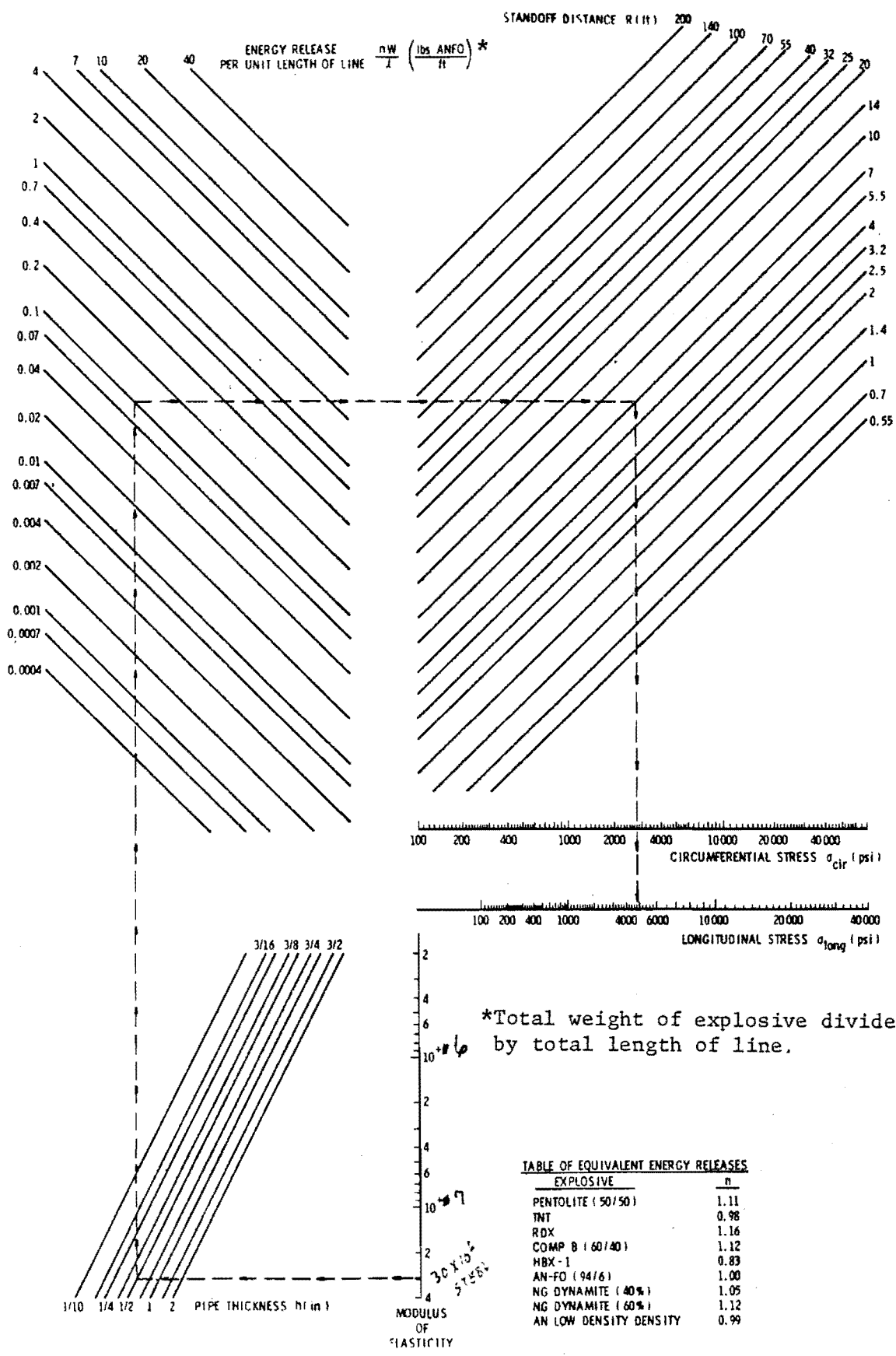


FIGURE 54. PIPE STRESS NOMOGRAPH FOR LINE SOURCES

Both nomographs represent graphical solutions to Equations (91), (95a), and (95b). Basically, logarithms are being added and subtracted until the quantity $\bar{\sigma}$ is computed. For a point source, Figure (53) is using Equation (91) in the form:

$$[\log \bar{\sigma}] = \frac{1}{2}[\log E] - \frac{1}{2}[\log h] + [\log nW] - \frac{5}{2}[\log R] + [\log 46.53] \quad (103)$$

The vertical line which finally descends to intersect the two stress axes is the $[\log \bar{\sigma}]$. Both of the stress axes are not log scales because Equations (95a) and (95b) are not log linear. But in both of these equations σ_{cir} and σ_{long} are unique functions of only $\bar{\sigma}$. This observation means that a stress axis can be computed from equations, and drawn from Equations (95a) and (95b). Although portions of this line may be approximated by log scales, all segments of this line will not maintain the same proportions.

The same illustrative example of a 40-lb charge of AN-FO placed 32 ft from a steel pipe 0.5-in. thick is presented in the point source solution, Figure 53. From this figure, one would estimate the circumferential stress as 2450 psi and the longitudinal stress as 4050 psi. Once again graphical accuracy prevents the solution from having the precision of an answer obtained by substituting into equations.

The illustrative example presented in the line source nomograph, Figure 54, is for a steel pipe, 0.5 in. thick, with 8 AN-FO explosive charges weighing 0.5 lb each spaced 5.0 ft apart in a line 7 ft from a pipeline which is parallel to the explosive line. The quantity nW/ℓ equals $8(0.5)/8(5.0)$ or 0.1 lb/ft. In this example, the circumferential stress is 2800 psi, and the longitudinal stress equals 4850 psi.

Both of these nomographs have the added advantage that they can easily be solved for limiting values of other parameters if a maximum stress is specified. For example, suppose that the longitudinal stress from blasting had to be limited to 4050 psi for a steel pipe 0.5 in. thick which had been buried in the ground. The crews in the field might wish to know which combinations of explosive charge weight and standoff distances constituted an acceptable threshold. In this case, a vertical line would be drawn from the 4050 longitudinal stress axis on the right hand side of Figure 53 if point sources were to be used. The same horizontal line would be drawn from E to

h, and a vertical line would also be drawn from h on the left hand side of Figure 53. Now the correct answer relating acceptable values of nW to R would be all horizontal lines intersecting the vertical lines on the left and the right of Figure 53. The horizontal line which is drawn connecting an nW of 40 lb to an R of 32 ft is but one answer. For a 20-lb charge, an R of 25 ft is acceptable; for a 2-lb charge, an R of 10 ft is acceptable; etcetera.

The great advantage of these nomographs is their simplicity once they are learned. No multiplications of powers have to be taken to read stresses or other quantities directly. Their weaknesses are that their use must be learned, inaccuracy can result if lines are not drawn carefully, and field personnel still have to read a graph which looks somewhat like a log scale. These nomographs have been drawn on a sheet of paper. Another presentation which might be more attractive in the field would be to make a linear or a circular slide rule for performing these same computations.

Tables for Various Pipe

This format could be applied for a particular company application. A field manual could be created in which all possible conditions had already been precalculated. The following four pages are such a table for a point source charge against a steel pipe which is 0.5-in. thick. This pipe may be of any diameter; however, as soon as a line source is used instead of a point source, a PVC pipe is used instead of a steel one, or if a pipe with a wall thickness other than 0.5-in. is used, four more pages of tables would be required. Listed in Table XVIII are circumferential stress (SC) and longitudinal stress (SL) for various equivalent charge weights (nW) in pounds of AN-FO and standoff distances (R). Use is very simple provided the conditions needed are included in the compilation.

For our example problem of 40-lb of AN-FO located 32 ft from a 0.5-in. steel pipe, the tables which we have compiled can be used provided the reader extrapolates. The following four conditions shown below can be found in Table XVIII.

TABLE XVIII

STRESS IN BURIED PIPE FROM POINT SOURCE BLASTING

E=29,500,000(P.SI) H=0.5(IN)

NW(LBS)	R(FT)	SC(P.SI)	SL(P.SI)
1.00000E+00	2.63793E+01	1.00000E+02	2.51254E+00
1.00000E+00	2.31271E+01	1.38950E+02	1.84717E+01
1.00000E+00	2.02758E+01	1.93071E+02	4.86710E+01
1.00000E+00	1.77760E+01	2.68272E+02	1.02955E+02
1.00000E+00	1.55844E+01	3.72764E+02	1.97304E+02
1.00000E+00	1.36630E+01	5.17956E+02	3.57461E+02
1.00000E+00	1.19785E+01	7.19699E+02	6.24619E+02
1.00000E+00	1.05017E+01	1.00002E+03	1.06436E+03
1.00000E+00	9.20696E+00	1.38953E+03	1.78060E+03
1.00000E+00	8.07185E+00	1.93075E+03	2.93741E+03
1.00000E+00	7.07668E+00	2.68305E+03	4.78018E+03
1.00000E+00	6.20421E+00	3.72689E+03	5.79260E+03
1.00000E+00	5.43930E+00	5.12284E+03	7.01945E+03
1.00000E+00	4.76869E+00	6.98158E+03	8.50614E+03
1.00000E+00	4.18077E+00	9.44717E+03	1.03077E+04
1.00000E+00	3.66533E+00	1.27069E+04	1.24908E+04
1.00000E+00	3.21343E+00	1.70038E+04	1.51363E+04
1.00000E+00	2.81725E+00	2.26532E+04	1.83421E+04
1.00000E+00	2.46992E+00	3.00634E+04	2.22269E+04
1.00000E+00	2.16540E+00	3.97628E+04	2.69345E+04
1.00000E+00	1.89843E+00	5.24345E+04	3.26391E+04
1.00000E+00	1.66438E+00	6.89610E+04	3.95519E+04
2.00000E+00	3.48077E+01	1.00000E+02	2.51254E+00
2.00000E+00	3.05163E+01	1.38950E+02	1.84717E+01
2.00000E+00	2.67540E+01	1.93071E+02	4.86710E+01
2.00000E+00	2.34555E+01	2.68272E+02	1.02955E+02
2.00000E+00	2.05637E+01	3.72764E+02	1.97304E+02
2.00000E+00	1.80285E+01	5.17956E+02	3.57461E+02
2.00000E+00	1.58058E+01	7.19699E+02	6.24619E+02
2.00000E+00	1.38571E+01	1.00002E+03	1.06436E+03
2.00000E+00	1.21487E+01	1.38953E+03	1.78060E+03
2.00000E+00	1.06509E+01	1.93075E+03	2.93741E+03
2.00000E+00	9.33774E+00	2.68305E+03	4.78018E+03
2.00000E+00	8.18650E+00	3.72689E+03	5.79260E+03
2.00000E+00	7.17720E+00	5.12284E+03	7.01945E+03
2.00000E+00	6.29233E+00	6.98158E+03	8.50614E+03
2.00000E+00	5.51656E+00	9.44717E+03	1.03077E+04
2.00000E+00	4.83643E+00	1.27069E+04	1.24908E+04
2.00000E+00	4.24015E+00	1.70038E+04	1.51363E+04
2.00000E+00	3.71739E+00	2.26532E+04	1.83421E+04
2.00000E+00	3.25907E+00	3.00634E+04	2.22269E+04
2.00000E+00	2.85727E+00	3.97628E+04	2.69345E+04
2.00000E+00	2.50500E+00	5.24345E+04	3.26391E+04
2.00000E+00	2.19616E+00	6.89610E+04	3.95519E+04
5.00000E+00	5.02171E+01	1.00000E+02	2.51254E+00
5.00000E+00	4.40259E+01	1.38950E+02	1.84717E+01
5.00000E+00	3.85980E+01	1.93071E+02	4.86710E+01
5.00000E+00	3.38393E+01	2.68272E+02	1.02955E+02
5.00000E+00	2.96673E+01	3.72764E+02	1.97304E+02

5.000000E+00	2.60097E+01	5.17956E+02	3.57461E+02
5.000000E+00	2.28030E+01	7.19699E+02	6.24619E+02
5.000000E+00	1.99916E+01	1.00002E+03	1.06436E+03
5.000000E+00	1.75269E+01	1.38953E+03	1.78060E+03
5.000000E+00	1.53660E+01	1.93075E+03	2.93741E+03
5.000000E+00	1.34716E+01	2.68305E+03	4.78018E+03
5.000000E+00	1.18107E+01	3.72689E+03	5.79260E+03
5.000000E+00	1.03545E+01	5.12284E+03	7.01945E+03
5.000000E+00	9.07794E+00	6.98158E+03	8.50614E+03
5.000000E+00	7.95873E+00	9.44717E+03	1.03077E+04
5.000000E+00	6.97751E+00	1.27069E+04	1.24908E+04
5.000000E+00	6.11726E+00	1.70038E+04	1.51363E+04
5.000000E+00	5.36307E+00	2.26532E+04	1.83421E+04
5.000000E+00	4.70187E+00	3.00634E+04	2.22269E+04
5.000000E+00	4.12218E+00	3.97628E+04	2.69345E+04
5.000000E+00	3.61396E+00	5.24345E+04	3.26391E+04
5.000000E+00	3.16840E+00	6.89610E+04	3.95519E+04

1.000000E+01	6.62619E+01	1.00000E+02	2.51254E+00
1.000000E+01	5.80925E+01	1.38950E+02	1.84717E+01
1.000000E+01	5.09304E+01	1.93071E+02	4.86710E+01
1.000000E+01	4.46512E+01	2.68272E+02	1.02955E+02
1.000000E+01	3.91462E+01	3.72764E+02	1.97304E+02
1.000000E+01	3.43200E+01	5.17956E+02	3.57461E+02
1.000000E+01	3.00887E+01	7.19699E+02	6.24619E+02
1.000000E+01	2.63791E+01	1.00002E+03	1.06436E+03
1.000000E+01	2.31268E+01	1.38953E+03	1.78060E+03
1.000000E+01	2.02756E+01	1.93075E+03	2.93741E+03
1.000000E+01	1.77758E+01	2.68305E+03	4.78018E+03
1.000000E+01	1.55843E+01	3.72689E+03	5.79260E+03
1.000000E+01	1.36629E+01	5.12284E+03	7.01945E+03
1.000000E+01	1.19784E+01	6.98158E+03	8.50614E+03
1.000000E+01	1.05016E+01	9.44717E+03	1.03077E+04
1.000000E+01	9.20688E+00	1.27069E+04	1.24908E+04
1.000000E+01	8.07178E+00	1.70038E+04	1.51363E+04
1.000000E+01	7.07662E+00	2.26532E+04	1.83421E+04
1.000000E+01	6.20415E+00	3.00634E+04	2.22269E+04
1.000000E+01	5.43925E+00	3.97628E+04	2.69345E+04
1.000000E+01	4.76865E+00	5.24345E+04	3.26391E+04
1.000000E+01	4.18073E+00	6.89610E+04	3.95519E+04

2.000000E+01	8.74331E+01	1.00000E+02	2.51254E+00
2.000000E+01	7.66536E+01	1.38950E+02	1.84717E+01
2.000000E+01	6.72031E+01	1.93071E+02	4.86710E+01
2.000000E+01	5.89177E+01	2.68272E+02	1.02955E+02
2.000000E+01	5.16538E+01	3.72764E+02	1.97304E+02
2.000000E+01	4.52855E+01	5.17956E+02	3.57461E+02
2.000000E+01	3.97023E+01	7.19699E+02	6.24619E+02
2.000000E+01	3.48074E+01	1.00002E+03	1.06436E+03
2.000000E+01	3.05161E+01	1.38953E+03	1.78060E+03
2.000000E+01	2.67538E+01	1.93075E+03	2.93741E+03
2.000000E+01	2.34553E+01	2.68305E+03	4.78018E+03
2.000000E+01	2.05636E+01	3.72689E+03	5.79260E+03
2.000000E+01	1.80283E+01	5.12284E+03	7.01945E+03
2.000000E+01	1.58056E+01	6.98158E+03	8.50614E+03
2.000000E+01	1.38570E+01	9.44717E+03	1.03077E+04
2.000000E+01	1.21486E+01	1.27069E+04	1.24908E+04
2.000000E+01	1.06508E+01	1.70038E+04	1.51363E+04
2.000000E+01	9.33765E+00	2.26532E+04	1.83421E+04

2.000000E+01	8.18642E+00	3.00634E+04	2.22269E+04
2.000000E+01	7.17713E+00	3.97628E+04	2.69345E+04
2.000000E+01	6.29227E+00	5.24345E+04	3.26391E+04
2.000000E+01	5.51650E+00	6.89610E+04	3.95519E+04
5.000000E+01	1.26140E+02	1.000000E+02	2.51254E+00
5.000000E+01	1.10588E+02	1.38950E+02	1.84717E+01
5.000000E+01	9.69538E+01	1.93071E+02	4.86710E+01
5.000000E+01	8.50005E+01	2.68272E+02	1.02955E+02
5.000000E+01	7.45209E+01	3.72764E+02	1.97304E+02
5.000000E+01	6.53333E+01	5.17956E+02	3.57461E+02
5.000000E+01	5.72785E+01	7.19699E+02	6.24619E+02
5.000000E+01	5.02167E+01	1.00002E+03	1.06436E+03
5.000000E+01	4.40255E+01	1.38953E+03	1.78060E+03
5.000000E+01	3.85977E+01	1.93075E+03	2.93741E+03
5.000000E+01	3.38390E+01	2.68305E+03	4.78018E+03
5.000000E+01	2.96670E+01	3.72689E+03	5.79260E+03
5.000000E+01	2.60094E+01	5.12204E+03	7.01945E+03
5.000000E+01	2.28020E+01	6.98158E+03	8.50614E+03
5.000000E+01	1.99914E+01	9.44717E+03	1.03077E+04
5.000000E+01	1.75267E+01	1.27069E+04	1.24908E+04
5.000000E+01	1.53659E+01	1.70038E+04	1.51363E+04
5.000000E+01	1.34714E+01	2.26532E+04	1.83421E+04
5.000000E+01	1.18106E+01	3.00634E+04	2.22269E+04
5.000000E+01	1.03544E+01	3.97628E+04	2.69345E+04
5.000000E+01	9.07786E+00	5.24345E+04	3.26391E+04
5.000000E+01	7.95866E+00	6.89610E+04	3.95519E+04
1.000000E+02	1.66442E+02	1.000000E+02	2.51254E+00
1.000000E+02	1.45922E+02	1.38950E+02	1.84717E+01
1.000000E+02	1.27931E+02	1.93071E+02	4.86710E+01
1.000000E+02	1.12159E+02	2.68272E+02	1.02955E+02
1.000000E+02	9.83309E+01	3.72764E+02	1.97304E+02
1.000000E+02	8.62070E+01	5.17956E+02	3.57461E+02
1.000000E+02	7.55794E+01	7.19699E+02	6.24619E+02
1.000000E+02	6.62613E+01	1.00002E+03	1.06436E+03
1.000000E+02	5.80920E+01	1.38953E+03	1.78060E+03
1.000000E+02	5.09299E+01	1.93075E+03	2.93741E+03
1.000000E+02	4.46508E+01	2.68305E+03	4.78018E+03
1.000000E+02	3.91459E+01	3.72689E+03	5.79260E+03
1.000000E+02	3.43196E+01	5.12204E+03	7.01945E+03
1.000000E+02	3.00884E+01	6.98158E+03	8.50614E+03
1.000000E+02	2.63789E+01	9.44717E+03	1.03077E+04
1.000000E+02	2.31266E+01	1.27069E+04	1.24908E+04
1.000000E+02	2.02754E+01	1.70038E+04	1.51363E+04
1.000000E+02	1.77757E+01	2.26532E+04	1.83421E+04
1.000000E+02	1.55841E+01	3.00634E+04	2.22269E+04
1.000000E+02	1.36628E+01	3.97628E+04	2.69345E+04
1.000000E+02	1.19783E+01	5.24345E+04	3.26391E+04
1.000000E+02	1.05015E+01	6.89610E+04	3.95519E+04
2.000000E+02	2.19622E+02	1.000000E+02	2.51254E+00
2.000000E+02	1.92545E+02	1.38950E+02	1.84717E+01
2.000000E+02	1.68806E+02	1.93071E+02	4.86710E+01
2.000000E+02	1.47995E+02	2.68272E+02	1.02955E+02
2.000000E+02	1.29748E+02	3.72764E+02	1.97304E+02
2.000000E+02	1.13752E+02	5.17956E+02	3.57461E+02
2.000000E+02	9.97276E+01	7.19699E+02	6.24619E+02
2.000000E+02	8.74323E+01	1.00002E+03	1.06436E+03

2.000000E+02	7.66529E+01	1.38953E+03	1.78060E+03
2.000000E+02	6.72024E+01	1.93075E+03	2.93741E+03
2.000000E+02	5.89171E+01	2.68305E+03	4.78018E+03
2.000000E+02	5.16533E+01	3.72689E+03	5.79260E+03
2.000000E+02	4.52850E+01	5.12284E+03	7.01945E+03
2.000000E+02	3.97019E+01	6.98158E+03	8.50614E+03
2.000000E+02	3.48071E+01	9.44717E+03	1.03077E+04
2.000000E+02	3.05158E+01	1.27069E+04	1.24908E+04
2.000000E+02	2.67535E+01	1.70038E+04	1.51363E+04
2.000000E+02	2.34551E+01	2.26532E+04	1.83421E+04
2.000000E+02	2.05634E+01	3.00634E+04	2.22269E+04
2.000000E+02	1.80281E+01	3.97628E+04	2.69345E+04
2.000000E+02	1.58055E+01	5.24345E+04	3.26391E+04
2.000000E+02	1.38568E+01	6.89610E+04	3.95519E+04
5.000000E+02	3.16849E+02	1.00000E+02	2.51254E+00
5.000000E+02	2.77785E+02	1.38950E+02	1.84717E+01
5.000000E+02	2.43537E+02	1.93071E+02	4.86710E+01
5.000000E+02	2.13512E+02	2.68272E+02	1.02955E+02
5.000000E+02	1.87188E+02	3.72764E+02	1.97304E+02
5.000000E+02	1.64110E+02	5.17956E+02	3.57461E+02
5.000000E+02	1.43877E+02	7.19699E+02	6.24619E+02
5.000000E+02	1.26139E+02	1.00002E+03	1.06436E+03
5.000000E+02	1.10587E+02	1.38953E+03	1.78060E+03
5.000000E+02	9.69530E+01	1.93075E+03	2.93741E+03
5.000000E+02	8.49997E+01	2.68305E+03	4.78018E+03
5.000000E+02	7.45202E+01	3.72689E+03	5.79260E+03
5.000000E+02	6.53327E+01	5.12284E+03	7.01945E+03
5.000000E+02	5.72779E+01	6.98158E+03	8.50614E+03
5.000000E+02	5.02162E+01	9.44717E+03	1.03077E+04
5.000000E+02	4.40251E+01	1.27069E+04	1.24908E+04
5.000000E+02	3.85973E+01	1.70038E+04	1.51363E+04
5.000000E+02	3.38387E+01	2.26532E+04	1.83421E+04
5.000000E+02	2.96668E+01	3.00634E+04	2.22269E+04
5.000000E+02	2.60092E+01	3.97628E+04	2.69345E+04
5.000000E+02	2.28026E+01	5.24345E+04	3.26391E+04
5.000000E+02	1.99913E+01	6.89610E+04	3.95519E+04
1.000000E+03	4.18084E+02	1.00000E+02	2.51254E+00
1.000000E+03	3.66539E+02	1.38950E+02	1.84717E+01
1.000000E+03	3.21349E+02	1.93071E+02	4.86710E+01
1.000000E+03	2.81730E+02	2.68272E+02	1.02955E+02
1.000000E+03	2.46996E+02	3.72764E+02	1.97304E+02
1.000000E+03	2.16544E+02	5.17956E+02	3.57461E+02
1.000000E+03	1.89847E+02	7.19699E+02	6.24619E+02
1.000000E+03	1.66441E+02	1.00002E+03	1.06436E+03
1.000000E+03	1.45921E+02	1.38953E+03	1.78060E+03
1.000000E+03	1.27930E+02	1.93075E+03	2.93741E+03
1.000000E+03	1.12158E+02	2.68305E+03	4.78018E+03
1.000000E+03	9.83300E+01	3.72689E+03	5.79260E+03
1.000000E+03	8.62071E+01	5.12284E+03	7.01945E+03
1.000000E+03	7.55787E+01	6.98158E+03	8.50614E+03
1.000000E+03	6.62607E+01	9.44717E+03	1.03077E+04
1.000000E+03	5.80915E+01	1.27069E+04	1.24908E+04
1.000000E+03	5.09295E+01	1.70038E+04	1.51363E+04
1.000000E+03	4.46504E+01	2.26532E+04	1.83421E+04
1.000000E+03	3.91455E+01	3.00634E+04	2.22269E+04
1.000000E+03	3.43193E+01	3.97628E+04	2.69345E+04
1.000000E+03	3.00881E+01	5.24345E+04	3.26391E+04
1.000000E+03	2.63786E+01	6.89610E+04	3.95519E+04

TABLE XIX. STRESSES USED IN EXTRAPOLATION

<u>nW</u>	<u>R</u>	<u>SC</u>	<u>SL</u>
20	34.8	1000	1064
20	30.5	1390	1781
50	33.8	2683	4780
50	29.7	3727	5793

Extrapolating first on standoff distance gives:

$$\sigma_{\text{cir}_{20} \text{ lb}} = 1390 - \frac{1390 - 1000}{34.8 - 30.5} = 1136 \text{ psi} \quad (104a)$$

$$\sigma_{\text{cir}_{50} \text{ lb}} = 3727 - \frac{3727 - 2683}{33.8 - 29.7} (33.8 - 32.0) = 3269 \text{ psi} \quad (104b)$$

$$\sigma_{\text{long}_{20} \text{ lb}} = 1781 - \frac{1781 - 1064}{34.8 - 30.5} (34.8 - 32.0) = 1314 \text{ psi} \quad (104c)$$

$$\sigma_{\text{long}_{50} \text{ lb}} = 5793 - \frac{5793 - 4780}{33.8 - 29.7} (33.8 - 32.0) = 5348 \text{ psi} \quad (104d)$$

And finally extrapolating on charge size gives:

$$\sigma_{\text{cir}_{40} \text{ lb}} = \frac{-(3269 - 1136)}{(50 - 20)} (50 - 40) + 3269 = 2558 \text{ psi} \quad (105a)$$

$$\sigma_{\text{long}_{40} \text{ lb}} = \frac{-(5348 - 1314)}{(50 - 20)} (50 - 40) + 5348 = 4003 \text{ psi} \quad (105b)$$

These answers are close but not exact because of the extrapolation procedure. The advantage is that error might be prevented because items have been precalculated. The disadvantage is the extrapolations which are required. This computation required a double extrapolation--the standoff distance, and the charge size. A third extrapolation could be required if the appropriate pipe thickness was not listed. In addition, the number of tables which could be required rapidly becomes very bulky especially if many pipe sizes, pipe materials, and line as well as point sources are to be considered.

Graphical Plot of Parameters

All of the information contained in the previous table, Table XVIII, can be displayed in a single graph plotting either σ_{cir} or σ_{long} versus (nW) and R for constant values of h and E . A series of these figures would be required for various values of h and E . Figure 55 is one of these figures drawn for a modulus of elasticity E in the pipe of 29.5×10^6 psi and a pipe wall thickness h of 0.5 in. The dashed lines in Figure 55 are for predictions of longitudinal stress σ_{long} , and the solid lines are for estimating circumferential stress σ_{cir} . The abscissa is the standoff distance R and the various isoclines are for constant values of equivalent energy release nW . No extrapolating is needed for the standoff distance R , and any extrapolation on energy release nW can be eyed. These are the major advantages in using this approach over the use of tables.

The example of a single 40-lb AN-FO charge located 32 ft from a 0.05-in. thick steel pipe can be accomplished by directly reading Figure 55 after judging where the 40-lb charge line should fall between the 20 and 50-lb charge contours. From Figure 55, we would estimate that the longitudinal stress σ_{long} was approximately 4000 psi and the circumferential stress was approximately 2400 psi.

The major advantage to using Figure 55 is that no computations are required. Several disadvantages are that no one figure or table suffices, and field people must know how to read a graph and log scales.

The entire family of figures has not been drawn because pipe sizes and charge ranges can vary from company to company. In general if this approach is used, a complete set would be required. The equations being used are the ones used throughout this chapter, Equations (91) through (95b).

General

In creating a company field manual, any of these approaches can be used to obtain essentially the same result. Notice that essentially the same estimates of circumferential and longitudinal stresses from blasting were obtained using all approaches because the same problem and equations were being solved.

Perhaps greater difficulties will be encountered when decisions are made as to how longitudinal and circumferential stresses from other environments

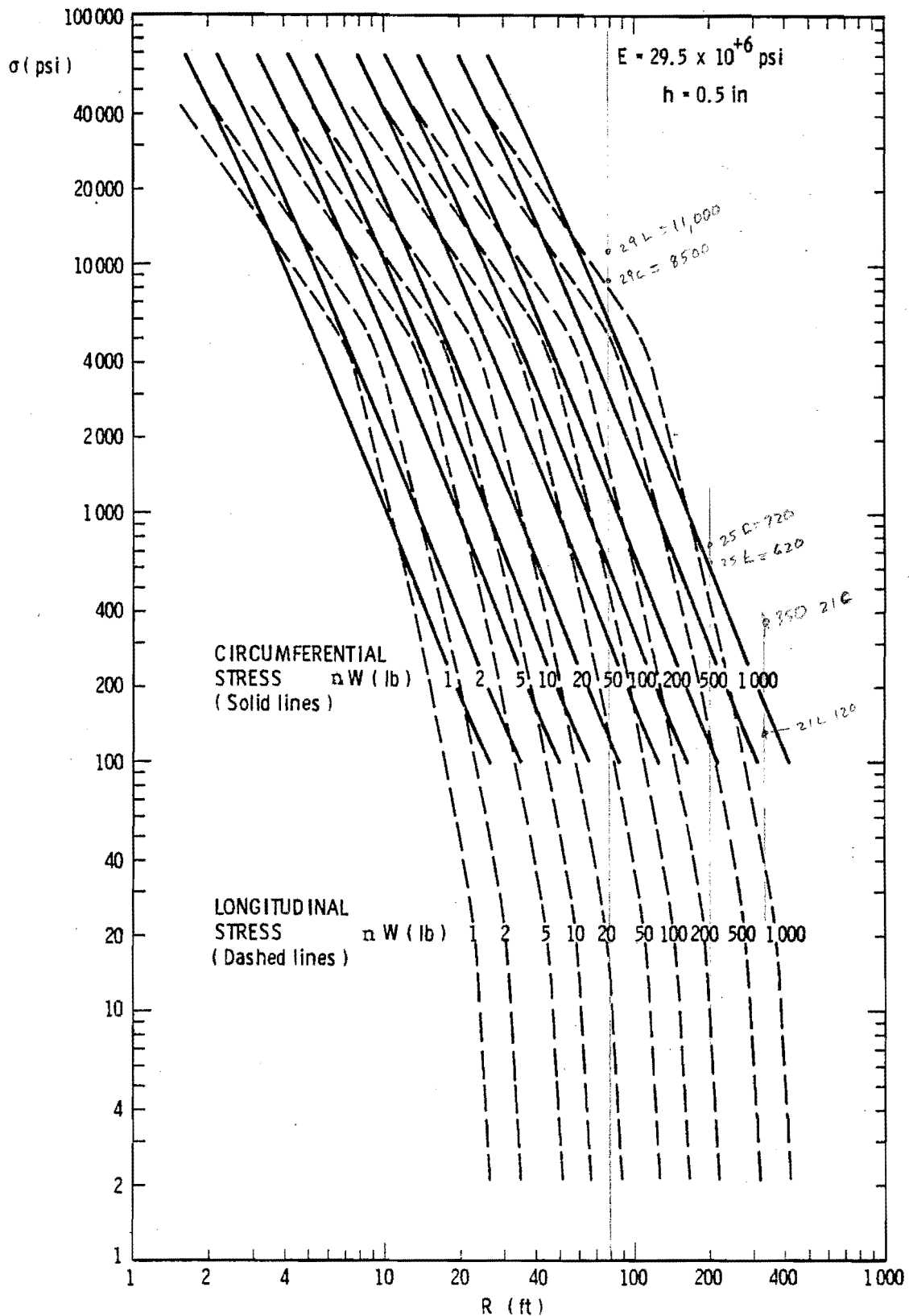


FIGURE 55. GRAPHICAL PLOT OF POINT SOURCE BLASTING PIPE STRESSES

are included. The solutions presented in this section give only those components of stress which are obtained from blasting. In addition, stresses from: 1) thermal expansion or contraction, 2) differential settlement of the pipe, 3) weight of overburden, and 4) internal pipe pressurization all add or subtract from the stresses caused by blasting. In addition, the subject of safety factors has not been discussed in detail and must reflect state laws and company policy. These added points are mentioned once again to emphasize that this solution for stresses from blasting near pipelines is only a partial one. The overall state-of-stress depends upon many factors, and to represent all in a field manual could be a very difficult task.

VIII. ANALYSIS OF STRESS SOLUTION

Example Problem

The solution for pipe stress which has just been presented is idealized. In reality problems are not point sources or line sources parallel to a pipeline. A problem which is more typical of a realistic field problem might be defined as follows:

- 1) A pipeline is 30-in. in diameter with a 0.250-in. wall thickness, and a SMYS of 60,000 psi. This pipeline is operated at a stress level of 50% of yield in the hoop direction.
- 2) Ammonium nitrate/fuel oil is to be used as an explosive in a 20 ft by 50 ft rectangular grid. The grid is rotated 30 degrees to the pipeline so that the nearest corner is 50 ft from the pipeline. The next corner which is 20 ft away is 61.5 ft from the pipeline. This charge configuration is illustrated in Figure 56. The parameter consists of fourteen 30-lb charges spaced 10 ft apart. These charges are to be detonated simultaneously. Four 50-lb charges lie within this parameter and are to be detonated with a delayed fuze (assumed to be 1.0 millisecond).
- 3) Soil conditions are unknown. Solve to see if this blasting will endanger the pipe.

The point made by this discussion is that real problems never correspond precisely with idealizations which are made for computational purposes. Engineering judgment is almost always required. There is no one answer to a problem such as this. Probably the best approach would be to solve this problem several different ways and use the answers giving the highest stresses.

One assumption might be to say all 620-lb of explosive detonates simultaneously as if it were located at a point in the geometric center of this array. Answers of the correct magnitude should result from this type of approximation, and might infer that no problem, a serious problem, or uncertainty exists as to the pipeline's safety for such a blasting operation.

By sketching out a problem such as this one, additional ideas also can be generated. For example, a delay-fuzing sequence should not be run towards the pipeline. Lower stresses would certainly occur if the charge nearest the

pipeline were detonated first and all delays progressed away from the pipe. Such a suggestion should automatically be company policy so shock waves from different sources have less chance of "shocking up" to form a more severe shock front at the pipeline.

This problem will not be solved because: 1) different quantitative numbers enter any problems and 2) various engineering judgments can be justified. Problems such as this one will be encountered and have to be faced by each individual pipeline company.

Solution Idealizations

Another reason for presenting the previous example was to emphasize that solutions are idealizations. No solution is properly understood unless these limitations are understood. Among the many limitations to these stress solutions are:

- 1) The charge and the center-line of the pipe are at the same depths.
- 2) A line charge is a continuous line rather than a series of point charges. A point source has no shape or finite size.
- 3) Any line source runs parallel to the pipeline.
- 4) The pipeline is straight without elbows or valves.
- 5) Wrapping, sand beds, and other potential shock isolation layers between the pipe and the soil have no effect.
- 6) The solution gives only the elastic stress contributions from blasting. No inelastic behavior is included in this solution.
- 7) Explosive sources always detonate instantly.
- 8) Reflections from the surface of the ground are insignificant.
- 9) No explosive energy (or at least a constant percentage of the energy) goes into cratering, air blast, and other phenomena.

Sensitivity Analysis

One of the best ways to determine how a solution responds to a change in some variable is to perform a sensitivity analysis. The variables which determine the circumferential stress σ_{cir} and the longitudinal stress σ_{long} from blasting are the modulus of elasticity for the pipe E , the charge size nW , the pipe wall thickness h , and the standoff distance R . For a line source, the energy release nW for a point source is replaced by an energy

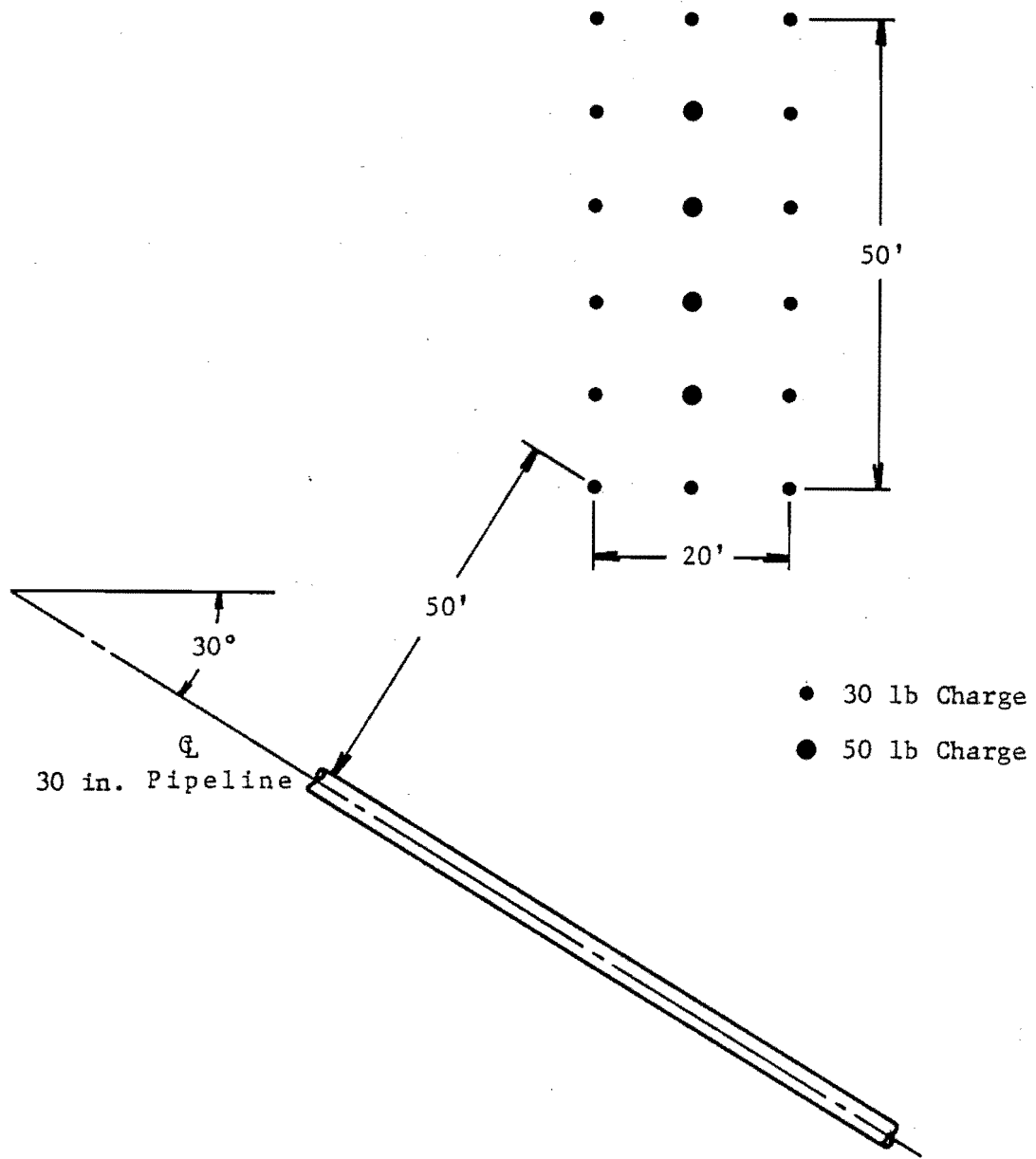


FIGURE 56. PLAN VIEW OF AN EXAMPLE FIELD BLASTING PROBLEM

release per unit length $\frac{nW}{\ell}$. Although the influence of E and h remain the same in both point and line source solutions, the standoff distance R and the energy releases nW for a point source and $\frac{nW}{\ell}$ for a line source have different influences on pipe stresses for point and line sources.

The solutions which have been developed can be seen in Figure 52. Whereas the circumferential stress solution is almost a straight line in Figure 52, the longitudinal stress solution has a sharp break at 2675 psi. This observation means that the influence of the various parameters E, h, nW, and R on stress differ for longitudinal stresses dependent upon $\bar{\sigma}$ being larger or smaller than 2675 psi. Probably this break is caused by the pipe responding in different modes. This influence on circumferential stresses is not great enough for a separate circumferential stress evaluation.

Table XX presents the results of a sensitivity analysis. In this table each parameter E, nW, h, and R are doubled independently. The number in the table shows how much σ_{cir} and σ_{long} increase or decrease because the parameter was double. If the number is greater than 1.0 as for E and nW, the stress increases. If the number is less than 1.0 as for h and R, the stress decreases. Two rows are used to present σ_{long} results, and are dependent upon $\bar{\sigma}$ being less than or greater than 2675 psi.

TABLE XX
Results of Sensitivity Analysis

Stress Component	Pipe Properties		Point Sources		Line Sources	
	E	h	nW	R	$\frac{nW}{\ell}$	R
σ_{cir}	1.41	0.71	2.00	0.18	2.00	0.35
σ_{long} large	1.22	0.82	1.50	0.37	1.50	0.55
σ_{long} small	1.75	0.57	3.08	0.06	3.08	0.19

Table XX indicates that stresses are most sensitive to standoff distance R and least sensitive to the pipe properties E and h. Changes in the stand-off distance also have a greater influence on point than line sources.

The list of parameters in Table XX, may seem small; however, these parameters are the main ones which determine the change in stress in a buried pipe from blasting. Particularly obvious by their omission are the pipe

diameter, the soil density, and the seismic propagation velocity in the soil. These parameters are absent because the solution is independent to them. In the case of larger diameter pipes, more kinetic energy is imparted to the pipe as its diameter increases, but more strain energy can also be stored in pipes with larger diameters. Because of the increase in kinetic energy and strain energy, both are increased by the first power of the pipe diameter. The pipe diameters cancel when these quantities are equated, and the resulting response becomes independent of pipe diameter. Experimental tests on 3-, 6-, 16-, 24- and 30-in pipe all yield results that show this observation is a correct one.

In a similar manner, the approximation that $\frac{X}{R} \left(\frac{p_0}{2}\right)^{1/2}$ is proportional to $\left(\frac{W}{2R^3}\right)$ eventually leads to ρ and c falling out of the analysis. If the more complex hyperbolic tangent relationship is used, the circumferential stress and the longitudinal stress become weak functions of ρ and c . The simpler format was used, because adequate engineering answers were obtained without appreciable benefit from added complexity.

Other Stress States

A knowledge of the state of stress caused by blasting is necessary but not sufficient information to determine if a buried pipe will yield. Other loading mechanisms also cause a pipe to be stressed. Because of symmetry, circumferential and longitudinal stresses from blasting and other effects are principle stresses. This observation means that an accurate estimate of the elastic state of stress can be made by superposition through addition of stresses with their signs considered. The purpose of this program does not include a discussion of states of stress from other causes. These stresses can be very significant, so readers should consider including longitudinal and circumferential stresses from such causes as:

- 1) Internal pipe pressurization
- 2) Thermal expansion or contraction
- 3) Surcharge or overburden
- 4) Residual stresses from welding and other assembly processes

After the resultant longitudinal and circumferential stresses have been obtained, a failure theory will have to be selected to determine if the pipe

yields. In this discussion we will only mention some of the theories which might be chosen. Actual selection of an appropriate failure theory must be left up to engineers in each company. Sometimes state law, politics, and other considerations beyond our control dictate the choice or selection of a particular process for determining yield. We will illustrate some of the theories which might be selected.

A biaxial state of stress may be plotted on a graph with one stress such as the circumferential one on the X axis and the other such as the longitudinal one on the Y axis. Figure 57 is such a plot, with the circumferential and longitudinal stresses normalized by dividing by a uniaxial yield stress σ_y . Four different quadrants exist in the solution shown in Figure 57 because these are the different combinations of tension and compression which could exist in the two orthogonal resultant stresses. Different yield theories have been applied by various investigators to determine what combinations of these resultant stresses constitute the onset of yield. Five of these different theories are illustrated in Figure 57. To determine if the pipe yields because of blasting and the other applied stresses, the reader will have to select one of these yield theories.

The five theories shown in Figure 57 are: 1) the maximum stress theory, 2) the maximum strain theory, 3) the maximum shear theory, 4) the maximum energy theory, and 5) the distortion energy theory. Additional details and discussions of these theories can be found in Section X of Timashenko (Reference 19). All of the lines in Figure 57 represent the threshold of yield. If any biaxial combination of stresses fall within the envelopes, no yield occurs, but if stresses fall outside the envelopes, yielding will occur. Notice that all theories agree on the yield criteria for a uniaxial state of stress; however, they differ for biaxial states of stress and also have different envelopes whenever the signs are the same and when the signs differ.

For all of these theories, the worse conditions occur in quadrants II and IV where the signs of the resultant stresses differ. Often regulations and specifications simplify yield criteria by taking absolute values of the resultant stresses, and use a yield criteria from a worse state quadrant such as quadrant II. Figure 58 is this plot for the five yield theories shown in Figure 57.

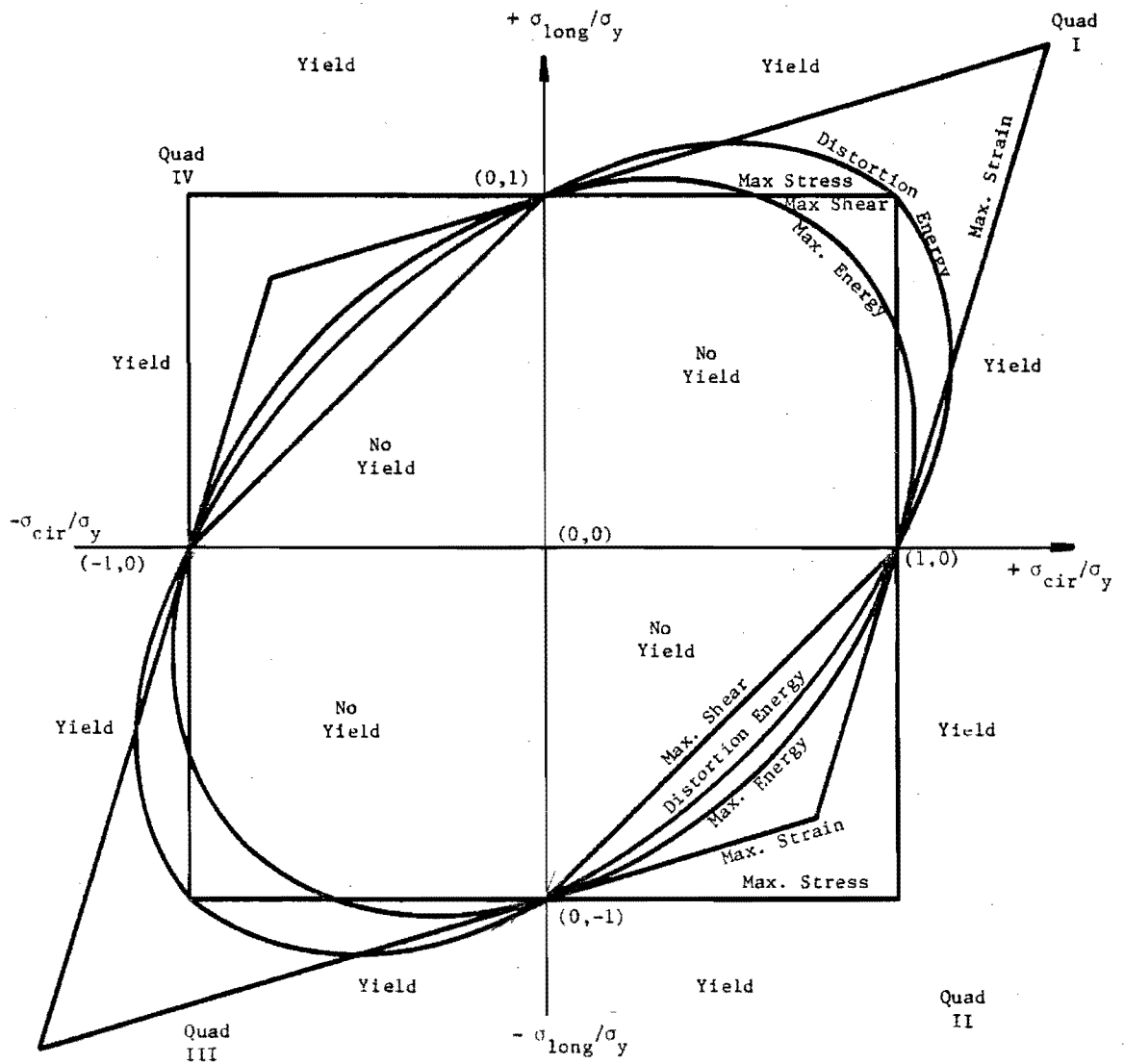


FIGURE 57. STRESS STATES FOR DIFFERENT YIELD THEORIES

Many states use the maximum shear theory because this is the most conservative and the equation to this straight line is very simple. Some people tend to use the distortion energy criteria as they believe this theory is the most accurate. Each reader will have to decide for his company which philosophy, approach, regulation, and company policy, is most applicable. We present this short discussion so different criteria will be discussed and can be compared in a meaningful way. Actual selection of any one approach as being the one theory to use is beyond the limits placed on this work by the A.G.A. All five theories combine circumferential and longitudinal stresses in the same manner to obtain resultant states of stress. This entire discussion is to emphasize that organizations may be using different yield criteria for different reasons in various sections of the country.

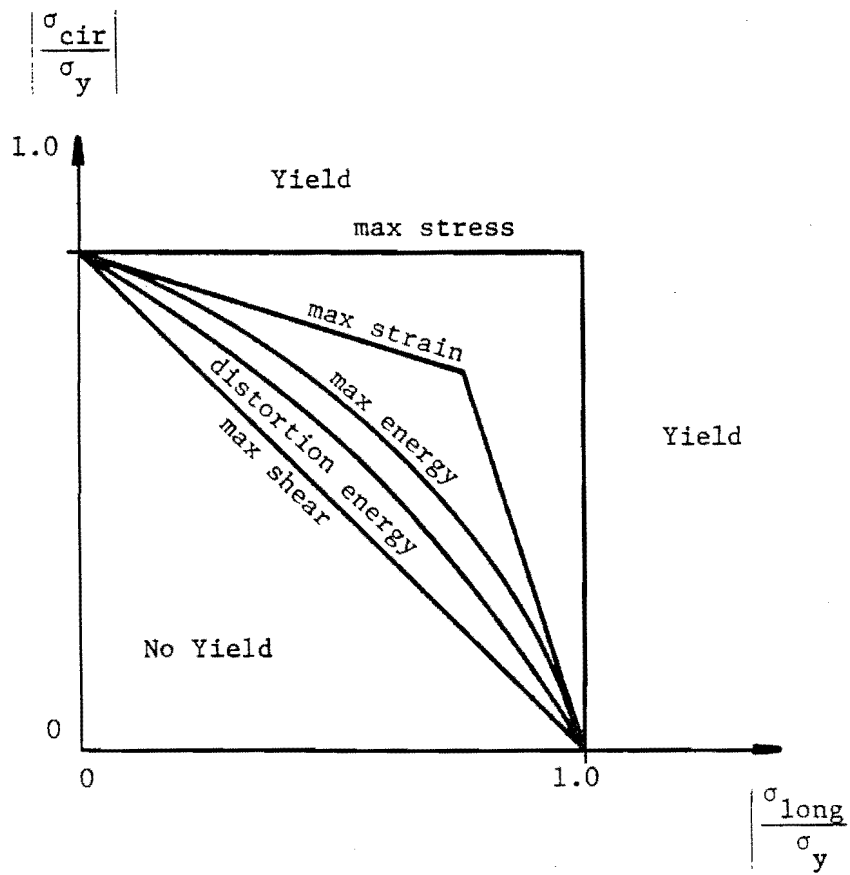


FIGURE 58. SIMPLIFIED YIELD THEORIES

Other Analysis Methods

Two methods in particular have found some usage, and should be discussed to place their misuse in proper perspective. The first of these is a series of maximum velocity criteria and sometimes, maximum acceleration criteria, which came into use in the 1940's. Unfortunately these efforts were concerned with very narrow bounds that pertain to some particular problem such as cracks in building and machinery misalignment. On occasion, the results would even conflict. These limiting ground motion criteria which have found their way into some state codes have been applied to pipelines and can be placed into perspective by looking at the following qualitative model.

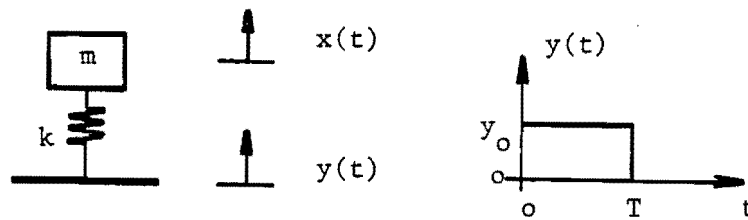


FIGURE 59. QUALITATIVE GROUND SHOCK MODEL

In this model a rectangular ground shock pulse of amplitude y_0 and duration T excites a linear elastic oscillator of mass m and spring constant k . If the relative motion $(x-y)$ max exceeds a certain magnitude, we assume that a building will crack, machinery will be misaligned, etc. The equations of motion are:

$$m \frac{d^2 x}{dt^2} + kx = k y_0 \quad \text{for } t < T \quad (106)$$

$$m \frac{d^2 x}{dt^2} + kx = 0 \quad \text{for } t > T \quad (107)$$

The initial conditions are at time $t=0$, $x=0$, and $\frac{dx}{dt} = 0$. Solving these equations for these initial conditions gives:

$$\frac{Y_o}{(x-y)_{\max}} = 0.5 \operatorname{csc} \left(\sqrt{\frac{k}{m}} \frac{T}{2} \right) \quad \text{if } \sqrt{\frac{k}{m}} T \leq \Pi \quad (108)$$

$$\frac{Y_o}{(x-y)_{\max}} = 0.5 \quad \text{if } \sqrt{\frac{k}{m}} T > \Pi \quad (109)$$

For short durations $\operatorname{csc} \sqrt{\frac{k}{m}} \frac{T}{2}$ approximately equals $\sqrt{\frac{in}{k}} \frac{2}{T}$ and:

$$\frac{\sqrt{\frac{k}{m}} (Y_o T)}{(x-y)_{\max}} = 1.0 \quad \text{if } \sqrt{\frac{k}{m}} T \leq \frac{\Pi}{3} \quad (110)$$

For a specific structure k , m , and $(x-y)$ are constants. This means that if $\sqrt{\frac{k}{m}} T > \Pi$ then y_o is equal to a constant and is a threshold for damage and for $\sqrt{\frac{k}{m}} T < \frac{\Pi}{3}$, $(y_o T)$ is equal to another constant and is also this threshold.

Usually investigators present what amounts to these same results by presenting results 180° out of phase. Acceleration corresponds to displacement and velocity corresponds to the time integral of displacement if this shift is made by multiplying and dividing by $\frac{k}{m}$, a constant for a specific structure.

In 1942 the Bureau of Mines [13] conducted experiments because of damage and litigation arising from blasting. In these tests, displacements were recorded for 10- to 10,000-lb charges at standoff distances from 100 to 6000 ft. Criterion for failure in surface buildings were the development of cracks in plaster. The Bureau of Mines investigators concluded that ground accelerations less than 0.1 g's would not cause damage, accelerations between 0.1 and 1.0 g's were in a caution range, and accelerations greater than 1.0 g's were dangerous. These were fairly long duration results with frequencies up to 10 cps. As already noted, an acceleration criterion applies for long duration results.

In 1949, Crandell [20] proposed a constant velocity (short duration) criterion for protecting structures from blasting. His lower limit for

caution to structures corresponds to a peak soil particle velocity of 3.0 in/sec. Crandell then created an arbitrary formula to relate this velocity to standoff distance, charge weight, and a ground transmission constant.

The present U. S. Bureau of Mines criteria [21] for blasting safety involve both a limiting soil particle velocity of 2 in/sec below 3 Hz and limiting ground acceleration of 0.10 g's above 3 Hz. Obviously these criteria are an effort to meet both low frequency and high frequency limiting conditions.

These criteria developed for buildings have been applied to pipelines under the assumptions that it does not matter if the structure is buried (incorrect because of the mass of soil which acts with the structure) and a pipe can be considered as a structure similar to a building (a very crude assumption).

By way of summary, this first velocity and acceleration criteria have some validity for building, but none at all for buried pipe. They also are often misapplied because people often ignore the $\sqrt{\frac{k}{m}} T$ or frequency limitations.

The second effort in common use is called the Battelle formula [22]. It uses the Morris [10] equation for ground motion, and assumes that the pipeline movements equal those of the surrounding soil. These assumptions lead to a quasi-static analysis and permits no diffraction of the shock front around the pipe. The equation for circumferential stress is given by

$$\sigma_{\text{cir}} = 4.26 \frac{K E h \sqrt{W}}{R D^2} \quad (111)$$

where

K is a site factor to account for soil conditions

E is pipe modulus (psi)

W is charge weight (lbs)

R is standoff distance (ft)

D is pipe diameter (in)

h is pipe thickness (in)

σ_{cir} is circumferential stress (psi)

Figure 60 shows a plot of test data versus this equation. To be perfectly fair, this evaluation is not a proper one because the authors state that Equation (111) is not valid for standoff distances less than 100 ft.

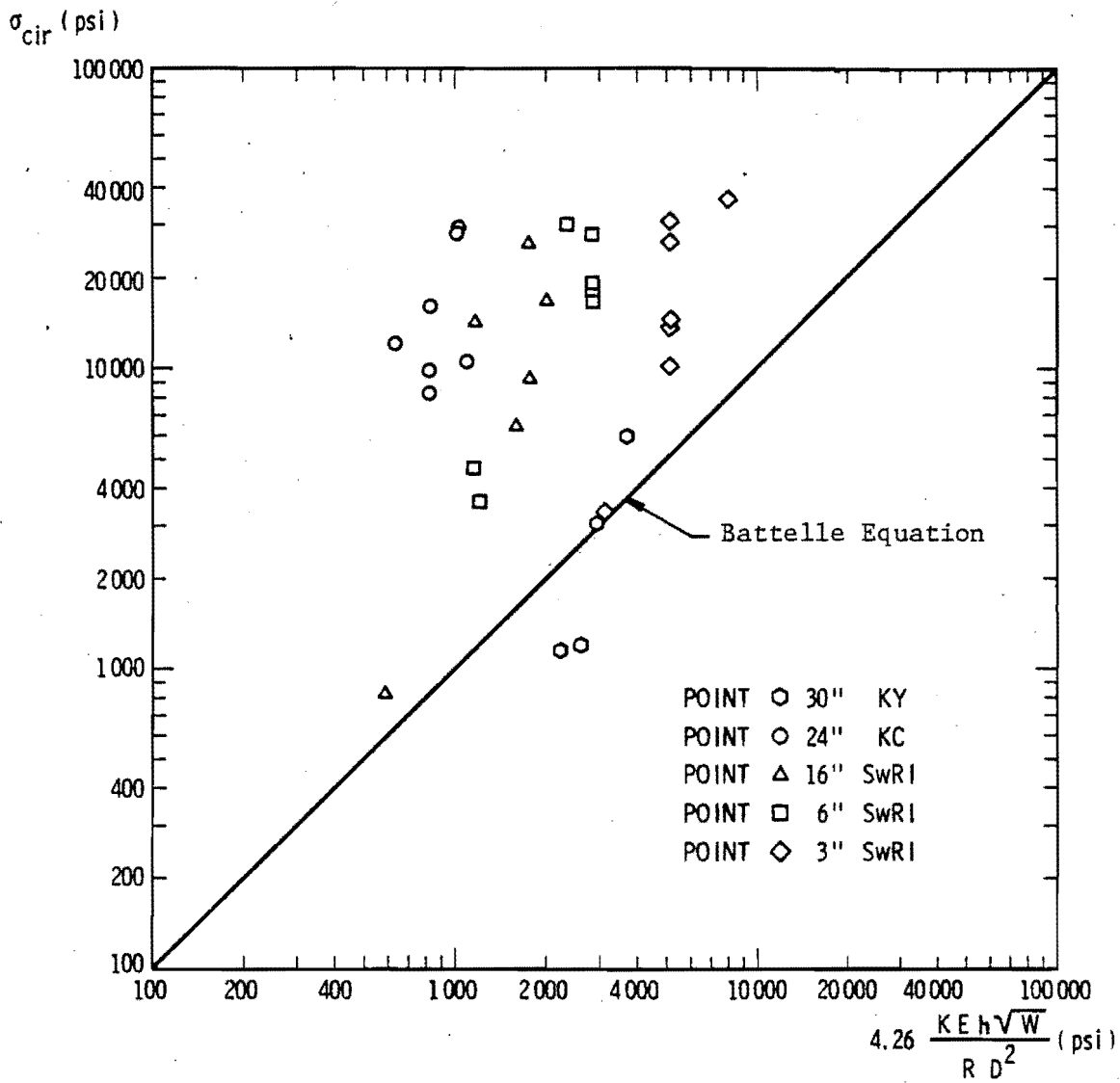


FIGURE 60. BATTELLE CIRCUMFERENTIAL STRESS FORMULA

Nevertheless this comparison is made because users have ignored the author's qualifying statement and have used the results. Equation (111) is not as accurate as our new relationships. In addition, misuse does not give conservative results as Figure 60 shows, as the measured stresses are higher than the predicted ones. Even if this formula were applied for standoff distances greater than 100 feet, its use would be questionable. Equation (111) shows that doubling the pipe thickness while keeping everything else constant doubles the stress in the pipe. This conclusion cannot be explained. Increases in pipe thickness h are expected to reduce the stress σ_{cir} .

A company's ability to use the results in this report may be restricted by regulations based on ground motion limitations or other criteria. When these circumstances arise, the reader should probably use both this report and the regulations, so blasting conditions can at least be limited to whichever gives the most conservative result.

Factor of Safety

The second question which must be faced by each company is "what factor of safety will we use?" This report will not answer this question either, but some guidance will be given.

No one number should be used as a factor of safety because many interactions are involved. Most newer pipes are manufactured from ductile materials, but some older pipes were manufactured from brittle materials. A ductile material can strain well beyond yield and still exhibit very little deformation. On the other hand, a brittle pipe material cannot exceed yield at all or the pipe will crack. Obviously the consequence of yielding is much more severe in a brittle than in a ductile pipeline, so much larger safety factors should be used in brittle as opposed to ductile pipelines.

One standard deviation for predicting both circumferential and longitudinal stresses from blasting equals essentially 45% of the predicted value (46% for circumferential stress and 44% for longitudinal stress). This statement infers that were the same blasting against pipeline experimental conditions repeated a large number of times, approximately 68% of the results would fall between $[1 \pm 0.45]$ times the predicted value, and 95% of the results would fall between $[1 \pm 0.90]$ times the predicted value. This

prediction of scatter assumes a normal distribution of test results which is not quite true, and it applies only to those stress components caused by blasting.

Knowing a standard deviation for the blasting components of stress helps, but it alone cannot determine the safety factor. Another key consideration is the magnitude of the blasting stresses relative to the total stresses. For example, in a pipeline with a yield stress of 60 ksi, a blasting stress of 10 ksi means one standard deviation is ± 4.5 ksi; whereas, a blasting stress of 40 ksi means one standard deviation is 18 ksi. Obviously one standard deviation of 4.5 ksi is fairly insignificant relative to a 60 ksi yield point especially when compared to one standard deviation of 18 ksi relative to 60 ksi. The magnitude of the blasting stress relative to the total state of stress must be considered in selecting an appropriate safety factor.

One final consideration in the selection of a safety factor is some concept of the consequences of failure. Loss of service in a major pipeline serving an entire region of the United States has to be more serious than loss of service in an artery into some building development. This observation implies that factor of safety might be presented as a function of pipe diameter because the larger lines are usually the most important ones.

As should be apparent by this discussion, factor of safety is not a one answer question. We must leave this consideration up to each individual company as regulations and company policy can also differ in various sections of the country.

IX CONCLUSIONS AND RECOMMENDATIONS

The following conclusions are reached from this program:

- (1) The functional relationships developed in this report represent a general solution to predict the maximum stress of a buried pipe to nearby point and line explosive sources in various types of soils. The final solution derived in Section VI uses both approximate analyses procedures to interrelate variables and empirical test results to develop the final functional format. Only elastic procedures were used because it was considered unacceptable to permit any stress to exceed yield in a pipeline.
- (2) The general solution to predict the pipe stresses from underground detonation requires knowledge of the maximum radial soil displacement. This relationship is needed because the ground motion defines the forcing function applied to a buried pipe from blasting.
- (3) Equations for predicting soil particle velocity and displacement for a wide range of single underground explosion energies (i.e. point sources), soils, and standoff distances were derived empirically applying SwRI as well as other investigation data, and are given in equations (30) and (31).
- (4) Equations (44) and (45) give the functional relationships for particle velocity and soil displacement for line sources (i.e. multiple detonation). Again, these equations were obtained empirically using SwRI measurements reported in Section IV.
- (5) Functional relationships to predict the pipe response to near underground detonations were derived for point and line sources and are presented in equations (91), (94) (95a) and (95b), for circumferential and longitudinal stresses. These close form solutions were obtained from the experiments reported in Section III and IV of this report.

- (6) The empirical data used to derive equation (95a) and (95b) infer that a change in mode of pipe response occurs around a $\bar{\sigma}$ of 2675 psi, which has a very pronounced effect on longitudinal response and only a small effect on circumferential response.
- (7) Analytical and experimental observations on 3-, 6-, 16-, 24- and 30-in. diameter pipe revealed that stresses were independent of both the pipe length and the pipe radius. Static analysis procedures do not yield this conclusion, and cannot be used to draw valid conclusions in this dynamic problem.
- (8) The sensitivity analysis given in Section VIII, Table XX indicated that pipe stresses are most sensitive to standoff distance R and least sensitive to pipe properties (i.e. modulus of elasticity E and thickness h). Changes in the standoff distance also have a greater influence on the stress for a point source than a line source.
- (9) The general solution is also independent of soil density ρ , and seismic P-wave velocity c, in the soil. These soil properties mathematically cancel out of the analysis in Section VI because a simplified linear approximation was used to interrelate soil displacement, soil properties, standoff distance and energy release. Had the more complex hyperbolic tangent relationship given in equation (30) been used, the circumferential and longitudinal stresses would become weak functions of ρ and c. The simplified format was used because adequate engineering answers were obtained without appreciable benefit from added complexity.
- (10) From the experimental data and analysis presented in this report, it was shown that ground motions and pipe response parameters from transient pulses can be scaled or modeled. This observation was verified with experiments at three different test sites in three different states using pipes with diameters ranging from 3 to 30 in.
- (11) A knowledge of the state of stress caused by blasting is necessary but not sufficient information to determine if a buried pipe will yield.

Other stresses such as those caused by internal pipe pressurization, thermal expansion or contraction, surcharge or overburden, and residual stress from welding and other assembly processes can be very significant. This program does not include a discussion of states of stress from other cause. However, an accurate estimate of the elastic state of stress can be made by superposition through additions of stresses with their signs considered. After the resultant longitudinal and circumferential stresses have been obtained a failure theory for yielding will have to be selected to determine if the pipe survives. Some of these theories are discussed in Section VIII.

- (12) Other analytical methods have been used in the past to predict structural response from underground detonation. Two methods in particular have found some usage. The first of these is a series of maximum soil velocity criteria, and sometimes acceleration criteria. The second is called the Battelle formula, which is based on Morris' equation for ground motion, and assumes that the pipeline movements equal those of the surrounding soil. The first criteria have some validity for surface structures such as buildings, but none at all for buried pipes. It is often misused because people find it easy to apply in spite of its limited applicability. The second criteria by the author's own admissions are not valid for standoff distances of less than 100 ft. However, users have ignored this limitation and have applied the results for much closer standoff distance, thereby predicting quite often lower stresses than those measured in this program. The Battelle formula (eq 111) is also suspect since it yields the questionable conclusion that doubling the pipe thickness while keeping everything else constant doubles the stress in the pipe.
- (13) The use of the results from this report may be restricted by regulatory codes based on either ground motion limitations and/or Battelle formula. When this circumstance arises, the reader should use both this report and regulatory codes, so blasting conditions can at least be limited to whichever gives the most conservative results.

- (14) What factors of safety can be used in applying these results is not answered, because many interactions are involved. The following factors interplay:
- a. Pipe ductility
 - b. Magnitude of the blasting stresses relative to the total stress
 - c. Failure theories used
 - d. Consequences of failure
 - e. Regulations and codes
 - f. Company policy
 - g. The charge should be buried at a standoff distance of 1.5 or greater pipe diameters from the center of the pipe.

Factor of safety considerations are to be determined by individual users.

- (15) One standard deviation for predicting both circumferential and longitudinal stresses from blasting equals essentially $\pm 45\%$ of the predicted value (46% for circumferential stress and 44% for longitudinal stress). This statistic infers that if a large number of the same blasting conditions were to be repeated, approximately 68% of the results would fall between $[1 \pm 0.45]$ times the predicted value, and 95% of the results would fall between $[1 \pm 0.90]$ times the predicted value. This calculation assumes a normal distribution of the test results and applies only to those stress components caused by blasting.

- (16) Assumptions and limitations associated with the general solution are:
- (a) The charge and the center-line of the pipe are at the same depth.
 - (b) A line charge is a continuous line rather than a series of point charges. A point source has no shape or finite size.
 - (c) Any line source runs parallel to the pipeline.
 - (d) The pipeline is straight without elbows or valves.
 - (e) Wrapping, sand beds, and other potential shock isolation layers between the pipe and the soil have no effect.
 - (f) The solution gives only the elastic stress contributions from blasting. No inelastic behavior is included in this solution.
 - (g) Explosive sources always detonate instantly.
 - (h) Reflections from the surface of the ground are insignificant.
 - (i) No explosive energy (or at least a constant percentage of the energy) goes into cratering, air blast, and other phenomena.

(j) Explosive charge and pipe are embedded in the same soil medium.

(k) Some conclusions for minimum standoff for application.

Because of the above limitations the following recommendations are made for additional investigation to improve the validation of these program results and broaden the usefulness of the data.

- (1) Conduct additional scale model tests to examine the results of blasting when the explosive charge is well below the center line of the pipe and no energy is vented to the atmosphere.
- (2) Conduct model tests in which the charge and pipeline are in different soil mediums to determine if any ground shock reflections occur which appreciably invalidate the analysis.
- (3) Develop procedures to model an explosive grid system and verify through model tests.

X. REFERENCES

1. Wilfred E. Baker, Peter S. Westine, and Franklin T. Dodge, Similarity Methods in Engineering Dynamics, Spartan Division of Hayden Books, Rochelle Park, N.J., 1978.
2. H. L. Langhaar, Dimensional Analysis and Theory of Models, John Wiley and Sons, New York, 1951.
3. G. Murphy, Similitude in Engineering, Ronald Press, New York, 1950.
4. L. I. Sedov, Similarity and Dimensional Methods in Mechanics, Edited by Maurice Holt, translated from Russian to English by Morris Feldman, Academic Press, New York, 1959.
5. D. S. Carder and W. K. Cloud, "Surface Motion from Large Underground Explosions," Journal of Geophysical Research, Vol. 64, No. 10, October 1959, pp. 1471-1487.
6. F. J. Crandell, "Transmission Coefficient for Ground Vibrations Due to Blasting," Journal of Boston Society of Civil Engineering, Vol. 47, No. 2, April 1960, pp. 152-168.
7. G. M. Habberjam and J. T. Whetton, "On the Relationship Between Seismic Amplitude and Charge of Explosive Fired to Routine Blasting Operations," Geophysics, Vol. 17, No. 1, January 1952, pp. 116-128.
8. D. E. Hudson, J. L. Alford, and W. D. Iwan, "Ground Accelerations Caused by Large Quarry Blasts," Bulletin of the Seismic Society of America, Vol. 51, No. 2, April 1961, pp. 191-202.
9. Ichiro Ito, "On the Relationship Between Seismic Ground Amplitude and the Quantity of Explosives in Blasting," reprint from Memoirs of the Faculty of Engineering, Kyoto University, Vol. 15, No. 11, April 1953, pp. 579-587.
10. G. Morris, "The Reduction of Ground Vibrations from Blasting Operations," Engineering, April 21, 1950, pp. 430-433.
11. N. Ricker, "The Form and Nature of Seismic Waves and the Structure of Seismograms," Geophysics, Vol. 5, No. 4, October 1940, pp. 348-366.
12. G. A. Teichmann and R. Westwater, "Blasting and Associated Vibrations," Engineering, April 12, 1957, pp. 460-465.
13. J. R. Thoenen and S. L. Windes, "Seismic Effects of Quarry Blasting," Bureau of Mines Bulletin 442, 1942, pp. 83.
14. D. E. Willis and J. T. Wilson, "Maximum Vertical Ground Displacement of Seismic Waves Generated by Explosive Blasts," Bulletin of the Seismic Society of America, Vol. 50, No. 3, July 1960, pp. 455-459.

15. B. F. Murphey, "Particle Motions Near Explosions in Halite," Journal of Geophysical Research, Vol. 66, No. 3, March 1961, pp. 947ff.
16. H. Nicholls, C. Johnson, and W. Duvall, "Blasting Vibrations and Their Effects on Structures," Final Report 1971, Denver Mining Research Center for Bureau of Mines, BuMines Report No. B 656, PB 231 971.
17. Anon., Project Dribble Salmon, "Analysis of Ground Motion and Containment, Roland F. Beers, Inc. report to Atomic Energy Commission on Tests in Tatum Salt Dome, Mississippi, Final Report VUF-1026, November 30, 1965.
18. W. M. Adams, R. G. Preston, P. L. Flanders, D. C. Sachs, and W. R. Perret, "Summary Report of Strong-Motion Measurements, Underground Nuclear Detonations," Journal of Geophysical Research, Vol. 66, No. 3, March 1961, pp. 903ff.
19. Stephen Timoshenko, Strength of Materials, Part II: Advanced Theory and Problems, Third Edition, Van Nostrand Company, Princeton, New Jersey, March 1956.
20. F. J. Crandell, "Ground Vibrations Due to Blasting and Its Effect Upon Structures", Journal Boston Soc. Civil Engineers, Vol. 36, 1949, p 245.
21. J. F. Wiss, "Effects of Blasting Vibrations on Buildings and People", Civil Engineering, July 1968, pp. 46-48.
22. George M. McClure, Thomas V. Atterbury, and Noah A. Frazier, "Analysis of Blast Effects on Pipelines", Journal of the Pipeline Division, Proceeding of the American Society of Civil Engineers, November 1964.

XI. LIST OF PARAMETERS AND SYMBOLS

English

A	Projected pipe area; peak amplitude for either velocity or displacement
A_1, A_2, \dots	Acceleration
C_D	Diffraction coefficient
c (ft/sec)	Seismic P-wave velocity in soil
D (in)	Pipe diameter
<u>d</u>	"Dimensionally equal to"
dx	Differential length of pipe
E (psi)	Modulus of elasticity for the pipe material
F, L, T	Fundamental units of measure; force, length and time, respectively
$f_1, f_2 \dots$	Symbol for function of
h (in)	Pipe wall thickness
I	Total applied impulse
i	Any applied specific impulse
i_s	Side-on specific impulse
J (in ⁴)	Second moment of area
K	Site factor for soil condition; a constant
KE	Kinetic energy
k	Spring constant in the qualitative structural response model
l (ft)	Length of explosive line (for uniform charges spaced equal distances apart, this length is the spacing between charges times the number of charges)
m	Ratio of impulse or pressure on the back of the pipe relative to impulse or pressure at the front of the pipe; also mass in the qualitative structural response mode.
n	Numerical constants

English

nW	Equivalent explosive energy release, see Equation (90) (lb AN-FO) and pp. 124 and 129.
p_o (psf)	Atmospheric pressure
P_s	Side-on pressure
R (ft)	Standoff distance from the center of the pipe to the charge
R_1, R_2 (ft)	Distance between charge and ground motion canister
r (in)	Pipe radius
S	One standard deviation as a percentage
SC (psi)	Circumferential stress
SE (in-lb)	Strain energy
SE_{cir} (in-lb)	Circumferential strain energy
SE_{long}	Longitudinal strain energy
SL (psi)	Longitudinal stress
T	Time constant associated with duration of the load
t	Variable constant
U (ft/sec)	Maximum radial peak particle velocity of the soil
$U_1, U_2 \dots$	Maximum radial particle velocity of the soil at location 1, 2... (in/sec)
U_{A1}	Particle velocity of soil obtained from accelerometer measurement at location 1
U/C	Scaled velocity
V	Velocity of shock front
W (ft-lb)	Energy released in an explosive point source; charge weight
$W/l \left(\frac{ft-lb}{ft} \right)$	Energy released per unit length in an explosive line source
w_o	Mid-span deformation
X (ft)	Maximum radial displacement of the soil
X/R	Scaled displacement

English

X_{U_1} Maximum radial displacement of the soil obtained by integrating the velocity at location 1

x (in) Displacement in the qualitative structural response model

x-y (in) Relative motion

Y (in) Assumed deformed shape

y_0 (in) Ground shock pulse of amplitude; threshold for damage

Greek Symbols

$\alpha_1 \dots, \alpha_{10}$	Exponents on parameters in the equation of dimensional homogeneity
θ	Angle (see Figure 49)
λ	Geometric scale factor
μ	Mass per unit length
$\mu\epsilon$	Micro strains
π term	Dimensionless group
$\rho, \rho_s, \left(\frac{\text{lb-sec}^2}{\text{ft}^4}\right)$	Mass density of soil or rock
$\rho_a \left(\frac{\text{lb-sec}^2}{\text{ft}^4}\right)$	Density behind the shock front
ρc^2 (psf)	Compressibility of the soil
$\rho c_p \theta$ (psf)	Heat capacity times temperature increase
ρ_p	Mass density of pipe
$\bar{\sigma}$ (psi)	Maximum circumferential stress for values <2675 psi
σ_{cir} (psi)	Maximum circumferential stress in the pipe
σ_{long} (psi)	Maximum longitudinal stress in the pipe
σ_{max} (psi)	Maximum pipe stress; may be either the longitudinal or circumferential direction
σ_{obs} (psi)	Observed stress
σ_{cal} (psi)	Calculated value
σ_y (psi)	Yield point for the pipe
τ (sec)	Period of pipe response
ω (rad/sec)	Fundamental natural frequency
η (psf)	Density times the heat of fusion